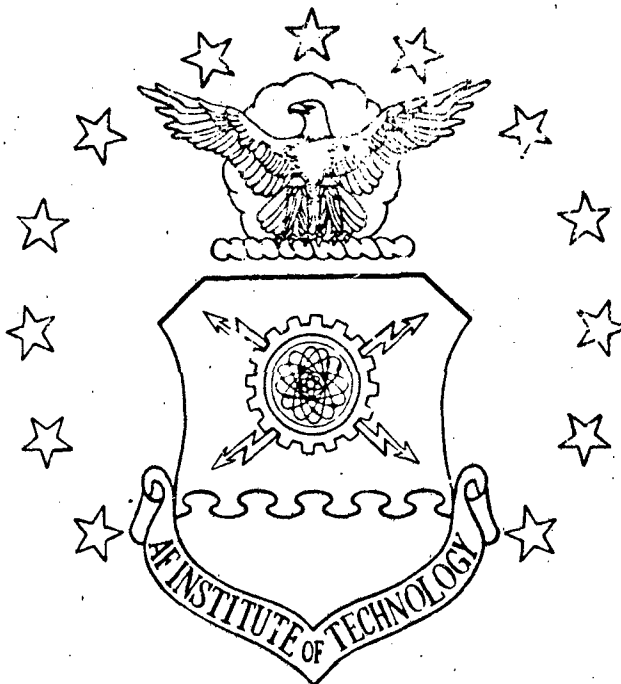


DTIC

①

AD-A153 100



20000814173

DESIGN OF ROBUST CONTROLLERS FOR A MULTIPLE  
 INPUT-MULTIPLE OUTPUT CONTROL SYSTEM WITH  
 UNCERTAIN PARAMETERS APPLICATION TO THE  
 LATERAL AND LONGITUDINAL MODES OF THE  
 KC-135 TRANSPORT AIRCRAFT

THESIS

AFIT/GE/ENG/84D-72

Harvey H. Russell  
Capt CAF

DTIC FILE COPY

DTIC  
 ELECTED  
 APR 29 1985  
 E

DEPARTMENT OF THE AIR FORCE  
AIR UNIVERSITY

**AIR FORCE INSTITUTE OF TECHNOLOGY**

Wright-Patterson Air Force Base, Ohio

This document has been approved  
 for public release  
 distribution is unlimited

85 04 26 010

UNCLASSIFIED

SECURITY CLASSIFICATION OF THIS PAGE

AD A 153 100

REPORT DOCUMENTATION PAGE

1. REPORT SECURITY CLASSIFICATION <b>UNCLASSIFIED</b>			1d. RESTRICTIVE MARKINGS			
2a. SECURITY CLASSIFICATION AUTHORITY			3. DISTRIBUTION/AVAILABILITY OF REPORT Approved for public release; distribution unlimited			
2b. DECLASSIFICATION/DOWNGRADING SCHEDULE						
4. PERFORMING ORGANIZATION REPORT NUMBER(S)			5. MONITORING ORGANIZATION REPORT NUMBER(S)			
6a. NAME OF PERFORMING ORGANIZATION AF Institute of Technology School of Engineering		6b. OFFICE SYMBOL (If applicable) AFIT/EN		7a. NAME OF MONITORING ORGANIZATION AFWAL/Flight Dynamics Laboratory Flight Control Division (FIG)		
6c. ADDRESS (City, State and ZIP Code) Wright-Patterson AFB OH 45433			7b. ADDRESS (City, State and ZIP Code) Wright-Patterson AFB OH 45433			
8a. NAME OF FUNDING/SPONSORING ORGANIZATION		8b. OFFICE SYMBOL (If applicable) AFWAL/FIG		9. PROCUREMENT INSTRUMENT IDENTIFICATION NUMBER		
8c. ADDRESS (City, State and ZIP Code)			10. SOURCE OF FUNDING NOS.			
			PROGRAM ELEMENT NO.	PROJECT NO.	TASK NO.	WORK UNIT NO.
11. TITLE (Include Security Classification) See Block 19						
12. PERSONAL AUTHOR(S) Harvey Hayward Russell, Captain, CAF						
13a. TYPE OF REPORT MS Thesis		13b. TIME COVERED FROM _____ TO _____		14. DATE OF REPORT (Yr., Mo., Day) 1984 December		15. PAGE COUNT 380
16. SUPPLEMENTARY NOTATION						
17. COSATI CODES			18. SUBJECT TERMS (Continue on reverse if necessary and identify by block number)			
FIELD	GROUP	SUB GR	Multiple Input-Multiple Output; Multivariable Control; Flight Control; Lateral Controllers; Longitudinal Con- trollers; Uncertain Plants; Robustness; Quantitative Feedback; Landing Modes; KC-135			
19. ABSTRACT (Continue on reverse if necessary and identify by block number)						
Title: DESIGN OF ROBUST CONTROLLERS FOR A MULTIPLE INPUT-MULTIPLE OUTPUT CONTROL SYSTEM WITH UNCERTAIN PARAMETERS APPLICATION TO THE LATERAL AND LONGITUDINAL MODES OF THE KC-135 TRANSPORT AIRCRAFT						
Thesis Chairman: Constantine H. Houpis						
20. DISTRIBUTION/AVAILABILITY OF ABSTRACT UNCLASSIFIED/UNLIMITED <input type="checkbox"/> SAME AS RPT <input checked="" type="checkbox"/> DTIC USERS <input type="checkbox"/>			21. ABSTRACT SECURITY CLASSIFICATION <b>UNCLASSIFIED</b>			
22a. NAME OF RESPONSIBLE INDIVIDUAL Constantine H. Houpis, Ph.D.			22b. TELEPHONE NUMBER (Include Area Code) 513-255-3576		22c. OFFICE SYMBOL AFIT/EN	

Approved for public release: IAW AFR 120-17.  
LYNN E. WELLS  
Dean for Research and Professional Development  
Air Force Institute of Technology (AFIT)  
Wright-Patterson AFB OH 45433

UNCLASSIFIED

SECURITY CLASSIFICATION OF THIS PAGE

A multiple input-multiple output flight control design on the KC-135 aircraft is completed using the Quantitative Feedback Theory (QFT), developed by Dr. Isaac Horowitz, Weizmann Institute of Science, Rehovot, Israel.

First, the three degrees-of-freedom model for the lateral mode is reduced to a two degrees-of-freedom model. From this model a robust controller is developed to perform two maneuvers over a wide range of the aircraft flight envelope.

Second, the three degrees-of-freedom model for the longitudinal mode is used to develop a robust controller to perform one maneuver. The first and second body bending modes are then added to remove the rigid body constraint and a robust control is developed for the non-rigid aircraft.

Finally, the robust controllers developed for the lateral and longitudinal modes are simulated over a large range of the aircraft's flight envelope.

The conclusion drawn from the research is that the methods developed by Dr. Horowitz are very effective in designing multiple input-multiple output systems with plant uncertainty.

UNCLASSIFIED

SECURITY CLASSIFICATION OF THIS PAGE

①

AFIT/GE/ENG/84D-72

DESIGN OF ROBUST CONTROLLERS FOR A MULTIPLE  
INPUT-MULTIPLE OUTPUT CONTROL SYSTEM WITH  
UNCERTAIN PARAMETERS APPLICATION TO THE  
LATERAL AND LONGITUDINAL MODES OF THE  
KC-135 TRANSPORT AIRCRAFT

THESIS

AFIT/GE/ENG/84D-72

Harvey H. Russell  
Capt                      CAF

Approved for public release; distribution unlimited

DTIC  
ELECTE  
APR 29 1985  
S  
E

AFIT/GE/ENG/84D-72

DESIGN OF ROBUST CONTROLLERS FOR A MULTIPLE INPUT-MULTIPLE  
OUTPUT CONTROL SYSTEM WITH UNCERTAIN PARAMETERS  
APPLICATION TO THE LATERAL AND LONGITUDINAL  
MODES OF THE KC-135 TRANSPORT AIRCRAFT

THESIS

Presented to the Faculty of the School of Engineering  
of the Air Force Institute of Technology  
Air University  
In Partial Fulfillment of the  
Requirements for the Degree of  
Master of Science in Electrical Engineering

Harvey H. Russell, B.S.E.E.  
Captain, CAF

December 1984

Accession	
NTIS	X
ERIC	
Univ.	
J.	

A-1

Approved for public release; distribution unlimited



## Preface

This thesis subject was sponsored by the Flight Dynamics Laboratory, Wright-Patterson AFB, Ohio. This topic was selected because of its importance in achieving robust flight control systems and the multiple input-multiple output design approach of Dr. Isaac Horowitz can readily be applied to such flight control problems.

I would like to thank Dr. Isaac Horowitz for his excellent support during this thesis. Without his support, this thesis would not have been possible. I would also like to thank Dr. Constantine Houppis, Thesis Co-advisor, for the support and direction given to me throughout this thesis endeavor. Also I extend my appreciation to Mr. Yin-Kuei Liao of the Chung-Shan Institute of Science, Republic of China, for giving me direction and use of a large number of software programs which aided in the numerical analysis and simulation phases of this thesis.

I wish to extend my greatest appreciation to my wife, Carol, for her understanding and patience during this very demanding period. Also, I would like to thank my children, Mark and Robin, for their devotion and understanding. Thank you and I love you.

Table of Contents

	Page
Preface . . . . .	ii
List of Figures . . . . .	vii
List of Tables . . . . .	xv
List of Symbols . . . . .	xix
Abstract . . . . .	xxvi
I. Introduction . . . . .	1
I-1 Problem . . . . .	3
I-2 Scope . . . . .	3
I-3 Assumptions . . . . .	3
I-4 Approach . . . . .	4
I-5 Presentation . . . . .	5
II. Quantitative Feedback Design Theory . . . . .	7
II-1 Introduction . . . . .	7
II-2 SISO Design Theory . . . . .	7
II-3 MIMO Design Theory (2x2 System) . . . . .	9
II-4 MIMO Design Theory (3x3 System) . . . . .	10
Control Structure . . . . .	10
Constraints on the Plant Matrix . . . . .	13
Effective SISO Loops . . . . .	14
Simplification of the Single- Loop Structure . . . . .	18
Performance Tolerances . . . . .	19

	Page
Improved Design Technique . . . . .	21
Equilibrium and Tradeoffs . . . . .	24
Summary . . . . .	25
III. Aircraft Model . . . . .	28
III-1 Introduction . . . . .	26
III-2 Equations of Motion . . . . .	27
III-3 Summary . . . . .	32
IV. Lateral Design . . . . .	33
IV-1 Introduction . . . . .	33
IV-2 Input and Output Matrices . . . . .	34
IV-3 Effective SISO Systems . . . . .	38
IV-4 Response Models . . . . .	39
IV-5 Loop Two Design . . . . .	41
BNIC Loop . . . . .	45
Tracking Loop . . . . .	48
Shaping the Nominal Loop Transmission, $L_{20}$ . . . . .	53
Pre-Filter Design $F_{22}$ . . . . .	55
IV-6 Loop One Design . . . . .	56
Shaping the Nominal Loop Transmission, $L_{1e}$ . . . . .	62
Pre-Filter Design $F_{11}$ . . . . .	64
IV-7 Summary . . . . .	65



	Page
V. Longitudinal Design . . . . .	67
V-1 Introduction . . . . .	67
V-2 Input and Output Matrices . . . . .	68
V-3 Effective SISO Systems . . . . .	71
V-4 Response Models . . . . .	73
V-5 Loop Three Design . . . . .	73
Loop One Design . . . . .	80
Tracking Loop (Loop Two) . . . . .	81
V-6 Longitudinal Design (Non-Rigid) Aircraft . . . . .	89
Addition of First and Second Body Bending Modes . . . . .	89
V-7 Loop Three Design . . . . .	91
V-8 Loop One Design . . . . .	92
V-9 Loop Two Design . . . . .	94
V-10 Comparison of Rigid and Non-Rigid Designs . . . . .	97
V-11 Summary . . . . .	98
VI. Simulation . . . . .	99
VI-1 Introduction . . . . .	99
VI-2 Lateral Simulation (2x2 Design) . . . . .	99
Bank Angle Command Response . . . . .	100
Sideslip Command . . . . .	109
VI-3 Longitudinal Simulation (3x3 Design). . . . .	119
VII. Conclusions and Recommendations . . . . .	134
VII-1 Thesis Summary . . . . .	134

	Page
VII-2 Discussion . . . . .	135
VII-3 Comparison to Porter Technique . . . . .	136
VII-4 Conclusion . . . . .	138
VII-5 Recommendations . . . . .	139
Appendix A: Single Input-Single Output Theory . . . . .	140
Appendix B: Multiple Input-Multiple Output Theory . . . . .	163
Appendix C: Aircraft Equations . . . . .	172
Appendix D: Sample Run of CAT Program . . . . .	206
Appendix E: Time Response Models . . . . .	211
Appendix F: The 3x3 Design Data and Response Models. . . . .	224
Appendix G: 2x2 Simulation Programs . . . . .	262
Appendix H: Simulation Responses for F.C.'s #1 and #2 . . . . .	296
Bibliography . . . . .	349
Vita . . . . .	351

List of Figures

Figure		Page
2-1	The 3x3 Multiple Input-Multiple Output Feedback Structure . . . . .	11
2-2	The Complete Three-by-Three MIMO Structure with Diagonal G . . . . .	11
2-3	The Final Equivalent Single Loop Feedback Structure which Replaces the 3x3 MIMO Problem . . . . .	15
4-1	Effective SISO Systems . . . . .	39
4-2	Loop 2 SISO Systems . . . . .	41
4-3	Upper and Lower Bound Specifications . . . . .	43
4-4	Basic Non-Interacting Loop Two . . . . .	45
4-5	Magnitude of $g_{22}$ for F.C.'s #1, #2, and #3 . . . . .	46
4-6	SISO System - $L_2$ - Tracking . . . . .	49
4-7	Effective Loops--Tracking . . . . .	49
4-8	Bounds on $L_{20}$ for $\omega = .1$ Radians/Sec. . . . .	52
4-9	Bounds and Nominal Loop Transmission, $L_{20}$ . . . . .	54
4-10	Magnitude and Phase of Nominal Loop Transmission of Loop Two . . . . .	55
4-11	Required Bounds on Pre-Filter $f_{22}$ . . . . .	56
4-12	Effective SISO System for Loop One . . . . .	56
4-13	Magnitude vs Frequency of Equivalent $g_{11e}$ 's . . . . .	60
4-14	Bounds on $L_{10e}$ . . . . .	63
4-15	Magnitude and Phase of Nominal Loop Transmission for Loop One . . . . .	64

Figure		Page
4-16	Bounds on Pre-Filter $F_{11}$ . . . . .	65
5-1	Effective SISO Systems for 3x3 MIMO Problem .	72
5-2	The Effective SISO System for Loop 3 . . . . .	74
5-3	Magnitude of $q_{33}$ for F.C.'s #1, #2, and #3 . .	76
5-4	Bounds and Nominal Loop Transmission, $L_{30}$ . .	78
5-5	Magnitude and Phase, $L_{30}$ . . . . .	79
5-6	Effective SISO System for Loop One . . . . .	80
5-7	Bounds and Nominal Loop Transmission, $L_{10}$ . .	82
5-8	Magnitude and Phase, $L_{10}$ . . . . .	83
5-9	Effective SISO System, Loop 2 . . . . .	83
5-10	Bounds and Nominal Loop Transmission, $L_{2oe}$ . .	86
5-11	Magnitude and Phase, $L_{2oe}$ . . . . .	87
5-12	Bounds and Nominal Loop Transmission $L_{10}$ . . . .	93
5-13	Magnitude and Phase-- $L_{10}$ . . . . .	94
5-14	Bounds and Nominal Loop Transmission, $L_{2oe}$ . . .	96
5-15	Magnitude and Phase-- $L_{2oe}$ . . . . .	97
6-1	Bank Angle Response--F.C. #3 . . . . .	101
6-2	Sideslip Response--F.C. #3 . . . . .	101
6-3	Control Wheel Deflection--F.C. #3 . . . . .	102
6-4	Rudder Deflection--F.C. #3 . . . . .	102
6-5	Bank Angle Response--F.C. #3 . . . . .	104
6-6	Sideslip Response--F.C. #3 . . . . .	104
6-7	Control Wheel Deflection--F.C. #3 . . . . .	105
6-8	Rudder Deflection--F.C. #3 . . . . .	105
6-9	Bank Angle Response--F.C. #3 . . . . .	107

Figure		Page
6-10	Sideslip Response--F.C. #3 . . . . .	107
6-11	Control Wheel Deflection--F.C. #3 . . . . .	108
6-12	Rudder Deflection--F.C. #3 . . . . .	108
6-13	Sideslip Response--F.C. #3 . . . . .	110
6-14	Bank Angle Response--F.C. #3 . . . . .	110
6-15	Control Wheel Deflection--F.C. #3 . . . . .	111
6-16	Rudder Deflection--F.C. #3 . . . . .	111
6-17	Sideslip Response--F.C. #3 . . . . .	113
6-18	Bank Angle Response--F.C. #3 . . . . .	113
6-19	Control Wheel Deflection--F.C. #3 . . . . .	114
6-20	Rudder Deflection--F.C. #3 . . . . .	114
6-21	Sideslip Response--F.C. #3 . . . . .	116
6-22	Bank Angle Response--F.C. #3 . . . . .	116
6-23	Control Wheel Deflection--F.C. #3 . . . . .	117
6-24	Rudder Deflection--F.C. #3 . . . . .	117
6-25	Robust Controller--Bank Angle Response . . . . .	118
6-26	Robust Controller--Sideslip Response . . . . .	119
6-27	Pitch Angle Response--F.C. #3 . . . . .	120
6-28	Perturbation Velocity Response--F.C. #3 . . . . .	121
6-29	Altitude Response--F.C. #3 . . . . .	121
6-30	Elevator Deflection--F.C. #3 . . . . .	122
6-31	Speed Brake Deflection--F.C. #3 . . . . .	122
6-32	Thrust Increase--F.C. #3 . . . . .	123
6-33	Pitch Angle Response--F.C. #3 . . . . .	124

Figure		Page
6-34	Perturbation Velocity Response--F.C. #3 . . . . .	125
6-35	Altitude Response--F.C. #3 . . . . .	125
6-36	Elevator Deflection--F.C. #3 . . . . .	126
6-37	Speed Brake Deflection--F.C. #3 . . . . .	126
6-38	Thrust Increase--F.C. #3 . . . . .	127
6-39	Pitch Angle Response--F.C. #2 . . . . .	128
6-40	Perturbation Velocity Response--F.C. #2 . . . . .	129
6-41	Altitude Response--F.C. #2 . . . . .	129
6-42	Elevator Deflection--F.C. #2 . . . . .	130
6-43	Speed Brake Deflection--F.C. #2 . . . . .	130
6-44	Thrust Increase--F.C. #2 . . . . .	131
6-45	Pitch Angle Response--F.C.'s #1, #2, and #3 (Rigid Aircraft) . . . . .	132
6-46	Pitch Angle Response--F.C.'s #1, #2, and #3 (Non-Rigid Aircraft) . . . . .	133
A-1	Two Degrees-of-Freedom Control Loop . . . . .	141
A-2	Time Domain Step Response Specifications . . . . .	144
A-3	Third-Order Control Ratio Pole-Zero Pattern . . . . .	145
A-4	Frequency Domain Specifications . . . . .	146
A-5	Nichols Chart with Plant Templates . . . . .	148
A-6	$L_o(j\omega_i)$ Bounds on the Nichols Chart . . . . .	153
A-7	Nominal $L_o(j\omega_i)$ . . . . .	157
A-8	Requirements of F . . . . .	160
A-9	Frequency Bounds on the Pre-Filter, F . . . . .	161
B-1	MIMO Plant . . . . .	164

Figure		Page
B-2	Standard State Space Diagram . . . . .	166
B-3	MIMO Control Structure . . . . .	167
B-4	Two-by-Two MIMO System . . . . .	168
B-5	Effective SISO Loops . . . . .	169
C-1	Sign Convention . . . . .	176
C-2	Lateral Sign Convention . . . . .	177
C-3	Longitudinal Sign Convention . . . . .	178
E-1	Frequency Response-- $a_{11}$ , $b_{11}$ and $b_{12}$ . . . . .	215
E-2	Frequency Response-- $a_{22}$ , $b_{22}$ and $b_{21}$ . . . . .	219
E-3	Templates for $q_{22}$ . . . . .	222
E-4	Templates for $q_{11e}$ . . . . .	223
F-1	Frequency Response-- $a_{22}$ , $b_{22}$ , $b_{12}$ and $b_{32}$ . . . . .	252
F-2	Templates-- $q_{11}$ --Rigid Aircraft . . . . .	253
F-3	Templates-- $q_{22}$ --Rigid Aircraft . . . . .	254
F-4	Templates-- $q_{22e}$ --Rigid Aircraft . . . . .	255
F-5	Templates-- $q_{33}$ --Rigid and Non-Rigid Aircraft . . . . .	256
F-6	Templates-- $q_{22}$ --Non-Rigid Aircraft . . . . .	257
F-7	Templates-- $q_{11}$ --Non-Rigid Aircraft . . . . .	258
F-8 (a)	Templates-- $q_{22e}$ --Non-Rigid Aircraft . . . . .	259
F-8 (b)	Templates-- $q_{22e}$ --Non-Rigid Aircraft . . . . .	260
G-1	Simulation Block Diagram . . . . .	262
H-1	Bank Angle Response--F.C. #1 . . . . .	297
H-2	Sideslip Response--F.C. #1 . . . . .	297
H-3	Control Wheel Deflection--F.C. #1 . . . . .	298
H-4	Rudder Deflection--F.C. #2 . . . . .	298

Figure		Page
H-5	Bank Angle Response--F.C. #1 . . . . .	300
H-6	Sideslip Response--F.C. #1 . . . . .	300
H-7	Control Wheel Deflection--F.C. #1 . . . . .	301
H-8	Rudder Deflection--F.C. #1 . . . . .	301
H-9	Bank Angle Response--F.C. #1 . . . . .	303
H-10	Sideslip Response--F.C. #1 . . . . .	303
H-11	Control Wheel Deflection--F.C. #1 . . . . .	304
H-12	Rudder Deflection--F.C. #1 . . . . .	304
H-13	Bank Angle Response--F.C. #2 . . . . .	306
H-14	Sideslip Response--F.C. #2 . . . . .	306
H-15	Control Wheel Deflection--F.C. #2 . . . . .	307
H-16	Rudder Deflection--F.C. #2 . . . . .	307
H-17	Bank Angle Response--F.C. #2 . . . . .	309
H-18	Sideslip Response--F.C. #2 . . . . .	309
H-19	Control Wheel Deflection--F.C. #2 . . . . .	310
H-20	Rudder Deflection--F.C. #2 . . . . .	310
H-21	Bank Angle Response--F.C. #2 . . . . .	312
H-22	Sideslip Response--F.C. #2 . . . . .	312
H-23	Control Wheel Deflection--F.C. #2 . . . . .	313
H-24	Rudder Deflection--F.C. #2 . . . . .	313
H-25	Sideslip Response--F.C. #1 . . . . .	315
H-26	Bank Angle Response--F.C. #1 . . . . .	315
H-27	Control Wheel Deflection--F.C. #1 . . . . .	316
H-28	Rudder Deflection--F.C. #1 . . . . .	316
H-29	Sideslip Response--F.C. #1 . . . . .	318



Figure		Page
H-30	Bank Angle Response--F.C. #1 . . . . .	318
H-31	Control Wheel Deflection--F.C. #1 . . . . .	319
H-32	Rudder Deflection--F.C. #1 . . . . .	319
H-33	Sideslip Response--F.C. #1 . . . . .	321
H-34	Bank Angle Response--F.C. #1 . . . . .	321
H-35	Control Wheel Deflection--F.C. #1 . . . . .	322
H-36	Rudder Deflection--F.C. #1 . . . . .	322
H-37	Sideslip Response--F.C. #2 . . . . .	324
H-38	Bank Angle Response--F.C. #2 . . . . .	324
H-39	Control Wheel Deflection--F.C. #2 . . . . .	325
H-40	Rudder Deflection--F.C. #2 . . . . .	325
H-41	Sideslip Response--F.C. #2 . . . . .	327
H-42	Bank Angle Response--F.C. #2 . . . . .	327
H-43	Control Wheel Deflection--F.C. #2 . . . . .	328
H-44	Rudder Deflection--F.C. #2 . . . . .	328
H-45	Sideslip Response--F.C. #2 . . . . .	330
H-46	Bank Angle Response--F.C. #2 . . . . .	330
H-47	Control Wheel Deflection--F.C. #2 . . . . .	331
H-48	Rudder Deflection--F.C. #2 . . . . .	331
H-49	Pitch Angle Response--F.C. #1 . . . . .	333
H-50	Perturbation Velocity Response--F.C. #1 . . . . .	333
H-51	Altitude Response--F.C. #1 . . . . .	334
H-52	Elevator Deflection--F.C. #1 . . . . .	334
H-53	Speed Brake Deflection--F.C. #1 . . . . .	335
H-54	Thrust Increase--F.C. #1 . . . . .	335

Figure		Page
H-55	Pitch Angle Response--F.C. #2 . . . . .	337
H-56	Perturbation Velocity Response--F.C. #3 . . . . .	337
H-57	Altitude Response--F.C. #2 . . . . .	338
H-58	Elevator Deflection--F.C. #2 . . . . .	338
H-59	Speed Brake Deflection--F.C. #2 . . . . .	339
H-60	Thrust Increase--F.C. #2 . . . . .	339
H-61	Pitch Angle Response--F.C. #1 . . . . .	341
H-62	Perturbation Velocity--F.C. #1 . . . . .	341
H-63	Altitude Response--F.C. #1 . . . . .	342
H-64	Elevator Deflection--F.C. #1 . . . . .	342
H-65	Speed Brake Deflection--F.C. #1 . . . . .	343
H-66	Thrust Increase--F.C. #1 . . . . .	343
H-67	Pitch Angle Response--F.C. #2 . . . . .	345
H-68	Perturbation Velocity Response--F.C. #2 . . . . .	345
H-69	Altitude Response--F.C. #2 . . . . .	346
H-70	Elevator Deflection--F.C. #2 . . . . .	346
H-71	Speed Brake Deflection--F.C. #2 . . . . .	347
H-72	Thrust Increase--F.C. #3 . . . . .	347

List of Tables

Table		Page
4-1	Elements for Design Equation at $\omega=0.1$ rad/sec . . . . .	47
4-2	Elements for Design Equation at $\omega=0.1$ rad/sec . . . . .	50
4-3	Elements for Design Equation at $\omega=1$ rad/sec . . . . .	61
5-1	Design Equation Elements for $\omega=0.1$ rad/sec . . . . .	76
6-1	Bank Angle Command--F.C. #3 . . . . .	100
6-2	Bank Angle Command--F.C. #3 . . . . .	103
6-3	Bank Angle Command--F.C. #3 . . . . .	106
6-4	Sideslip Command--F.C. #3 . . . . .	109
6-5	Sideslip Command--F.C. #3 . . . . .	112
6-6	Sideslip Command--F.C. #3 . . . . .	115
6-7	Pitch Angle Command--F.C. #3 . . . . .	120
6-8	Pitch Angle Command--F.C. #3 . . . . .	124
6-9	Pitch Angle Command--F.C. #2 (Control Surface Saturation) . . . . .	128
C-1	KC-135 Aircraft Data . . . . .	187
C-2	Nondimensional Stability Axes Derivatives for F.C. #1 . . . . .	188
C-3	Nondimensional Stability Axes Derivatives for F.C. #2 . . . . .	189
C-4	Nondimensional Stability Axes Derivatives for F.C. #3 . . . . .	190

Table	Page
C-5	Dimensional Input and Output Matrix Coefficients for F.C. #1 . . . . . 191
C-6	Dimensional Input and Output Matrix Coefficients for F.C. #2 . . . . . 193
C-7	Dimensional Input and Output Matrix Coefficients for F.C. #3 . . . . . 195
E-1	$b_{11}$ Time Domain Specifications . . . . . 212
E-2	Log Magnitude-- $b_{11}$ . . . . . 212
E-3	$a_{11}$ Time Domain Specifications . . . . . 213
E-4	Log Magnitude-- $a_{11}$ . . . . . 213
E-5	$b_{12}$ Time Domain Specifications . . . . . 214
E-6	Log Magnitude-- $b_{12}$ . . . . . 214
E-7	$b_{22}$ Time Domain Specifications . . . . . 216
E-8	Log Magnitude-- $b_{22}$ . . . . . 216
E-9	$a_{22}$ Time Domain Specifications . . . . . 217
E-10	Log Magnitude-- $a_{22}$ . . . . . 217
E-11	$b_{21}$ Time Domain Specifications . . . . . 218
E-12	Log Magnitude-- $b_{21}$ . . . . . 219
F-1	Magnitude (db) and Phase (Deg)-- $q_{11}$ . . . . . 225
F-2	Magnitude (db)-- $q_{12}$ . . . . . 226
F-3	Magnitude (db)-- $q_{13}$ . . . . . 227
F-4	Magnitude (db)-- $q_{21}$ . . . . . 228
F-5	Magnitude (db) and Phase (Deg)-- $q_{22}$ . . . . . 229
F-6	Magnitude (db) and Phase (Deg)-- $q_{22e}$ . . . . . 230
F-7	Magnitude (db)-- $q_{23}$ . . . . . 231
F-8	Magnitude (db)-- $q_{31}$ . . . . . 232

Table		Page
F-9	Magnitude (db)-- $q_{32}$ . . . . .	233
F-10	Magnitude (db) and Phase (Deg)-- $q_{33}$ . . . . .	234
F-11	Magnitude and Phase $q_{11}$ . . . . .	236
F-12	Magnitude (db)-- $q_{12}$ . . . . .	237
F-13	Magnitude (db)-- $q_{13}$ . . . . .	238
F-14	Magnitude (db)-- $q_{21}$ . . . . .	239
F-15	Magnitude (db) and Phase-- $q_{22}$ . . . . .	240
F-16	Magnitude (db)-- $q_{23}$ . . . . .	241
F-17	Magnitude (db)-- $q_{31}$ . . . . .	242
F-18	Magnitude (db)-- $q_{32}$ . . . . .	243
F-19	Magnitude (db) and Phase (Deg)-- $q_{33}$ . . . . .	244
F-20	Magnitude (db) and Phase (Deg)-- $q_{22e}$ . . . . .	245
F-21	$b_{22}$ Time Domain Specifications . . . . .	247
F-22	Log Magnitude-- $b_{22}$ . . . . .	248
F-23	$a_{22}$ Time Domain Specifications . . . . .	248
F-24	Log Magnitude-- $a_{22}$ . . . . .	249
F-25	$b_{12}$ Time Domain Specifications . . . . .	250
F-26	Log Magnitude-- $b_{12}$ . . . . .	250
F-27	$b_{32}$ Time Domain Specifications . . . . .	251
F-28	Log Magnitude-- $b_{32}$ . . . . .	251
H-1	Bank Angle Command--F.C. #1 . . . . .	296
H-2	Bank Angle Command--F.C. #1 . . . . .	299
H-3	Bank Angle Command--F.C. #1 . . . . .	302
H-4	Bank Angle Command--F.C. #2 . . . . .	305
H-5	Bank Angle Command--F.C. #2 . . . . .	308

Table	Page
H-6 Bank Angle Command--F.C. #2 . . . . .	311
H-7 Sideslip Command--F.C. #1 . . . . .	314
H-8 Sideslip Command--F.C. #1 . . . . .	317
H-9 Sideslip Command--F.C. #1 . . . . .	320
H-10 Sideslip Command--F.C. #2 . . . . .	323
H-11 Sideslip Command--F.C. #2 . . . . .	326
H-12 Sideslip Command--F.C. #2 . . . . .	329
H-13 Pitch Angle Command--F.C. #1 . . . . .	332
H-14 Pitch Angle Command--F.C. #1 . . . . .	336
H-15 Pitch Angle Command--F.C. #1 . . . . .	340
H-16 Pitch Angle Command--F.C. #2 . . . . .	344

### List of Symbols

AC	Aerodynamic center
$a_{ij}$	Model response bound--lower
$\alpha$	Angle of attack
$\alpha_0$	Trim angle of attack
b	Wing span
$b_{ij}$	Model response bound--upper
$\beta$	Sideslip angle
c	Mean aerodynamic cord
CG, cg	Center of gravity
$C_D$	Nondimensional coefficient of drag (along velocity vector)
$C_{D_\alpha}$	Nondimensional variation of drag with angle of attack
$C_{D_u}$	Nondimensional variation of drag with forward velocity perturbations from trim velocity
$C_L$	Nondimensional coefficient of lift (normal to velocity vector)
$C_{L_\alpha}$	Nondimensional variation of lift with angle of attack
$C_{L_\alpha}$	Nondimensional variation of lift with the rate of change of angle of attack
$C_{L_\delta}$	Nondimensional variation of lift with elevator ( $\delta_e$ ) or speed brakes ( $\delta_{sb}$ )
$C_{L_q}$	Nondimensional variation of lift with pitch rate
$C_{l_\beta}$	Nondimensional variation of rolling moment with sideslip angle

$C_{l\delta}$	Nondimensional variation of rolling moment with control wheel ( $\delta_w$ ) or rudder ( $\delta_r$ )
$C_{lp}$	Nondimensional variation of rolling moment with roll rate
$C_{lr}$	Nondimensional variation of rolling moment with yaw rate
$C_m$	Nondimensional variation of pitching moment
$C_{m\alpha}$	Nondimensional variation of pitching moment with angle of attack
$C_{m\delta}$	Nondimensional variation of pitching moment with elevator ( $\delta_e$ ) or speed brakes ( $\delta_{sb}$ )
$C_{mq}$	Nondimensional variation of pitching moment with pitch rate
$C_{mu}$	Nondimensional variation of pitching moment with forward velocity perturbations
$C_{n\beta}$	Nondimensional variation of yawing moment with sideslip angle
$C_{n\delta}$	Nondimensional variation of yawing moment with control wheel ( $\delta_w$ ) or rudder ( $\delta_r$ )
$C_{np}$	Nondimensional variation of yawing moment with roll rate
$C_{nr}$	Nondimensional variation of yawing moment with yaw rate
cos	Cosine
$C_{x\alpha}$	Nondimensional variation of x-force with angle of attack
$C_{x\delta}$	Nondimensional variation of x-force with elevator ( $\delta_e$ ) or speed brakes ( $\delta_{sb}$ )
$C_{xq}$	Nondimensional variation of x-force with pitch rate
$C_{xu}$	Nondimensional variation of x-force with forward velocity perturbations
$C_{y\beta}$	Nondimensional variation of y-force with sideslip angle



$C_{Y\delta}$	Nondimensional variation of y-force with control wheel ( $\delta_w$ ) or rudder ( $\delta_r$ )
$C_{Yp}$	Nondimensional variation of y-force with roll rate
$C_{Yr}$	Nondimensional variation of y-force with yaw rate
$C_{Z\alpha}$	Nondimensional variation of z-force with angle of attack
$C_{Z\dot{\alpha}}$	Nondimensional variation of z-force with the rate of change of angle of attack
$C_{Z\delta}$	Nondimensional variation of z-force with elevator ( $\delta_e$ ) or speed brakes ( $\delta_{sb}$ )
$C_{Zq}$	Nondimensional variation of z-force with pitch rate
$C_{Zu}$	Nondimensional variation of z-force with forward velocity perturbation
Deg	Degree
$d_{ij}$	Effective disturbance
$\delta$	Plant input vector
$\delta_w$	Control wheel deflection
$\delta_e$	Elevator deflection
$\delta_{sb}$	Speed brake deflection
$\delta_T$	Percent engine thrust, change from trim
$e$	Body bending displacement
$F$	Pre-filter in single loop design
$\underline{F}$	Pre-filter matrix
$f_{ij}$	Element of $\underline{F}$
ft	Feet
$g$	Gravity
$G$	Primary compensator element in single loop design

$\underline{G}$	Compensator matrix
$g_i$	Element of diagonal $\underline{G}$
$h$	Altitude
$I_{xx}$	Moment of inertia about x-axis
$I_{yy}$	Moment of inertia about y-axis
$I_{zz}$	Moment of inertia about z-axis
$I_{xz}$	Product of inertia about xz-axis
$L$	Control loop transmission ( $L = GP$ )
$L_o$	Nominal loop transmission
$L$	Rolling moment
lbs	Pounds
$L_\beta$	Dimensional variation of rolling moment with sideslip angle
$L_\delta$	Dimensional variation of rolling moment with control wheel ( $\delta_w$ ) or rudder ( $\delta_r$ )
$L_p$	Dimensional variation of rolling moment with roll rate
$L_r$	Dimensional variation of rolling moment with yaw rate
$m$	Aircraft mass
MAC	Mean Aerodynamic Cord
$M_\alpha$	Dimensional variation of pitching moment with angle of attack
$M_\dot{\alpha}$	Dimensional variation of pitching moment with the rate of change of angle of attack
$M_q$	Dimensional variation of pitching moment with pitch rate
$M_x$	Moment about the x-axis
$M_y$	Moment about the y-axis

$M_z$	Moment about the z-axis
$N$	Yawing moment
$N_\beta$	Dimensional variation of yawing moment with sideslip angle
$N_\delta$	Dimensional variation of yawing moment with control wheel ( $\delta_w$ ) or rudder ( $\delta_r$ )
$N_r$	Dimensional variation of yawing moment with yaw rate
$N_p$	Dimensional variation of yawing moment with roll rate
$P$	Plant transfer function
$P_o$	Nominal plant transfer function
$\underline{P}$	Plant matrix of system transfer function
$P_{ij}$	Element of $\underline{P}$
$p$	Roll rate
$\underline{Q}'$	Inverse of plant matrix $(P)^{-1}$
$q'_{ij}$	Element of $\underline{Q}'$
$q_{ij}$	$(1/(q'_{ij}))$
$q_{ij0}$	Nominal $q_{ij}$
$q$	Pitch rate
$q$	Dynamic pressure
$r$	Yaw rate
rad	Radians
$S$	Surface area
$s$	Laplace operator ( $s=j\omega$ )
sec	Seconds
sin	Sine

T	Compensated system transfer function
$T_R$	Command response transfer function
$T_D$	Disturbance response transfer function
U	Velocity in x-direction
$U_0$	Equilibrium x-axis velocity
u	Perturbation velocity along x-axis
V	Velocity along y-axis
v	Perturbation velocity along y-axis
$V_0$	Equilibrium y-axis velocity
$W_0$	Equilibrium z-axis velocity
w	Aircraft weight
w	Perturbation velocity along z-axis
X	Force in x-direction
$X_\alpha$	Dimensional variation of x-force with angle of attack
$\dot{X}_\alpha$	Dimensional variation of x-force with rate of change of angle of attack
$X_\delta$	Dimensional variation of x-force with elevator ( $\delta_e$ ) or speed brakes ( $\delta_{sb}$ )
$X_q$	Dimensional variation of x-force with pitch rate
$X_u$	Dimensional variation of x-force with forward velocity perturbation
Y	Force in y-direction
$Y_\beta$	Dimensional variation of y-force with sideslip angle
$Y_\delta$	Dimensional variation of y-force with control wheel ( $\delta_w$ ) or rudder ( $\delta_r$ )
$Y_p$	Dimensional variation of y-force with roll rate
$Y_r$	Dimensional variation of y-force with yaw rate

$Z$	Force in z-direction
$Z_{\alpha}$	Dimensional variation of z-force with angle of attack
$Z_{\dot{\alpha}}$	Dimensional variation of z-force with rate of change of angle of attack
$Z_{\delta}$	Dimensional variation of z-force with the elevator ( $\delta_e$ ) or speed brakes ( $\delta_{sb}$ )
$Z_q$	Dimensional variation of z-force with pitch rate
$Z_u$	Dimensional variation of z-force with forward velocity perturbation
$\theta$	Pitch angle
$\theta_0$	Equilibrium pitch angle
$\phi$	Roll angle
$\psi$	Yaw angle
$\gamma$	Ratio of effective plant transfer functions
$\omega$	Unit of frequency (rad/sec)

Abstract

A multiple input-multiple output flight control design on the KC-135 aircraft is completed using the Quantitative Feedback Theory (QFT) developed by Dr. Isaac Horowitz, Weizmann Institute of Science, Rehovot, Israel.

First, the three degrees-of-freedom model for the lateral mode is reduced to a two degrees-of-freedom model. From this model a robust controller is developed to perform two maneuvers over a wide range of the aircraft flight envelope.

Second, the three degrees-of-freedom model for the longitudinal mode is used to develop a robust controller to perform one maneuver. The first and second body bending modes are then added to remove the rigid body constraint and a robust control is developed for the non-rigid aircraft.

Finally, the robust controllers developed for the lateral and longitudinal modes are simulated over a large range of the aircraft's flight envelope.

The conclusion drawn from the research is that the methods developed by Dr. Horowitz are very effective in designing multiple input-multiple output systems with plant uncertainty.

DESIGN OF ROBUST CONTROLLERS FOR A MULTIPLE INPUT-MULTIPLE  
OUTPUT CONTROL SYSTEM WITH UNCERTAIN PARAMETERS  
APPLICATION TO THE LATERAL AND LONGITUDINAL  
MODES OF THE KC-135 TRANSPORT AIRCRAFT

I. Introduction

An aircraft in flight is a nonlinear, multiple input-multiple output (MIMO) control system. New design techniques have been developed which give the design engineer more insight into the design of such MIMO systems. Two such design techniques, the Dr. Brian Porter technique and the Dr. Isaac Horowitz technique, have been demonstrated to be effective means of designing these MIMO systems.

Two designs have been demonstrated using the KC-135 transport aircraft as a model (3; 17), one using the Porter approach and the other the Horowitz approach. Both design methods have proven to be effective methods for the design of robust controllers for MIMO systems. The Horowitz design approach (3) included one flight maneuver in the lateral mode which included two inputs and two outputs. Since there was only one command input, the design considered only one column of the set of equivalent SISO systems.

The Porter design approach (7) demonstrated a design of a 2x2 system in the lateral mode. A robust controller was developed to perform two maneuvers over the entire flight envelope of the KC-135 aircraft. A controller was also developed for a 3x3 system in the longitudinal mode. However, only one maneuver was demonstrated and a robust controller could not be found that would operate over the entire flight envelope. Three controllers were developed, one for each flight condition.

This thesis is an extension of the work completed on the KC-135 aircraft using the Horowitz design approach (3). The design is for similar maneuvers as demonstrated by the Porter technique (17).

#### I-1 Problem

The problem is to design lateral and longitudinal robust controllers for the KC-135 transport aircraft. Thus the purpose of this research is to apply the Quantitative Feedback Theory (QFT) design technique developed by Dr. Isaac Horowitz to design two robust controllers for this aircraft. The first design develops a robust controller to handle two maneuvers in the lateral mode. This system includes two inputs and two outputs. The second design develops a robust controller to handle one maneuver in the longitudinal mode. This design includes three inputs and three outputs. Both controllers are designed to operate over the entire flight envelope of the aircraft.



I-2      Scope

This study examines both a longitudinal and lateral flight control design for the KC-135 transport.

The lateral robust control design includes:

1. coordinated turn, and
2. sideslip maneuver.

The longitudinal robust design is a pitch pointing maneuver. This design includes the first and second body bending modes while the lateral design considers the aircraft as a rigid body. The above designs are for the following flight conditions (F.C):

F.C. #1: High altitude cruise (45,500 ft at mach 0.77)

F.C. #2: Medium altitude cruise (28,500 ft at mach 0.77)

F.C. #3: Approach (sea level at mach 0.21)

The resulting design is compared against compensator bandwidth for each flight condition. A qualitative comparison is also completed between this design and the design completed by Captain Locken using the Porter design technique (17).

I-3      Assumptions

The following assumptions are used to simplify the design process (4:21):

1. The aircraft is a rigid body (lateral mode only).

2. Flat, non-rotating earth inertial reference frame.
3. Mass of the aircraft remains constant during any particular dynamic analysis.
4. Aircraft is always considered to be in equilibrium before a disturbance is introduced.
5. The perturbations from equilibrium are small.
6. Quasi-steady airflow.

The resulting design is analyzed with aid of a computer-aided design program. It is assumed that these simulations or analyses will provide realistic responses of the aircraft motion during each flight maneuver.

#### I-4 Approach

The first step in the approach to this design is to develop the required lateral equations of motion for the aircraft, thus developing the required matrix equations for the three F.C.'s which are to be used for the lateral control design.

The second step is to develop the longitudinal equations of motion for the aircraft, thus developing the required matrix equations for the three F.C.'s which are to be used for the longitudinal control design.

The third step is to derive a frequency domain representation of the desired specifications for each of the lateral and longitudinal control designs. These specifications are obtained from the design using the Porter technique (17).

The fourth is to apply the Horowitz design technique to the resulting aircraft matrices. The lateral and longitudinal robust controllers are thus designed to the required specifications obtained in step three.

The fifth step is to simulate the design on a computer-aided design program. The aircraft responses are plotted for different control inputs for each of the three flight conditions.

The last step is to compare the design in terms of compensator bandwidth against each of the Quantitative Feedback Technique designs, one for each maneuver. A qualitative comparison is made between the Horowitz design approach and the Porter design approach using the work completed by Captain Locken (17) and this design.

#### I-5 Presentation

This thesis is contained in seven chapters. Chapter II contains an overview of the SISO and MIMO design technique with an in-depth look at the 3x3 design philosophy. Chapter III describes the basic KC-135 aircraft and the derived aircraft equations of motion for both the lateral and longitudinal modes. Chapter IV covers the design of the robust lateral controller for a 2x2 system. Chapter V outlines the design of the robust longitudinal controller for a 3x3 system. Chapter VI shows the simulation of the robust controllers designed in the preceding

two chapters. Chapter VII draws conclusions from this study and outlines recommendations for future study in this area.

## II. Quantitative Feedback Design Theory

### II-1 Introduction

This chapter contains a basic overview of the SISO and MIMO system designs with emphasis placed on a 3x3 system. The SISO system design philosophy is outlined in detail in Appendix A and the MIMO (2x2) system design is outlined in Appendix B. Thus the emphasis in this chapter is placed on the 3x3 design using Dr. Horowitz's technique. Also the improved technique is discussed.

### II-2 SISO Design Theory

This section is a brief overview of the design philosophy for the SISO system. The reader is referred to Appendix A for a more detailed analysis of the design approach.

The SISO design approach assumes that there are two degrees-of-freedom (i.e., the input and output are readily accessible and measurable quantities). Thus the problem is defined such that there are two elements,  $F$  and  $G$ , which are designed to enable the system or plant to be controlled for a given input and desired output. The plant, compensator  $G$ , and pre-filter  $F$  are also assumed to be Laplace transfer functions.

Once the problem is defined, the time domain design specifications, which describe the upper and lower limits of the closed loop system for an acceptable response to a desired input or disturbance, are transformed into the frequency domain. These specifications generate an upper and lower bound on the acceptable responses for a desired input. The last bound required for the SISO design is the maximum allowable response of the system to a disturbance input. This specification is normally defined in the time domain and thus it must also be transformed to the frequency domain. There is only a maximum or upper bound on the disturbance response since the only concern in the design is that the response be below a certain maximum allowable value.

Once the problem is defined and the specifications are transformed to the frequency domain, the actual design can now be completed. One of the most important tools in the design is the Nichols Chart. The uncertainty in the plant is plotted on the Nichols Chart for a given frequency which generates a template of the uncertainty in the plant at that particular frequency. This is done over a desired range of frequencies, and the resulting templates are then used in the design of the nominal loop transmission  $L_o$ , which is defined as the open loop transfer function ( $GP_o$ ), for the nominal plant. This nominal loop transfer function is derived from the use of these templates (plant

uncertainty) and the upper and lower bound specifications on the acceptable responses for a desired input. In designing the nominal loop transmission, a Universal High Frequency (UHF) is defined which ensures that the loop transmission  $L$  has a positive phase and gain margin.

Once the nominal loop transmission is designed, then the compensator,  $G$ , can be obtained directly from the nominal loop transmission function (i.e.,  $L_0 = GP_0$ ). The last part of the design process is to synthesize the pre-filter  $F$ , which positions the desired response within the frequency domain specifications.

The above is a brief description of the SISO design approach and is not meant to be a comprehensive outline of the design approach. For a complete understanding of the design technique refer to Appendix A.

### II-3 MIMO Design Theory (2x2 System)

The MIMO design is accomplished using the SISO design approach. For a SISO system there is one loop to be designed which enables the system to track a desired input and to reject any unwanted disturbance input. For a 2x2 system, there are two loops which have to be designed. Thus as the size of the system increases, the number of loops increases by a factor of  $n$ , where  $n$  is the size of the system (i.e., the number of inputs-outputs). This appears to be a limiting factor to the size of the system which can be designed using this technique. However, this

is not the case as there are many methods for reducing the complexity of the system required in the design process (to be discussed later in this chapter). For a complete outline of a 2x2 MIMO design refer to Appendix B.

#### II-4 MIMO Design Theory (3x3 System)

This section is devoted to a 3x3 MIMO system structure with extension to a general nxn system. Several methods are discussed of ways to reduce the complexity required in the design process. Finally, a discussion of the improved design technique is highlighted.

##### Control Structure

The system structure is similar to that of the 2x2 system (Appendix A). The basic structure is shown in Figure 2-1 where P is the uncertainty plant matrix, G is the compensator matrix, and F is the pre-filter matrix. The purpose of G and F is identical to those of the SISO system. Figure 2-2 shows the 3x3 MIMO structure with G being diagonal. The general form of the aircraft equations of motion, for a 3x3 MIMO system, are of the form:

$$\begin{aligned} (aS + b)Y_1 + (cS + d)Y_2 + (eS + f)Y_3 \\ = gU_1 + hU_2 + iU_3 \end{aligned} \quad (2-1)$$

$$\begin{aligned} (jS + k)Y_1 + (lS + m)Y_2 + (nS + o)Y_3 \\ = pU_1 + qU_2 + rU_3 \end{aligned} \quad (2-2)$$



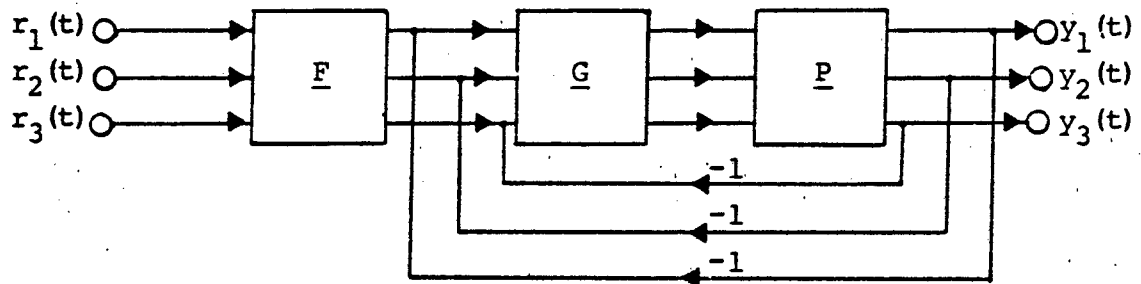


Fig. 2-1. The 3x3 Multiple Input-Multiple Output Feedback Structure

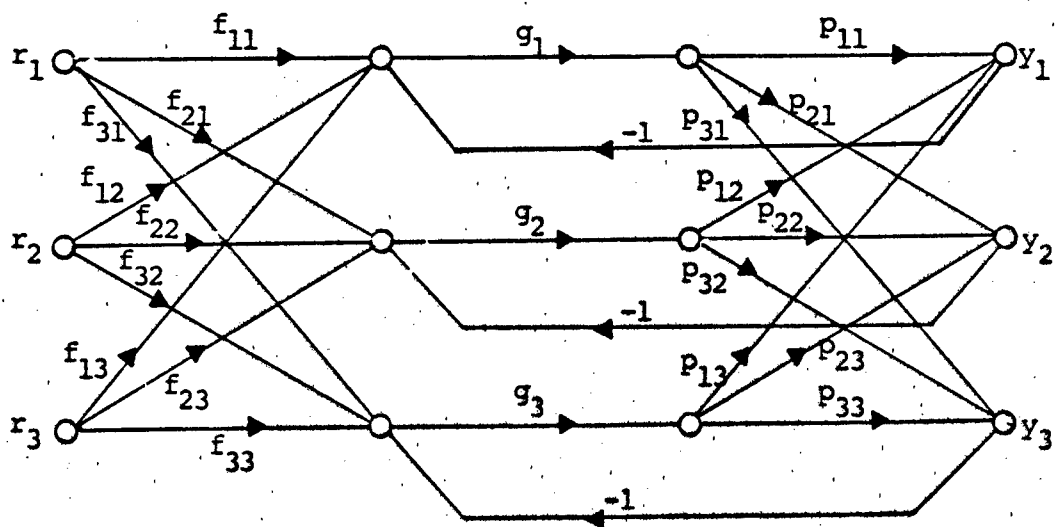


Fig. 2-2. The Complete Three-by-Three MIMO Structure with Diagonal G

$$\begin{aligned}
 (tS + v)Y_1 + (wS + x)Y_2 + (aS + b)Y_3 \\
 = ccU_1 + ddU_2 + eeU_3
 \end{aligned}
 \tag{2-3}$$

Where a through ee are constant coefficients. Equations (2-1) through (2-3) can be written in matrix notation as:

$$\begin{bmatrix} aS + b & cS + d & eS + f \\ jS + k & lS + m & nS + o \\ tS + v & wS + x & aaS + bb \end{bmatrix} \begin{bmatrix} Y_1 \\ Y_2 \\ Y_3 \end{bmatrix} = \begin{bmatrix} g & h & i \\ p & q & r \\ cc & dd & ee \end{bmatrix} \begin{bmatrix} U_1 \\ U_2 \\ U_3 \end{bmatrix}$$

(2-4)

Equation (2-4) is of the form:

$$\underline{M}\underline{y} = \underline{N}\underline{u}$$

(2-5)

where the output matrix M multiplies the output vector y and the input matrix N multiplies the input vector u.

Equation (2-5) is manipulated to

$$\underline{y} = \underline{M}^{-1}\underline{N}\underline{u}$$

(2-6)

where  $\underline{P} = \underline{M}^{-1}\underline{N}$  (2-7)

is defined as the plant matrix. Thus equation (2-6) becomes

$$\underline{y} = \underline{P}\underline{u}$$

(2-8)

The remaining elements of the 3x3 MIMO system can be represented in matrix form as:

$$F = \begin{bmatrix} f_{11} & f_{12} & f_{13} \\ f_{21} & f_{22} & f_{23} \\ f_{31} & f_{32} & f_{33} \end{bmatrix}; \quad G = \begin{bmatrix} g_1 & 0 & 0 \\ 0 & g_2 & 0 \\ 0 & 0 & g_3 \end{bmatrix} \quad (2-9)$$

In this thesis G is treated as a diagonal matrix but G can be a full matrix which gives the designer more flexibility in the design technique.

#### Constraints on the Plant Matrix

There are two constraints on the P matrix which must be satisfied. These constraints are:

1. The plant matrix P must be invertible. That is,  $P^{-1}$  must exist (i.e., P must not be singular).
2. As  $S \rightarrow \infty$

$$\begin{aligned} & |P_{11}P_{22}P_{33}| > |P_{11}P_{23}P_{21}| + |P_{12}P_{21}P_{33}| \\ & + |P_{12}P_{23}P_{31}| + |P_{13}P_{22}P_{31}| + |P_{13}P_{21}P_{32}| \end{aligned}$$

for all possible plants (10).

The first constraint ensures that the plant is controllable. If constraint 2 is not satisfied, then the original order of the input and output matrices may be changed to ensure that this constraint is met. It is to be noted that constraint 2 is not required for the improved design method. The only requirement is that the diagonal terms do not change sign as  $S \rightarrow \infty$  (i.e.,  $q_{11}$ ,  $q_{22}$ , through  $q_{ij}$  where  $i=j$ ).

### Effective SISO Loops

First define a matrix  $Q' = P^{-1}$  having elements  $q'_{ij}$  and a matrix  $Q = [q_{ij}]$  where  $q_{ij} = 1/q'_{ij}$ . Thus  $q_{ij}$  are the  $n^2$  effective transfer functions that are needed for the QFT technique. Using the above transformation the 3x3 system is now treated as  $n^2$  (nine) SISO problems (10). Figure 2-3 shows the resulting nine effective SISO loops. Note that the first subscript on  $d_{ij}$ ,  $f_{ij}$  and  $y_{ij}$  refers to the  $i$ th input and the second subscript to the  $j$ th output. Since  $q_{ij} = 1/q'_{ij}$ , therefore  $Q$  can be represented in matrix form as

$$Q = \begin{bmatrix} q_{11} & q_{12} & q_{13} \\ q_{21} & q_{22} & q_{23} \\ q_{31} & q_{32} & q_{33} \end{bmatrix} \quad (2-10)$$

Using Figure 2-3 the input/output relationship is defined as:

$$t_{ij} = y_{ij}/r_{ij} \quad (2-11)$$

where  $r_{ij} = 1$

Therefore the final equations for the nine SISO effective loops are:

$$T_{11} = \frac{f_{11}g_1q_{11}}{1 + g_1q_{11}} + \frac{q_{11}d_{11}}{1 + g_1q_{11}} \quad (2-12)$$

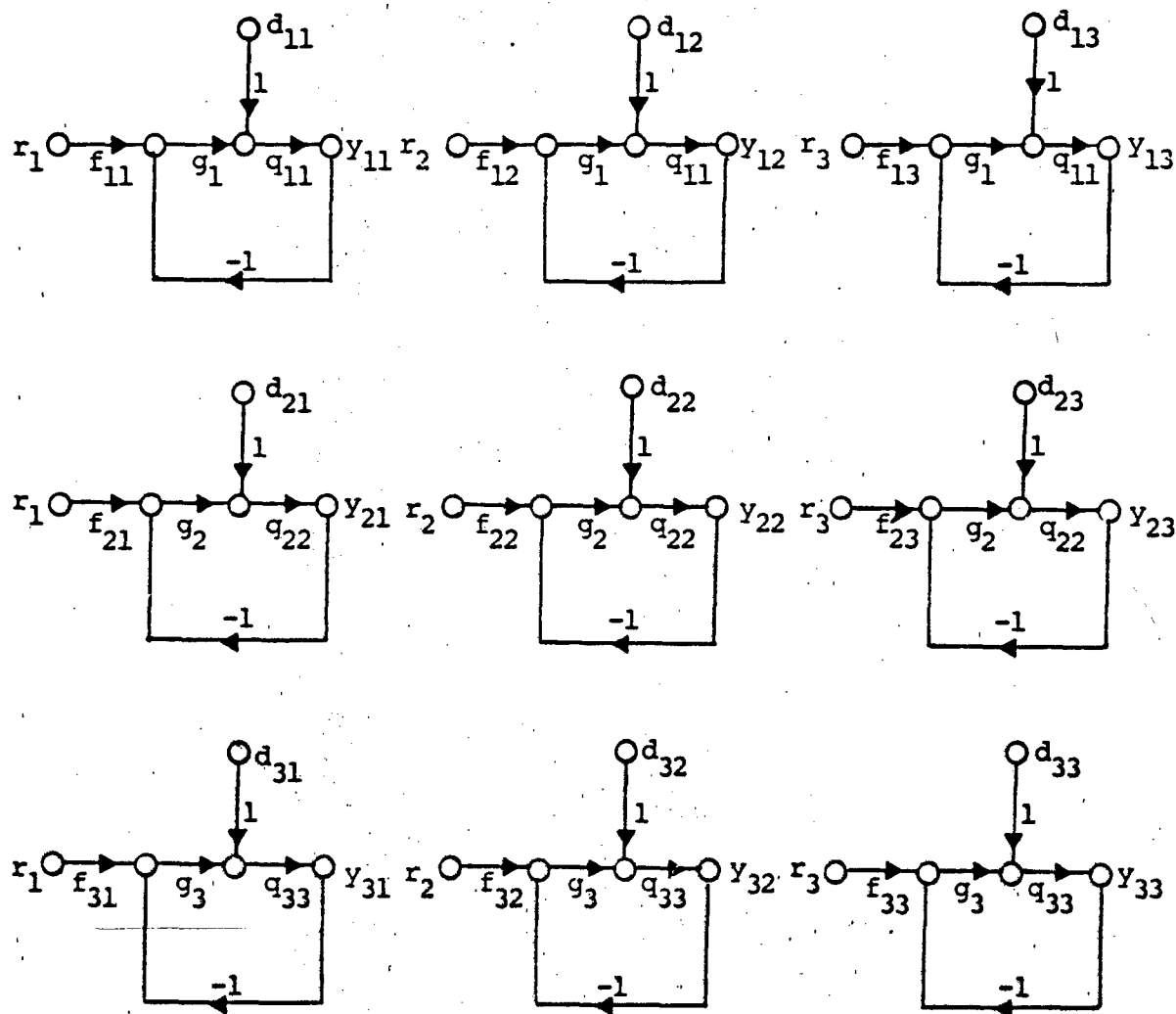


Fig. 2-3. The Final Equivalent Single Loop Feedback Structure which Replaces the 3x3 MIMO Problem

$$t_{12} = \frac{f_{12}g_1q_{11}}{1 + g_1q_{11}} + \frac{q_{11}d_{12}}{1 + g_1q_{11}} \quad (2-12a)$$

$$t_{13} = \frac{f_{13}g_1q_{11}}{1 + g_1q_{11}} + \frac{q_{11}d_{13}}{1 + g_1q_{11}} \quad (2-12b)$$

$$t_{21} = \frac{f_{21}g_2q_{22}}{1 + g_2q_{22}} + \frac{q_{22}d_{21}}{1 + g_2q_{22}} \quad (2-12c)$$

$$t_{22} = \frac{f_{22}g_2q_{22}}{1 + g_2q_{22}} + \frac{q_{22}d_{22}}{1 + g_2q_{22}} \quad (2-12d)$$

$$t_{23} = \frac{f_{23}g_2q_{22}}{1 + g_2q_{22}} + \frac{q_{22}d_{23}}{1 + g_2q_{22}} \quad (2-12e)$$

$$t_{31} = \frac{f_{31}g_3q_{33}}{1 + g_3q_{33}} + \frac{q_{33}d_{31}}{1 + g_3q_{33}} \quad (2-12f)$$

$$t_{32} = \frac{f_{32}g_3q_{33}}{1 + g_3q_{33}} + \frac{q_{33}d_{32}}{1 + g_3q_{33}} \quad (2-12g)$$

$$t_{33} = \frac{f_{33}g_3q_{33}}{1 + g_3q_{33}} + \frac{q_{33}d_{33}}{1 + g_3q_{33}} \quad (2-12h)$$

where:

$$d_{11} = - [t_{21}/q_{12} + t_{31}/q_{13}] \quad (2-13)$$

$$d_{12} = - [t_{22}/q_{12} + t_{32}/q_{13}] \quad (2-13a)$$

$$d_{13} = - [t_{23}/q_{12} + t_{33}/q_{13}] \quad (2-13b)$$

$$d_{21} = - [t_{11}/q_{21} + t_{31}/q_{23}] \quad (2-13c)$$

$$d_{22} = - [t_{12}/q_{21} + t_{32}/q_{23}] \quad (2-13d)$$

$$d_{23} = - [t_{13}/q_{21} + t_{33}/q_{23}] \quad (2-13e)$$

$$d_{31} = - [t_{11}/q_{31} + t_{21}/q_{32}] \quad (2-13f)$$

$$d_{32} = - [t_{12}/q_{31} + t_{22}/q_{32}] \quad (2-13g)$$

$$d_{33} = - [t_{13}/q_{31} + t_{33}/q_{32}] \quad (2-13h)$$

Finally, the above equations can be written in a general form for any  $n^2$  equivalent single loop feedback structure (10:680). Thus in general form:

$$t_{ij} = \frac{f_{ij}g_iq_{ii} + d_{ij}q_{ii}}{1 + g_iq_{ii}} \quad (2-14)$$

where:  $d_{ij} = - \sum_k T_{kj}/q_{ik}$  and  $k \neq j$

Equation (2-14) can be expressed as

$$t_{ij} = \frac{f_{ij}L_i + d_{ij}q_{ii}}{1 + L_i} \quad (2-15)$$

where  $L_i = g_iq_{ii}$

### Simplification of the Single-Loop Structure

The single-loop structure in Figure 2-3 has two components, one due to the input  $r_i$  (assume  $r_i=1$ ) and one due to the disturbance input  $d_{ij}$ . Therefore, the control ratio  $t_{ij}$  is the sum of control ratios each involving the  $j$ th input and can be written:

$$t_{ij} = \tau_{ij} + \tau_{d_{ij}} \quad (2-16)$$

where

$$\tau_{ij} = \frac{f_{ij}L_i}{1 + L_i}; \quad \tau_{d_{ij}} = \frac{d_{ij}q_{ii}}{1 + L_i} \quad (2-17)$$

For a fixed  $P$  which is an element of the universal set  $p$ ,  $|t_{ij}|_{\max}$  occurs at

$$|d_{ij}|_{\max} = \sum_{k \neq i} |t_{kj}/q_{ik}|_{\max} \quad (2-18)$$

Since the relative phases of  $T_{kj}/q_{ik}$  are not known, the design process must use the extreme cases:

$$\sum_{k \neq i} \frac{|t_{kj}|_{\max}}{|q_{ik}|} = \sum_{k \neq i} \frac{|b_{ij}|}{|q_{ik}|} \triangleq d_{ij} \quad (2-19)$$

The term  $b_{kj}$  is the control ratio that represents the maximum allowable magnitude of the output due to the disturbance input which is one of the required design specifications.



### Performance Tolerances

The performance tolerances are divided into two separate portions. One set of tolerances for the interacting loop (tracking loop) and a second tolerance for the Basically Non-Interacting (BNIC) loop (Appendix A). Thus, for the BNIC loop it is necessary that:

$$\begin{aligned} \left| \tau_{ij}(j\omega) + \tau_{d_{ij}}(j\omega) \right|_{\max} &\leq \left| \tau_{ij} \right|_{\max} + \left| \tau_{d_{ij}} \right|_{\max} \\ &= \left| \tau_{d_{ij}} \right|_{\max} \leq b_{ij}(\omega) \end{aligned} \quad (2-20)$$

The above equation can be justified since the relative phase of the two terms ( $\tau_{ij}(j\omega)$  and  $\tau_{d_{ij}}(j\omega)$ ) are not known. Then  $\tau_{ij}(j\omega)$  can be forced to zero by simply selecting  $f_{ij}$ , for  $i=j$ , to be zero.  $b_{ij}(j\omega)$  is the upper bounds for the design specification on the disturbance rejection (10:681). The performance tolerance for the interacting loop is:

$$a_{ij}(\omega) \leq \left| \tau_{ij}(j\omega) + \tau_{d_{ij}}(j\omega) \right| \leq b_{ij}(\omega) \quad (2-21)$$

where  $a_{ij}$  and  $b_{ij}$  are the upper and lower bounds of the design specifications for the interacting loop. Applying the above tolerances to the BNIC loop results in the following inequality:

$$\left| \tau_{ij} \right| = \frac{|q_{ij}| |d_{ij}|}{|1 + L_i|} \leq |b_{ij}| \quad (2-22)$$

where for the 3x3 system

$$|d_{ij}| = |b_{kj}/q_{jk} + b_{ki}/q_{ik}| \quad k \neq i$$

Rearranging Equation (2-22) yields the following inequality:

$$|1 + L_i| \geq \frac{|b_{kj}/q_{jk} + b_{ki}/q_{ik}|}{|b_{ij}|} \times |q_{ii}| \quad (2-23)$$

Equation (2-23) is used in the design of all BNIC loops, which generates the required bounds on the loop transmission for a disturbance input.

The interacting loop tolerance generates the following conditions which must be satisfied in the design:

$$\tau_{ij} = \frac{f_{ij}L_i}{1+L_i} \quad ; \quad \tau_{d_{ij}} = \frac{d_{ij}q_{ii}}{1+L_i} \quad (2-24)$$

where the bounds on  $\tau_{d_{ij}}$  are found exactly as outlined above and the bounds on  $\tau_{ij}$  are determined using the plant uncertainty (templates) and the given tolerances  $a_{ij}$  and  $b_{ij}$  on the interacting loop. It must be noted that the tolerances given by  $a_{ij}$  and  $b_{ij}$  are for the bounds on the entire interacting loop. Therefore, the tolerances must be divided between the interacting and BNIC cases. If one of the equations of Equation (2-24) is much more dominant than the other, then the entire bounds can be dedicated to that particular portion. The designer is

cautioned that if one of  $\tau_{ij}$  or  $\tau_{d_{ij}}$  dominates, it must be verified over the entire frequency range of interest.

Improved Design Technique

The improved technique reduces the inherent over-design. The unimproved technique does not exploit the correlation between the  $t_{ij}$  of the system. With the improved technique this correlation between the  $t_{ij}$ 's is taken into account for the second and subsequent loop design. This technique is highlighted using a 3x3 MIMO system as an example.

Assume that loop one is the first loop to be designed. Therefore the general equation for these three SISO problems is obtained from Equation (2-14) (9:977-988) and is given as:

$$t_{1j} = \frac{f_{ij}L_1 + d_{1j}q_{11}}{1 + L_1} \quad j = 1, 2, 3 \quad (2-25)$$

and  $L_1 = g_1 q_{11}$  ;  $d_{1j} = \sum_{k \neq i}^3 t_{ij} / q_{1k}$

Using Equation (2-25) the element  $L_1$  and  $f_{ij}$  are designed such that  $t_{ij}$ 's are stable and meet the desired tolerances or specifications. With loop one design completed, the second loop design can now be accomplished. The general equations for loop two are obtained using Equation (2-14). The resulting equation is:

$$t_{2j} = \frac{f_{2j}L_2 + d_{2j}q_{22}}{1 + L_2} \quad (2-26)$$

$$d_{2j} = \sum_{k \neq i}^3 t_{2j}/q_{2k} \quad j = 1, 2, 3$$

By solving for  $t_{ij}$  in Equation (2-25) and substituting these into Equation (2-26) it can be shown (9) that

$$t_{2j} = \frac{f_{2j}L_{2e} + d_{2e}}{1 + L_{2e}} \quad (2-27)$$

where  $L_{2e} = \frac{q_{22}q_{22}}{1 - \gamma_{12}/(1+L_1)}$  (2-27a)

$$\gamma_{12} = \frac{q_{11}q_{22}}{q_{12}q_{21}} \quad (2-27b)$$

$$q_{22e} = \frac{q_{22}(1 + L_1)}{(1 + L_1) - \gamma_{12}} \quad (2-27c)$$

$$d_{2j} = \frac{L_{2e}}{q_2} \left[ t_{3j} \left( \frac{q_{11}}{q_{21}q_{13}(1 + L_1)} \right) - \frac{f_{1j}L_1}{q_{21}(1 + L_1)} \right] \quad (2-27d)$$

Using equations (2-27a) through (2-27d) the elements  $L_{2e}$  and  $f_{2j}$  can be designed to meet the desired tolerances since  $L_1$  and  $f_{1j}$  are known from the first loop design.

The final loop is accomplished in a similar manner as the second loop design. The resulting equations are:

$$t_{3j} = \frac{f_{3j}L_{3e} + d_{3e}}{(1 + L_{3e})} \quad (2-28a)$$

$$L_{3e} = \frac{L_3 \epsilon}{\epsilon - \Lambda} \quad (2-28b)$$

$$L_{3e} = q_{33e} g_3 \quad (2-28c)$$

$$q_{33e} = \frac{q_{33} \epsilon}{\epsilon - \Lambda} \quad (2-28d)$$

$$\Lambda = \gamma_{23}(1 + L_1) + \gamma_{13}(1 + L_2) - (\gamma_{12}u_1 + \gamma_{13}u_2) \quad (2-28e)$$

$$\epsilon = (1 + L_1)(1 + L_2) - \gamma_{12} \quad (2-28f)$$

$$u_1 = \frac{q_{21}q_{33}}{q_{23}q_{31}} ; \quad u_2 = \frac{q_{31}q_{22}}{q_{32}q_{21}} \quad (2-28g)$$

$$\gamma_{12} = \frac{q_{11}q_{22}}{q_{12}q_{21}} ; \quad \gamma_{23} = \frac{q_{22}q_{33}}{q_{23}q_{32}} \quad (2-28h)$$

$$\gamma_{13} = \frac{q_{11}q_{33}}{q_{13}q_{31}} \quad (2-28i)$$

$$d_{3i} = \frac{f_{1i}L_1q_{33}n_1 + f_{2i}L_2q_{33}n_2}{\epsilon - \Lambda} \quad (2-28j)$$

$$n_1 = \frac{q_{22}}{q_{21}q_{31}} - (1 + L_2)/q_{31} \quad (2-28k)$$

$$n_2 = \frac{q_{11}}{q_{12}q_{31}} - (1 + L_1)/q_{32} \quad (2-28L)$$

In Equations (2-28a) through (2-28L)  $L_1$ ,  $L_2$ ,  $f_{1j}$ ,  $f_{2j}$ , are all known; therefore, the only unknowns are  $f_{3i}$  and  $g_3$ . These now constitute single-loop uncertainty problems and can be designed using the methods outlined in Appendix A. The required elements are designed to the desired tolerances or specifications. This completes the improved 3x3 MIMO design technique. If all loops are designed to meet the given tolerances, then the desired response from the MIMO system is guaranteed.

#### Equilibrium and Tradeoffs

Equilibrium exists when it is impossible to reduce the burden on any  $L_i$ , without increasing it on some other  $L_j$  (10:683). This simply states that some of the design tolerances may be decreased or increased for certain loops without making it more difficult on other loops. This results in only one column of the equivalent SISO systems being dominant. However, after equilibrium is reached, it may be desirable to sacrifice one loop for the sake of

another. This involves "tradeoffs" between the different loops. It should be noted that these tradeoffs, when used, always make it harder on one loop when reduction is accomplished in another.

#### II-5 Summary

This chapter describes the design technique used in the design of single input-single output and multiple input-multiple output systems. First, the SISO system technique is outlined and, second, the technique is expanded to the MIMO system. Finally, the guidelines for reducing the MIMO system to a simple SISO system problem is illustrated with a 3x3 design overview with extension to any general  $n^2$  MIMO system.

### III. Aircraft Model

#### III-1 Introduction

The model used in this thesis is the KC-135 transport aircraft. A linear three degree-of-freedom model is generated for both the lateral and longitudinal modes for each of the three selected flight conditions (F.C.). These conditions are selected to represent the aircraft over a wide range of performance which represent the uncertainty in the plant parameters. This uncertainty is the variation in the aircraft stability derivatives between the respective F.C.'s. One robust controller is designed to operate over a wide range of the aircraft flight envelope which is represented by the given F.C.'s. The conditions selected for this design are a high altitude, high speed cruise at 45,500 feet and Mach 0.77 (745 ft/sec), a medium altitude cruise at 28,500 feet and Mach 0.77 (771 ft/sec), and a low speed landing condition at Mach 0.21 (235 ft/sec).

This chapter and Appendix C outline the basic aircraft, sign convention, axis system, and the linearized equations of motion used in the design for this thesis. Appendix C also outlines the conversion of the nondimensional stability axis derivatives to the dimensional body axis and the addition of the first and second body bending



modes for the longitudinal plane which is used in this thesis.

### III-2 Equations of Motion

The aircraft models used in this thesis are developed using six degree-of-freedom equations of motion. It is assumed that there is no coupling between the lateral and longitudinal modes of operation. Thus the six degree-of-freedom model is reduced to two models with three degrees-of-motion. One model for the lateral plane and a second model for the longitudinal plane.

The assumptions stated in Chapter I are used in the development of these models in conjunction with the following assumptions:

1.  $\phi_0 = P_0 = Q_0 = R_0 = 0$
2.  $X_{\dot{\alpha}} = Z_{\dot{\alpha}} = 0$
3.  $U_0 = \text{Constant} \ \& \ V_0 = W_0 = 0$
4.  $W = U_0 \alpha \ \& \ \dot{W} = U_0 \dot{\alpha}$
5.  $V = U_0 \beta \ \& \ \dot{V} = U_0 \dot{\beta}$

The equations of motion developed for the lateral plane are as follows:

$$\begin{aligned} \dot{v} = & -U_0 r + g \phi \cos \theta_0 + Y_{\beta} \beta + Y_p p + U_0 \alpha_{\dot{p}} + Y_r r \\ & + Y_{\delta_r} \delta_r + Y_{\delta_w} \delta_w \end{aligned} \quad (3-1)$$

$$\begin{aligned} \dot{p} = & (I_{xz}/I_{xx})\dot{r} + L_{\beta}\beta + L_p p + L_r r \\ & + L_{\delta_r}\delta_r + L_{\delta_w}\delta_w \end{aligned} \quad (3-2)$$

$$\begin{aligned} \dot{r} = & (I_{xz}/I_{zz})\dot{p} + N_{\beta}\beta + N_p p + N_r r \\ & + N_{\delta_r}\delta_r + N_{\delta_w}\delta_w \end{aligned} \quad (3-3)$$

$$\phi = p \quad (3-4)$$

$$\dot{\psi} = r \quad (3-5)$$

Equations (3-4) and (3-5) are justified since the perturbations from equilibrium are assumed to be small. The relationship between the sideslip velocity  $v$  and the sideslip angle  $\beta$  is given by the following:

$$\tan \beta = \frac{v}{U_0} \quad (3-6)$$

Since  $\beta$  is small, the small angle approximation is used and assumed valid for this thesis. Therefore,

$$\beta = \frac{v}{U_0} \quad (3-6a)$$

$\delta_r$  and  $\delta_w$  represent displacement in the rudder and control wheel respectively. Substituting Equations (3-4) through (3-6a) into Equations (3-1) through (3-3) and taking the Laplace Transform yields the following three equations:

$$\begin{aligned}
(S - Y_{\beta}/U_0)\beta - [(Y_p/U_0 + \alpha_0)S + g\cos\theta_0/U_0]\phi \\
+ [1(1 - Y_r/U_0)S]\psi = Y_{\delta_r}/U_0\delta_r + Y_{\delta_w}/U_0\delta_w
\end{aligned} \tag{3-7}$$

$$\begin{aligned}
-L_{\beta}\beta + (S^2 - L_p S)\phi - [(I_{xz}/I_{xx})S^2 + L_r S]\psi \\
= L_{\delta_r}\delta_r + L_{\delta_w}\delta_w
\end{aligned} \tag{3-8}$$

$$\begin{aligned}
-N_{\beta}\beta - [(I_{xz}/I_{zz})S^2 + N_p S]\phi + [S^2 - N_r S]\psi \\
= N_{\delta_r}\delta_r + N_{\delta_w}\delta_w
\end{aligned} \tag{3-9}$$

Using Appendix C, Equations (3-7) to (3-9) are converted to a prime notation which now places all coefficients in the body axis system which is used in the design for this thesis. Thus, the equations are written as:

$$\begin{aligned}
(S - Y_{\beta'})\beta - [Y_p' S + Y_{\phi}']\phi - (Y_r' S)\psi \\
= Y_{\delta_r'}\delta_r + Y_{\delta_w'}\delta_w
\end{aligned} \tag{3-10}$$

$$\begin{aligned}
-L_{\beta'}\beta + (S^2 - L_p')\phi - (L_r' S)\psi \\
= L_{\delta_r'}\delta_r + L_{\delta_w'}\delta_w
\end{aligned} \tag{3-11}$$

$$\begin{aligned}
-N_{\beta'}\beta - (N_p' S)\phi + (S^2 - N_r' S)\psi \\
= N_{\delta_r'}\delta_r + N_{\delta_w'}\delta_w
\end{aligned} \tag{3-12}$$

Equations (3-10) to (3-12) are the actual equations used in Chapter IV for the design of a robust lateral controller.

The equations developed for the longitudinal plane are as follows:

$$\begin{aligned} \dot{u} = & -g\theta\cos\theta_0 + X_u u + X_\alpha \alpha + X_{\dot{\alpha}} \dot{\alpha} + X_q q - U_0 \alpha q \\ & + X_{\delta_e} \delta_e + X_{\delta_{sb}} \delta_{sb} + X_{\delta_T} \delta_T \end{aligned} \quad (3-13)$$

$$\begin{aligned} \dot{w} = & U_0 q - g\theta\sin\theta_0 + Z_u u + Z_{\dot{\alpha}} \dot{\alpha} + Z_\alpha \alpha + Z_q q \\ & + Z_{\delta_e} \delta_e + Z_{\delta_{sb}} \delta_{sb} \end{aligned} \quad (3-14)$$

$$q = M_u u + M_{\dot{\alpha}} \dot{\alpha} + M_\alpha \alpha + M_q q + M_{\delta_e} \delta_e + M_{\delta_{sb}} \delta_{sb} \quad (3-15)$$

$$\dot{\theta} = q \quad (3-16)$$

$$\dot{h} = U_0 (\theta - \alpha) \quad (3-17)$$

$$w = U_0 \alpha \quad (3-18)$$

$$\dot{w} = U_0 \dot{\alpha} \quad (3-19)$$

where  $\delta_e$ ,  $\delta_{sb}$ , and  $\delta_T$  represent displacement in elevator, speed brakes, and thrust respectively. Substituting Equations (3-16) to (3-19) into Equations (3-13) to (3-15) and taking the Laplace Transform yields the following three equations:

$$\begin{aligned}
x_{\alpha} Sh/U_0 - [SX_q + (x_{\alpha} - g \cos \theta_0)] \theta + (S - x_u) u \\
= x_{\delta_e} \delta_e + x_{\delta_{sb}} \delta_{sb} + x_{\delta_T} \delta_T
\end{aligned} \tag{3-20}$$

$$\begin{aligned}
(S - z_{\alpha}/U_0)(\theta - Sh/U_0) - [S(1 + z_q/U_0 + g \sin \theta_0) \theta \\
- z_u u/U] = [z_{\delta_e} \delta_e + z_{\delta_{sb}} \delta_{sb}] / u_0
\end{aligned} \tag{3-21}$$

$$\begin{aligned}
(S\theta^2) - M_u u - M_{\alpha} (\theta - Sh/U_0) - M_q S \theta \\
= M_{\delta_e} \delta_e + M_{\delta_{sb}} \delta_{sb}
\end{aligned} \tag{3-22}$$

Using Appendix C, Equations (3-20) to (3-22) are converted to a primed notation which now places all coefficients in the body axis. Thus, the equation becomes:

$$\begin{aligned}
(S - x_u) u - [SX_{q'} + (x_{\alpha} - x_{\theta'})] \theta - x_{\alpha} h/U_0 \\
= x_{\delta_e'} \delta_e + x_{\delta_{sb}'} \delta_{sb} + x_{\delta_T'} \delta_T
\end{aligned} \tag{3-23}$$

$$\begin{aligned}
-z_{u'} u - [S(1 - z_{q'}) - (z_{\theta'} + z_{\alpha'})] \theta + S(S - z_{\alpha'}) h/U_0 \\
= z_{\delta_e'} \delta_e + z_{\delta_{sb}'} \delta_{sb}
\end{aligned} \tag{3-24}$$

$$\begin{aligned}
-M_{u'} u + [S^2 - M_{q'} S + (M_{\theta'} - M_{\alpha'})] - (M_{\alpha'} S) h/U_0 \\
= M_{\delta_e'} \delta_e + M_{\delta_{sb}'} \delta_{sb}
\end{aligned} \tag{3-25}$$

Equations (3-23) to (3-25) are used in Chapter V for the design of a robust controller in the longitudinal plane.

### III-3 Summary

This chapter outlines the lateral and longitudinal equations of motion. These equations are used in Chapters IV and V for the design of the lateral and longitudinal controllers. Appendix C gives a basic aircraft description, sign convention, and the conversion of the nondimensional stability axis derivatives to the dimensional body axis system. Finally, Appendix C develops the first and second body bending modes used in Chapter V to eliminate the assumption that the aircraft is a rigid body. The body bending modes are only considered for the longitudinal case.

## IV. Lateral Design

### IV-1 Introduction

This chapter is devoted to the design of a robust lateral controller for the KC-135 aircraft. The three degrees-of-freedom model derived in Chapter III is reduced to two inputs and two outputs. These equations are used in the design of a lateral control to perform two maneuvers. One maneuver is a coordinated turn (i.e., bank angle commands with minimum sideslip). The second maneuver is a commanded sideslip with minimum bank angle. This design is completed using the improved design technique outlined in Chapter III and in Appendix B.

The  $q_{ij}$ 's are determined using the 2x2 input and output matrices which are required in this design. The specifications are modeled in the time domain and converted to the frequency domain. Using the above specifications, the nominal loop transmission,  $L_{20}$ , is designed by the standard QFT technique and the required pre-filter,  $F_{22}$ , is developed. The improved design technique is used to synthesize the nominal loop transmission,  $L_{10}$ , and the final step in the design is the development of the pre-filter  $F_{11}$  which places the derived response within the frequency domain specifications.

IV-2 Input and Output Matrices

The required equations of motion developed in Chapter III are as follows:

$$-(Y_{\phi, \phi} + Y_{p, S})\phi + (S - Y_{\beta, \beta})\beta - Y_{r, S}\psi = Y_{\delta, w}\delta w + Y_{\delta, r}\delta r \quad (4-1)$$

$$(-S^2 - L_{p, S})\phi - L_{\beta, \beta} - L_{r, S}\psi = L_{\delta, w}\delta w + L_{\delta, r}\delta r \quad (4-2)$$

$$N_{p, S}\phi - N_{\beta, \beta} + (S - N_{r, S})\psi = N_{\delta, w}\delta w + N_{\delta, r}\delta r \quad (4-3)$$

Substituting the dimensional body axes coefficients into Equations (4-1) to (4-3) for F.C. #1 yields:

$$\begin{aligned} &-(.039665S + .04322)\phi + (S + .076917\beta + .99629S)\psi \\ &= -.00074615\delta w + .026647\delta r \end{aligned} \quad (4-4)$$

$$\begin{aligned} &(S^2 + .75011S)\phi + 4.4499\beta - .24613S\psi \\ &= .3633103\delta w + .618646\delta r \end{aligned} \quad (4-5)$$

$$\begin{aligned} &.012277S\phi - 1.42597\beta + (S^2 + .15052S)\psi \\ &= .020775\delta w - 1.01653\delta r \end{aligned} \quad (4-6)$$

The resulting equations for F.C.'s #2 and #3 are included in Appendix E.

Equations (4-4) to (4-6) have two inputs and three outputs. This design technique requires that the number of inputs be equal to the number of outputs. Thus, one of the outputs must be eliminated from these equations. The



desired outputs are bank angle  $\phi$  and sideslip  $\beta$ ; therefore, the output  $\psi$  is mathematically eliminated from the equations. This is accomplished by solving for  $\psi$  in Equation (4-4) and substituting this into Equations (4-5) and (4-6). Therefore, solving for  $\psi$  in Equation (4-4) yields:

$$\psi = 1/s[(.03981s + .04338)\phi - (s + .0772)\beta - .00749\delta w + .02675\delta r] \quad (4-7)$$

Substituting Equations (4-7) into (4-5) and (4-6) yields the desired two input-two output model. These equations are:

$$(s^2 + .74628s - .010714)\phi - (.24789s + 4.46897)\beta = .363103\delta w + .61846\delta r \quad (4-8)$$

$$(.039665s^2 + .05142s + .0065)\phi - (s^2 + .227437s + 1.43226)\beta = (.00074615s + .207051)\delta w - (.026647s + .909021)\delta r \quad (4-9)$$

Equations (4-8) and (4-9) no longer explicitly represent the rolling and yawing movements of the aircraft since sideforces are now included in each equation. However, the mathematical representation of the aircraft in flight is retained.

As outlined in Appendix B, input and output vectors are defined respectively as:

$$\underline{\delta} = \begin{bmatrix} \delta w \\ \delta r \end{bmatrix} \quad \text{and} \quad \underline{y} = \begin{bmatrix} \phi \\ \beta \end{bmatrix}$$

Also define an input matrix N which premultiplies the input vector and an output matrix M which premultiplies the output vector. Therefore, Equations (4-8) and (4-9) can be represented in matrix form as:

$$\begin{aligned}
 & \begin{bmatrix} (s^2 + .74028s - .010714) & (.24789s + 4.46897) \\ (.039665s^2 + .06142s + .0065) & (s^2 + .227437s + 1.43226) \end{bmatrix} \begin{bmatrix} \phi \\ \beta \end{bmatrix} \\
 = & \begin{bmatrix} .363103s & .618646 \\ (.0074615s + .207051) & -(.026647s - .909021) \end{bmatrix} \begin{bmatrix} \delta_w \\ \delta_r \end{bmatrix} \quad (4-10)
 \end{aligned}$$

Representing Equation (4-10) in general terms

$$\underline{M}\underline{Y} = \underline{N}\delta$$

$$\underline{Y} = \underline{M}^{-1}\underline{N}\delta$$

Let  $\underline{P} = \underline{M}\underline{N}^{-1}$

and  $\underline{P}^{-1} = \underline{N}^{-1}\underline{M} = \underline{Q}'$

The first constraint on the system is that the inverse of P exists. Since the inverse of N exists (i.e., N is non-singular), then the inverse of P exists. Likewise, the inverse of M exists; therefore P is non-singular.

Q' is computed using a computer program and the resulting  $q'_{ij}$ 's are obtained. The  $q_{ij}$ 's required in the design process are:  $q_{ij}$ 's =  $1/q'_{ij}$ 's

The resulting  $q_{ij}$ 's for each of the flight conditions are as follows:

Flight Condition #1:

$$q_{11} = \frac{.3906 (S + 45.19)}{S - .00732 (S + .7675) (S + 35.02)} \quad (4-11)$$

$$q_{12} = \frac{-.01656 (S + 45.19)}{(S + 2.114) (S - 2.442)} \quad (4-12)$$

$$q_{21} = \frac{13.64 (S + 45.19)}{(S - .03275) (S + .7104) (S + 258.2)} \quad (4-13)$$

$$q_{22} = \frac{.0279 (S + 45.19)}{(S + .1884 \pm j 1.983)} \quad (4-14)$$

Flight Condition #2:

$$q_{11} = \frac{.4897 (S + 44.36)}{(S - .01033) (S + .9217) (S + 46.40)} \quad (4-15)$$

$$q_{12} = \frac{-.01333 (S + 44.36)}{(S + 2.219) (S + 2.590)} \quad (4-16)$$

$$q_{21} = \frac{17.49 (S + 44.36)}{(S + .4450) (S - 1.152) (S + 11.09)} \quad (4-17)$$

$$q_{22} = \frac{.0280 (S + 44.36)}{(S + .1480 \pm j 1.485)} \quad (4-18)$$

Flight Condition #3:

$$q_{11} = \frac{.4006 (S + 11.36)}{(S + .07322) (S + 1.026 \pm j 1.494)} \quad (4-19)$$

$$q_{12} = \frac{.4503 (S + 11.36)}{(S + .05108 \pm j .6652)} \quad (4-20)$$

$$q_{21} = \frac{6.318 (S + 11.36)}{(S - .1196)(S + 1.049)(S + 181.6)} \quad (4-21)$$

$$q_{22} = \frac{.04033 (S + 11.36)}{(S + .6041 \pm j 1.789)} \quad (4-22)$$

The second constraint on the system is:

$$|P_{11} P_{22}| > |P_{21} P_{12}| \quad \text{as } S \rightarrow \infty$$

or

$$\left| \frac{P_{21} P_{12}}{P_{11} P_{22}} \right| < 1$$

and equivalent

$$\left| \frac{q_{11} q_{22}}{q_{12} q_{21}} \right| < 1$$

For each of the three flight conditions the above inequality holds true (i.e., as  $S \rightarrow \infty$  the denominator is always larger than the numerator). Therefore, the magnitude is always less than one over the entire frequency of interest.

#### IV-3 Effective SISO Systems

A 2x2 MIMO system is represented as four SISO systems as demonstrated in Appendix B. These four SISO systems are shown in Figure 4-1.

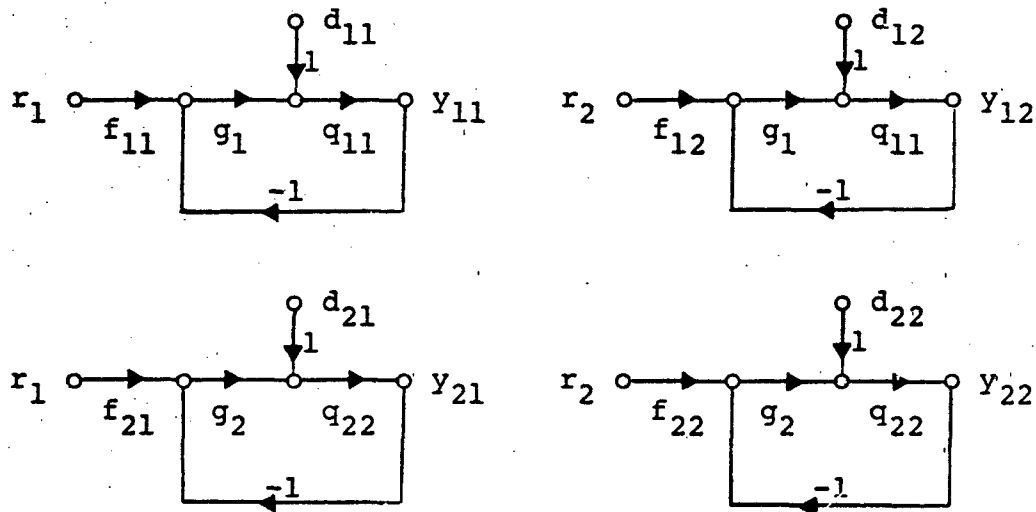


Fig. 4-1. Effective SISO Systems

In this design the command inputs,  $r_1$  and  $r_2$  are:  
 $r_1$  (Bank angle command) = 30;  $r_2$  (Sideslip angle command) = 5. It is desired that the outputs  $Y_{11}$  and  $Y_{22}$  track the inputs  $r_1$  and  $r_2$  respectively and the outputs  $Y_{12}$  and  $Y_{21}$  responses due to  $r_2$  and  $r_1$  respectively be ideally zero. Thus the next step in the design is to model the desired responses that are considered acceptable for the system for any given input.

#### IV-4 Response Models

The response models used in this thesis are developed from Reference 17 which demonstrated identical maneuvers for the Porter design technique. However, it is not required that such specification be available. For example, the user will specify an acceptable range of response or specification which is desired from the system. These

specifications are normally in the form of  $t_s$ ,  $T_s$ ,  $M_p$ ,  $T_p$ , etc. These specifications are modeled in the time domain and then transformed to the frequency domain.

The specifications used in the design of this thesis are as follows:

1. Bank Angle Command:

$T_U$  - Optimal settling time,  $t_s$ , of 4 seconds  
(i.e.,  $t_s$ , is  $\pm 2\%$  of final value).

$T_L$  - Worst acceptable case is a settling time,  $t_s$ , of 10 seconds.

$T_D$  - The acceptable or worst case for sideslip during the coordinated turn maneuver is a peak value,  $M_p$ , of 1 which settles to zero in approximately 10 seconds.

2. Sideslip Angle Command:

$T_U$  - Optimal settling time,  $t_s$ , of 8 seconds.

$T_L$  - Worst acceptable case is a settling time,  $t_s$ , of 15 seconds.

$T_D$  - The acceptable or worst case for bank angle  $\phi$  during the sideslip maneuver is a peak value,  $M_p$ , of 1 which settles to zero in approximately 20 seconds.

The time domain specification models are included in Appendix E.

#### IV-5 Loop Two Design

The selection of which loop to design first is entirely up to the designer. However, it is recommended that the loop with the smallest amount of uncertainty be designed first and the loop with the largest amount of uncertainty be designed last via the improved design technique. This reduces the overdesign inherent in the design technique. In this thesis, loop two is selected to be designed first.

In this design, one compensator is to be selected which performs two functions. The first is for the system to track a given input (i.e.,  $r_2$ ) and the second is to reject the unwanted output  $y_{21}$  due to the bank angle command; i.e., for  $y_{21}$  to be ideally zero.

The SISO systems used in this design are shown in Figure 4-2.

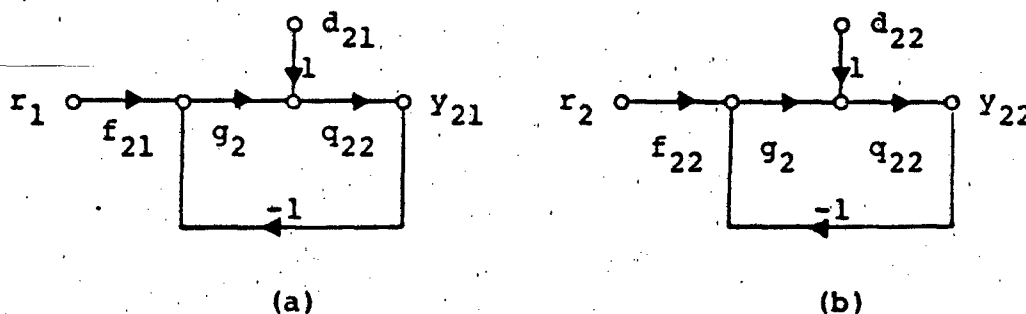
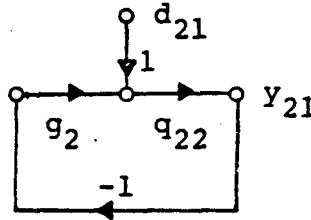


Fig. 4-2. Loop 2 SISO Systems

Since it is desired to have  $y_{21}$  approach zero (Figure 4-2a), the pre-filter  $f_{21}$  can be selected to equal zero. Therefore, this loop now becomes a BNIC (Appendix A).



The equation for the BNIC loop is given as:

$$t_{21} = \frac{q_{22}d_{21}}{1 + q_{22}g_2} \quad (4-23)$$

where  $d_{21} = -t_{11}/q_{21}$

Therefore  $t_{21} = \frac{-[q_{22}/q_{21}] \times t_{11}}{1 + L_2} \quad (4-24)$

where  $L_2 = g_2q_{22}$

It is desired that the magnitude of  $t_{21}$  be below some acceptable maximum (i.e., the bound  $T_D = b_{21}$ ) and that the worst case for  $t_{11}$  is the maximum allowable response (i.e., the bound  $t_u = b_{11}$ ). Therefore, Equation (4-24) can be rearranged to yield the following inequality:

$$|t_{21}| = \frac{|q_{22}| |b_{11}|}{|q_{21}| |1 + L_2|} \leq |b_{21}| \quad (4-25)$$

Therefore  $|1 + L_2| \geq \frac{|q_{22}| |b_{11}|}{|b_{21}| |q_{21}|} \quad (4-26)$



Equation (4-26) is used in the design to determine the required bounds on the nominal loop transmission,  $L_{20}$ , for the BNIC loop.

The second equation of interest is derived from Figure 4-2b. This equation is:

$$t_{22} = \frac{f_{22}g_2q_{22} + d_{22}}{1 + g_2q_{22}} \quad (4-27)$$

where  $d_{22} = (-t_{12} * q_{22}) / (q_{21})$

$$\text{Therefore } t_{22} = \frac{f_{22}L_2}{1 + L_2} - \frac{t_{12}q_{22}}{q_{21}(1 + L_2)} \quad (4-28)$$

Since there are two inputs, a commanded input and a disturbance input, the bounds on  $t_{22}$  must be broken into two parts.

$$\text{Therefore } t_{22} = \tau_{22} + \tau_{d_{22}} \quad (4-29)$$

Figure 4-3 illustrates the use of Equation (4-29).

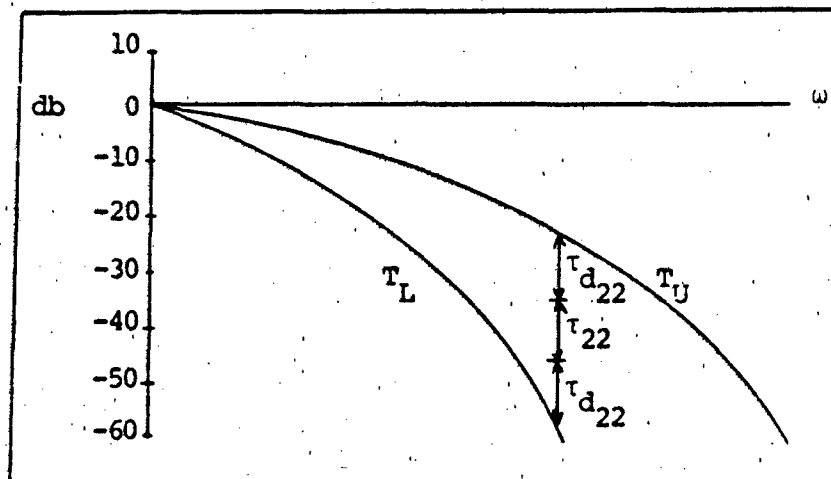


Fig. 4-3. Upper and Lower Bound Specifications

The relative weighting placed on  $\tau_{22}$  and  $\tau_{d_{22}}$  can be determined from the following equations.

$$\tau_{22} = \frac{f_{22} L_2}{1 + L_2} \quad (4-30)$$

and

$$\tau_{d_{22}} = \frac{-t_{12} q_{22}}{q_{21} (1 + L_2)} \quad (4-31)$$

If, for example, Equation (4-31) has a much smaller magnitude than Equation (4-30), then the entire bound on  $\tau_{22}$  can be used for Equation (4-30). However, if this is not the case, the designer must select the ratio of  $\tau_{22}$  to  $\tau_{d_{22}}$ .

Since  $f_{22}$  is to be designed, there is no uncertainty in the pre-filter. Thus, for the design of loop two (Figure 4-2b) set  $f_{22}$  equal to one (note: this is for design purposes only).

Therefore

$$t_{22} = \frac{L_2}{1 + L_2} \quad (4-32)$$

Equations (4-26), (4-31), and (4-32) are now used in the design of the nominal loop transmission for loop two.

The design process is illustrated for determining the bounds on  $L_{20}$  at one particular frequency.

### BNIC Loop

The BNIC loop is selected first to determine the required bounds at  $\omega = 0.1$  radians/sec. The BNIC loop is shown in Figure 4-4.

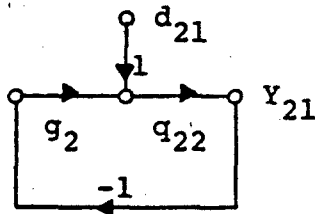


Fig. 4-4. Basic Non-Interacting Loop Two

The design equation for this loop is given as:

$$|1 + L_2| \geq \frac{|q_{22}| |b_{11}|}{|b_{21}| |q_{21}|} \quad (4-33)$$

Where  $b_{11}$  and  $b_{21}$  are the upper bounds or specifications on the two responses. The magnitudes only are required for the above inequality for determining the bounds on  $L_{20}$ . Thus this equation can be redefined using log magnitudes as

$$\begin{aligned} \text{Lm}(1 + L_2) &= \text{Lm}(q_{22}) + \text{Lm}(b_{11}) - \text{Lm}(q_{21}) \\ &\quad - \text{Lm}(b_{21}) \end{aligned} \quad (4-34)$$

To ensure positive phase and gain margin the universal high frequency bound is selected to be the -3db contour line on the inverted Nichols Chart as outlined in Appendix A. Thus the design requires that

$$Lm(1 + L_2) \geq -3db$$

The magnitudes of the  $q_{22}$ 's for each of the three flight conditions are shown in Figure 4-5. For the design of  $L_{20}$ , flight condition #3 is selected as the nominal plant. The nominal loop transmission is defined as

$$L_{20} = g_2 q_{220} = \frac{g_2 q_{22} q_{220}}{q_{22}} \quad (4-35)$$

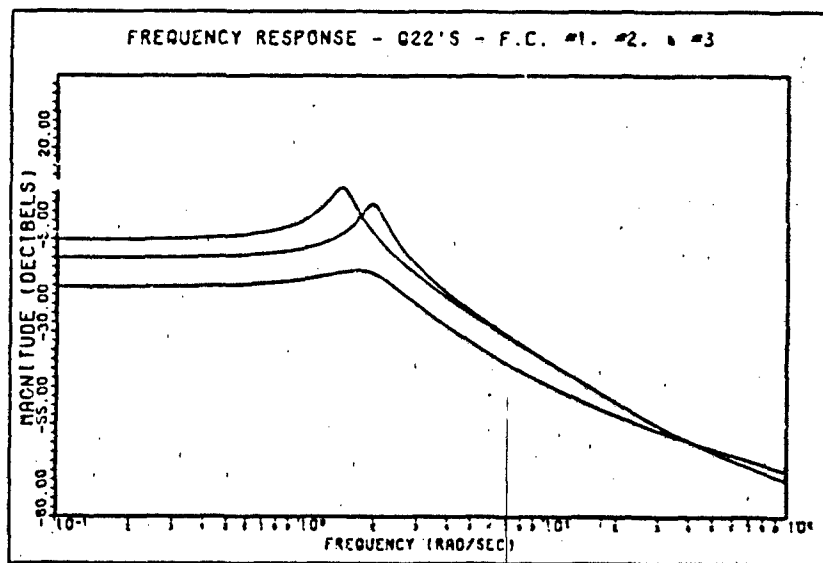


Fig. 4-5. Magnitude of  $q_{22}$  for F.C.'s #1, #2, and #3

Therefore 
$$L_{20} = \frac{L_2 q_{220}}{q_{22}}$$

The above transformation is required since the design is for the nominal loop transmission,  $L_{20}$  and not for  $L_2$ .

Thus 
$$Lm(L_{20}) = Lm(L_2) + Lm(q_{220}) - Lm(q_{22}) \quad (4-36)$$

Table 4-1 contains the log magnitude of each of the required elements of Equation (4-33) used in the design for  $\omega = 0.1$  rad/sec.

TABLE 4-1  
ELEMENT FOR DESIGN EQUATION AT  $\omega=0.1$  RAD/SEC

Element	F.C. #1	F.C. #2	F.C. #3
$ b_{11} $	-0.05	-0.05	-0.05
$ b_{21} $	-34.2	-34.2	-34.2
$ q_{220} $	-17.8	-17.8	-17.8
$ q_{21} $	30.0	42.46	7.63
$ q_{22} $	-9.87	-5.03	-17.8

Note: F.C. = Flight Condition.

For each of the three F.C. the bounds on  $L_m(1 + L_2)$  are determined using Equation (4-33). These bounds are:

$$\text{F.C. \#1: } L_m(1 + L_2) = -5.72\text{db}$$

$$\text{F.C. \#2: } L_m(1 + L_2) = -13.34\text{db}$$

$$\text{F.C. \#3: } L_m(1 + L_2) = 8.72\text{db}$$

On the inverted Nichols Chart the  $L_m(1 + L_2)$  is given by the contour lines and  $L_m(L_2)$  can be obtained from the vertical scale of the Nichols Chart.

Converting the loop transmission to nominal loop transmission requires that the contour of  $L_m(1 + L_2)$  must be translated up or down the Nichols Chart the

required amount given by Equation (4-35). For example, F.C. #1 requires that

$$Lm (1 + L_2) \geq -5.72db$$

Now  $Lm (L_{20}) = Lm (L_2) + Lm (q_{220}) - Lm (q_{22})$

And for this example, the variation in  $Lm (L_2)$  is approximately -6.2db to 3db. The maximum magnitude is selected to determine the allowable magnitude of  $L_{20}$ .

Thus  $Lm (L_{20}) = 3db - 17.8db + 9.87db = -4.92db$

Therefore,  $Lm (1 + L_{20}) \geq -10.64db$  which means that, for F.C. #1, the nominal loop transmission must be on or above the -10.64db contour. This process is repeated for the remaining two flight conditions. The dominant bounds for  $\omega = 0.1$  rad/sec occur for F.C. #3 and is

$$Lm (1 + L_{20}) \geq 8.72db$$

### Tracking Loop

The next step in the design is to determine the required bound on the tracking loop. This loop is shown in Figure 4-6. There are two inputs for this loop. The command input,  $r_2$ , and a disturbance input,  $d_{22}$ . The disturbance input being the interaction of loop one with loop two. The equivalent JISO systems for this portion of the design are given in Figure 4-7.

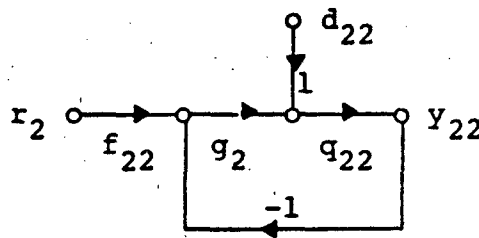


Fig. 4-6. SISO System -  $L_2$  - Tracking

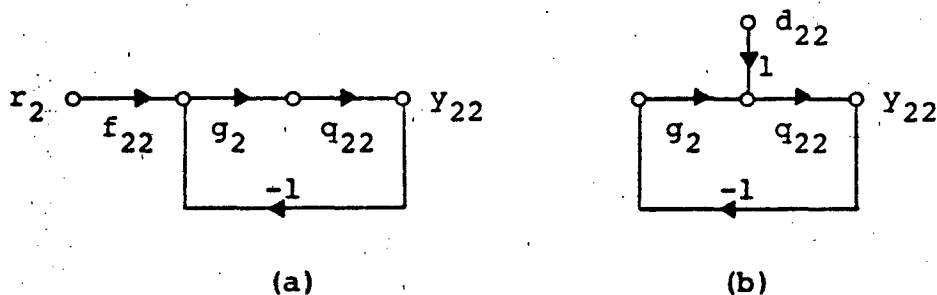


Fig. 4-7. Effective Loops--Tracking

Equation (4-31) is used in the determination of the bounds required for Figure 4-7(b). Dividing top and bottom of Equation (4-31) by  $q_{220}$  and rearranging yields the following design equation:

$$|\tau_{d_{22}}| = \left| \frac{[b_{12}/q_{21}] \times q_{22}}{1 + L_{20} (q_{22}/q_{220})} \right| \quad (4-37)$$

The magnitude of  $\tau_{d_{22}}$  can now be determined using Equation (4-37) and Table 4-2.

TABLE 4-2

ELEMENTS FOR DESIGN EQUATION AT  $\omega=0.1$  RAD/SEC

Element	F.C. #1	F.C. #2	F.C. #3
$ b_{12} $	-23.11	-23.11	-23.11
$ a_{22} $	-0.5025	-0.5025	-0.5025
$ b_{22} $	-0.2208	-0.2208	-0.2208
$ q_{22} $	-9.87	-5.03	-17.8
$ q_{21} $	30.0	42.46	7.63
$ q_{220} $	-17.8	-17.8	-17.8

The magnitude  $|1/1 + L_{20}|$  is the required bound on the BNIC loop. Thus to determine the magnitude of

$$\left| \frac{1}{1 + L_{20} q_{22}/q_{220}} \right| L_{20} \text{ must be adjusted by the amount given}$$

by the magnitude of  $q_{22}/q_{220}$ . Therefore, the bounds on

$\tau_{d_{22}}$  are as follows:

$$\text{F.C. \#1: } \tau_{d_{22}} \geq -79.63\text{db}$$

$$\text{F.C. \#2: } \tau_{d_{22}} \geq -92.12\text{db}$$

$$\text{F.C. \#3: } \tau_{d_{22}} \geq -57.26\text{db}$$

The above bounds on  $\tau_{d_{22}}$  are considered small. Therefore, the entire bounds can be devoted to the  $\tau_{22}$



term in Equation (4-29). For  $\omega = 0.1$  radians/second, these bounds are given by

$$Lm (b_{22}) - Lm (a_{22}) = 0.282\text{db}$$

Now determine if the bounds on the BNIC loop satisfy the bounds for the tracking loop. This is given by  $|t_{22}|_{\text{max}}$  minus  $|t_{22}|_{\text{min}}$ . The template of  $q_{22}$  (the uncertainty in the plant at  $\omega = 0.1$  rad/sec) is used in this determination. However, first the bounds for the BNIC loop must be converted from the inverse Nichols Chart to the regular (upright) Nichols Chart. The template of  $q_{22}$  for  $\omega = 0.1$  rad/sec is a straight line with a magnitude of 7.92db. It is seen from the Nichols Chart (Figure 4-8) that the bounds on the BNIC loop do not meet the required bounds or specifications for the tracking loop. Therefore, the worst case is selected as the dominant bound at  $\omega = 0.1$  rad/sec. This bound is generated by using the template of  $q_{22}$  as outlined in Appendix A. The templates of  $q_{22}$  for each of the frequencies of interest are included in Appendix E.

This process is repeated every octave over the frequency from  $\omega = 0.1$  rad/sec to  $\omega = 500$  rad/sec. It is to be noted, as shown in Figure 4-8, that for certain frequencies such as for  $\omega = 0.1$  rad/sec the BNIC loop dominates for a portion of the bound on  $L_{20}$  and the tracking loop dominates for the remaining portion. Thus, the

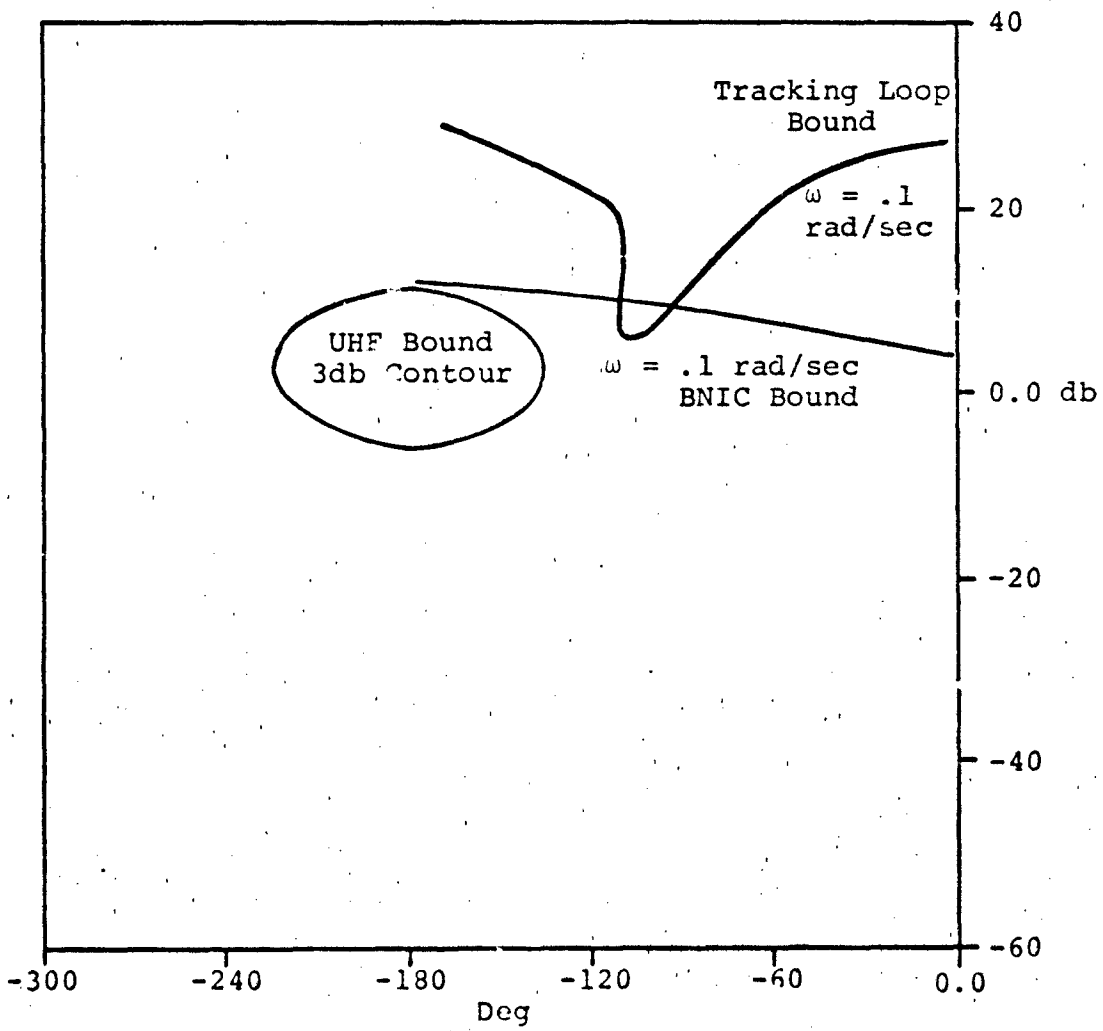


Fig. 4-8. Bounds on  $L_{20}$  for  $\omega = .1$  Radians/Sec.

composite of the two bounds must be used to form the bounds on the nominal loop transmission,  $L_{20}$ . At and above  $\omega = 1$  rad/sec the BNIC loop generates the dominant bounds on  $L_{20}$ . Also at and above  $\omega = 1$  rad/sec the BNIC bound becomes the -3db oval (i.e., the UHF bounds). The requirement on the design above  $\omega = 20$  rad/sec is that the templates not penetrate the 3db UHF bounds as shown in Figure 4-9. This completes the determination of the bounds on  $L_{20}$ .

Shaping the Nominal Loop Transmission,  $L_{20}$

The shaping of the nominal loop transmission is a crucial step in the design process. The designer must ensure that, for each frequency, the nominal loop transmission is on or above the bound at that given frequency. It is important that, for each bound, the nominal loop transmission falls as close as possible to the bound for each frequency. As the nominal loop is shaped care must be taken to guarantee that  $L_{20}$  does not penetrate the UHF bounds which ensure positive phase and gain margin. The resulting  $L_{20}$  as shown in Figure 4-9 is as follows:

$$L_{20} = \frac{(9.523)10^5 (s + 7)(s + 11.36)}{(s + .6041 \pm j1.789)(s + 50)(s + 96 \pm j128)} \quad (4-38)$$

and using the relationship

$$L_{20} = g_2 q_{220}$$

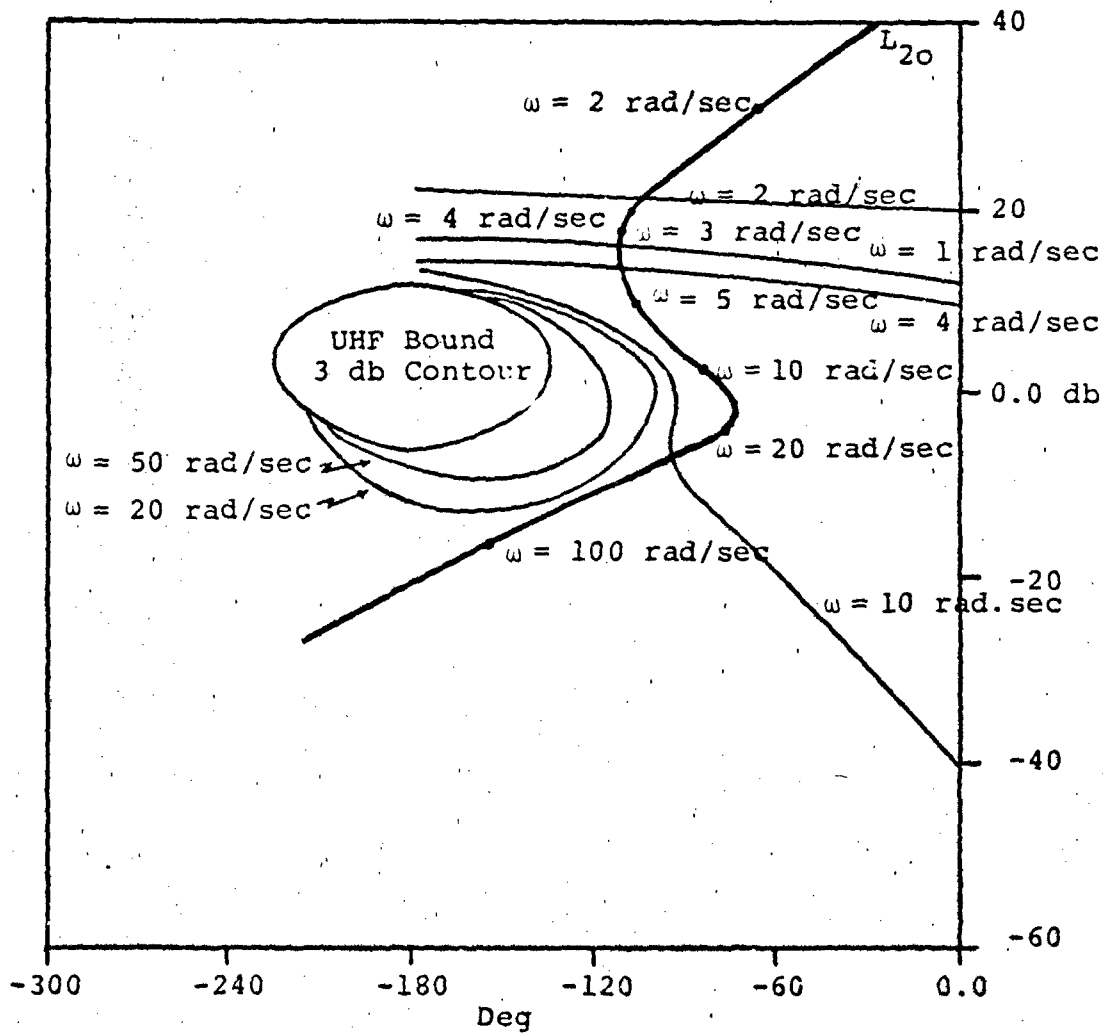


Fig. 4-9. Bounds and Nominal Loop Transmission,  $L_{20}$

the corresponding compensator  $g_2$  is

$$g_2 = \frac{(2.361)10^7 (s + 7)}{(s + 50)(s + 96 \pm j128)} \quad (4-39)$$

The magnitude and phase of  $L_{20}$  is shown in Figure 4-10.

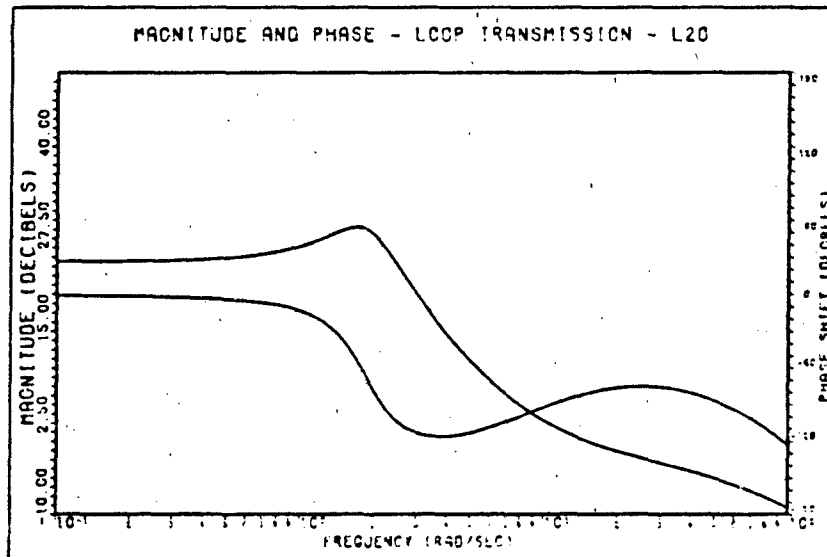


Fig. 4-10. Magnitude and Phase of Nominal Loop Transmission of Loop Two

#### Pre-Filter Design $F_{22}$

The design of loop one using the improved design technique requires that the pre-filter  $f_{22}$  be known. Therefore,  $f_{22}$  is determined using the approach stated in Appendix A. The resulting pre-filter that places the desired response within the frequency domain specifications is derived from Figure 4-11 and is:

$$F_{22} = \frac{0.512}{(s + .512)(s + 1)} \quad (4-40)$$

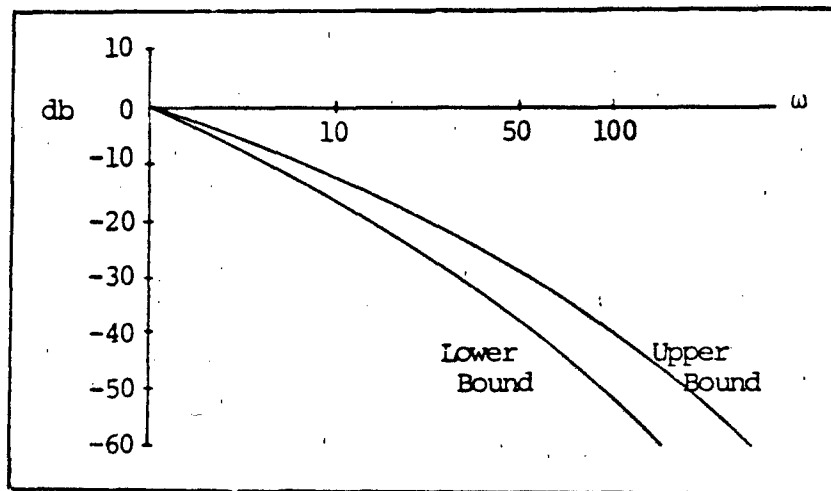


Fig. 4-11. Required Bounds on Pre-Filter  $f_{22}$

IV-6 Loop One Design

This loop is designed using the improved design technique; that is, the elements designed in loop two are now used in the design of loop one. The equation required in the design of loop one is briefly highlighted. As in loop two, the effective SISO loop is shown in Figure 4-12.

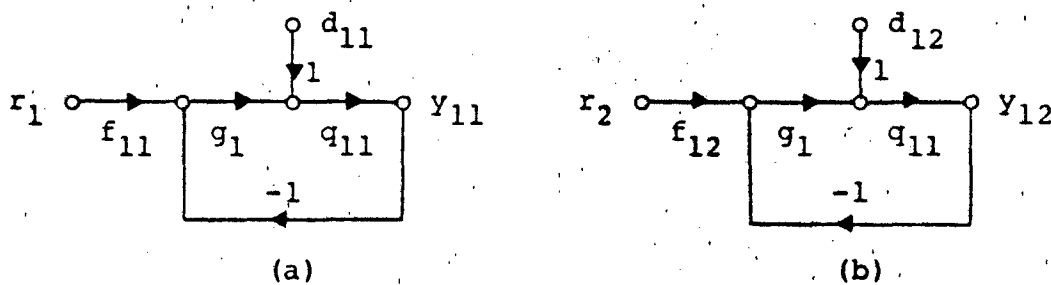
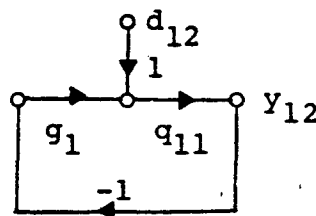


Fig. 4-12. Effective SISO System for Loop One

It is required that the sideslip response, due to the commanded bank angle, be ideally zero. Therefore, the pre-filter  $f_{12}$  in Figure 4-12b can be set equal to zero resulting in the SISO system:



Equation (4-41) developed from the above diagram is

$$t_{12} = \frac{d_{12}q_{11}}{1 + g_1q_{11}} \quad (4-41)$$

where  $L_1 = g_1q_{11}$  and  $d_{12} = -t_{22}/q_{12}$

From Figure 4-12a Equation (4-42) is developed and is given as:

$$t_{11} = \frac{f_{11}L_1}{1 + L_1} + \frac{d_{11}q_{11}}{1 + L_1} \quad (4-42)$$

where  $d_{11} = -t_{21}/q_{12}$

Using the design developed for loop two, the elements which are known are now substituted into Equations (4-41) and (4-42) (i.e., the equations for  $t_{21}$  and  $t_{22}$ ). The resulting equations can be manipulated into the following form (11:102):

1. For the tracking loop:

$$t_{11} = \frac{f_{11}L_{1e}}{1 + L_{1e}} \quad (4-42a)$$

where  $L_{1e} = g_1 q_{11e}$  (4-42b)

and  $q_{11e} = \frac{q_{11}(1 + L_2)}{1 + L_2 - \gamma}$  (4-42c)

and  $\gamma = \frac{q_{11}q_{22}}{q_{12}q_{21}}$  (4-42d)

2. For the BNIC loop:

$$t_{12} = \frac{d_{12e}}{1 + L_{1e}} \quad (4-42e)$$

where  $L_{1e}$  is given in Equation (4-29a) and

$$d_{12e} = \frac{f_{22}L_2q_{11}}{q_{12}(1 + L_2 - \gamma)} \quad (4-42f)$$

where  $\gamma$  is given in Equation (4-42d). The design of  $L_{1oe}$  can now be accomplished as a simple single loop problem where  $q_{11oe}$  is the nominal plant transfer function.

Therefore, the required design equations to be used in this design are given in Equations (4-43) and (4-44). The required tracking loop design equation is:

$$t_{11} = \frac{L_{1e}}{1 + L_{1e}} \quad (4-43)$$



since  $f_{11}$  is to be designed and is considered to have no uncertainty. The required BNIC loop equation is:

$$|1 + L_{1e}| \geq \frac{|d_{12e}|}{|b_{12}|} \quad (4-44)$$

As in the design of loop two, the design is for  $L_{1oe}$  and not for  $L_{1e}$ . Therefore,  $L_{1oe}$  is given as:

$$L_{1oe} = \frac{L_{1e} q_{11oe}}{q_{11o}} \quad (4-45)$$

The equivalent  $q_{11e}$ 's for each of the three flight conditions are as follows:

F.C. #1:

$$q_{11e} = \frac{.3726(s + 12.76 \pm j4.644)(s + 56.45)}{(s - .00712)(s + 8.476 \pm j6.512)(s + 65.21)(s + .7681)}$$

F.C. #2:

$$q_{11e} = \frac{.4625(s + 57.43)}{(s - .01005)(s + .9221)(s + 54.46)}$$

F.C. #3:

$$q_{11e} = \frac{.3791(s + 4.53 \pm j4.51)}{(s + .06889)(s + .7536 \pm j1.665)(s + 3.24)}$$

The magnitude response for each of the equivalent  $q_{11e}$ 's is given in Figure 4-13.

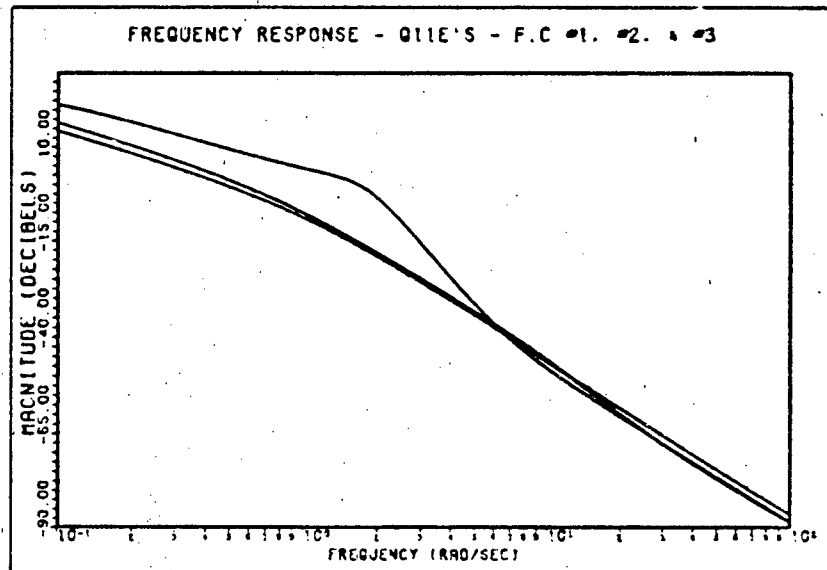


Fig. 4-13. Magnitude vs Frequency of Equivalent  $q_{11e}$ 's

Since it is normally much easier to determine the bounds on the BNIC loop, the bound on this loop is determined first. Once this bound is determined for a particular frequency, it is checked against the required bound for the tracking loop (i.e., use of the templates which represent the uncertainty in the plant). If the bound on BNIC loop does not satisfy the bound on the tracking loop, then the bound on the tracking loop is used in the determination of the nominal loop transmission.

As an example, the determination of the bound for  $\omega = 1$  rad/sec is illustrated. Using design Equation (4-44) the bound on the BNIC loop is determined first. This equation is:

$$|1 + L_{ie}| \geq \frac{|d_{12e}|}{|b_{12}|}$$

From Table 4-3 the bound on  $|1 + L_{1e}|$  is determined.

TABLE 4-3  
ELEMENTS FOR DESIGN EQUATION AT  $\omega = 1$  RAD/SEC

Element	F.C. #1	F.C. #2	F.C. #3
$ q_{11e} $	-7.67	-8.91	4.29
$ q_{11oe} $	-8.91	-8.91	-8.91
$ d_{12e} $	-0.675	0.827	-6.77
$ b_{12} $	-11.76	-11.76	-11.76

The resulting bounds for each of the three flight conditions are:

$$\text{F.C. \#1: } |1 + L_{1e}| \geq 12.35\text{db}$$

$$\text{F.C. \#2: } |1 + L_{1e}| \geq 12.59\text{db}$$

$$\text{F.C. \#3: } |1 + L_{1e}| \geq 4.99\text{db}$$

As in the design of loop two, the nominal loop transmission is required. Flight Condition #2 is selected as the nominal point for the design of loop one. Therefore, using Equation (4-45) the bounds on  $L_{1e}$  are converted to bounds on  $L_{1oe}$  by

$$L_{1oe} = \frac{L_{1e} q_{11oe}}{q_{11e}}$$

Thus, using the above relationship, the dominant bound is found to occur for F.C. #3 and is

$$|1 + L_{1oe}| \geq 18.19\text{db}$$

Now the above bound is checked to determine if it meets the bound required for the tracking loop. The template for  $\omega = 1$  rad/sec has an allowable tolerance of 6.99db (i.e.,  $b_{11} - a_{11}$ ) and as can be seen from Figure 4-14 the bound on the BNIC loop also satisfies the required bound on the tracking loop. At and above  $\omega = 4$  rad/sec the bound on the BNIC loop becomes the -3db UHF contour. Therefore, at and above this frequency, the only concern is that the template of  $q_{11e}$  over the entire frequency range of interest (i.e.,  $\omega = 4$  rad/sec to 500 rad/sec), does not penetrate the 3db UHF bound. Thus, these templates generate bounds for each particular frequency as shown in Figure 4-15. The templates of  $q_{11e}$  for each of the frequencies of interest are included in Appendix E.

Shaping the Nominal Loop Transmission,  $L_{1e}$

The nominal loop transmission is shaped in the same manner as for  $L_{2o}$ . The resulting nominal loop transmission is shown in Figure 4-14.

$$L_{1oe} = \frac{(9)10^9 (s + 4)^2 (s + 17) (s + 50) (s + 57.43)}{(s - 0.01005) (s + .9921) (s + 10)^2 (s + 54.46) (s + 83) \times (s + 100) (s + 900 \pm j1200)}$$

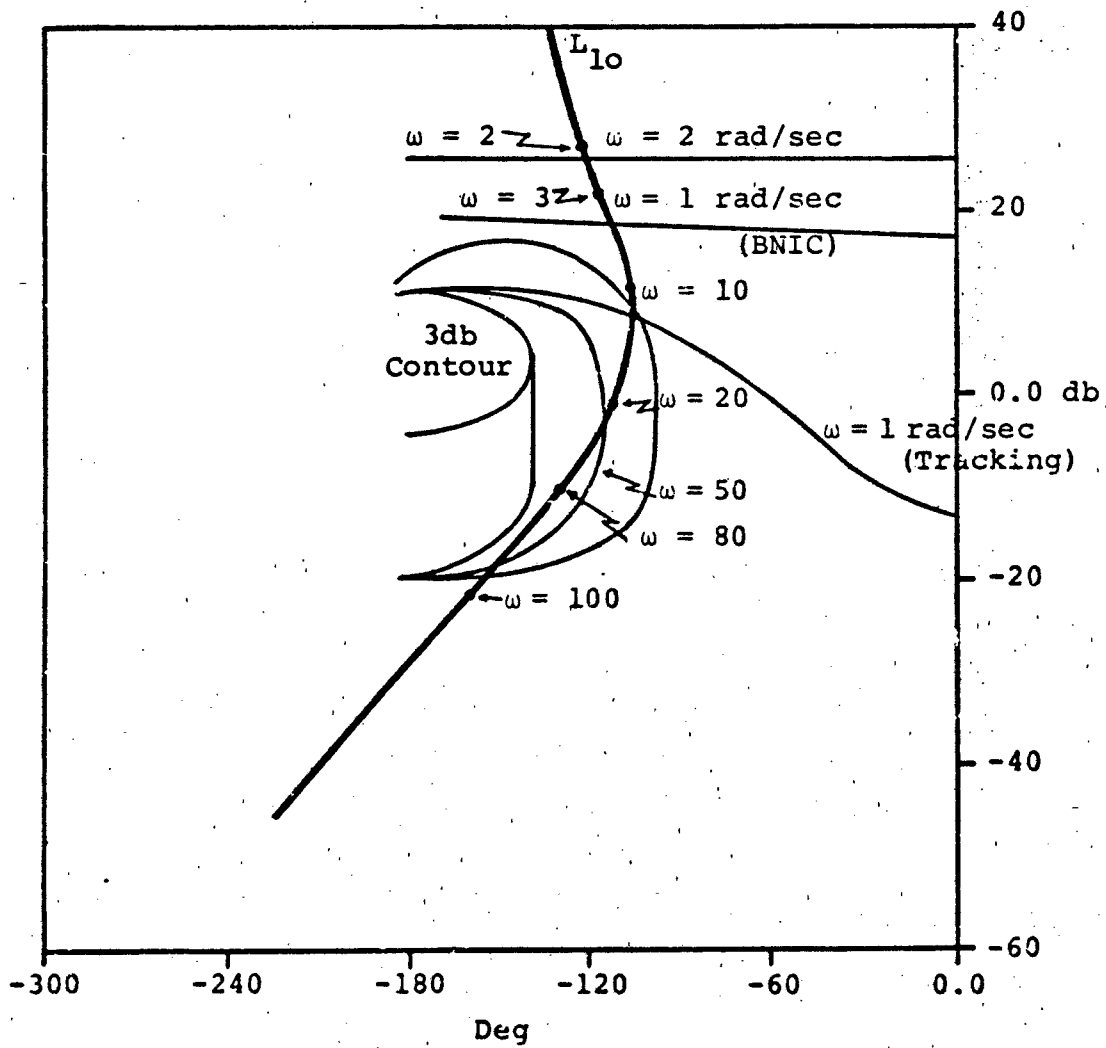


Fig. 4-14. Bounds on  $L_{10e}$

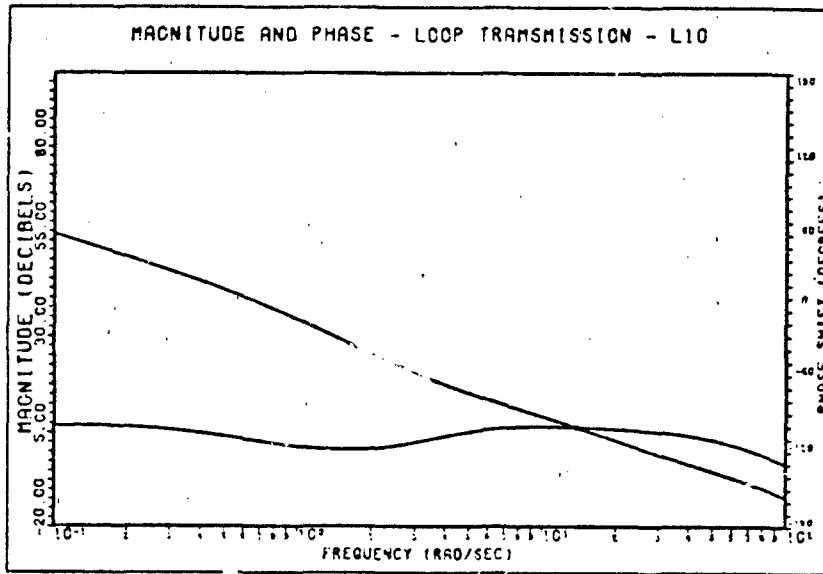


Fig. 4-15. Magnitude and Phase of Nominal Loop Transmission for Loop One

and using the relationship

$$L_{1oe} = g_1 q_{11oe}$$

The corresponding compensator  $g_1$  is

$$g_1 = \frac{(1.946)10^{10} (s + 4)^2 (s + 17) (s + 50)}{(s + 10)^2 (s + 83) (s + 100) (s + 900 \pm j1200)}$$

The magnitude and phase of  $L_{1oe}$  is shown in Figure 4-15.

#### Pre-Filter Design $F_{11}$

The design of the pre-filter is accomplished in the same manner as for the pre-filter  $f_{22}$ . The required bounds of  $f_{11}$  are shown in Figure 4-16. The resulting pre-filter is:

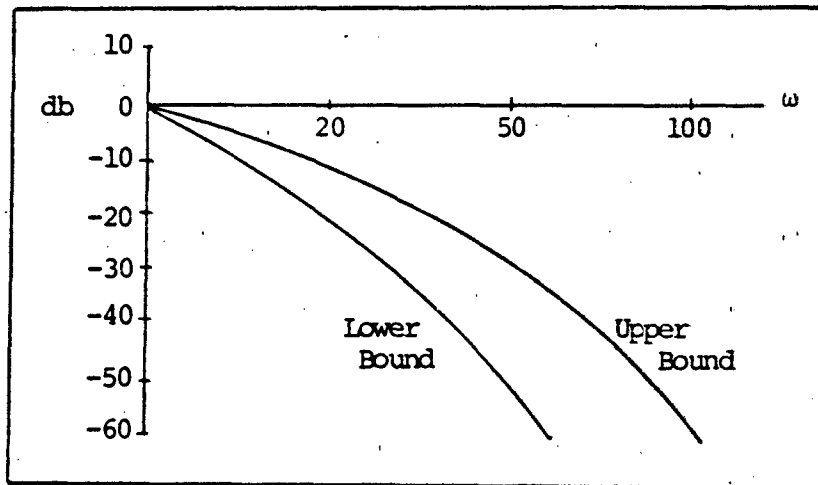


Fig. 4-16. Bounds on Pre-Filter  $F_{11}$

$$f_{11} = \frac{0.9}{(s + 0.9)(s + 1)}$$

This pre-filter now positions the desired response within the given frequency tolerances.

This concludes the design of the robust lateral controller for the sideslip and coordinated turn maneuvers.

#### IV-7 Summary

This chapter illustrates the method used in the development of the required 2x2 MIMO system by mathematically eliminating the yaw angle output from the model. This 2x2 MIMO system is then used to show the design methodology in developing the required elements,  $g_1$ ,  $g_2$ ,

$f_{11}$ , and  $f_{22}$ , used to develop a controller which is capable of operating over the three flight conditions selected for this thesis.

The resulting responses of the system for a given input are simulated in Chapter VI.



## V. Longitudinal Design

### V-1 Introduction

This chapter contains the design of a robust longitudinal controller for the KC-135 aircraft. The three-degrees-of-freedom model developed in Chapter III is used in the design to perform one maneuver. This is a commanded pitch pointing maneuver. For this maneuver, a four-degree pitch angle is commanded with minimum change in altitude  $h$ , and horizontal velocity  $u$ . Ideally, the outputs wanted for  $h$  and  $u$  respectively are zero. The design of the longitudinal controller is completed using the improved design technique outlined in Chapter III.

The  $q_{ij}$ 's are determined using the  $3 \times 3$  input and output matrices which are required in this design. The specifications are modeled in the time domain and converted to the frequency domain. For these specifications, the nominal loop transmission  $L_{30}$  is designed. The second loop designed is loop 1 and the nominal loop transmission  $L_{10}$  is obtained using the unimproved design technique. The last loop designed is loop two and the required nominal loop transmission  $L_{20}$  is obtained using the improved design approach. The first part of this design is accomplished using the equations for the rigid aircraft. The second

part of the design includes the first and second bending modes thus eliminating the rigid body constraint. A comparison is made between the design for the rigid aircraft and the design which includes the bending modes. Appendix F contains the data for the  $q_{ij}$ 's derived from the numerical analysis program. Also outlined in Appendix F are the required models for F.C.'s #2, #3 and the time domain specification models required in this design. The numerical analysis program and required subroutines are included in Reference 19.

#### V-2 Input and Output Matrices

The equations of motion required in this design are developed in Chapter III. The required equations are:

$$\begin{aligned} \frac{(X_1, S)h}{U_0} &= [X_{q, S} + (X_{\theta} - X_1)]\theta + (S - X_u)u \\ &= X_{e, S} \delta_e + X_{sb, S} \delta_{sb} + X_{T, S} T \end{aligned} \quad (5-1)$$

$$\begin{aligned} \frac{-S(S - Z_1, h)}{U_0} &+ [S(1 - Z_{q, S}) - (Z_{\theta, S} + Z_{u, S})]\theta - Z_{u, S}u \\ &= Z_{e, S} \delta_e + Z_{sb, S} \delta_{sb} \end{aligned} \quad (5-2)$$

$$\begin{aligned} \frac{(M_1, S)h}{U_0} &+ [S^2 - M_{q, S} - (M_{\theta, S} + M_{u, S})]\theta - M_{u, S}u \\ &= M_{e, S} \delta_e + M_{sb, S} \delta_{sb} \end{aligned} \quad (5-3)$$

Substituting the primed body axis coefficients listed in Appendix C for F.C. #1 into Equations (5-1) to (5-3) and writing in matrix form yields:

$$\begin{bmatrix}
 .0411S & .53477S - .02669 & S + .0029646 \\
 -.07691S^2 - .0417S & .007034S + .54404 & .004883 \\
 -.21507S & S^2 + .7537S + 2.79589 & -.010529
 \end{bmatrix}
 \begin{bmatrix}
 h \\
 \theta \\
 u
 \end{bmatrix}
 =
 \begin{bmatrix}
 .011617 & -.082712 & .0495 \\
 -.021319 & .031962 & 0 \\
 -1.64897 & .173339 & 0
 \end{bmatrix}
 \begin{bmatrix}
 \delta_e \\
 \delta_{sb} \\
 \delta_T
 \end{bmatrix}
 \quad (5-4)$$

The resulting equations for F.C.'s #2 and #3 are included in Appendix F.

Equation (5-4) is in the general form

$$\underline{MY} = \underline{N}\delta$$

$$\underline{Y} = \underline{M}^{-1} \underline{N}\delta$$

where  $\underline{P} = \underline{M}^{-1} \underline{N}$

and  $\underline{P}^{-1} = \underline{N}^{-1} \underline{M} = \underline{Q}'$

The first constraint on the system is that the inverse of  $\underline{P}$  must exist. Since the inverse of  $\underline{N}$  exists (i.e.,  $\underline{N}$  is nonsingular), then the inverse of  $\underline{P}$  exists. Likewise, the inverse of  $\underline{M}$  exists; therefore,  $\underline{P}$  is nonsingular.

Q' is computed using a numerical analysis program (Reference 19) and the resulting magnitude and phase of  $q_{ij}$  are obtained. The  $q_{ij}$ 's required in the design process are:  $q_{ij} = 1/q'_{ij}$ . Therefore, the inverse of the  $q'_{ij}$ 's are obtained. The resulting  $q_{ij}$ 's are synthesized from the numerical data obtained from the computer program. The three required diagonal  $q_{ij}$ 's for the design of the three nominal loop transmissions for each F.C. are as follows.

Flight Condition #1:

$$q_{11} = \frac{-3.673}{s(s + 0.0271)}$$

$$q_{22} = \frac{-2.253887}{(s + 6.359)(s - 6.147)}$$

$$q_{33} = \frac{0.0498}{(s + 0.01663)}$$

Flight Condition #2:

$$q_{11} = \frac{-2.71289}{s(s + .175125)}$$

$$q_{22} = \frac{-2.36022}{(s + 6.545)(s - 6.4353)}$$

$$q_{33} = \frac{0.034}{(s + 0.01846)}$$

Flight Condition #3

$$q_{11} = \frac{-2.40529}{s(s + 0.051)}$$

$$q_{22} = \frac{-1.49166}{(S + 4.385)(S - 4.1163)}$$

$$q_{33} = \frac{0.126802}{(S + 0.0854)}$$

For this design the improved design technique is used. Therefore, the second constraint on the system is that, as  $S \rightarrow \infty$ ,  $q_{11}$ ,  $q_{22}$  and  $q_{33}$  do not change sign. This constraint is met for the above functions.

### V-3 Effective SISO Systems

The 3x3 system is represented as nine SISO systems. These nine SISO systems are shown in Figure 5-1. In general, the SISO equations are written as

$$t_{ij} = \frac{f_{ij}L_i + d_{ij}q_{ii}}{1 + L_i} \quad (5-5)$$

where  $L_i = g_i q_{ii}$

and  $d_{ij} = -\sum_k t_{kj}/q_{ij}$  for  $k \neq i$

For this design the command inputs  $r_1$  and  $r_3$  are zero. The command input  $r_2$  (pitch angle) is 4 degrees. It is desired that for the given input,  $r_2$ , the output  $Y_{22}$  tracks the input and the outputs  $Y_{12}$  and  $Y_{32}$  be ideally zero.

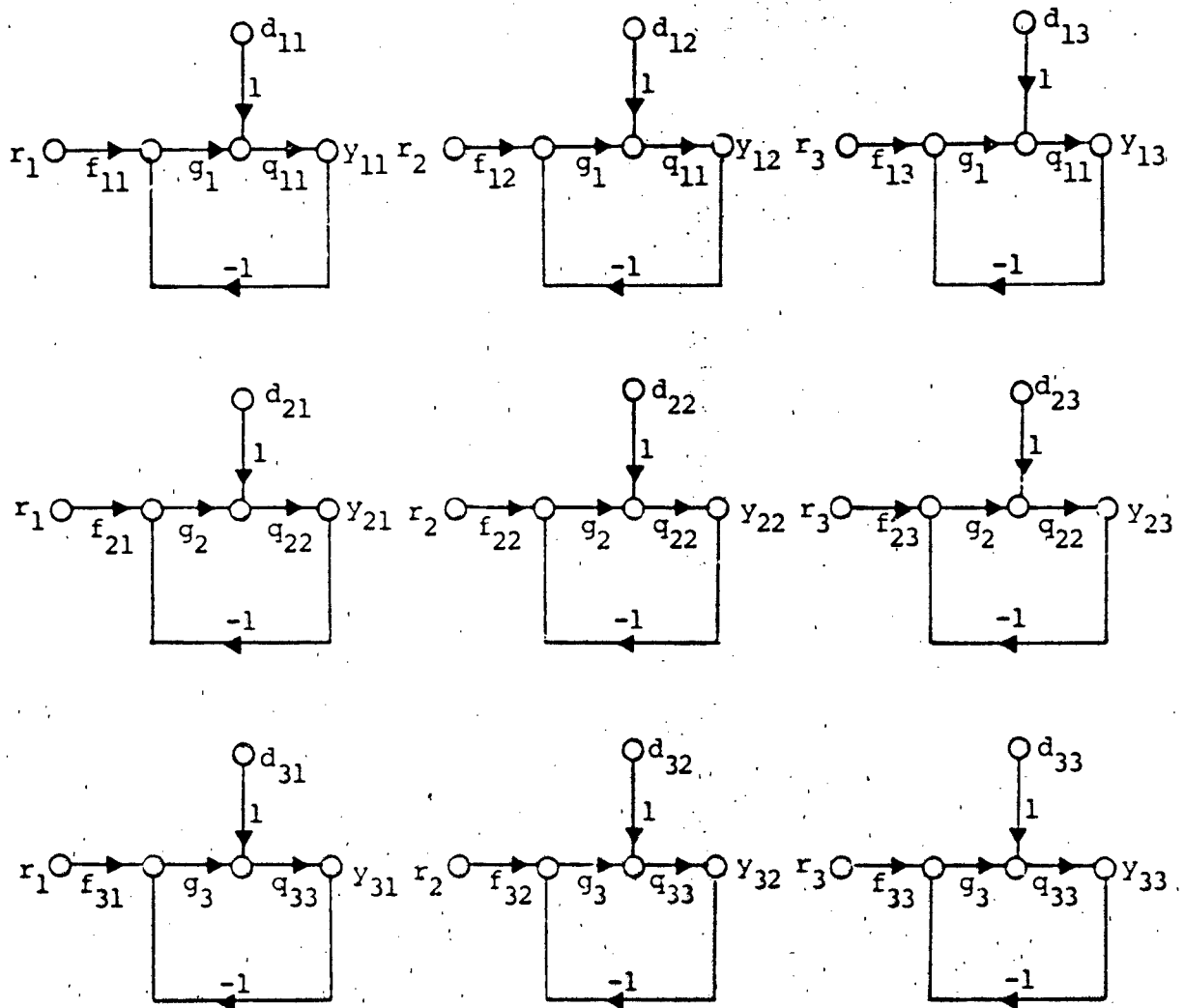


Fig. 5-1. Effective SISO Systems for 3x3 MIMO Problem

V-4      Response Models

The response models for this design are developed from Reference 17. In this reference an identical maneuver was designed and demonstrated using the Porter design technique. The specifications selected for this design are as follows:

Pitch angle command (pitch pointing maneuver):

$T_U$  -- optimal settling time,  $t_s$ , of 6 seconds  
(i.e.,  $t_s$  is  $\pm 2$  percent of final value).

$T_L$  -- worst acceptable case is a settling time,  $t_s$ , of 10 seconds.

$T_D$  -- the acceptable or worst case for the outputs  $h$  and  $u$  ( $Y_{32}$ ,  $Y_{12}$ ) is a peak value,  $M_p$ , of 0.5 and 1.0 respectively and they approach zero in approximately 10 seconds.

The above time domain-specification models are included in Appendix F.

V-5      Loop Three Design

The design of loop three is selected to be designed first since it has the smallest amount of uncertainty.

Also, loop three is a BNIC loop which simplifies the design process since the only requirement on this loop is that the output  $Y_{32}$  be below a certain allowable maximum,  $T_D$ , for the given input  $r_2$ .

The SISO system used in this design is shown in Figure 5-2. Note that this SISO system is obtained due to the fact that  $r_1$  and  $r_3$  are zero and the pre-filter  $f_{32}$  is selected to be zero. Therefore, the three effective loops shown in Figure 5-1 reduce to Figure 5-2.

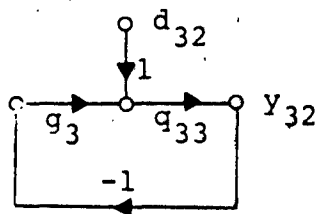


Fig. 5-2. The Effective SISO System for Loop 3

where 
$$d_{32} = - \left[ \frac{t_{12}}{q_{31}} + \frac{t_{22}}{q_{32}} \right]$$

The required equation for the design of the loop transmission is as follows:

$$t_{32} = - \left[ \frac{t_{12}q_{33}}{q_{31}(1+L_3)} + \frac{t_{22}q_{33}}{q_{32}(1+L_3)} \right] \quad (5-6)$$

where  $L_3 = g_3q_{33}$

It is desired that the magnitude of  $t_{32}$  be below some acceptable maximum (i.e., the bound  $T_D = b_{32}$ ). Also, the magnitudes selected for  $t_{12}$  and  $t_{22}$  are the maximum allowable responses. These responses are  $b_{12}$  and  $b_{22}$  respectively. Thus equation (5-6) is rearranged into the desired design equation (5-7).



$$|1 + L_3| \geq \left| \frac{1}{b_{32}} \left[ \frac{b_{12}q_{33}}{q_{31}} + \frac{b_{22}q_{33}}{q_{32}} \right] \right| \quad (5-7)$$

For low frequencies assume  $L_3 \gg 1$ ; therefore, the  $q_{33}$  term in Equation (5-7) cancels. Thus multiplying Equation (5-7) by  $q_{330}$  and assuming the worst case situation yields

$$|L_{30}| \geq \left| \frac{q_{330}}{b_{32}} \left[ \frac{|b_{12}|}{|q_{31}|} + \frac{|b_{22}|}{|q_{32}|} \right] \right| \quad (5-8)$$

Equation (5-8) is used in determining the required bounds on  $L_{30}$  at low frequencies. To ensure positive phase and gain margins the universal high frequency bound is selected to be the -3db contour line on the inverted Nichols Chart as outlined in Appendix A. Thus the design requires that

$$\text{Lm } |1 + L_3| \geq -3\text{db}$$

The magnitudes of  $q_{33}$  for each of the three F.C.'s are shown in Figure 5-3.

For the design of  $L_{30}$ , F.C. #2 is selected as the nominal plant. Table 5-1 contains the magnitude of the elements of Equation (5-8) required in the determination of  $L_{30}$  for  $\omega = 0.1$  rad/sec.

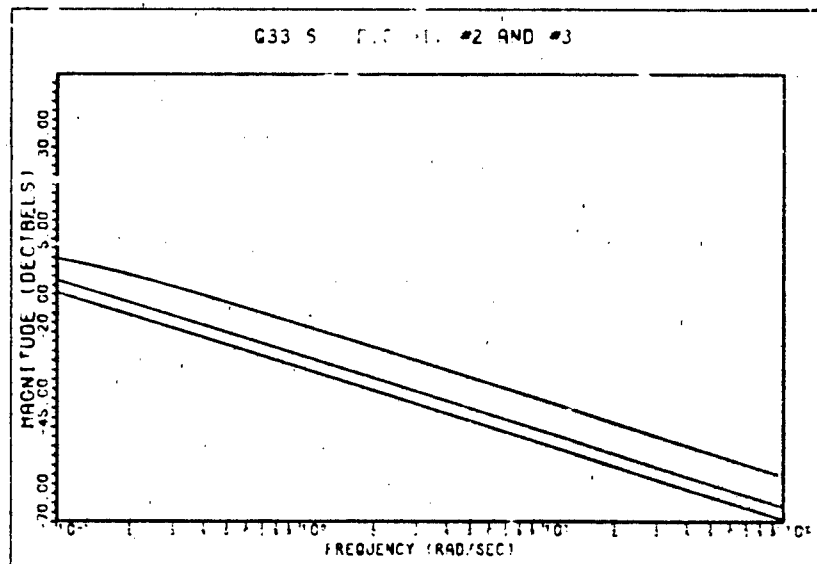


Fig. 5-3. Magnitude of  $q_{33}$  for F.C.'s #1, #2 and #3

TABLE 5-1

DESIGN EQUATION ELEMENTS FOR  $\omega = 0.1$  RAD/SEC

Element	F.C. #1	F.C. #2	F.C. #3
$ b_{12} $	-12.9	-12.9	-12.9
$ b_{22} $	0	0	0
$ b_{32} $	-6.9	-6.9	-6.9
$ q_{330} $	-9.6	-9.6	-9.6
$ q_{31} $	17.0	13.8	23.3
$ q_{32} $	-28.9	-32.5	-13.9

For each of the three F.C.'s the bound on  $Lm[L_{30}]$  is determined using Equation (5-8). The bound for each flight condition is as follows:

$$\text{F.C. \#1: } Lm |L_{30}| \geq 26.2 \text{ db}$$

$$\text{F.C. \#2: } Lm |L_{30}| \geq 29.8 \text{ db}$$

$$\text{F.C. \#3: } Lm |L_{30}| \geq 10.9 \text{ db}$$

The dominant bound occurs for F.C. #2 and is 29.8db. Therefore, at this frequency,  $L_{30}$  must be on or above 29.8db. It is to be noted that at this frequency the assumption that  $|L_3| \gg 1$  is a good assumption.

At and above  $\omega = 1.0$  rad/sec the approximation given by Equation (5-8) no longer holds true. Therefore, at and above  $\omega = 1.0$  rad/sec, the template of  $q_{33}$  must be used in the determination of the required bounds on  $L_{30}$  in conjunction with Equation (5-7).

It is found that at and above  $\omega = 1.0$  rad/sec the -3db contour (UHF bound) becomes the constraining bound on  $L_{30}$ . The other constraint is that at each frequency the template  $q_{33}$  not penetrate the -3db contour. The template of  $q_{33}$  at and above  $\omega = 1.0$  rad/sec is a straight line with a magnitude of 11.4db. The bounds for the loop transmission,  $L_{30}$ , are shown in Figure 5-4. Note that the magnitude of the  $q_{33}$  template generates the length of the barrel

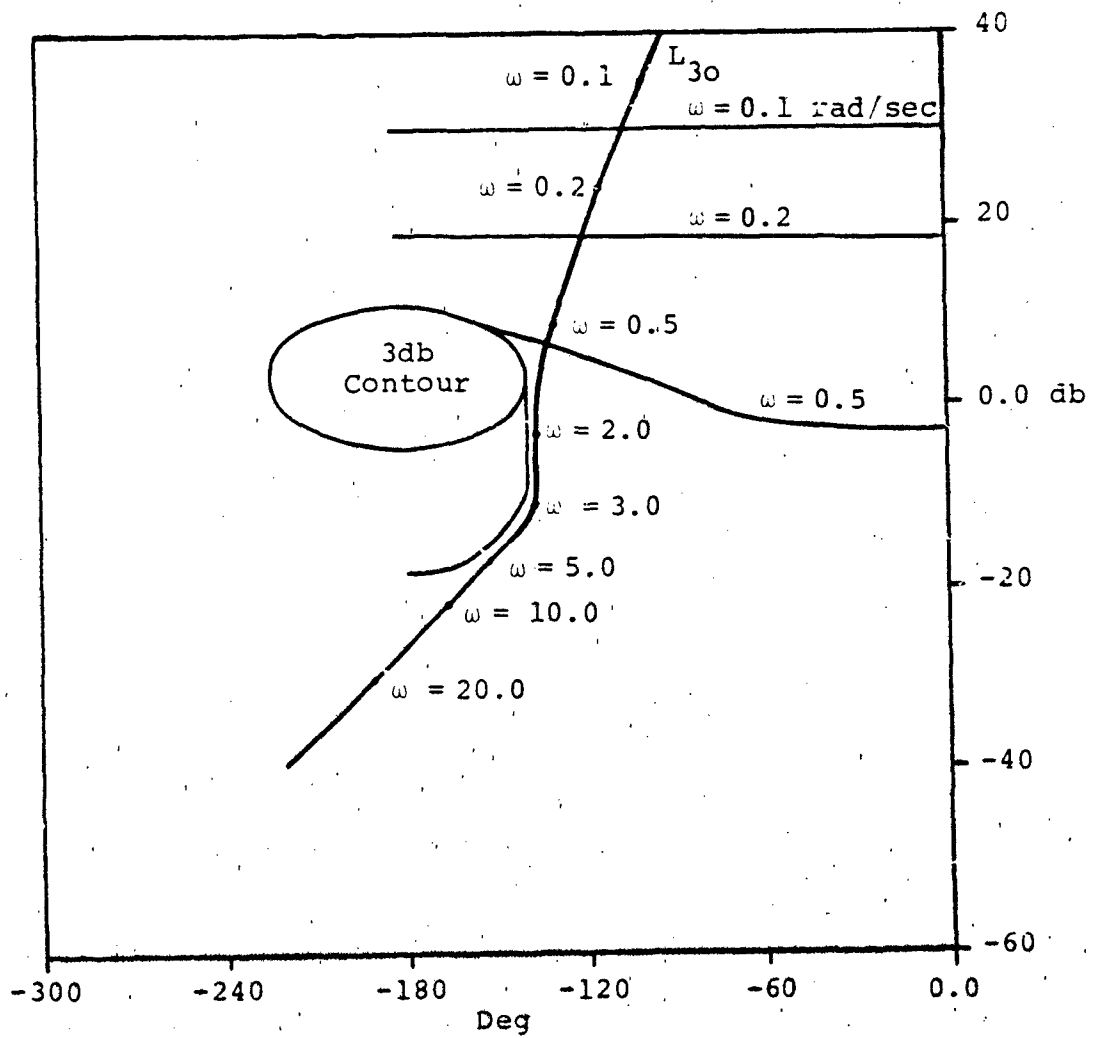


Fig. 5-4. Bounds and Nominal Loop Transmission,  $L_{30}$

extending down from the 3db contour. The templates of  $q_{33}$  are shown in Appendix F.

The nominal loop transmission,  $L_{30}$ , is derived using Figure 5-4 and the resulting nominal loop transmission is as follows:

$$L_{30} = \frac{7290 (S + 2)}{S(S + 0.5)(S + 10)(S + 18 \pm j24)}$$

and the resulting compensator,  $g_3$ , is derived from

$$L_{30} = g_3 q_{330}$$

Therefore  $g_3 = \frac{(2.144)(10^5)(S + 2)(S + 0.01846)}{S(S + 0.5)(S + 10)(S + 18 \pm j24)}$

The magnitude and phase of  $L_{30}$  is shown in Figure 5-5.

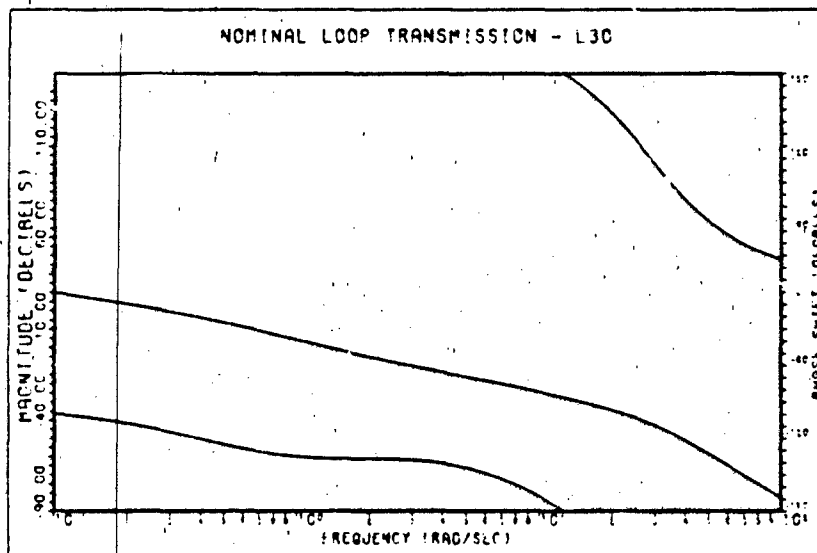


Figure 5-5. Magnitude and Phase,  $L_{30}$

### Loop One Design

This loop is selected to be designed second since loop one is also a BNIC loop. The effective SISO system reduces to the form shown in Figure 5-6.

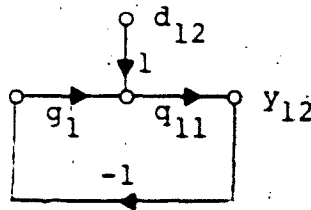


Fig. 5-6. Effective SISO System for Loop One

The required design equation developed from Figure 5-6 is

$$t_{12} = \frac{d_{12}q_{11}}{1 + L_1} \quad (5-9)$$

where

$$d_{12} = - \left[ \frac{t_{22}}{q_{12}} + \frac{t_{32}}{q_{13}} \right]$$

Equation (5-9) is rearranged to form the design equation

$$|1 + L_1| \leq \left| \frac{q_{11}}{b_{12}} \left[ \frac{b_{22}}{q_{12}} + \frac{b_{32}}{q_{13}} \right] \right| \quad (5-10)$$

where  $t_{12}$ ,  $t_{22}$ , and  $t_{32}$  are selected as the maximum allowable design specification responses  $b_{12}$ ,  $b_{22}$ , and  $b_{32}$  respectively. However, at low frequency, it is assumed that  $L_1 \gg 1$ . Therefore  $q_{11}$  in Equation (5-10) cancels. Thus multiply Equation (5-10) by  $q_{11}$  it can be written as

$$L_{10} = \frac{a_{110}}{b_{12}} \left[ \frac{b_{22}}{a_{12}} + \frac{b_{32}}{a_{13}} \right] \quad (5-11)$$

Note that Equation (5-11) is only valid over the frequency range where  $L_1 \gg 1$ . Thus it must be verified that the assumption is a good approximation. The development of  $L_{10}$  is accomplished in a similar manner as for the nominal loop transmission,  $L_{30}$ . Thus the design of this loop is not highlighted. The resulting bounds and the nominal loop transmission,  $L_{10}$ , are shown in Figure 5-7. The nominal loop transmission is:

$$L_{10} = \frac{3940(S + 4)}{S(S + 0.1751)(S + 24 \pm j32)} \quad (5-12)$$

and the resulting compensator  $g_1$  is

$$g_1 = \frac{-1455(S + 4)}{(S + 24 \pm j32)} \quad (5-13)$$

The magnitude and phase of  $L_{10}$  are shown in Figure 5-8.

#### Tracking Loop (Loop Two)

The last loop to be designed is loop 2 and this is accomplished using the improved design technique. Thus the next step in the design is to determine the required bounds on the tracking loop. The effective SISO system for this design is shown in Figure 5-9.

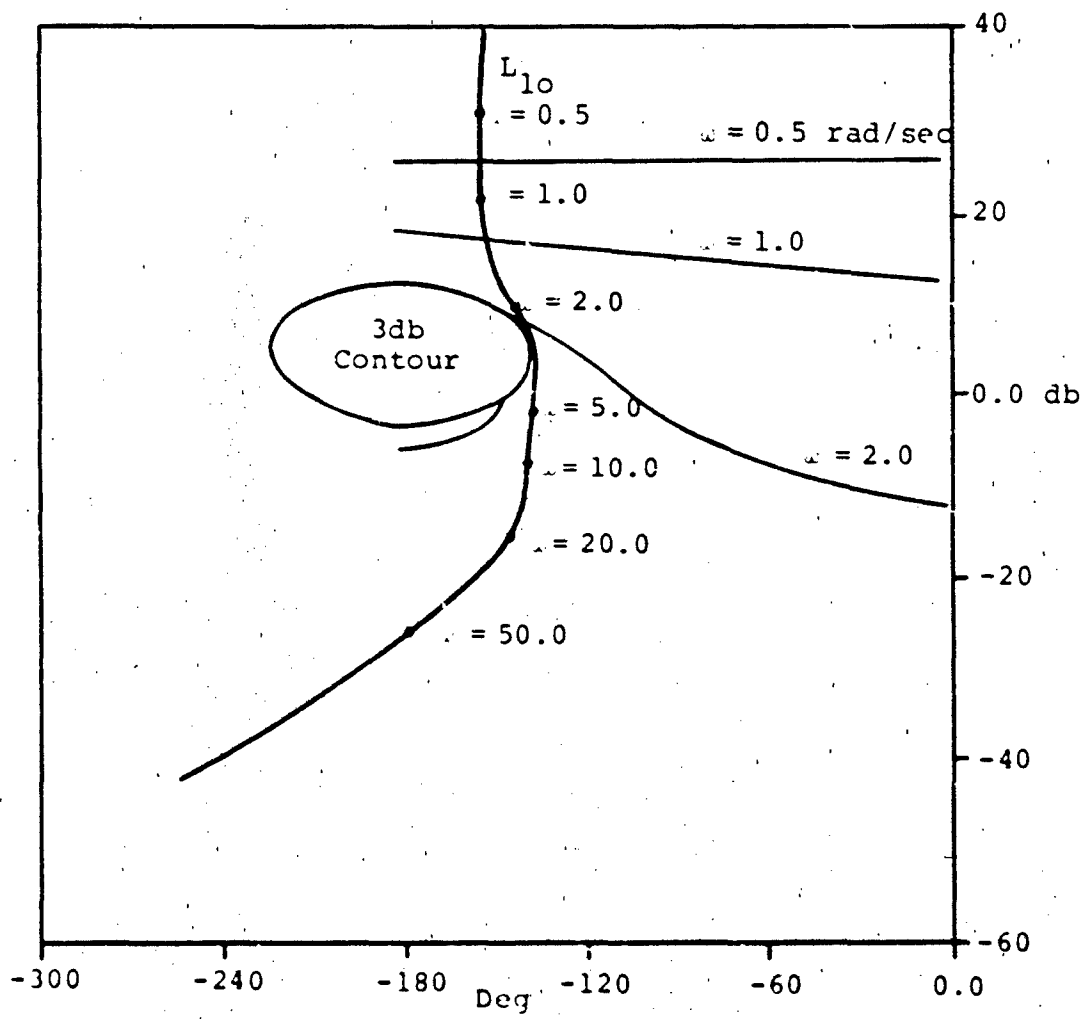


Fig. 5-7. Bounds and Nominal Loop Transmission,  $L_{10}$



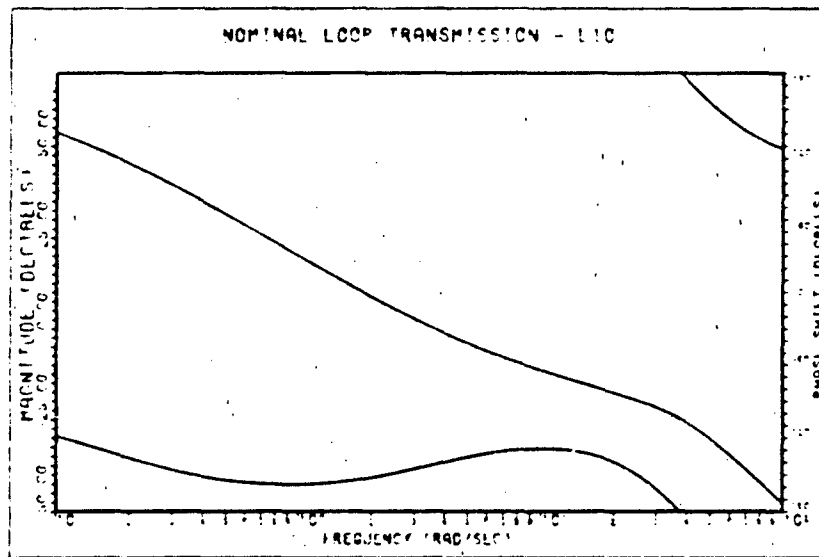


Fig. 5-8. Magnitude and Phase,  $L_{10}$

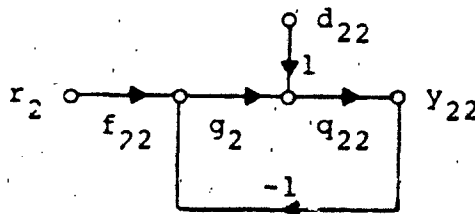


Fig. 5-9. Effective SISO System, Loop 2

Equation (5-14) is developed from Figure 5-5 and is

$$t_{22} = \frac{f_{22}L_2 + d_{22}q_{22}}{1 + L_2} \quad (5-14)$$

where

$$d_{22} = - \left[ \frac{t_{12}}{q_{21}} + \frac{t_{32}}{q_{23}} \right]$$

The design of loop two is accomplished using the improved design technique. The required equations as developed in Chapter III are:

$$t_{22} = \frac{f_{22}L_{2e} - d_{22e}}{1 + L_{2e}} \quad (5-15)$$

where

$$L_{2e} = \frac{L_2 \varepsilon}{\varepsilon + \Delta} \quad (5-16)$$

$$\varepsilon = (1 + L_1)(1 + L_3) - \gamma_{13}$$

$$\Delta = \gamma_{32}(1 + L_1) + \gamma_{12}(1 + L_3) - (\gamma_{13}u_2 + \gamma_{12}u_3)$$

$$L_{2e} = g_2 q_{22e} : \gamma_{32} = \frac{q_{22}q_{33}}{q_{32}q_{23}}$$

$$\gamma_{12} = \frac{q_{11}q_{22}}{q_{12}q_{21}} \quad \gamma_{13} = \frac{q_{11}q_{33}}{q_{13}q_{31}}$$

$$u_2 = \frac{q_{31}q_{22}}{q_{32}q_{21}} \quad u_2 = \frac{q_{21}q_{33}}{q_{23}q_{31}}$$

and

$$q_{22e} = \frac{q_{22} \varepsilon}{\varepsilon + \Delta} \quad (5-17)$$

$$d_{22e} = \frac{f_{12} L_1 q_{22}^{n_1} + f_{32} L_3 q_{22}^{n_2}}{\epsilon - \lambda} \quad (5-18)$$

Since  $f_{12}$  and  $f_{32}$  are zero, then the design is a simple tracking loop problem. Thus the bounds on  $L_{2oe}$  are determined using the templates of  $q_{22e}$ . The nominal point selected for this design is F.C. #2 and the desired  $q_{22oe}$  is shown in Equation (5-19). The magnitude, phase and templates of  $q_{22e}$  are included in Appendix F.

$$q_{22e} = \frac{0.001745 (S+0.6237+j1.177) (S+0.9812+j3.163) (S+0.1808) (S+125)}{(S+0.585+j1.209) (S+1.944+j1.479) (S-1.394+j2.122) (S+0.1718)} \quad (5-19)$$

Therefore, using the templates generated by  $q_{22e}$  for the three F.C.'s and the upper and lower bounds on the responses, the bounds on  $L_{2oe}$  are determined. The desired bounds on the loop transmission  $L_{2oe}$  are shown in Figure 5-10. Using these bounds the resulting loop transmission is

$$L_{2oe} = \frac{(7.846) (10^6) (S+1) (S+0.6237+j1.177) (S+0.912+j3.163) (S+0.1808) (S+125)}{(S+0.585+j1.209) (S+1.944+j1.479) (S-1.394+j2.121)(S+30) \times (S+390+j520) (S+0.1718)} \quad (5-20)$$

where  $L_{2oe} = g_2 q_{22oe}$

Therefore  $g_2 = \frac{(4.496) (10^9) (S+1)}{(S+30) (S+390+j520)} \quad (5-21)$

It is to be noted that the  $q_{22e}$ 's for each of the three F.C.'s have two poles in the right half plane.

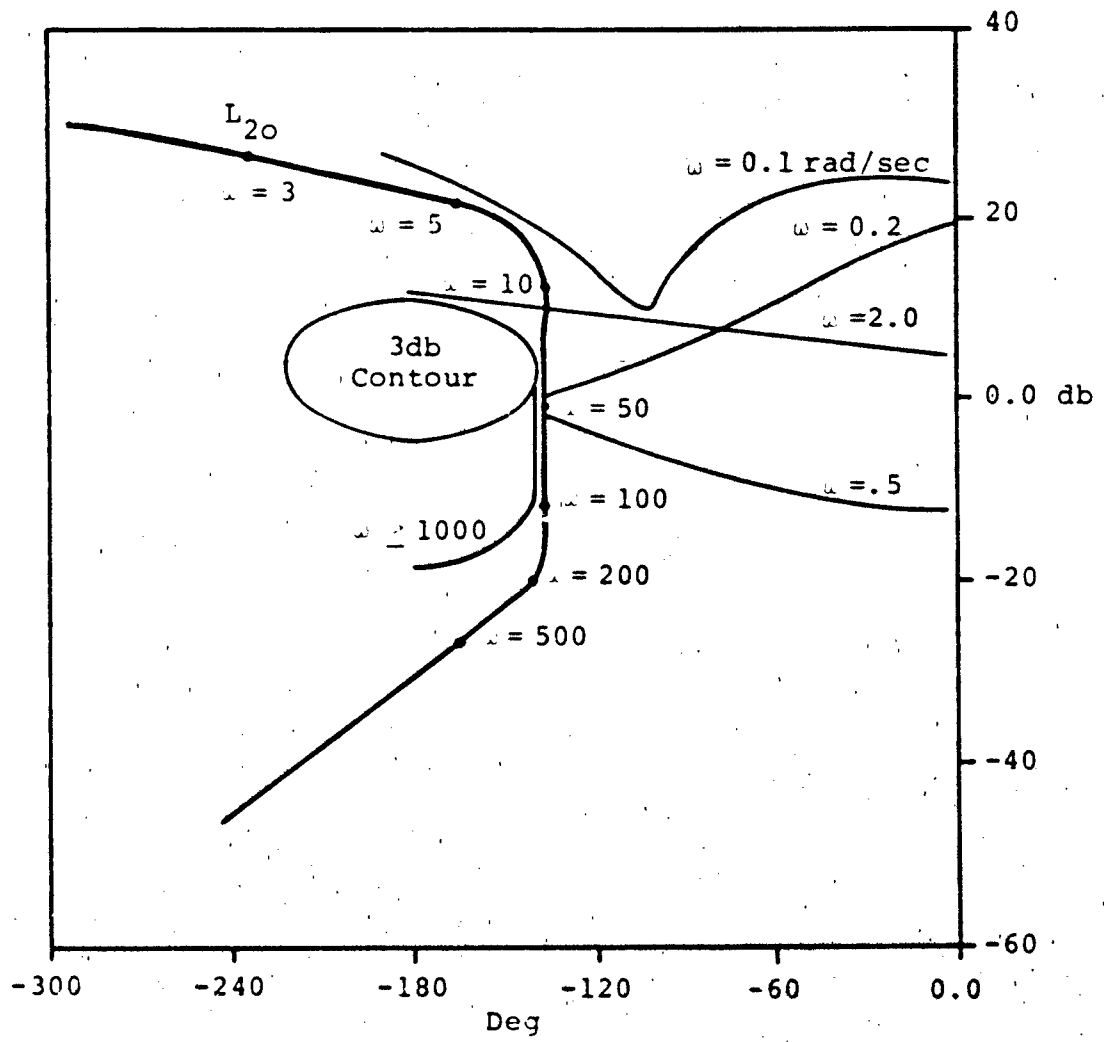


Fig. 5-10. Bounds and Nominal Loop Transmission,  $L_{20e}$

Therefore, these poles must be included in the shaping of  $L_{2oe}$  to guarantee a stable response.

A very important result is obtained in the design of this loop. If this loop is designed using the unimproved design technique a stable response cannot be obtained. This is due to the fact that  $q_{22}$ 's for each of the three F.C.'s has only one pole in the right half plane while the  $q_{22e}$ 's has two poles in the right half plane. These poles result from the designs of loops one and three being taken into account in the design of loop two. Thus it is important to include the previous loop designs in the design of all subsequent loops. The magnitude and phase of  $L_{2oe}$  is shown in Figure 5-11.

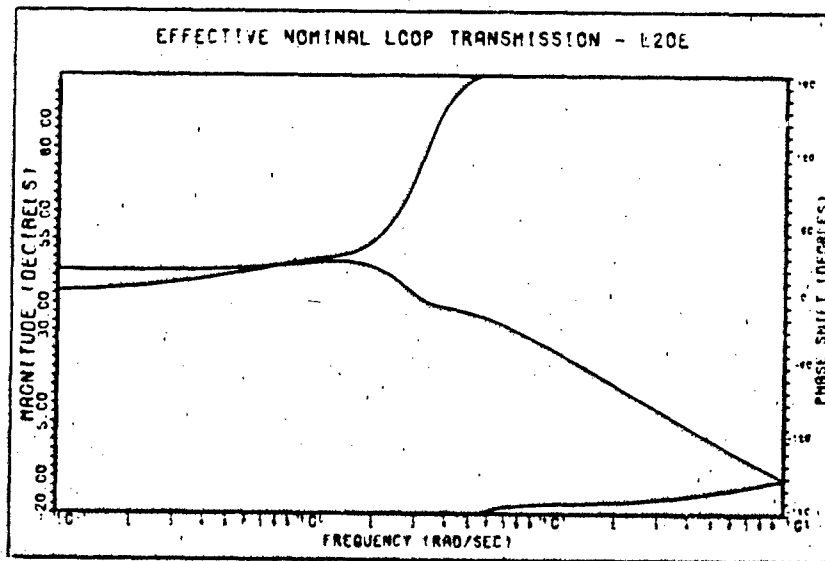


Fig. 5-11. Magnitude and Phase,  $L_{2oe}$

The last part of the loop two design is the development of the required pre-filter,  $f_{22}$ , which places the desired response within the frequency domain specifications. The design of the pre-filter is accomplished as outlined in Appendix A and the resulting pre-filter is

$$f_{22} = \frac{0.3506}{(s + 0.5)(s + 0.54 \pm j0.64)} \quad (5-22)$$

This concludes the design of the 3x3 MIMO system which considers the aircraft as a rigid body. The next section removes the rigid body assumption and treats the aircraft as being elastic (i.e., the first and second body bending modes are included in the 3x3 model).

V-6      Longitudinal Design  
          (Non-Rigid Aircraft)

This design is accomplished using the numerical data obtained from the programs outlined in Reference 19. The third loop is designed first, followed by the first and second loops. The nominal loop transmissions are designed in this order due to the differences in the uncertainties of  $q_{11}$ ,  $q_{22}$  and  $q_{33}$ .

Addition of First and Second  
Body Bending Modes

The first step in this design is to incorporate the bending and rigid models to form a non-rigid model. The form of the rigid aircraft equation is

$$\underline{M}_R \underline{Y} = \underline{N}_R \delta \quad (5-23)$$

where  $\underline{M}_R$  and  $\underline{N}_R$  are defined as the rigid output and input matrices respectively. The form of the elastic aircraft equation is

$$\underline{M}_e \underline{Y} = \underline{N}_e \delta \quad (5-24)$$

where  $\underline{M}_e$  and  $\underline{N}_e$  are defined as the elastic output and input matrices respectively. The required elastic equations are included in Appendix C. Equations (5-23) and (5-24) are written in the following form

$$\underline{Y} = \underline{M}_R^{-1} \underline{N}_R \delta \quad (5-25)$$

and 
$$\underline{Y} = \underline{M}_e^{-1} \underline{N}_e \underline{\delta} \quad (5-26)$$

The input vector  $\underline{\delta}$  is defined as

$$\underline{\delta} = \begin{bmatrix} \delta_e \\ \delta_{sb} \\ \delta_T \end{bmatrix}$$

and the output vector  $\underline{Y}$  is defined as

$$\underline{Y} = \begin{bmatrix} h \\ \theta \\ u \end{bmatrix}$$

Combining the rigid and bending mode equations yields

$$\underline{Y} = \left[ \underline{M}_R^{-1} \underline{N}_R + \underline{M}_e^{-1} \underline{N}_e \right] \underline{\delta} \quad (5-27)$$

Therefore 
$$\underline{P} = \underline{M}_R^{-1} \underline{N}_R + \underline{M}_e^{-1} \underline{N}_e$$

However,  $\underline{P}^{-1}$  is required in the design process. Therefore,  $\underline{P}^{-1}$  is

$$\underline{P}^{-1} = \left[ \underline{M}_R^{-1} \underline{N}_R + \underline{M}_e^{-1} \underline{N}_e \right]^{-1} \quad (5-28)$$

Equation (5-28) is evaluated using numerical analysis with the aid of a computer program (Reference 19). The generated data points for the  $q_{ij}$ 's are included in



Appendix F. Thus with the required magnitudes of the  $q_{ij}$ 's, the design of the 3x3 system including bending modes can now be completed. It is to be noted that the magnitudes of the  $q_{ij}$ 's at low frequencies are essentially unchanged from that of the rigid case. The differences in magnitude and phase occur around the bending mode's natural frequency.

#### V-7 Loop Three Design

The design of loop three is the same as that completed for the rigid aircraft. Since there is no change in the magnitude and phase of  $q_{33}$  over the three F.C.'s, the bounds on  $L_{30}$  do not change over the entire frequency of interest. The only concern in the design of this loop is that the magnitudes of  $q_{31}$  and  $q_{32}$  at and around the first and second bending mode natural frequencies do not change the determined bounds (Equation 5-7) of the rigid aircraft. Since the dominant bound, at  $\omega = 1$  rad/sec and higher, is the 3db UHF oval, the change in magnitudes of  $q_{31}$  and  $q_{32}$  have no effect on the bounds of  $L_{30}$  at the natural frequencies. Therefore, the nominal loop transmission,  $L_{30}$ , design for the rigid aircraft is also used for the non-rigid design.

V-8 Loop One Design

The design of this loop is similar to the design completed for loop one for the rigid aircraft. The only difference between the two designs is that at and around the body bending mode frequencies, large changes in magnitude and phase can occur. However, for this aircraft, the magnitudes of the first and second body bending modes are very small. Therefore, there is only a small change in magnitude and phase of  $q_{11}$  between the rigid and non-rigid aircraft.

The bounds and the nominal loop transmission  $L_{10}$  are shown in Figure 5-12. The resulting nominal loop transmission and compensator are given in Equations (5-29) and (5-30). The magnitude and phase of  $L_{10}$  are shown in Figure 5-13.

$$L_{10} = \frac{3940(S + 4)}{S(S + 0.1751)(S + 24 \pm j32)} \quad (5-29)$$

and

$$g_1 = \frac{-1455(S + 4)}{(S + 24 \pm j32)} \quad (5-30)$$

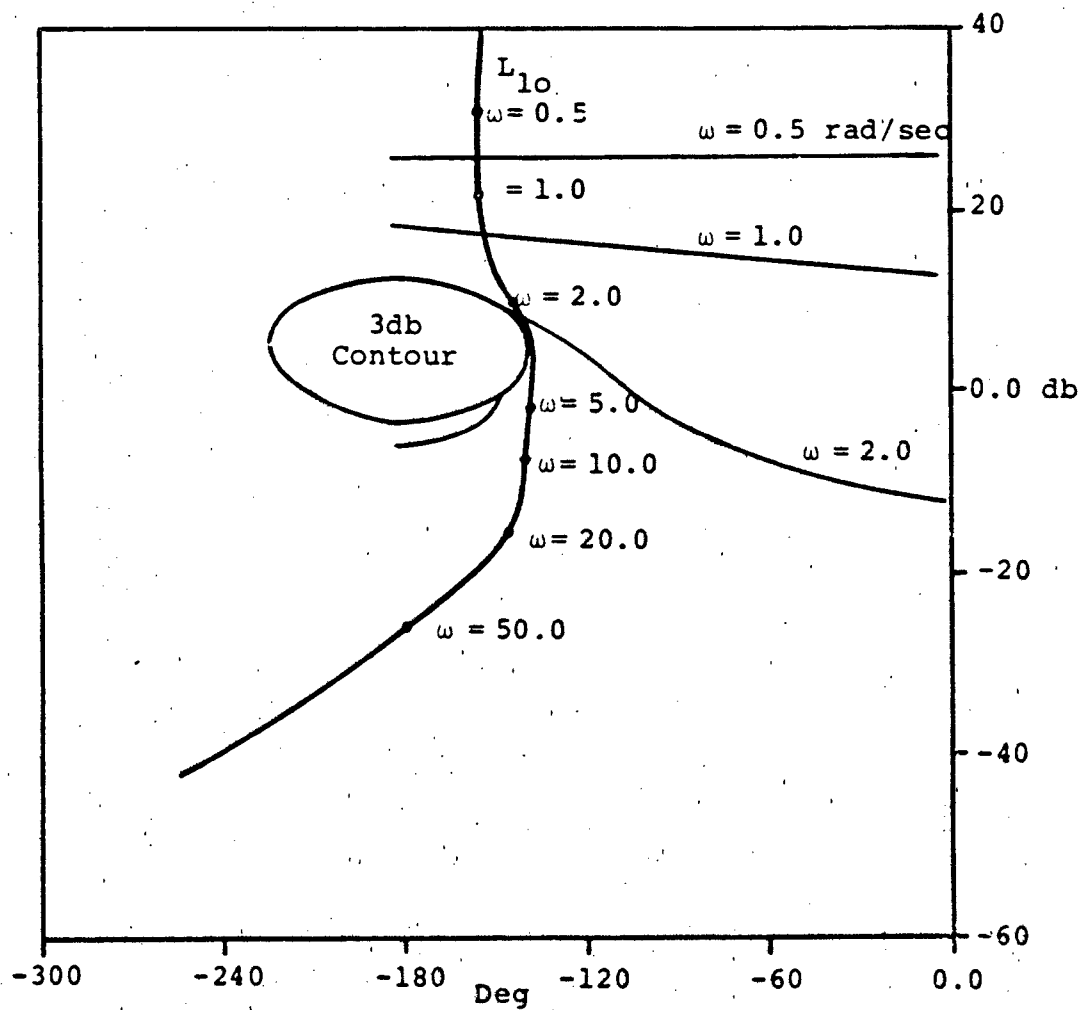


Fig. 5-12. Bounds and Nominal Loop Transmission  $L_{10}$

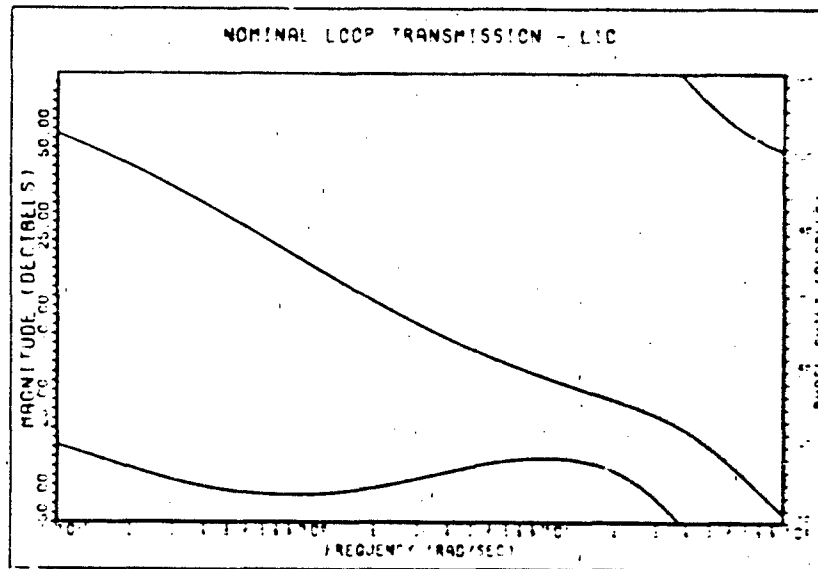


Fig. 5-13. Magnitude and Phase--L<sub>10</sub>

V-9 Loop Two Design

The design of loop two is completed using the improved design technique. This design is similar to the design of loop two for the rigid aircraft. The only difference is that any uncertainty introduced by the body bending modes must be taken into account during the design process. The difference in magnitude and phase of  $q_{22e}$  between the rigid and non-rigid design is very small. Thus the design of this loop is similar to the design of loop two for the rigid aircraft. This design will not be highlighted since it is similar to the design of loop two completed for the rigid aircraft. The  $q_{22e}$ 's for each of the three F.C.'s are included in Appendix F.

The resulting bounds and nominal loop transmission are shown in Figure 5-14. The required nominal loop transmission,  $L_{20}$ , is shown in Equation (5-31) and the resulting compensator,  $g_2$ , is shown in Equation (5-32).

$$L_{20} = \frac{(7.846)(10^6)(s+1)(s+0.6237+j1.177)(s+0.912+j3.163)(s+0.1808)(s+125)}{(s+0.585+j1.209)(s+1.944+j1.479)(s-1.394+j2.121)(s+30) \times (s+390+j520)(s+0.1718)} \quad (5-31)$$

and

$$g_2 = \frac{(4.496)(10^9)(s+1)}{(s+30)(s+390 \pm j520)} \quad (5-32)$$

The magnitude and phase of  $L_{20}$  are shown in Figure 5-15. The desired pre-filter,  $f_{22}$ , is obtained as outlined in Appendix A and the resulting pre-filter is shown in Equation (5-33).

$$f_{22} = \frac{0.3506}{(s+0.5)(s+0.54 \pm j0.64)} \quad (5-33)$$

This concludes the design of the 3x3 system.

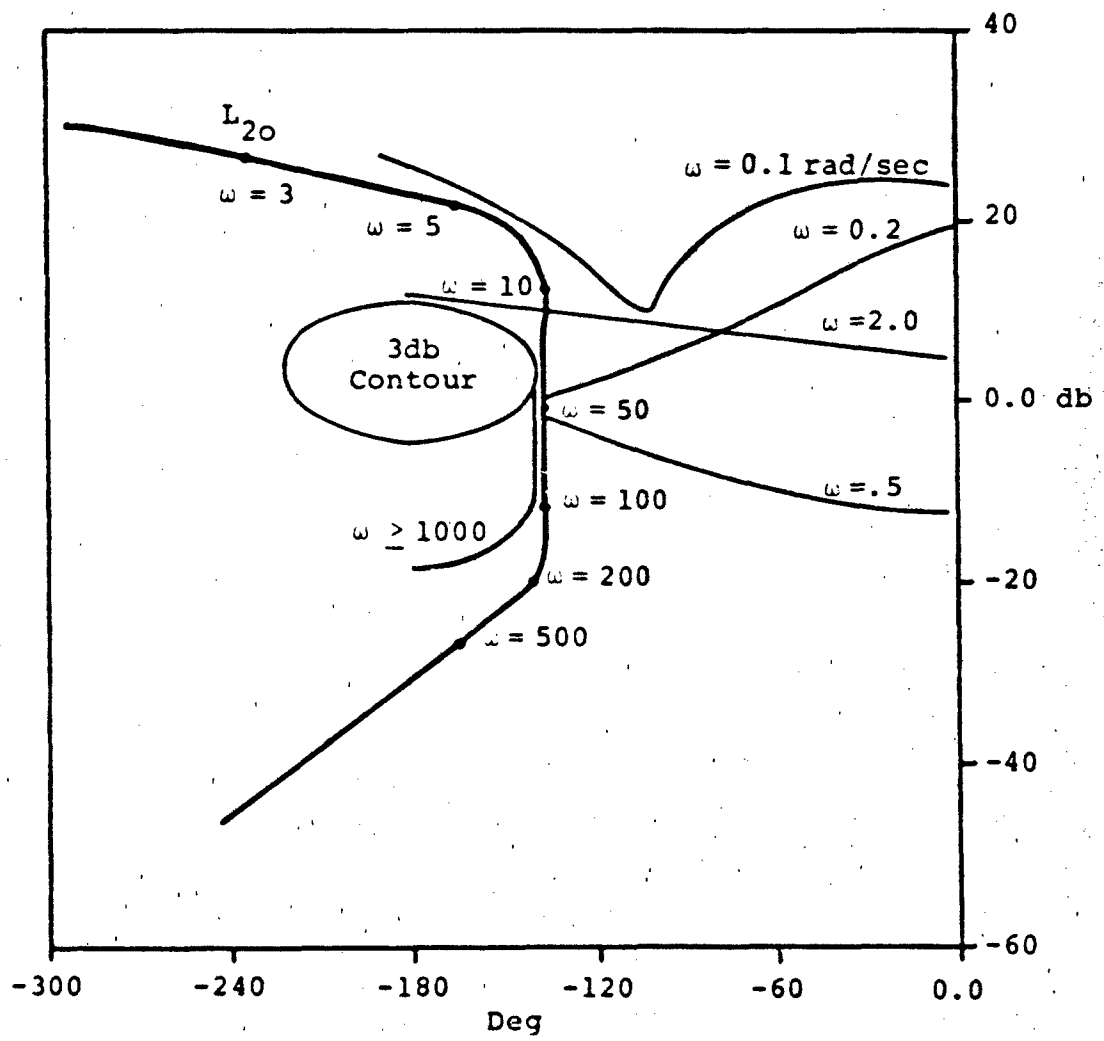


Fig. 5-14. Bounds and Nominal Loop Transmission  $L_{20e}$

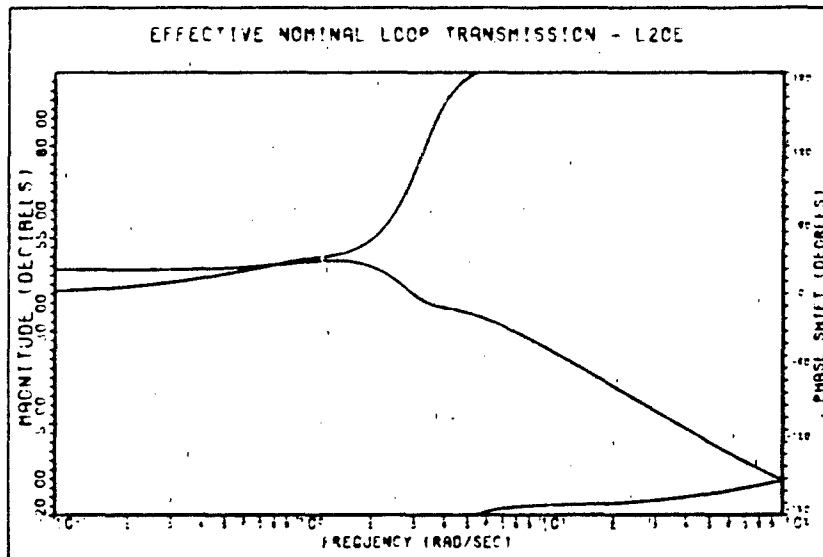


Fig. 5-15. Magnitude and Phase--L<sub>2oe</sub>

V-10 Comparison of Rigid and Non-Rigid Designs

The design, over the entire frequency, for both the rigid and non-rigid models is essentially the same. Thus the design completed for the rigid aircraft is the same as the design for the non-rigid aircraft. The reason that the addition of the first and second body bending modes had very little affect on the design is due to the small magnitudes of both these bending modes.

V-11 Summary

This chapter highlights the design of a 3x3 system with only one command input. The design is first accomplished using the rigid aircraft model and second, the controller is redesigned with the first and second body bending modes (i.e., the rigid constraint on the aircraft model is eliminated). Finally, the effect of introducing the first and second body bending modes is outlined.



## VI. Simulation

### VI-1 Introduction

This chapter contains the simulated responses for both the lateral and longitudinal robust controllers. The first section illustrates the simulated responses obtained for F.C. #3 using the controller developed for the lateral maneuvers and robustness of the lateral design is illustrated. The next section illustrates the simulated responses for F.C. #3 using the controller developed for the longitudinal maneuver and robustness of the design is also illustrated. The simulated responses for F.C.'s #1 and #2 are included in Appendix H.

### VI-2 Lateral Simulation (2x2 Design)

The simulation of this design is obtained using a computer-aided program (Appendix G). It is assumed that this simulation yields realistic motions of the aircraft for each of the given F.C.'s. The first lateral controller developed is for a 30 degree command bank angle maneuver with minimum sideslip (i.e., coordinated turn) and the second maneuver is a 5 degree command sideslip angle with minimum bank angle. This design is demonstrated using two different pre-filters. The first pre-filter has a pair of complex poles with a damping factor of  $\zeta = 0.6$ . The second pre-filter has a pair of real poles. The difference in the response to a step command input is highlighted.

Finally the design is illustrated using a ramp input with a rise time of 1 second for the pre-filters with real roots.

Bank Angle Command Response

The responses shown in Figures 6-1 through 6-4 are for a 30 degree step input bank angle command (complex pre-filter poles). As can be seen from Figure 6-1, the bank angle response has very desirable characteristics. The response starts out slowly and then increases more rapidly as time increases. This is desired in a heavy transport aircraft since it cannot react to rapid changes as can a fighter aircraft. Also if a faster response is required the control surface deflections and rates will be too high. Figure 6-1 is the command bank angle response while Figure 6-2 is the sideslip response due to the bank angle command. Figures 6-3 and 6-4 are the control surface deflections due to a 30 degree step bank angle command. The characteristics of these responses are given in Table 6-1.

TABLE 6-1

BANK ANGLE COMMAND--F.C. #3

	Peak Value	Final Value	Rise Time	Settling Time
$\phi$ (deg)	30.6	30.0	5.52	7.35
$\beta$ (deg)	0.0276	0.0181	--	--
$\delta_r$ (deg)	3.56	--	--	--
$\delta_w$ (deg)	21.9	--	--	--

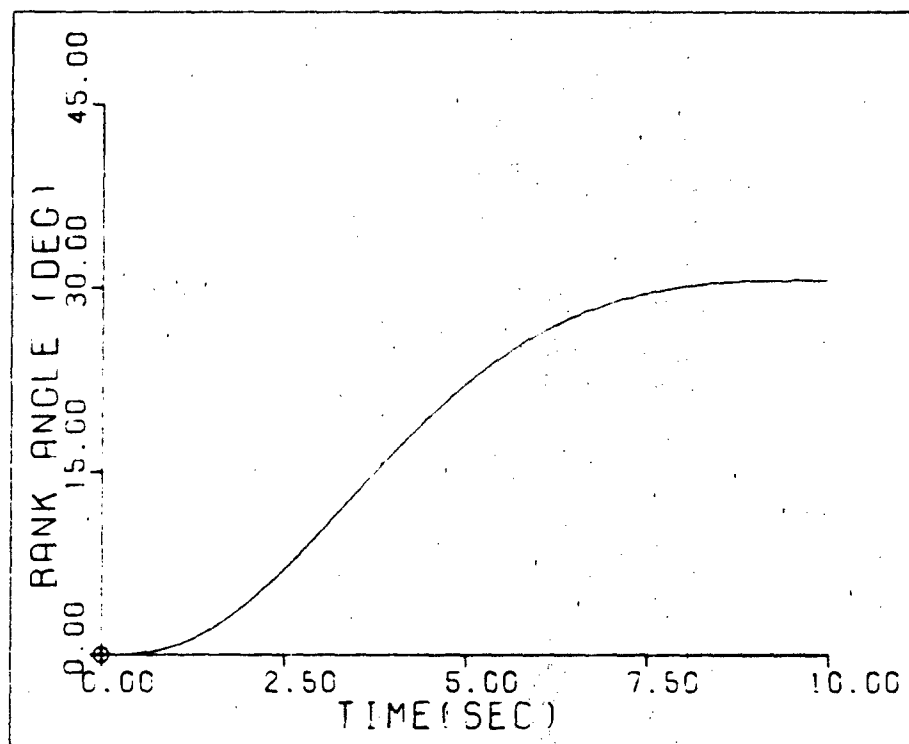


Fig. 6-1. Bank Angle Response--F.C. #3

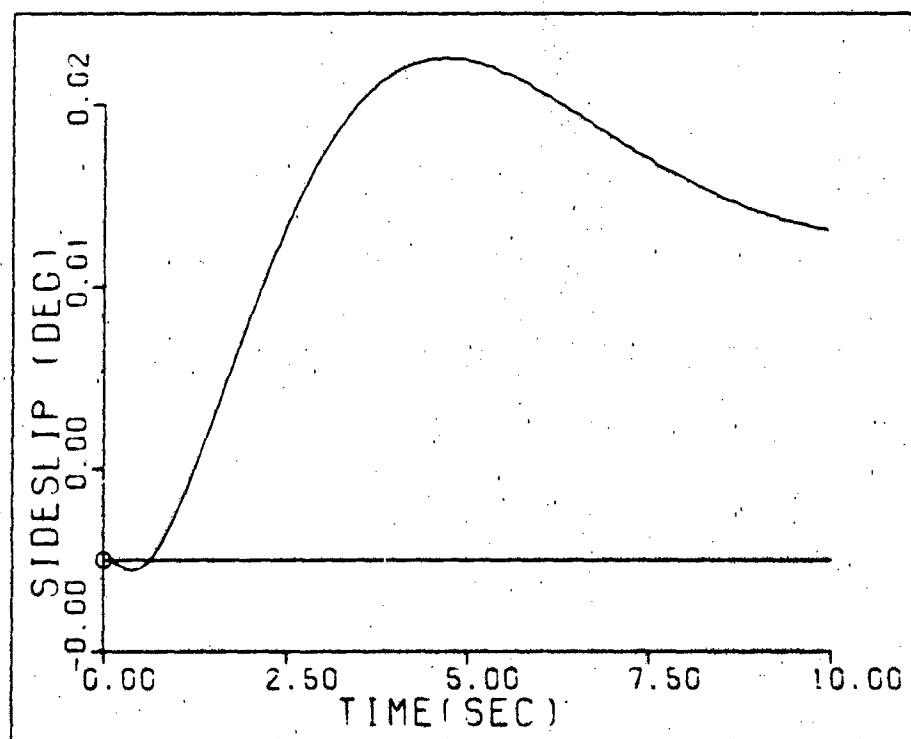


Fig. 6-2. Sideslip Response--F.C. #3

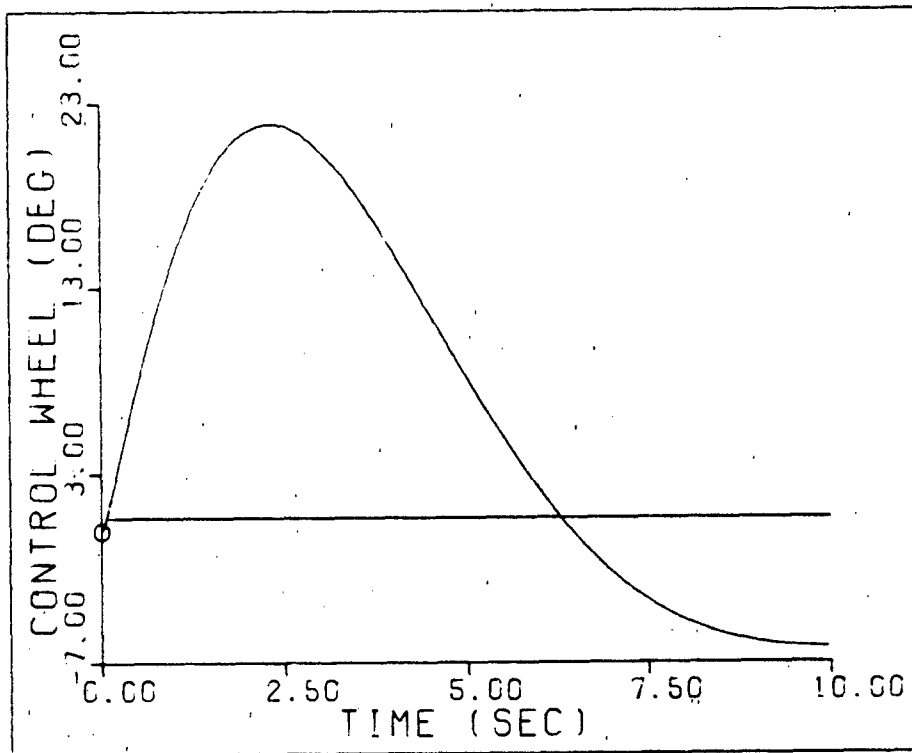


Fig. 6-3. Control Wheel Deflection--F.C. #3

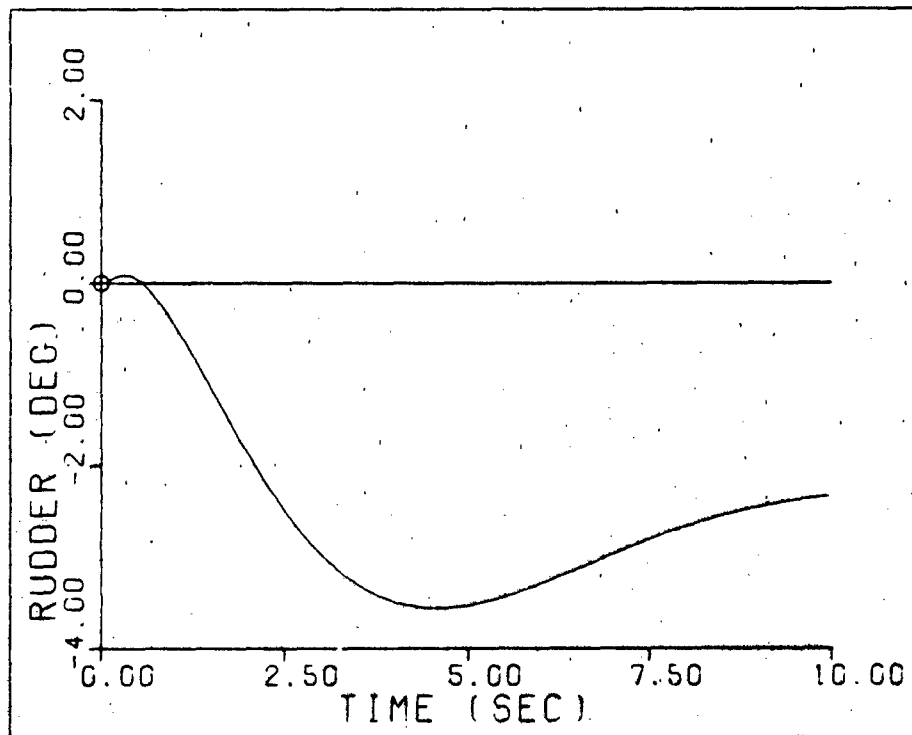


Fig. 6-4. Rudder Deflection--F.C. #3

The responses shown in Figures 6-5 through 6-8 are for a 30 degree step input bank angle command (real pre-filter poles). It is to be noted that the response due to this command input is much faster and the control surface rates are much higher than for the pre-filter with the complex poles. Thus, the pre-filter plays a very important role in the determination of the final output response. Table 6-2 outlines the characteristics of the response due to a 30 degree bank angle command.

TABLE 6-2

BANK ANGLE COMMAND--F.C. #3

	Peak Value	Final Value	Rise Time	Settling Time
$\phi$ (deg)	30.0	30.0	3.50	6.05
$\beta$ (deg)	0.0361	0.0179	--	--
$\delta_r$ (deg)	-4.68	--	--	--
$\delta_w$ (deg)	64.8	--	--	--

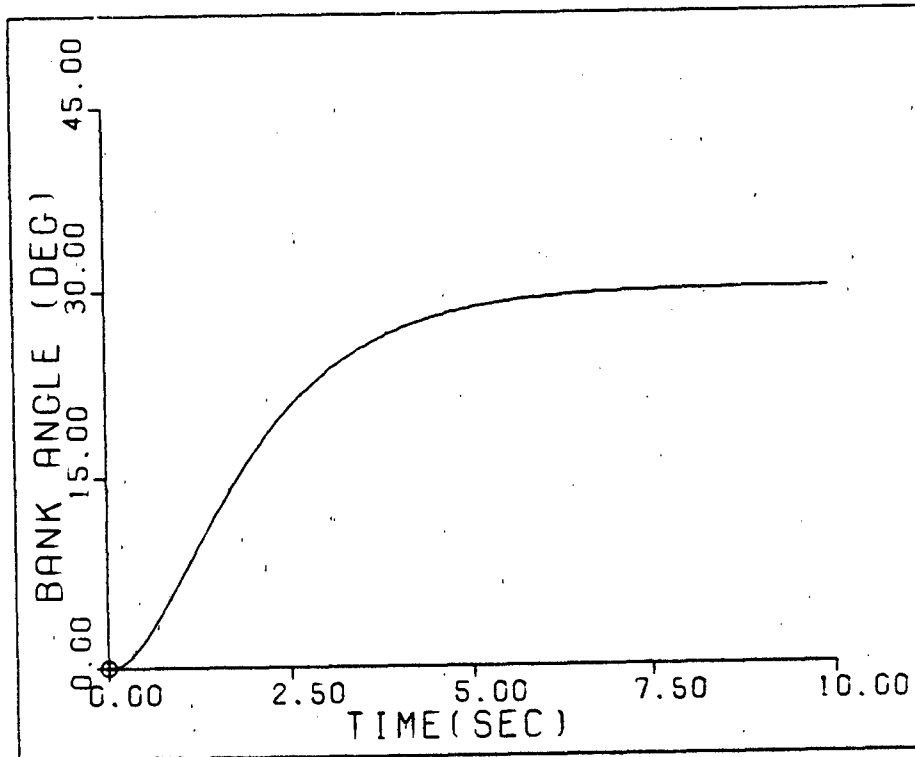


Fig. 6-5. Bank Angle Response--F.C. #3

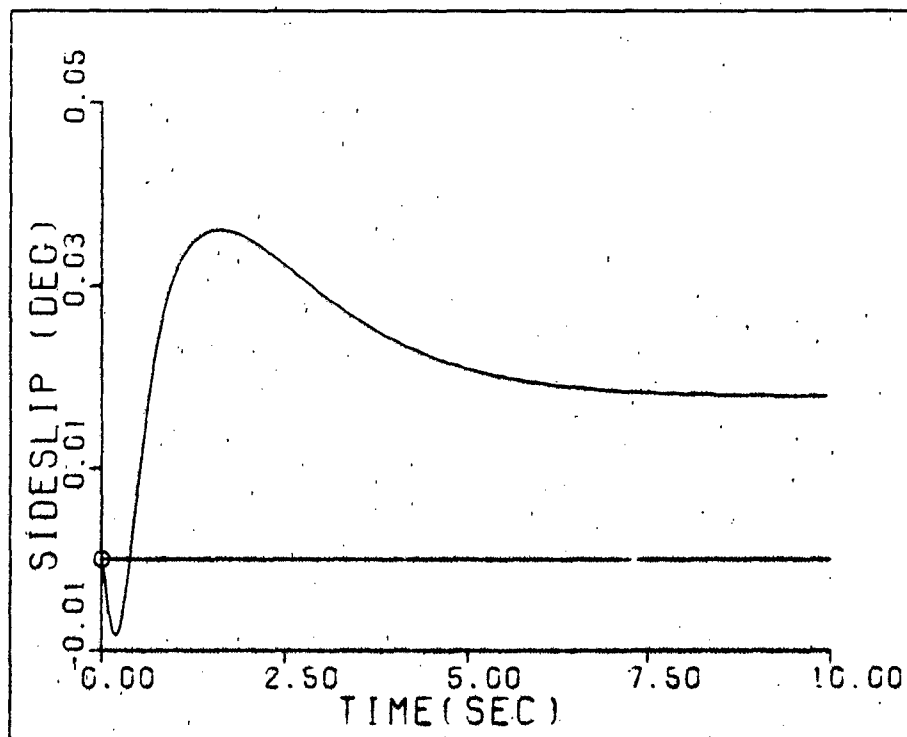


Fig. 6-6. Sideslip Response--F.C. #3

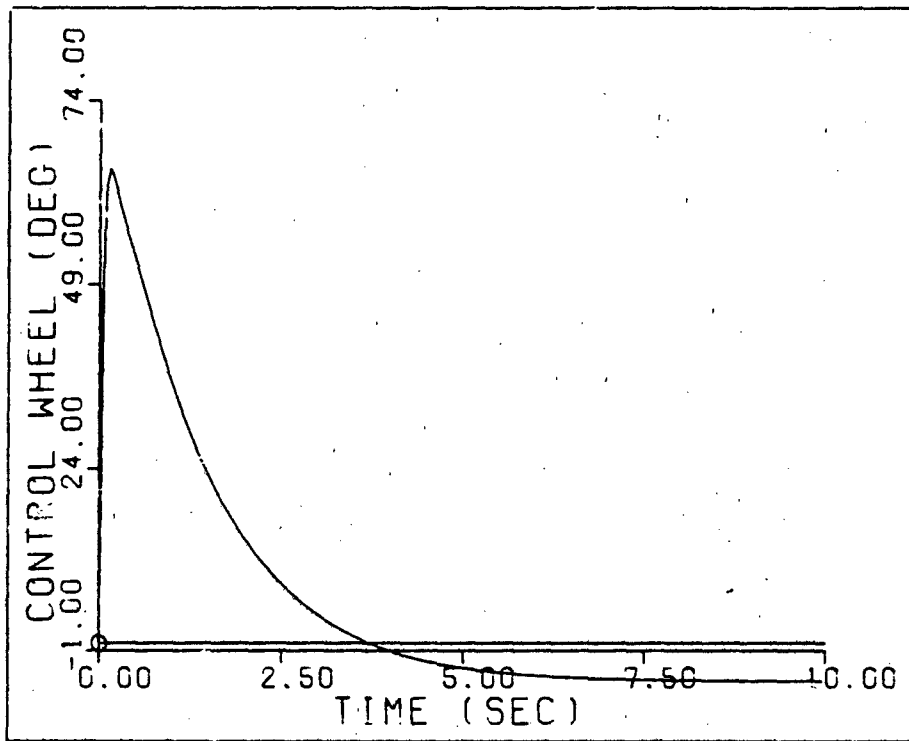


Fig. 6-7. Control Wheel Deflection--F.C. #3

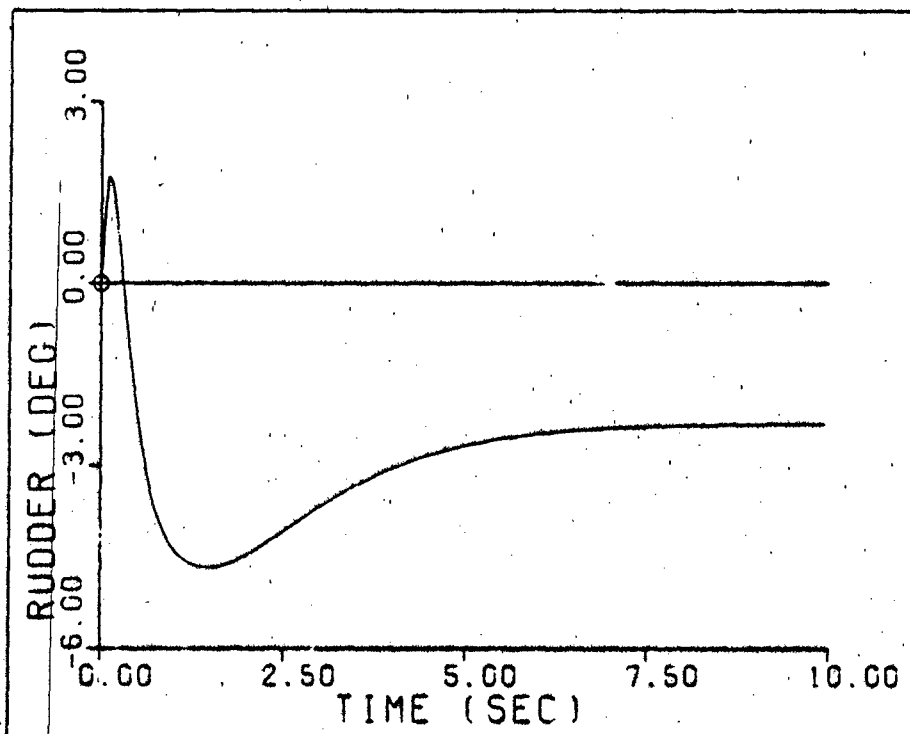


Fig. 6-8. Rudder Deflection--F.C. #3

The responses shown in Figures 6-9 through 6-12 are for a 30 degree bank angle command (real pre-filter poles) with a ramp input having a rise time of 1 second. This is a more realistic output response. As can be seen from Figure 6-9, the bank angle response is similar to that generated by the complex pre-filter but now the settling time is reduced by approximately 0.8 seconds. The response is thus very close to that of the bank angle model which is used as the design criteria. Table 5-2 shows the characteristics due to a 30 degree bank angle command.

TABLE 6-3

BANK ANGLE COMMAND--F.C. #3

	Peak Value	Final Value	Rise Time	Settling Time
$\phi$ (deg)	30.0	30.0	3.60	6.55
$\beta$ (deg)	0.0354	0.0179	--	--
$\delta_r$ (deg)	-.222	--	--	--
$\delta_w$ (deg)	36.9	--	--	--



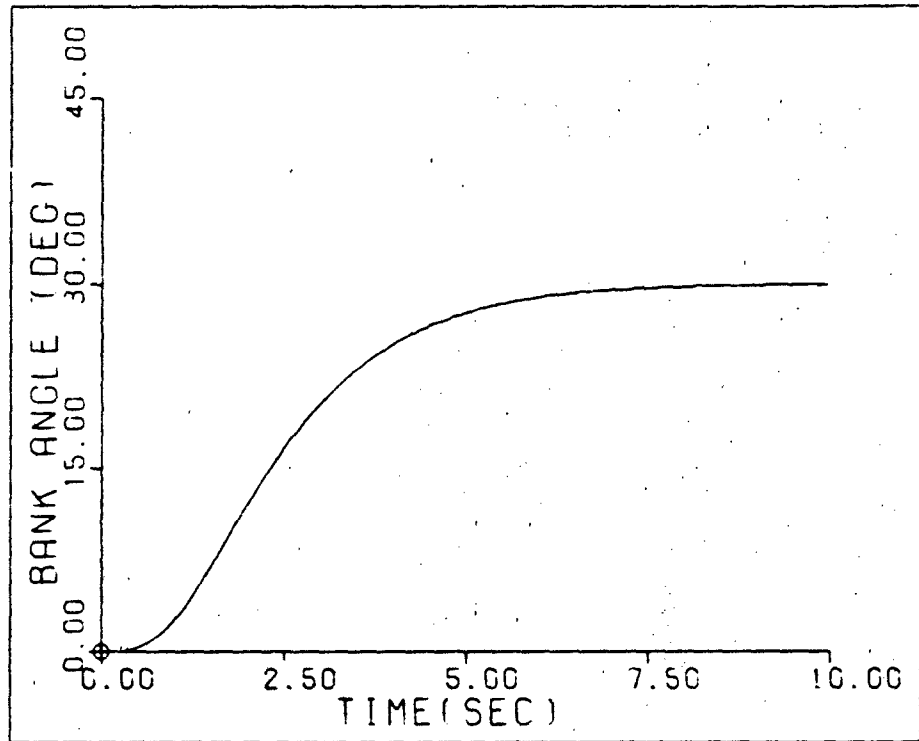


Fig. 6-9. Bank Angle Response--F.C. #3

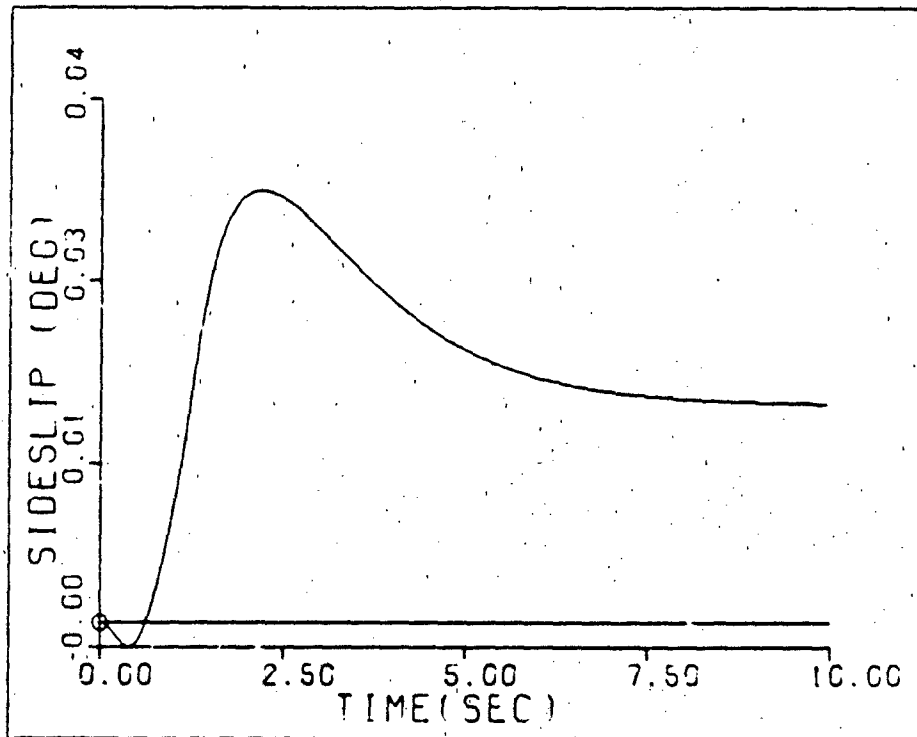


Fig. 6-10. Sideslip Response--F.C. #3

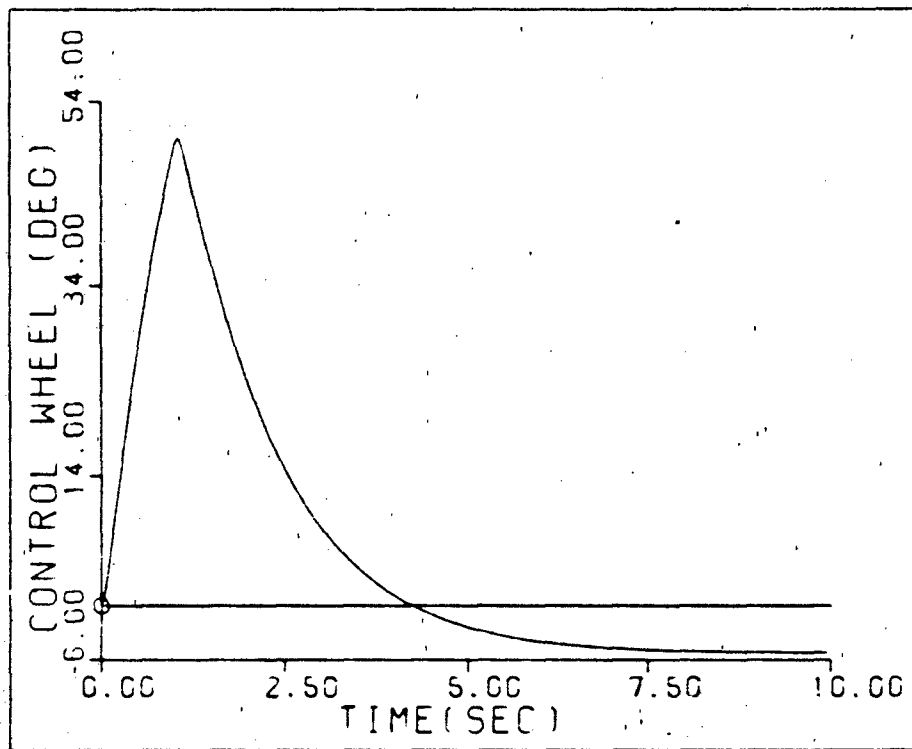


Fig. 6-11. Control Wheel Deflection--F.C. #3

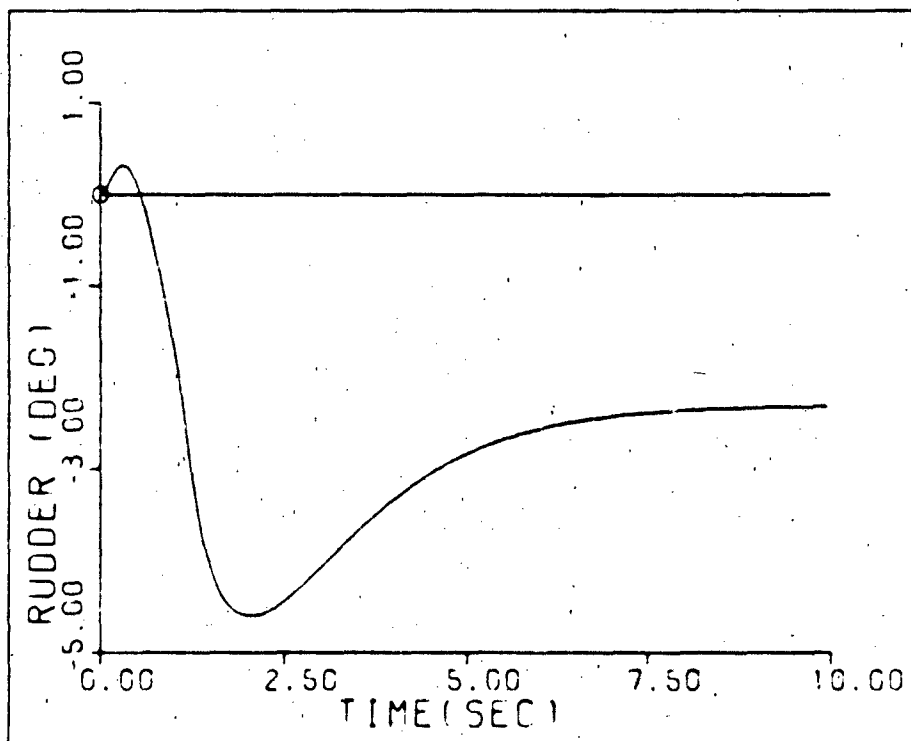


Fig. 6-12. Rudder Deflection--F.C. #3

### Sideslip Command

The responses shown in Figures 6-13 through 6-16 are for a 5 degree step input sideslip angle command (complex pre-filter poles). The sideslip response due to a 5 degree command input has desirable characteristics similar to those of the bank angle command. Table 6-4 outlines the characteristics of the responses due to a 5 degree sideslip command.

TABLE 6-4

SIDESLIP COMMAND--F.C. #3

	Peak Value	Final Value	Rise Time	Settling Time
$\beta$ (deg)	5.18	4.94	1.78	4.50
$\dot{\beta}$ (deg)	-.179	-.179	--	--
$\beta_r$ (deg)	12.0	--	--	--
$\beta_w$ (deg)	28.3	--	--	--

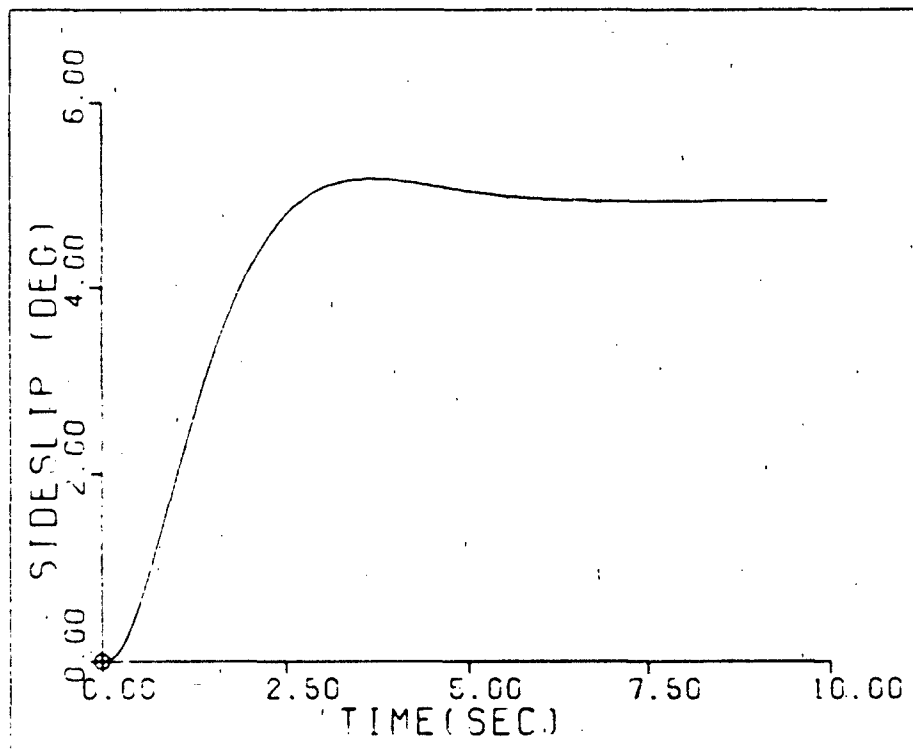


Fig. 6-13. Sideslip Response--F.C. #3

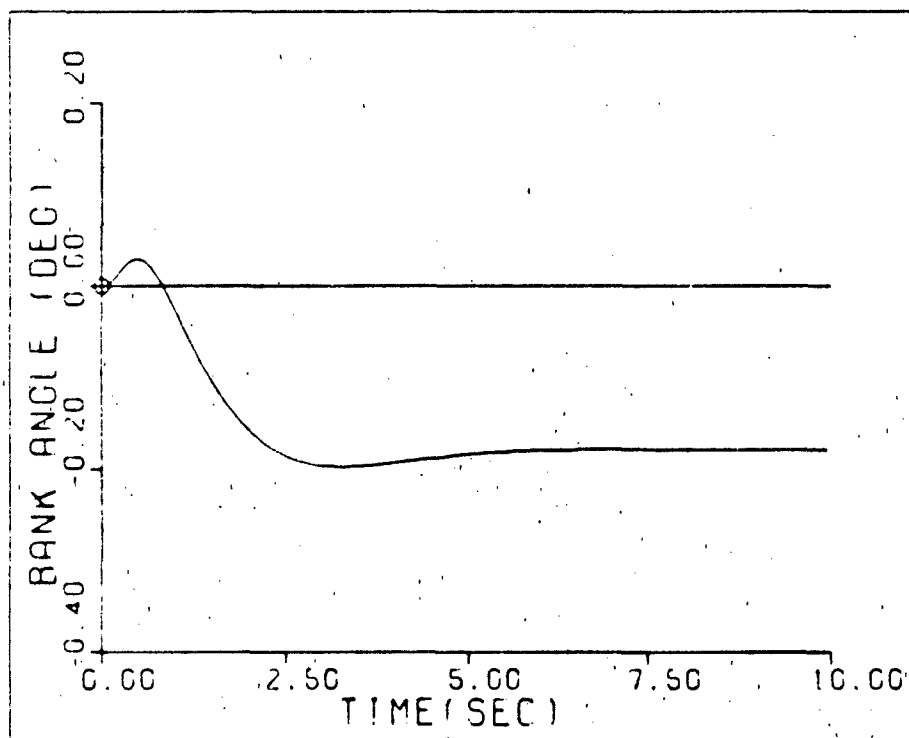


Fig. 6-14. Bank Angle Response--F.C. #3

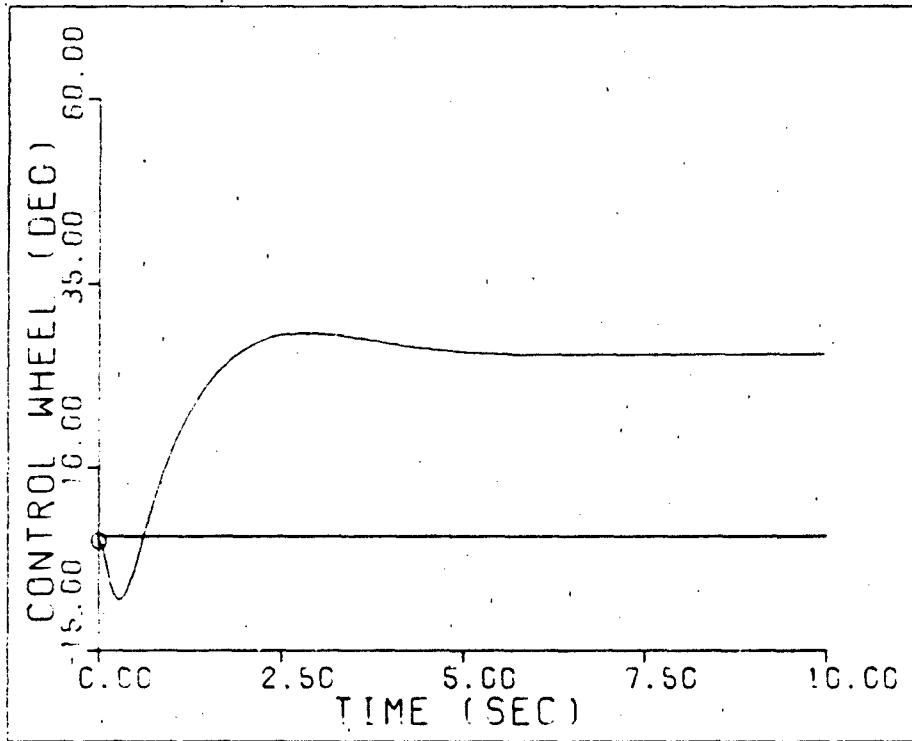


Fig. 6-15. Control Wheel Deflection--F.C. #3

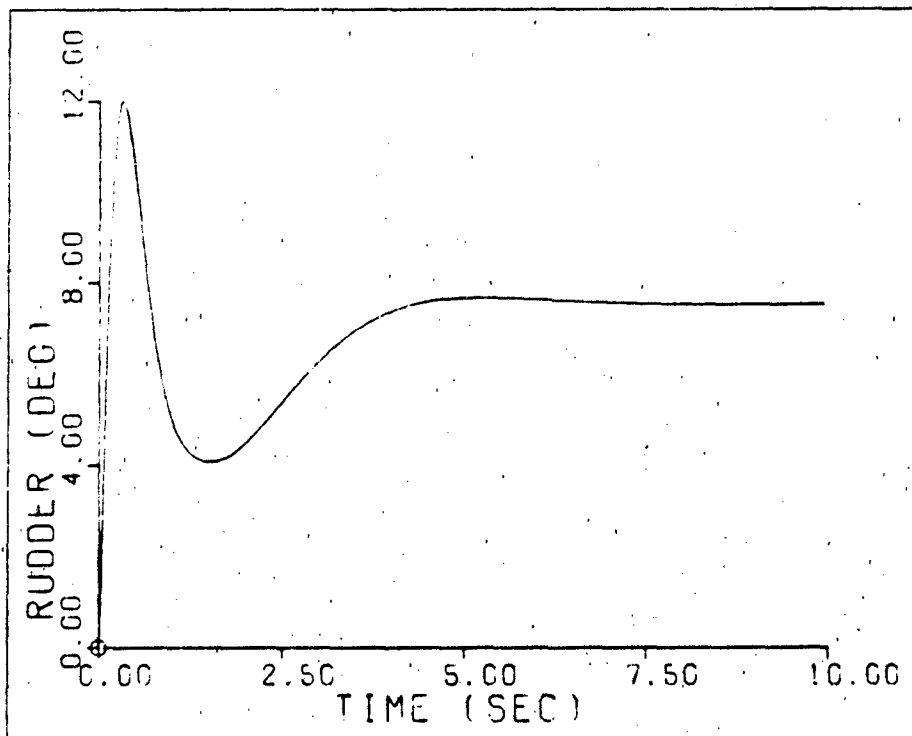


Fig. 6-16. Rudder Deflection--F.C. #3

The responses shown in Figures 6-17 through 6-20 are for a 5 degree step input sideslip command (real pre-filter poles). It is to be noted that the rise time and settling time are slower than that of the previous design using the complex poles for the pre-filter. This may be desirable, since the rates of the control surface deflection decrease due to the slower rise and settling times. Table 6-5 outlines the characteristics of the responses due to a 5 degree step input sideslip command.

TABLE 6-5  
SIDESLIP COMMAND--F.C. #3

	Peak Value	Final Value	Rise Time	Settling Time
$\beta$ (deg)	5.0	5.0	4.98	9.25
$\phi$ (deg)	-0.181	-0.181	--	--
$\epsilon_r$ (deg)	7.58	--	--	--
$\epsilon_w$ (deg)	25.7	--	--	--

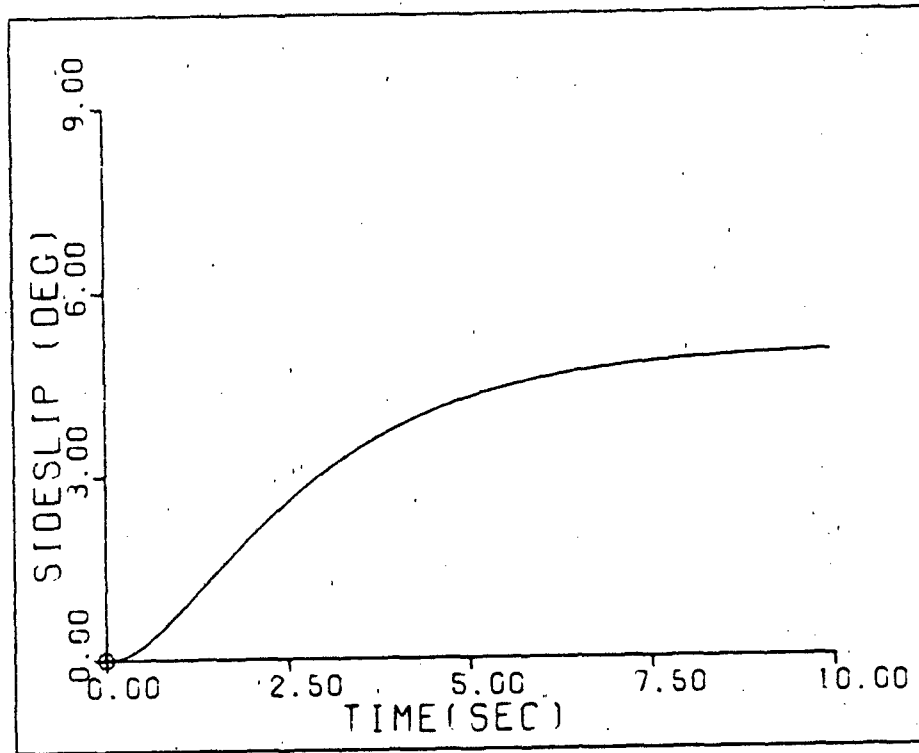


Fig. 6-17. Sideslip Response--F.C. #3

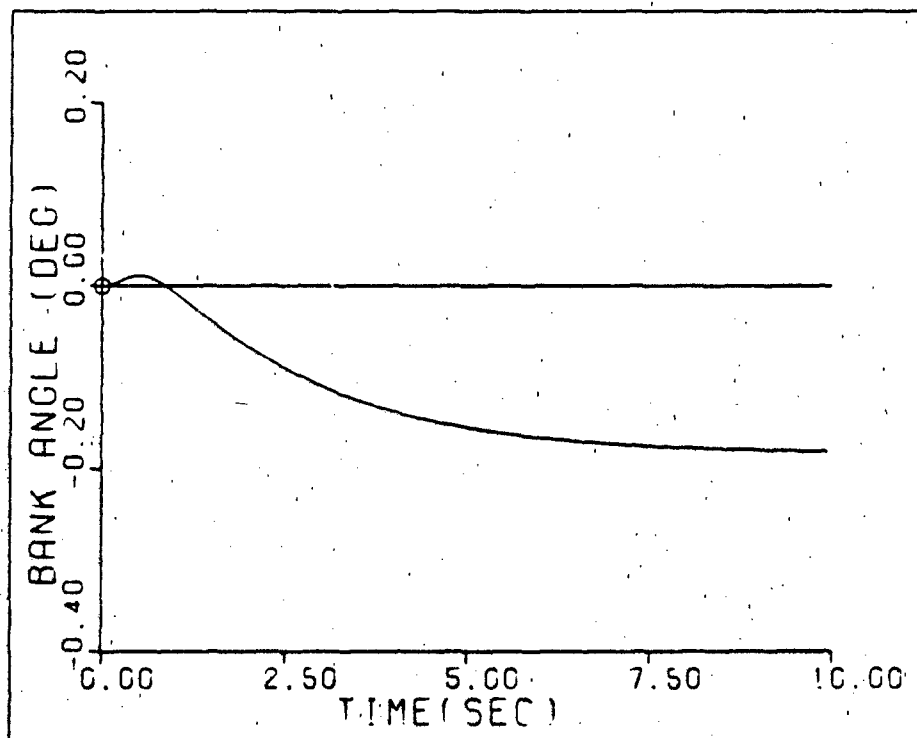


Fig. 6-18. Bank Angle Response--F.C. #3

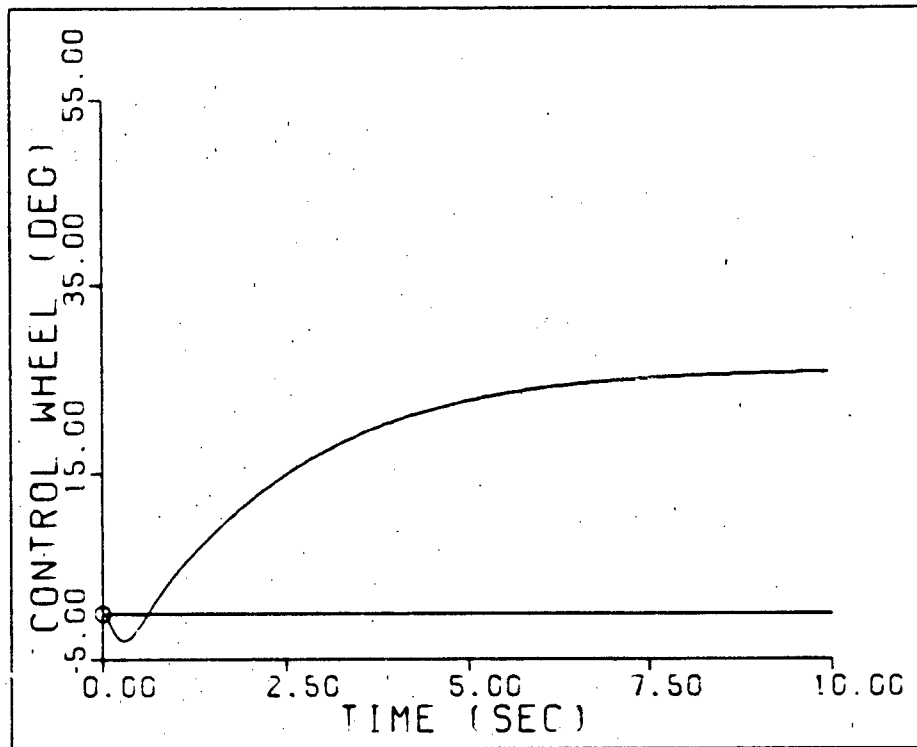


Fig. 6-19. Control Wheel Deflection--F.C. #3

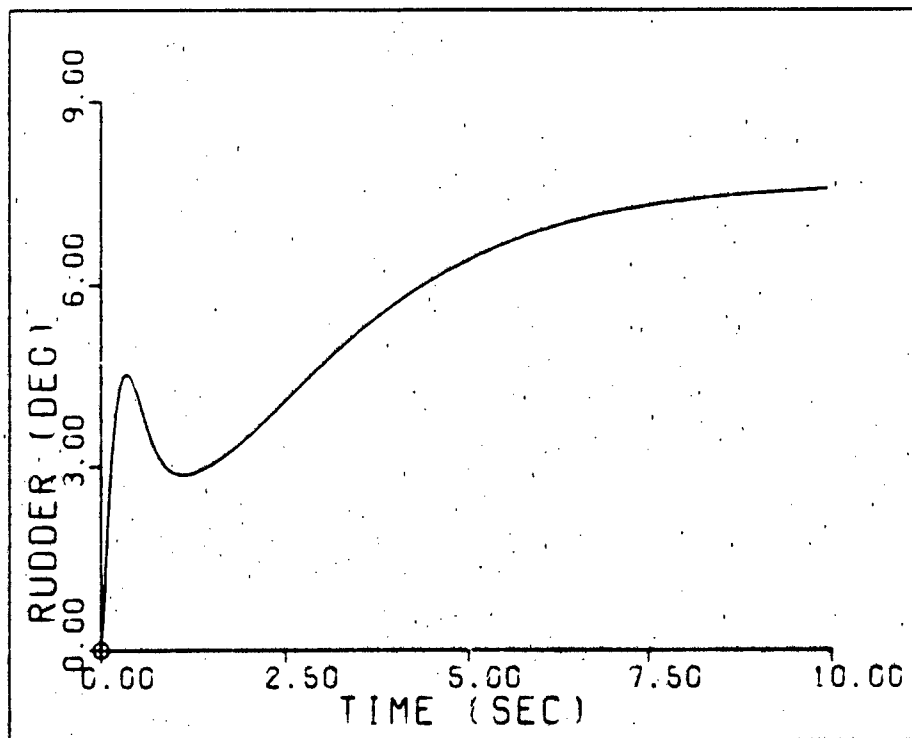


Fig. 6-20. Rudder Deflection--F.C. #3



The responses shown in Figures 6-21 through 6-24 are for a 5 degree sideslip command (real pre-filter poles). The command input is a ramp with a rise time of 1 second. As shown in Figure 6-21 the sideslip response has good characteristics. The response, due to this command input, is very close to that of the desired response model. Table 6-6 outlines the characteristics of the responses due to a 5 degree ramp input.

TABLE 6-6

SIDESLIP COMMAND--F.C. #3

	Peak Value	Final Value	Rise Time	Settling Time
$\beta$ (deg)	5.0	5.0	5.0	8.75
$\dot{\beta}$ (deg)	-0.180	-0.180	0	0
$\delta_r$ (deg)	7.55	--	--	--
$\delta_w$ (deg)	25.6	--	--	--

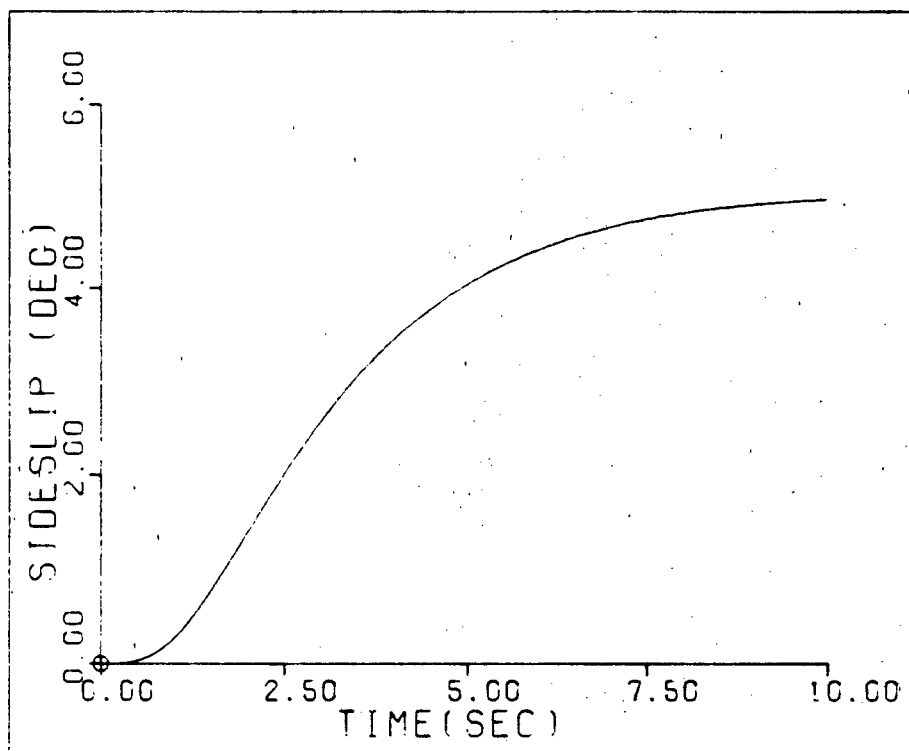


Fig. 6-21. Sideslip Response--F.C. #3

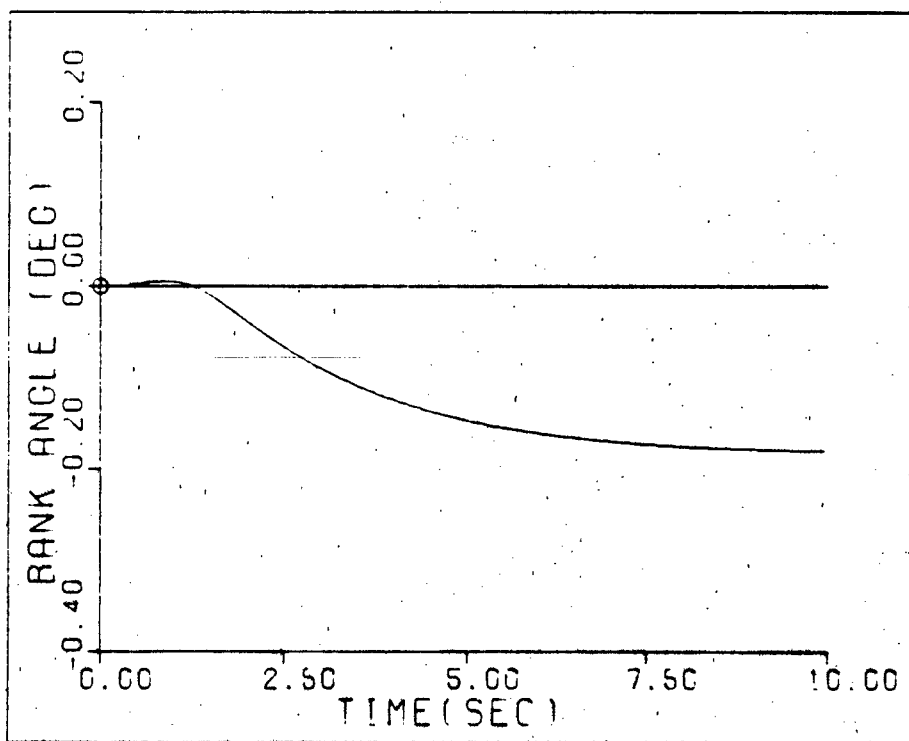


Fig. 6-22. Bank Angle Response--F.C. #3

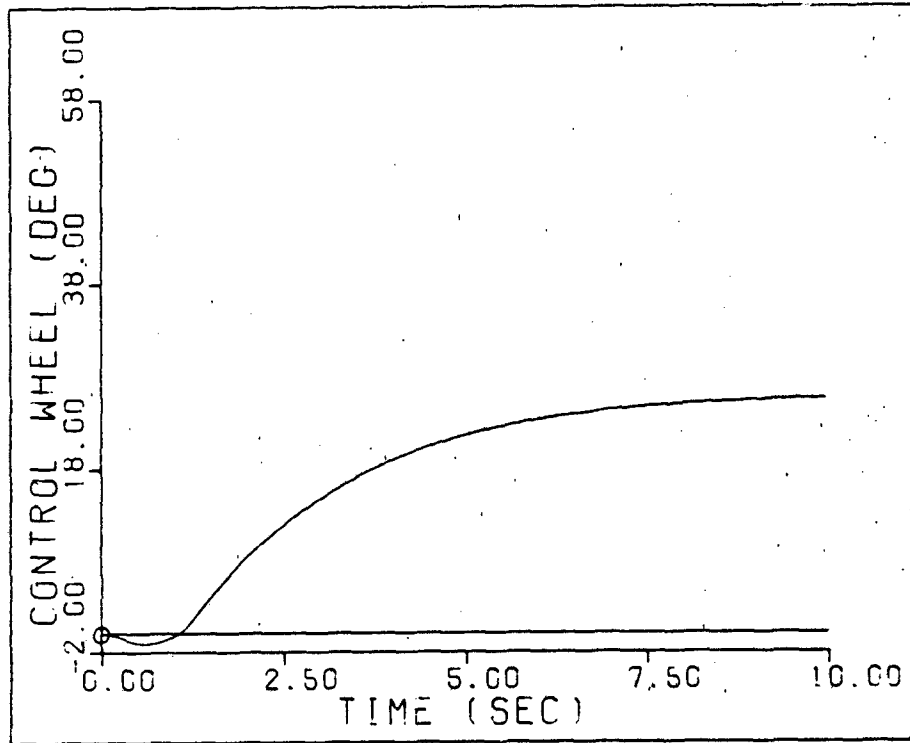


Fig. 6-23. Control Wheel Deflection--F.C. #3

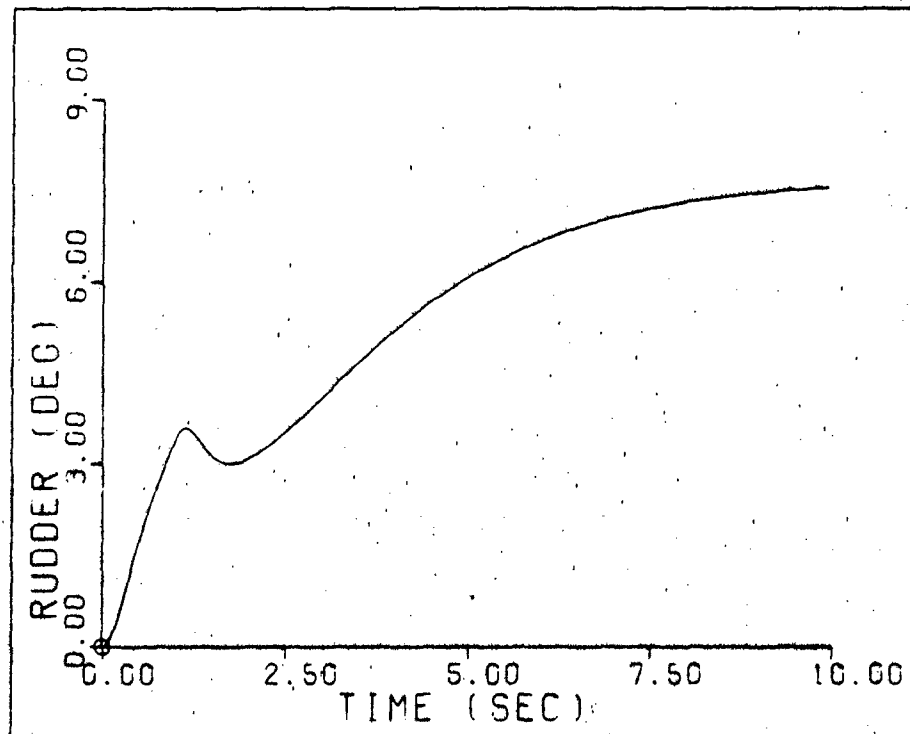


Fig. 6-24. Rudder Deflection--F.C. #3

Robustness of the designs for both the bank angle command and the sideslip command are illustrated in Figures 6-25 and 6-26. The responses for both designs, over the entire F.C.'s have very little variation. The actual output responses approach the responses of the models developed during the design process. Thus this design method has demonstrated that it is a very effective tool for the design of multi-variable control systems. This concludes the 2x2 design simulation.

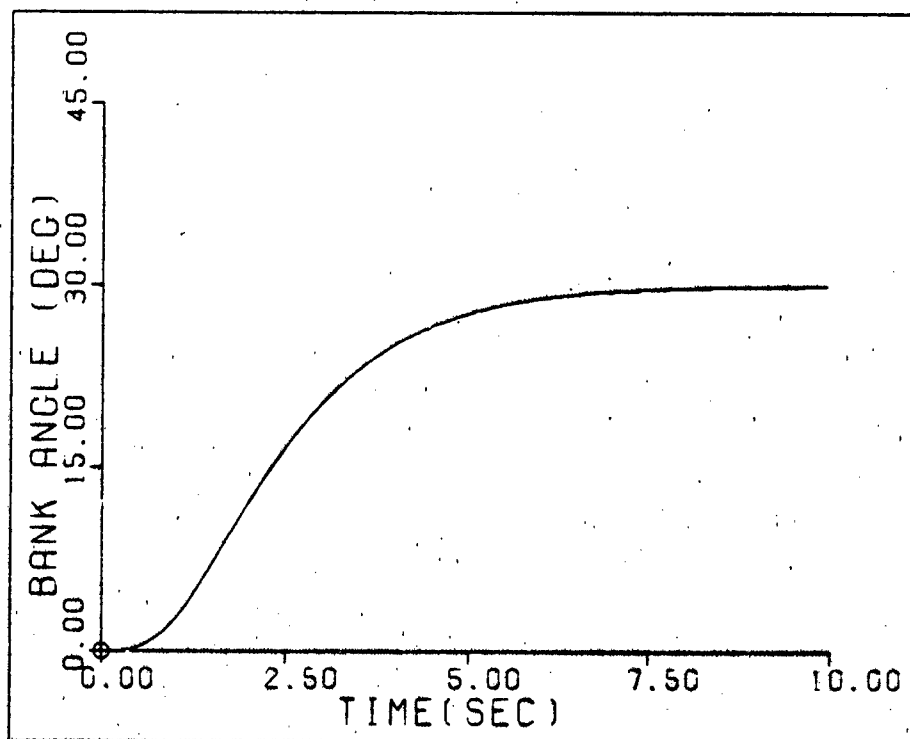


Fig. 6-25. Robust Controller--Bank Angle Response.

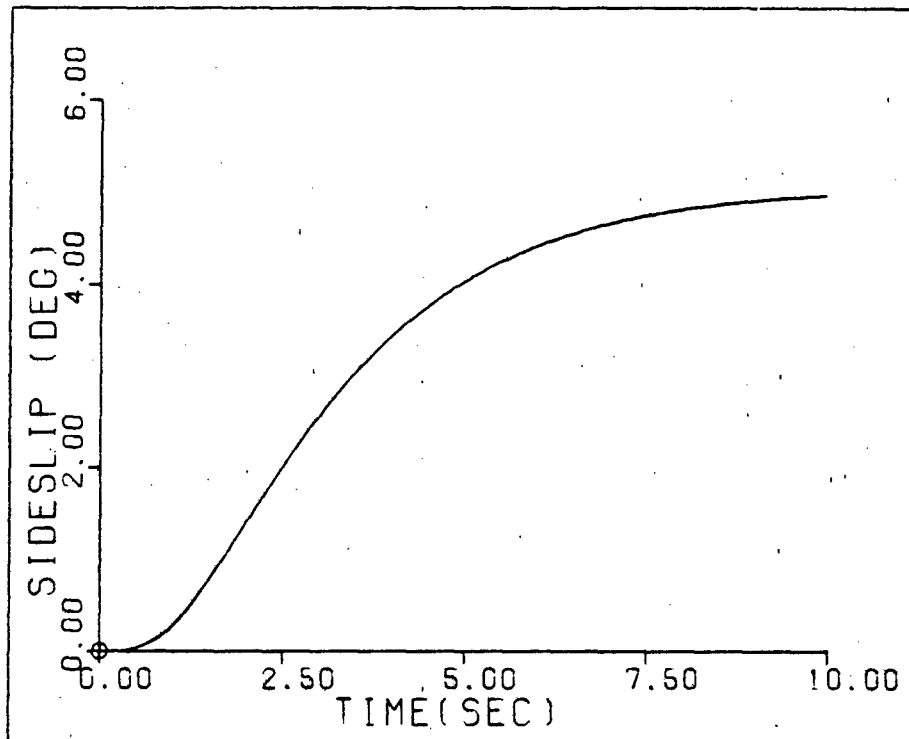


Fig. 6-26. Robust Controller--Sideslip Response

VI-3 Longitudinal Simulation  
(3x3 Design)

This design is completed for a one command input. The simulation is for a 4 degree pitch angle command and the input is a ramp which rises to a magnitude of 4 in 1 second. The output responses of the rigid aircraft for F.C. #3 are shown in Figures 6-27 through 6-29 and the control surface deflections are shown in Figures 6-30 through 6-32. Table 6-7 outlines the characteristics of each response. These responses do not include control surface deflection saturation.

TABLE 6-7

PITCH ANGLE COMMAND--F.C. #3

	Peak Value	Final Value	Rise Time	Settling Time
$\theta$	4.0	4.0	4.3	6.65
h	-0.581	0.107	--	--
u	-0.277	-0.171	--	--
$\delta_e$	-2.30	--	--	--
$\delta_{sb}$	48.4	--	--	--
$\delta_T$	19.7	--	--	--

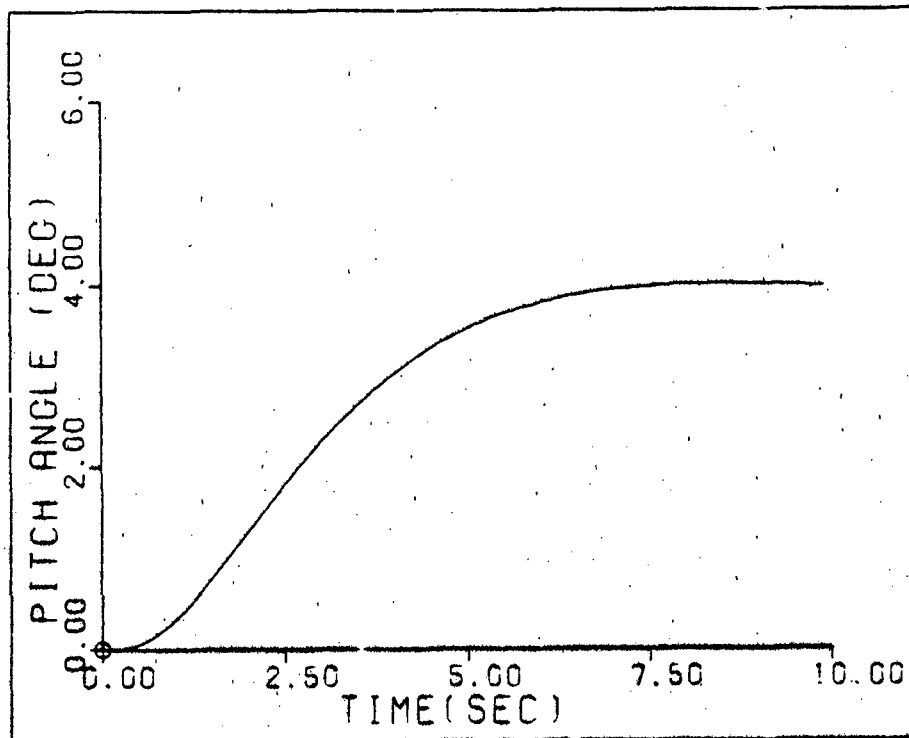


Fig. 6-27--Pitch Angle Response--F.C. #3

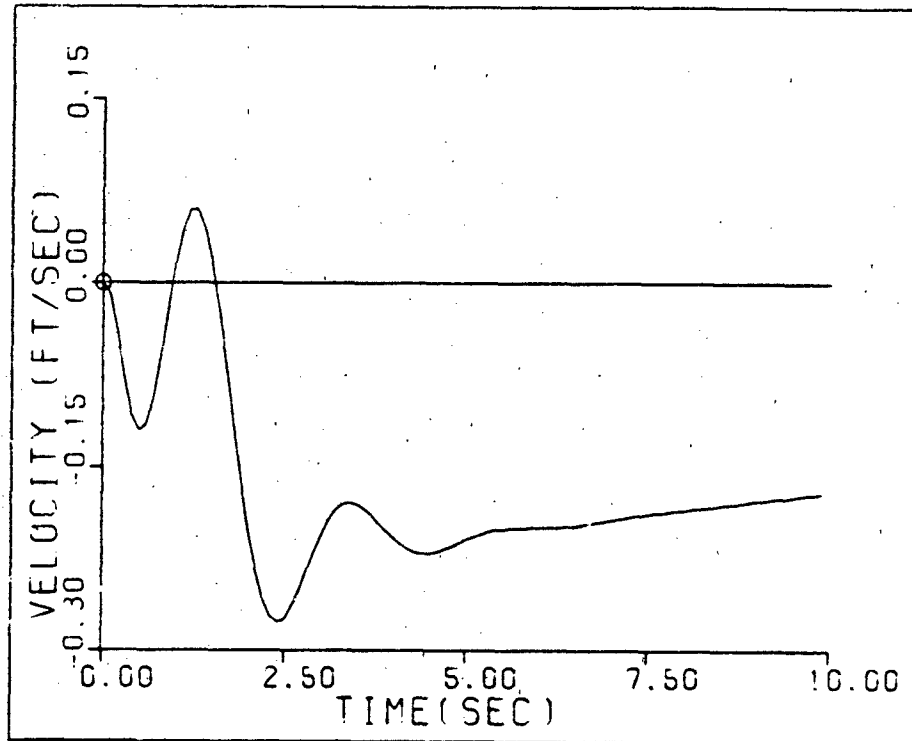


Fig. 6-28. Perturbation Velocity Response--F.C. #3

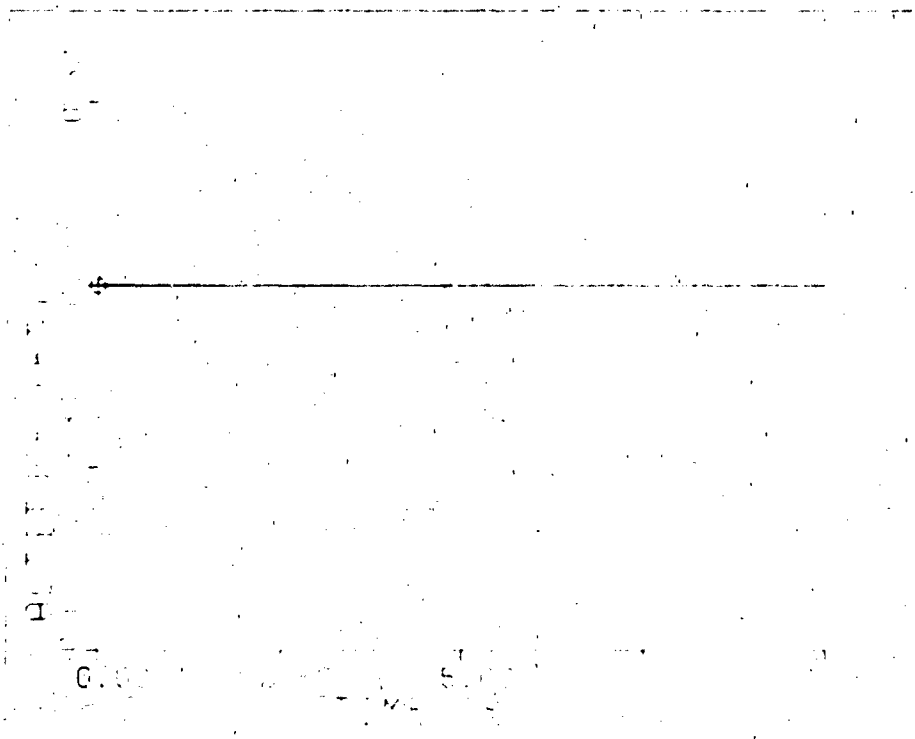


Fig. 6-29. Altitude Response--F.C. #3

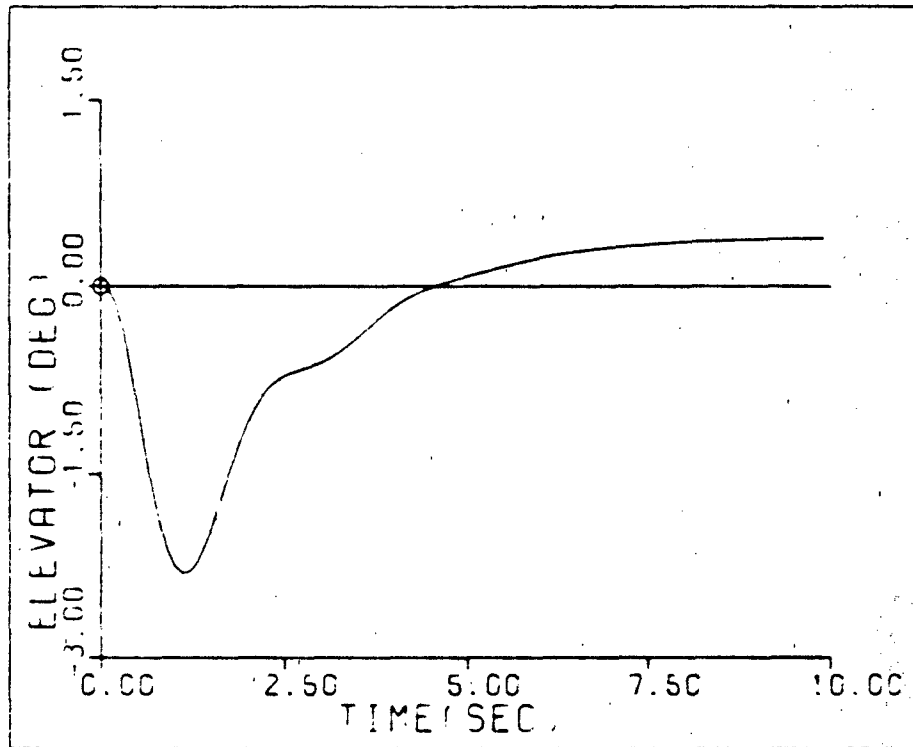


Fig. 6-30. Elevator Deflection--F.C. #3

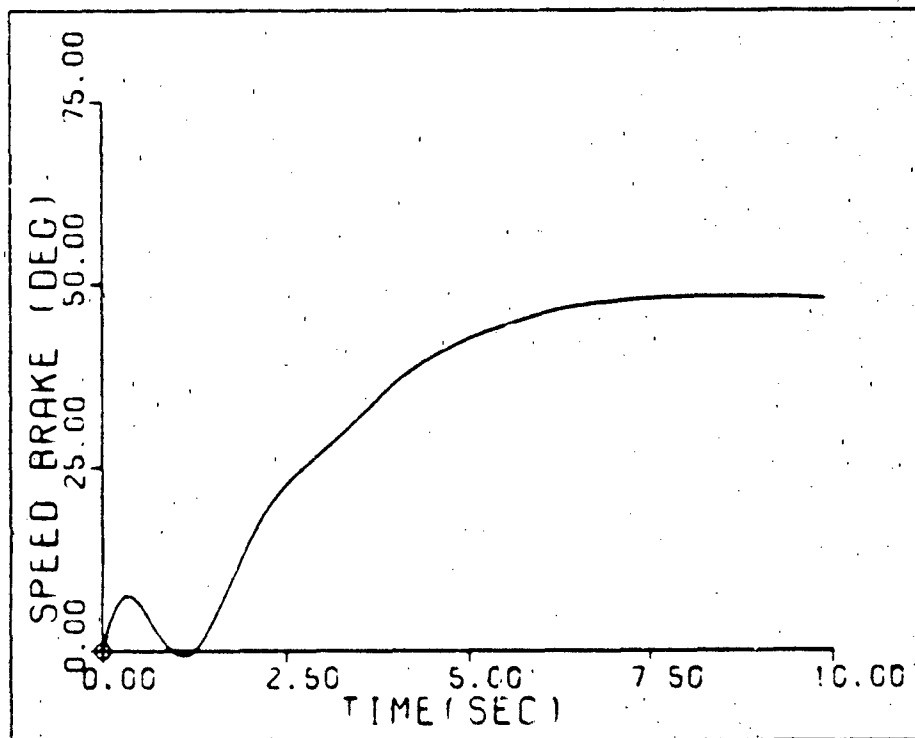


Fig. 6-31. Speed Brake Deflection--F.C. #3



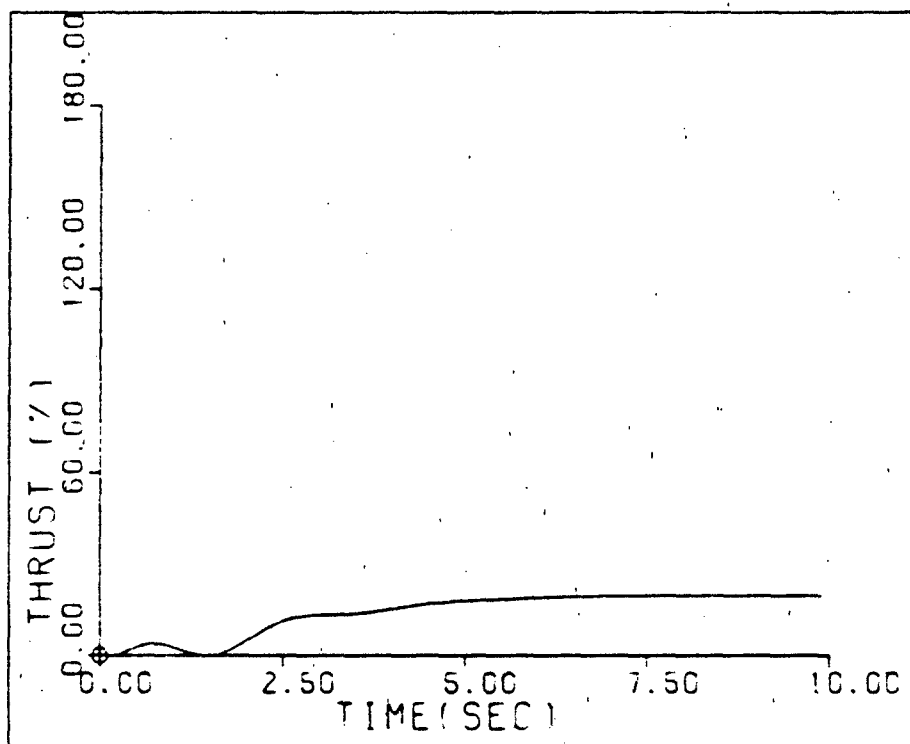


Fig. 6-32. Thrust Increase--F.C. #3

The output responses for the non-rigid aircraft design are shown in Figures 6-33 through 6-35 and the control surface deflections are shown in Figures 6-36 through 6-38. The simulation is for a 1 degree pitch angle command. The input is a ramp which rises to a magnitude of 1 in 1 second. Table 6-8 outlines the characteristics of each response.

TABLE 6-8

PITCH ANGLE COMMAND--F.C. #3

	Peak Value	Final Value	Rise Time	Settling Time
e	1.0	1.0	5.6	8.3
h	0.349	0.349	--	--
u	-0.073	-0.065	--	--
e	1.27	--	--	--
sb	12.2	--	--	--
T	7.05	--	--	--

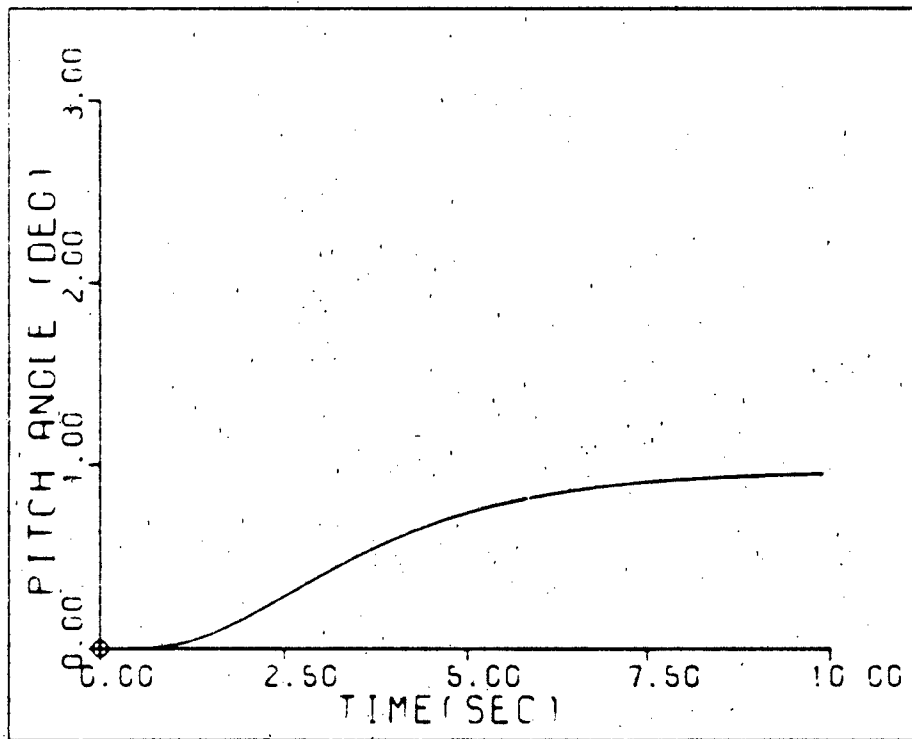


Fig. 6-33. Pitch Angle Response--F.C. #3

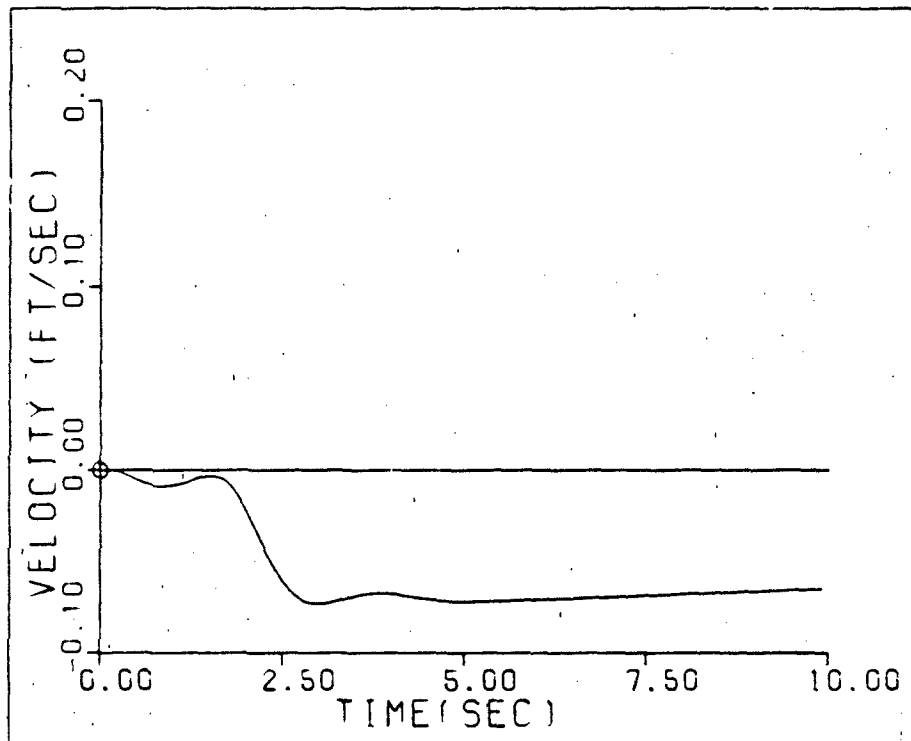


Fig. 6-34. Perturbation Velocity Response--F.C. #3

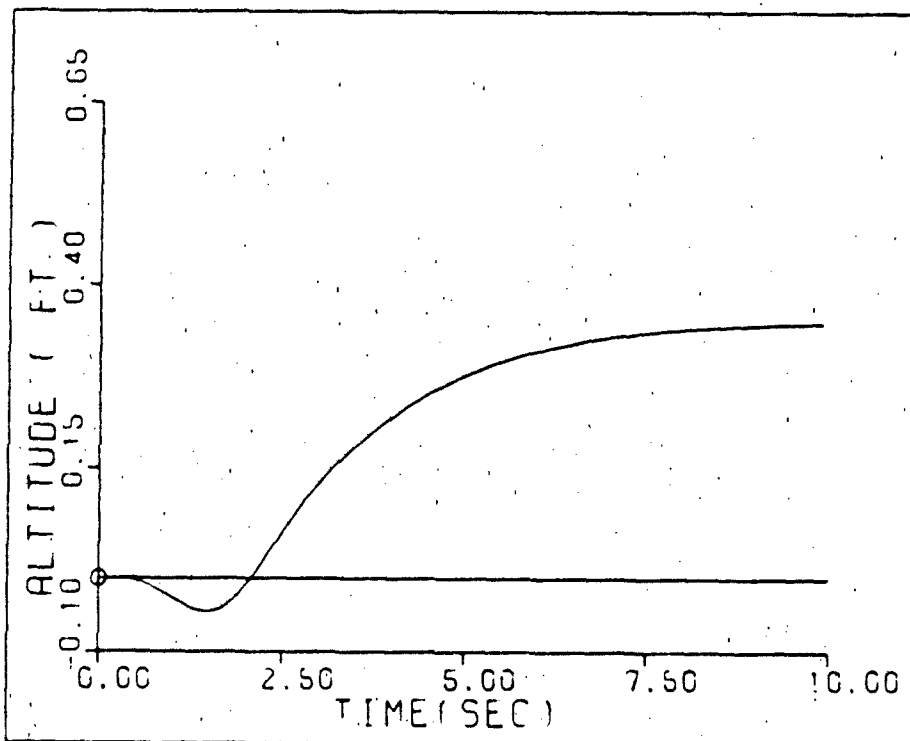


Fig. 6-35. Altitude Response--F. C. #3

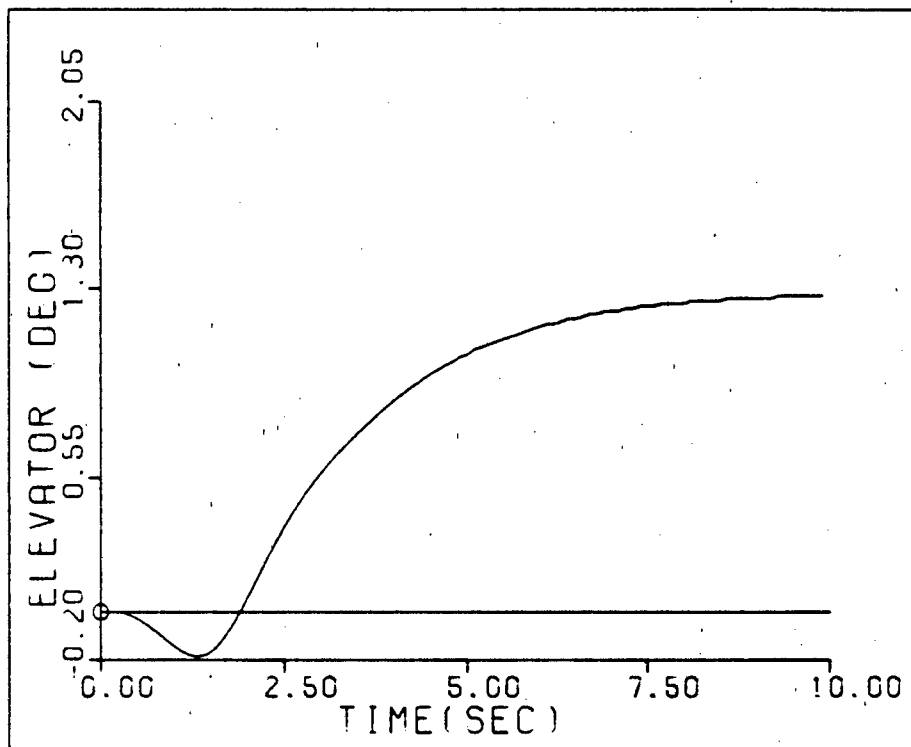


Fig. 6-36. Elevator Deflection--F.C. #3

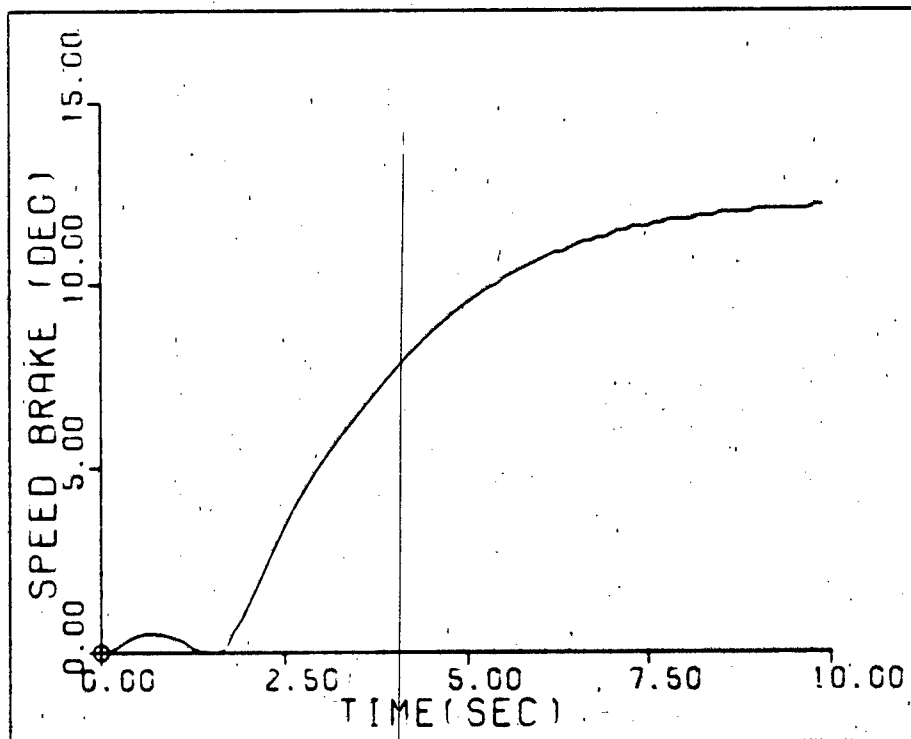


Fig. 6-37. Speed Brake Deflection--F.C. #3

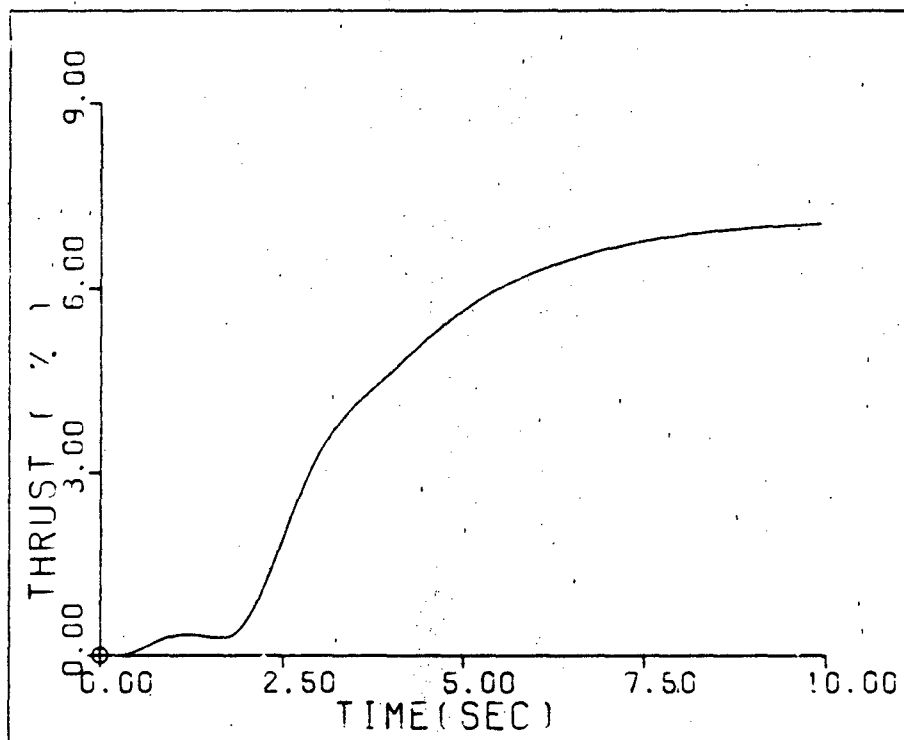


Fig. 6-38. Thrust Increase--F.C. #3

The response for F.C.'s #1 and #2 causes control surface saturation. Thus the responses of the rigid aircraft design with control surface deflection saturation for F.C. #2 are shown in Figures 6-39 through 6-44. The simulation is for a 4 degree pitch angle command. The input is a ramp which rises to a magnitude of 4 in 1 second. Table 6-9 outlines the characteristics of each response.

TABLE 6-9

PITCH ANGLE COMMAND--F.C. #2  
(CONTROL SURFACE SATURATION)

	Peak Value	Final Value	Rise Time	Settling Time
$\theta$	3.49	3.30	4.45	10.0
$h$	1.13	1.13	--	--
$u$	-18.8	-18.8	--	--
$\delta_e$	4.95	--	--	--
$\delta_{sb}$	60.0	--	--	--
$\delta_T$	50.0	--	--	--

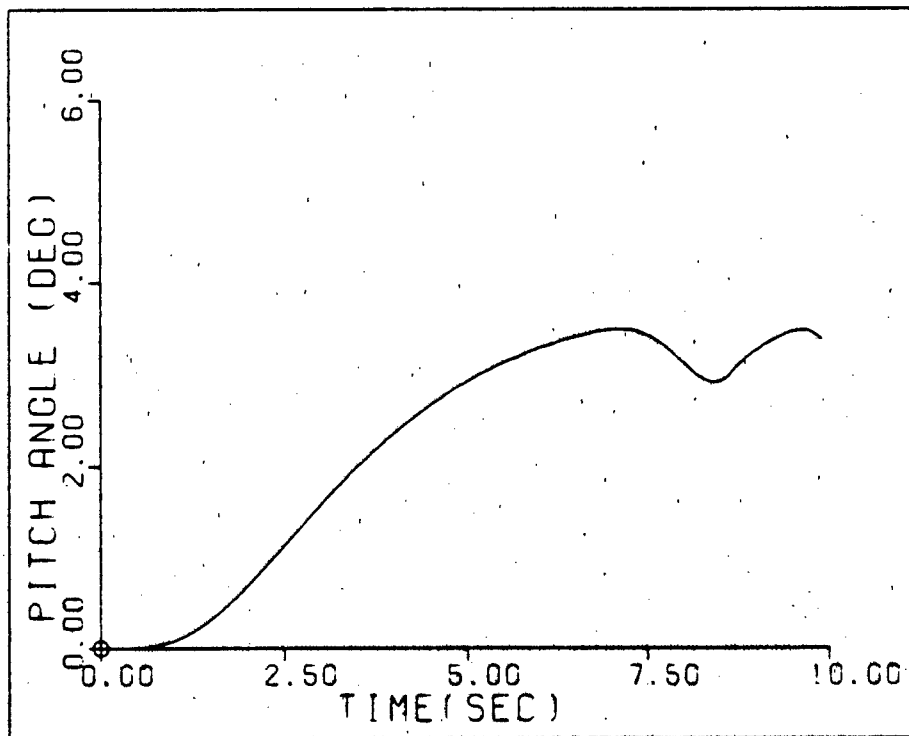


Fig. 6-39. Pitch Angle Response--F.C. #2

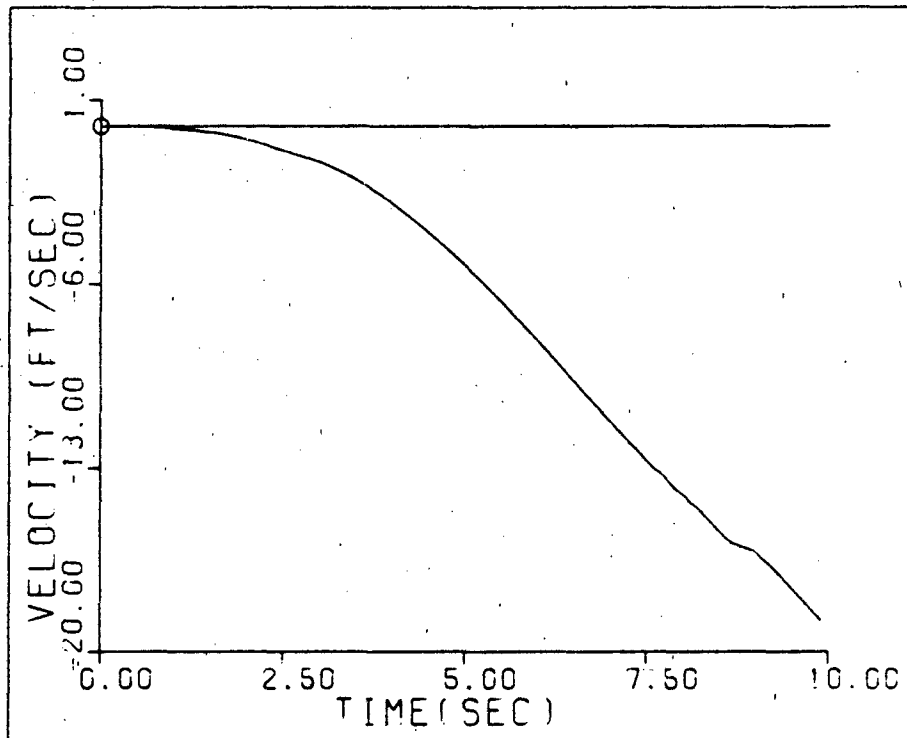


Fig. 6-40. Perturbation Velocity Response--F.C. #2

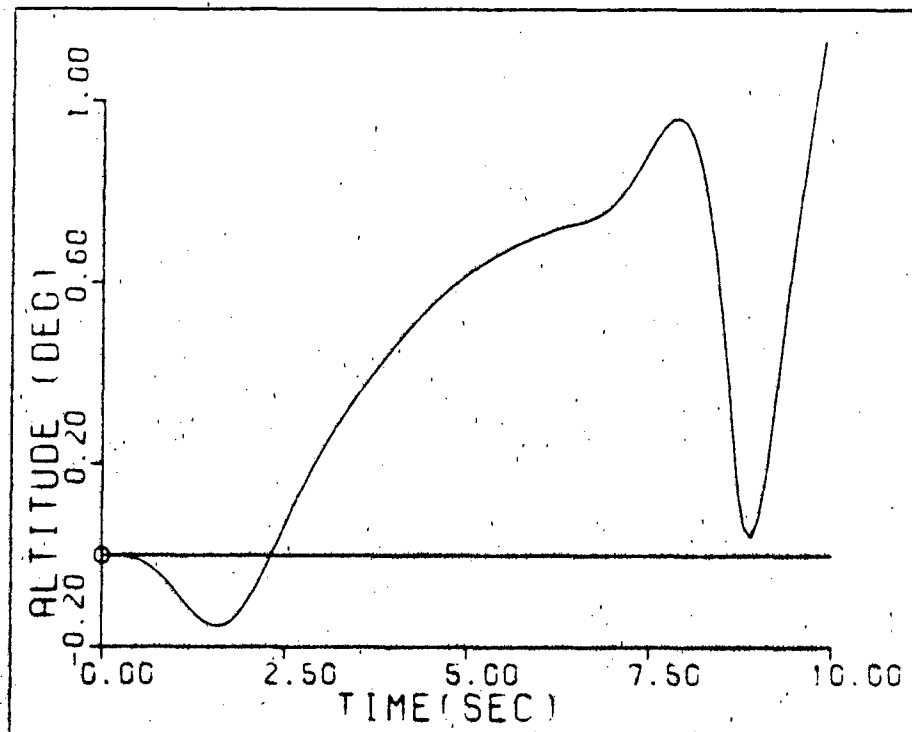


Fig. 6-41. Altitude Response--F.C. #2

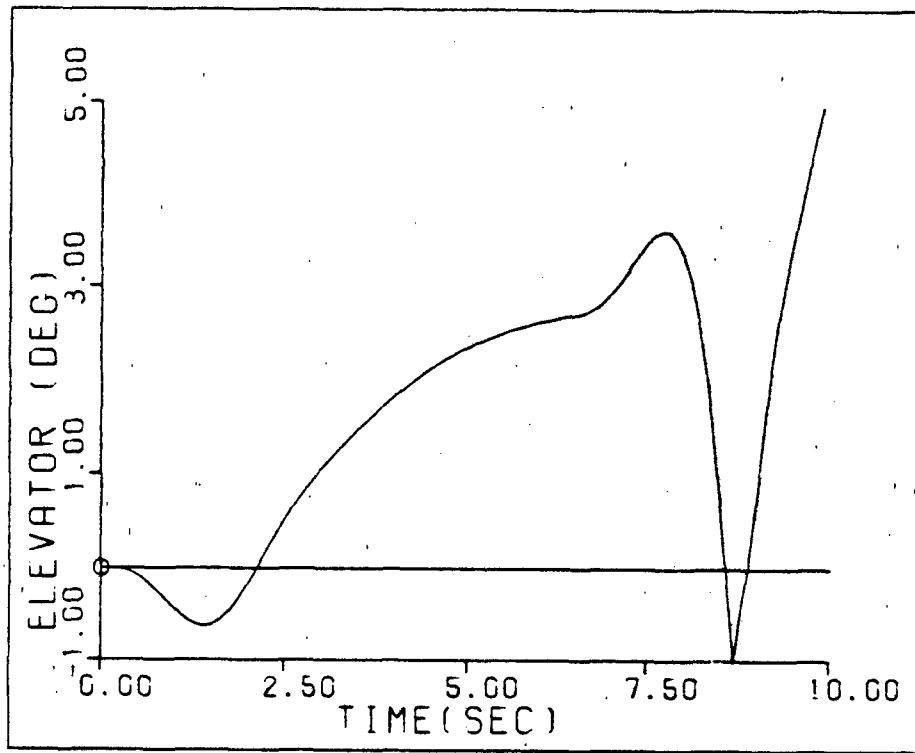


Fig. 6-42. Elevator Deflection--F.C. #2

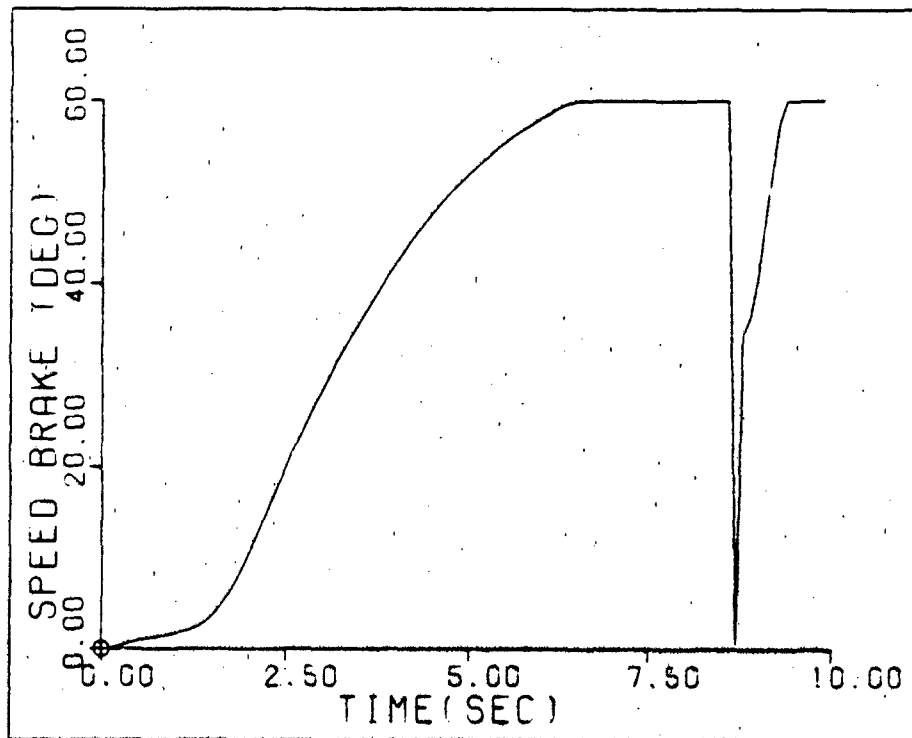


Fig. 6-43. Speed Brake Deflection--F.C. #2



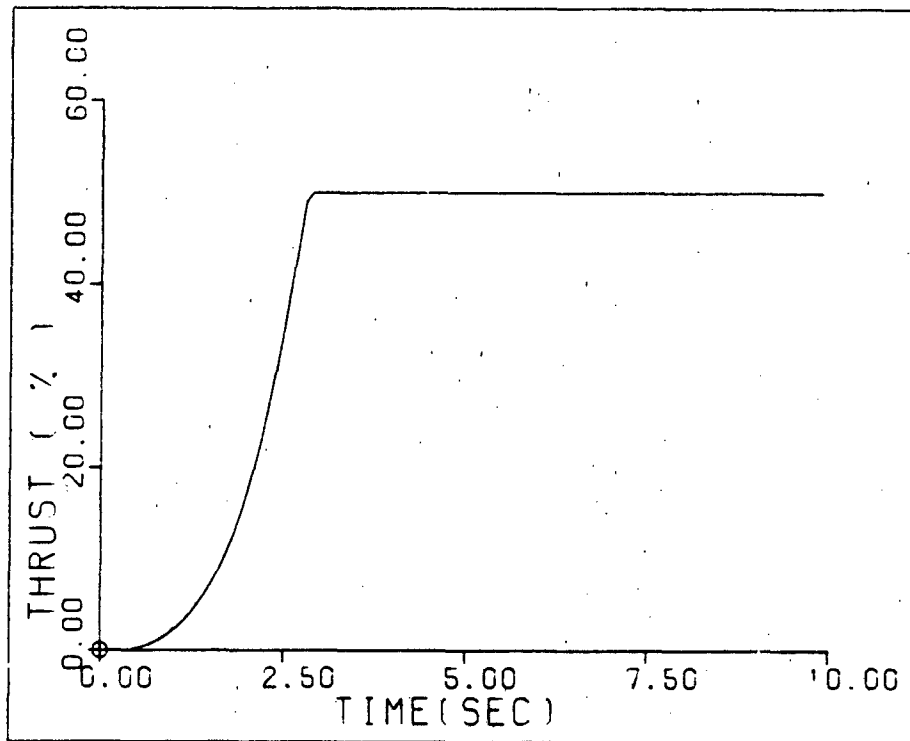


Fig. 6-44. Thrust Increase--F.C. #2

The desired pitch angle output of 4 degrees cannot be achieved due to control surface saturation for F.C.'s #1 and #2. Thus the pitch angle command is reduced from 4 degrees to 1 degree. The responses for the command input are included in Appendix H. Figure 6-45 demonstrates robustness of the 3x3 design of the rigid aircraft for a 1-degree command input.

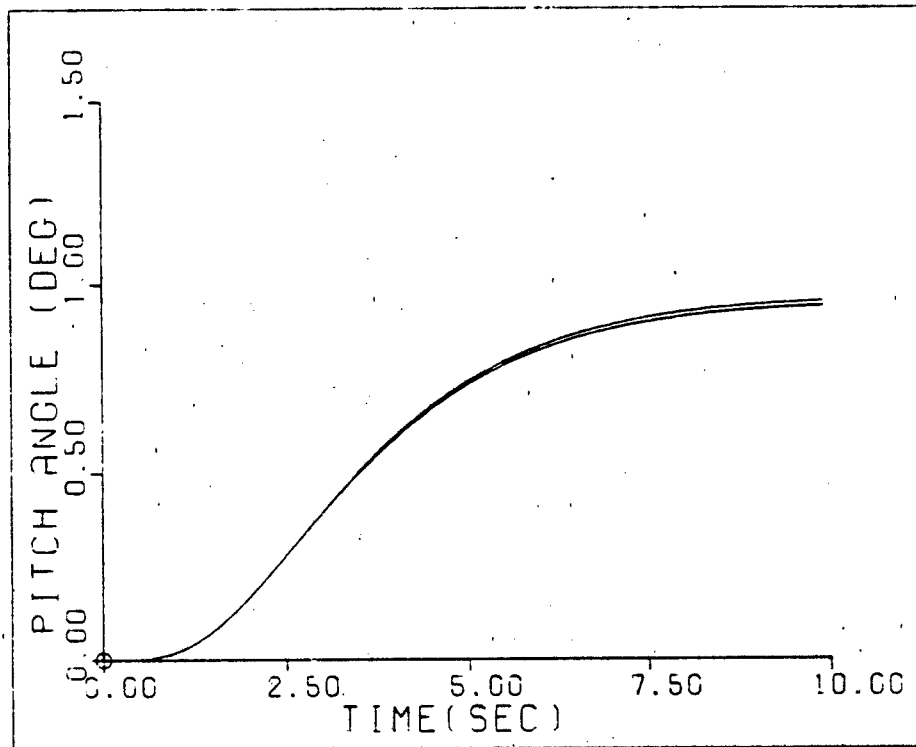


Fig. 6-45. Pitch Angle Response--F.C.'s #1, #2, and #3 (Rigid Aircraft)

Figure 6-46 demonstrates robustness of the 3x3 design with the first and second body bending modes included. These responses are for a 1-degree ramp command input which rises to 1 in 1 second.

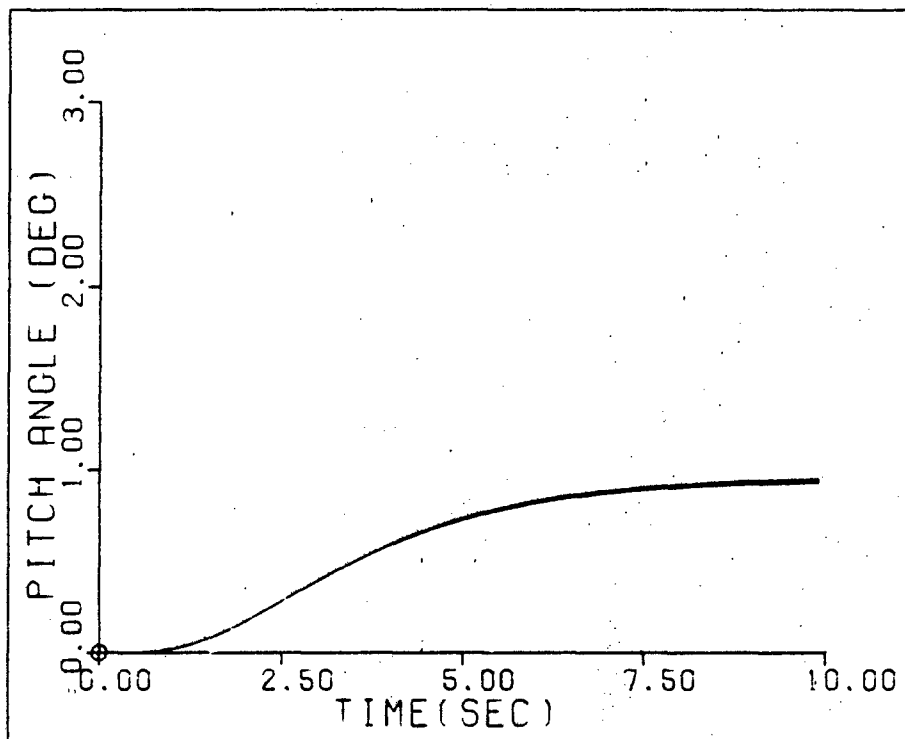


Fig. 6-46. Pitch Angle Response--F.C.'s #1, #2, and #3 (Non-Rigid Aircraft)

VI-4 Summary

This chapter outlines the simulations for both the lateral and longitudinal designs. The simulations are illustrated for F.C. #3. Finally, robustness of both designs is highlighted.

## VII. Conclusions and Recommendations

### VII-1 Thesis Summary

This thesis demonstrated the applications of Dr. Isaac Horowitz's Quantitative Feedback Theory to the design of multiple input-multiple output control systems.

Chapter I is an introduction and an explanation of the design problem including the assumptions used in the design process. Chapter II outlines the basic single input-single output design process which is expanded to the design of a 2x2 and 3x3 MIMO system and finally expanded to an nxn system. Chapter III is the development of the required aircraft equation for both the lateral and longitudinal modes. Chapters IV and V are the design of the lateral and longitudinal controllers respectively. Chapter VI contains the simulations and a demonstration of robustness for each design is highlighted.

Appendices A and B contain a detailed derivation of the SISO and MIMO systems. Appendix C outlines the basic aircraft and includes the transformation of the stability axis derivatives to the body axis system. Also included are the required equations for the first and second bending modes. Appendix D is a sample run of the computer program used in this transformation. Appendix E is the time

response models derived for the 2x2 lateral design. Appendix G is the computer programs used in the simulation of the 2x2 lateral design. Appendix H contains the numerical analysis data and time response models used in the 3x3 longitudinal design.

#### VII-2 Discussion

This design has demonstrated the transparency of the quantitative design technique developed by Dr. Horowitz. An important result is obtained during the design of the 3x3 longitudinal controller for the rigid aircraft equations. The first design attempted was done using the unimproved design technique. The three loop transmissions are designed, taking into account the right half plane poles (i.e., contained in  $q_{11}$ ,  $q_{22}$  and  $q_{33}$ ), so that each loop transmission is on or above the required bound at each frequency. This design was simulated and the system was unstable. The question is: why is the system unstable since none of the bounds is violated? This design technique ensures a stable response if all the bounds on the system are satisfied. The reason the system is unstable, using the unimproved technique, is that the design of the first two loops is not taken into account in the design of the last loop. The last loop designed is loop two and the  $q_{22}$ 's for each flight condition have one pole in the right half plane. However, due to the design of loops one and

three, a second pole in the right half plane appears in the effective  $q_{22}$ 's for each of the three flight conditions. Since this additional -180 degree phase change was not accounted for in the unimproved design, a stable response could not be obtained. When this phase change is taken into account, using the improved design technique, a stable response is obtained. Thus it is shown that this technique is very transparent in isolating and determining problem areas during the design process. This technique also allows the designer to determine if such problems can or cannot be resolved and thus obtain the desired response from the system.

#### VII-3 Comparison to Porter Technique

The designs accomplished during this thesis are for the same maneuvers as shown in Reference 17. This reference covers the designs accomplished by Captain Locken using the Porter Technique. The results obtained using the quantitative feedback technique are quite similar to those achieved via the Porter Technique. The control surface deflection and output responses are the same for both designs. There is only one difference between the two designs and this appears in the control surface deflection. The control surface rates obtained from this design are lower than those obtained using the Porter Technique. This is possibly due to the fact that the Porter Technique

uses high gain feedback thus causing higher control surface rates. Since each control surface has a maximum allowable rate, this may be critical in some design applications.

The second comparison made between the two design techniques is that a robust controller could not be obtained for the pitch pointing maneuver using the Porter Technique. However, while using the Quantitative Feedback Technique, a robust controller was obtained. One possible explanation is in using the Porter Technique, the problems encountered and recognized in the Quantitative Feedback Technique are not apparent, thus they cannot be accounted for in Porter's design process.

One very important difference between the two techniques is that the desired responses wanted from the system, using the Quantitative Feedback Technique, are taken into account at the beginning of each design while this is not done in the Porter Technique. Also, the bandwidth of the system is known using QFT while with the Porter Technique this is unknown. The bandwidth of the system is important since the larger the bandwidth the greater the effect noise will have on the overall system.

At present, a design using the Porter Technique can be accomplished more quickly than that using QFT. This is due to the use of a computer-aided design package. However, if a number of iterations are required, then the

design process may indeed take much longer than the Quantitative Feedback Technique.

The results obtained using this technique compare well with the results obtained using the Porter Technique. The advantage of QFT over the Porter Technique is that it is very transparent and compensator bandwidth is known for each design.

#### VII-4 Conclusion

This thesis concludes that the Quantitative Feedback Technique developed by Dr. Isaac Horowitz is an effective tool in the design of multiple input-multiple output control systems. The insight given the designer due to the transparency of the design process is extremely important. The design engineer, using this technique, has the ability to make design tradeoffs between the design responses, compensator bandwidth, and determine whether a stable response is achievable.

The addition of the first and second body bending modes has very little affect on the overall design of the non-rigid aircraft. The uncertainty in the plant of the rigid and non-rigid models is essentially the same.



This technique is a viable method in the design of multiple input-multiple output robust flight control systems.

#### VII-5 Recommendations

It is recommended that this design technique be demonstrated using an aircraft where the longitudinal and lateral modes are not decoupled. The advantages of this design technique can be readily applied to such a flight control design problem.

It is highly recommended that a computer-aided design package be developed to allow the design of larger and more complex flight control systems. With the development of such a package, the design engineer can design more complex systems using the insight given by this technique.

## Appendix A: Single Input-Single Output Theory

(This appendix was taken from Reference 3 with minor changes.)

### Introduction

Appendices A and B present an overview of the Quantitative Feedback Technique used in the design of multiple input-multiple output flight control systems for this thesis. Examples are presented to aid in the understanding of the material. The technique is valid for the general  $n \times n$  case. However, for simplicity, the examples below are either single loop or  $2 \times 2$  systems. A discussion of the  $3 \times 3$  case is outlined in Chapter II.

The flight control problem involves a multiple input-multiple output (MIMO) plant requiring regulation and control due to parameter uncertainty and disturbances. The mathematical equations describing the motion of an aircraft are highly nonlinear. For design purposes, these equations are linearized about a point in the flight envelope or flight condition. Uncertainty arises as the linearized coefficients vary with airspeed and altitude (see Chapter IV).

The Quantitative Feedback Synthesis Technique developed by Dr. Isaac Horowitz uses feedback to achieve closed-loop system response within performance tolerances

despite plant uncertainty. The range of plant uncertainty and the output performance specifications are quantitative parameters in the design process (12:81). The fundamentals of the design method are presented in the discussion of the single input-single output design. The multiple input-multiple output design procedure is described in Appendix B, using the fundamentals developed in Appendix A.

#### Problem Definition

The general single input-single output (SISO) problem involves a plant transfer function,  $P$ , with uncertain parameters (gain, poles, and zeros) known only to be members of finite sets. The design specifications dictate the desired response of the plant to inputs and/or disturbances. The problem is to obtain a controller forcing the plant output to satisfy performance tolerances over the range of plant uncertainty.

The basic SISO control loop structure is shown in Figure A-1.

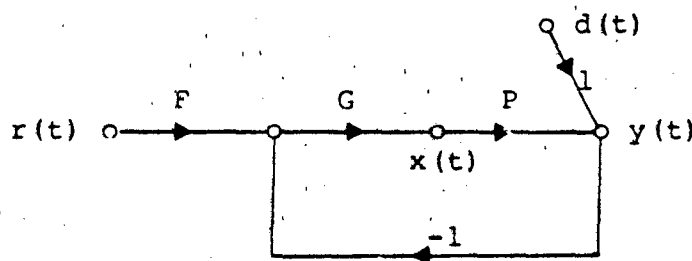


Fig. A-1. Two Degrees-of-Freedom Control Loop

In this figure,  $r(t)$  is the command input to the system and  $d(t)$  is a disturbance input to be attenuated.  $P$  is the plant transfer function, the characteristics of which are not precisely known. The compensator,  $G$ , and the pre-filter,  $F$ , are to be designed to force the system output,  $y(t)$ , to be an element of a set of acceptable responses, despite the uncertainty in  $P$  and the disturbance input  $d(t)$ . The plant input signal,  $x(t)$ , is identified since it is generally of interest because of physical constraints. The signals,  $r(t)$  and  $y(t)$  are assumed measurable quantities and the latter is available for feedback. Access to both signals allows the use of the two degree-of-freedom structure of Figure A-1 and provides the designer with two independent compensator elements,  $F$  and  $G$  (13:13). It is also assumed that  $r(t)$ ,  $y(t)$ , and (for now)  $P$ , such that  $y(t) = Px(t)$ , are all Laplace transformable functions (13:8).

There are four transfer functions of interest in Figure A-1 where the loop transmission,  $L$ , is defined as  $L = GP$ . The system output due to the command disturbance inputs, respectively, are:

$$T_R = Y(s)/R(s) = \frac{F G P}{(1 + G P)} = \frac{F G}{(1 + L)} \quad (A-1)$$

$$T_D = Y(s)/D(s) = \frac{1}{(1 + G P)} = \frac{1}{(1 + L)} \quad (A-2)$$

and the plant input due to the command and disturbance inputs, respectively, are:

$$I_R = X(s)/R(s) = \frac{F G}{(1 + G P)} = \frac{F G}{(1 + L)} \quad (A-3)$$

$$I_D = X(s)/D(s) = \frac{-G}{(1 + G P)} = \frac{-G}{(1 + L)} \quad (A-4)$$

The design specifications may impose constraints on any or all of these transfer functions, but for the purpose of this example, only the first two are considered.

#### Design Specifications

The design specifications, or closed-loop system response tolerances, describe the upper and lower limits for acceptable output response to a desired input or disturbance. Any output response between the two bounds is assumed acceptable. The response specifications must be determined prior to applying the design method. Typically, response specifications are given in the time domain, such as the figures of merit  $M_p$ ,  $t_s$ ,  $t_p$ , and  $K_m$  based upon a step forcing function (8:346), or as a bounded region as shown in Figure A-2. Response to a step input is a good initial test of system response. Bounds ( $T_L$ ) and ( $T_U$ ) of the figure are the acceptable lower and upper limits of a system's tracking performance to a step input. Desired system response to a step disturbance generally requires maintaining the output below a given value, thus only an upper bound is necessary as shown by curve ( $T_D$ ) in Figure A-2. Additional similar bounds are needed if other inputs are to be considered.

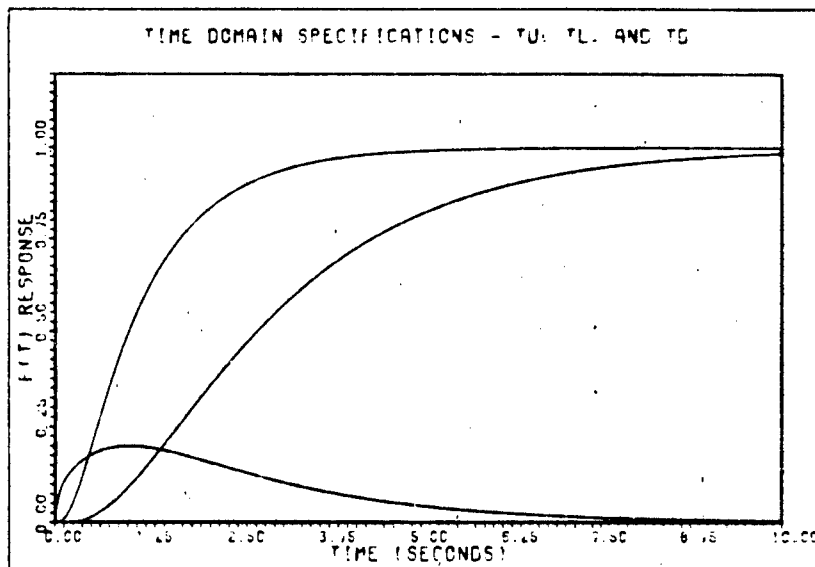


Fig. A-2. Time Domain Step Response Specifications

The design technique is a frequency domain approach; therefore, the time domain specifications must be translated to bounds in the frequency domain. Desired control ratios,  $T_{MR} = [Y/R]_{MR}$  and  $T_{MD} = [Y/D]_{MD}$ , are modeled to satisfy the performance specifications using the pole-zero placement method as described in Section 12-2 of Reference 8. For response to a step input, a third-order model with one zero is suggested.

$$T_M = \frac{A(s + z_1)}{(s + 2w_n s + w_n)(s + p_3)} \quad (A-5)$$

The pole-zero pattern of Equation (A-5) is shown in Figure A-3. The locations of the roots are adjusted until the step response of the modeled control ratio matches the bound.

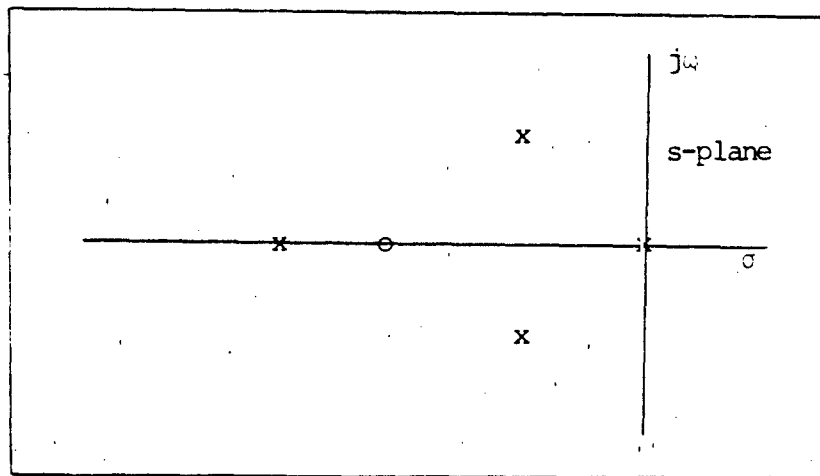


Fig. A-3. Third-Order Control Ratio Pole-Zero Pattern

The frequency domain characteristics are considered during the response modeling. It is desirable to keep the magnitude difference (as a function of frequency) between the upper and lower bound models of  $T_{MR}(j\omega)$  as large as possible at all frequencies. Choosing a lower bound model with a greater pole to zero ratio than the upper one ensures that the magnitude difference approaches infinity in the limit as  $\omega$  approaches infinity.

Errors made during this modeling process manifest themselves in one of two ways. First, if the worst acceptable response model is not really acceptable, the system may not meet the specifications over the assumed range of uncertainty in  $P$ . And, second, if the entire range of

allowable outputs is not considered, the bandwidth of the compensation will be higher than necessary, increasing the cost of the compensator (13:5).

Once control ratios are obtained for each time response bound, a magnitude plot of the frequency response (Bode plot) for each  $T_M(j\omega)$  is made on the same graph as shown in Figure A-4. These plots are the frequency domain representation of the design specifications on  $T_R$  and  $T_D$ . These derived frequency domain specifications are used to obtain the bounds on the loop transmission,  $\underline{L}(j\omega)$ , as described later.

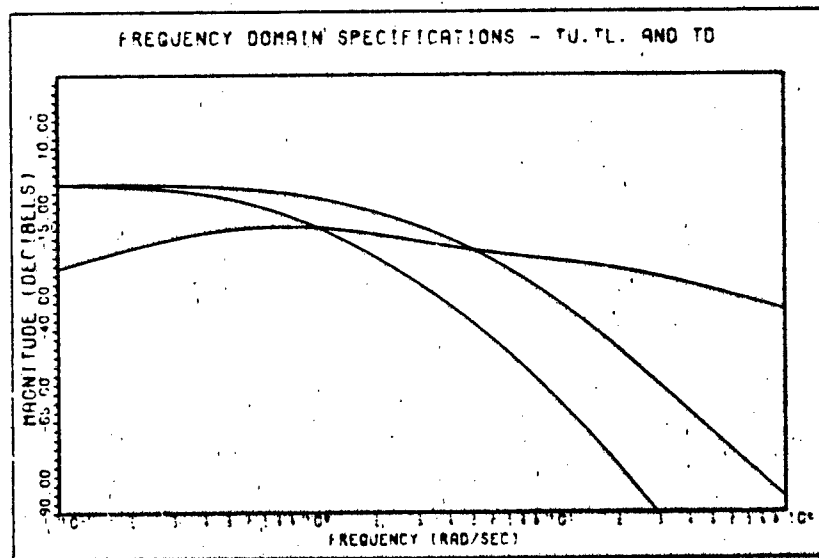


Fig. A-4. Frequency Domain Specifications

#### Nichols Chart

The primary tool used in the design of the compensator elements,  $G$  and  $F$  is the Nichols chart, shown in



Figure A-5. If the open loop transmission of a unity feedback system ( $L=GP$ , assuming  $F=1$  for now, in Figure A-1) is plotted using the horizontal and vertical scales on the chart, then at any given frequency, the magnitude and phase angle of  $T_R=L/(1+L)$  can be read directly from the curved scales. Conversely, any point corresponding to the magnitude and angle of  $T_R$  on the curved scales provides a point corresponding to the magnitude and angle of  $L$  on the horizontal and vertical scales (8:332-334). This correspondence between  $L$  and  $T_R$  on the Nichols chart is very important.

Likewise, the Nichols chart can be used for the disturbance response. Recall that  $T_D=1/(1+L)$ . By way of Sidi's transformation,  $L=1/m$  (1:152-155) the system control ratio due to the disturbance becomes  $T_D=m/(1+m)$ , which is of the same form as  $T_R=L/(1+L)$ . One could design the inverse of the loop transmission,  $m$ , directly on the Nichols chart, but it is much easier to realize that by turning the Nichols chart upside down, reflecting the vertical angle of  $L$  lines about the  $-180$  degree line (i.e.,  $-190$  becomes  $-170$ ,  $-210$  becomes  $-150$ , etc.), and reversing the signs on all magnitude lines, the chart can be used directly to design  $L$  itself. The horizontal and vertical lines still correspond to the magnitude and angle of  $L$ , and the curved magnitude lines correspond to the magnitude of  $(1+L)$  (1:155). For design purposes, only the magnitude of  $(1+L)$  is required. Therefore, the curved angle lines

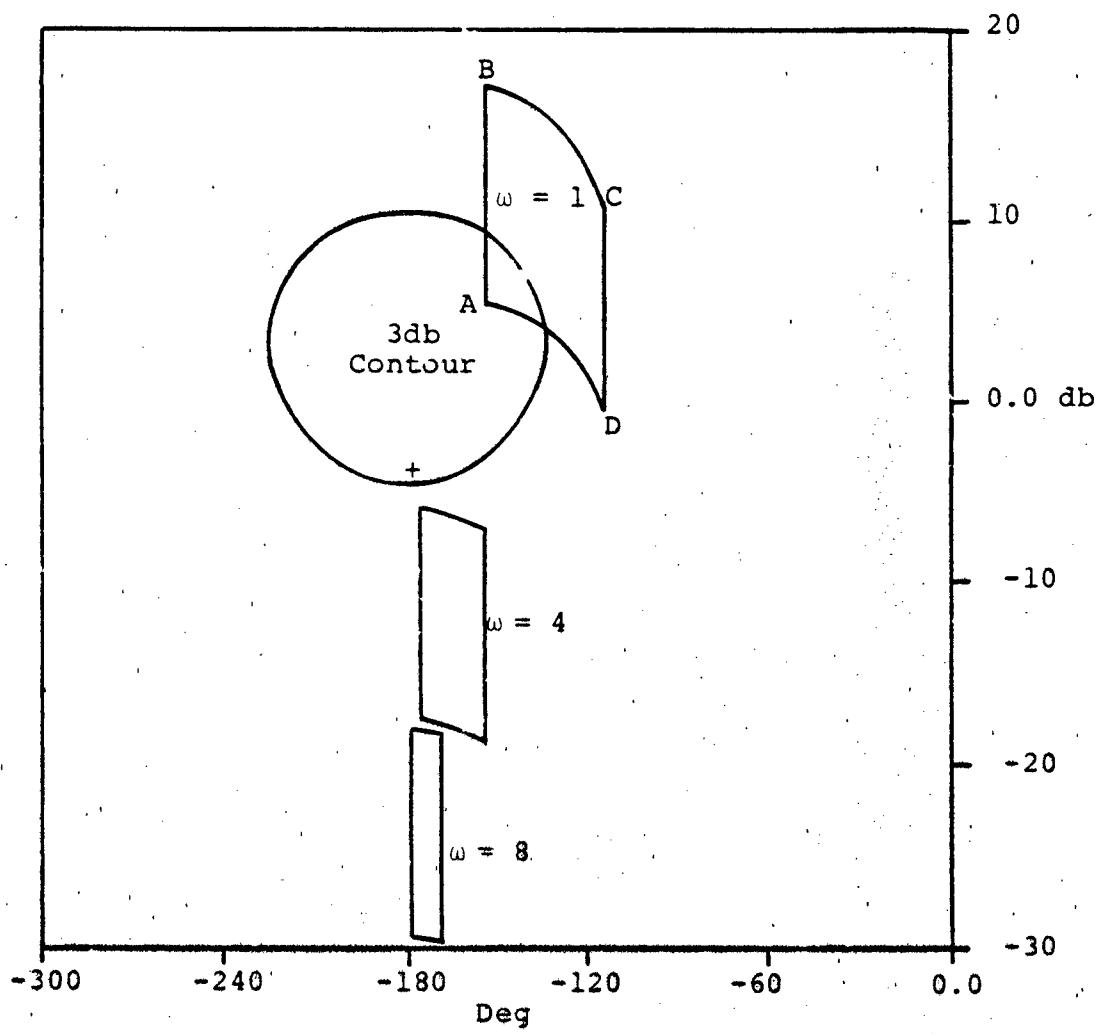


Fig. A-5. Nichols Chart with Plant Templates

on the chart can be ignored. In practice, Sidi's transformation is merely implied by turning the Nichols chart upside down and modifying the scales as described above. The dummy variable,  $m$ , need not be considered further.

#### Plant Templates

A plant template is a plot on the Nichols chart of the range of uncertainty in the plant  $P$  at a given frequency (14:290). Consider the example  $P(s) = Ks(s-a)$  where the gain  $K$  is described by:  $2 \leq K \leq 8$ , and the location of the second pole is given by:  $0.5 \leq a \leq 2.0$ . An infinite number of possible  $P$ 's exist due to the variation in parameters,  $K$  and  $a$ ; however, each parameter is a member of a set with finite boundaries. Likewise, the magnitude and phase angle of all possible  $P$ 's lie within finite boundaries when plotted at a given frequency. The plant template is obtained by plotting  $\text{Mag}[P(j\omega)]$  vs.  $\text{Ang}[P(j\omega)]$  for all possible  $P(j\omega)$ 's, that is over the range of uncertainty at a given frequency on the Nichols chart. Note, only the outer edges of the template need be calculated. The plant transfer functions at the boundaries are found by holding one parameter constant at a boundary value, i.e., set  $K=2$ , and vary  $a$  in increments from 0.5 to 2.0. The frequency response at  $\omega=1$  for the  $P$ 's obtained above provides a set of points from A, ( $K=2, a=0.5$ ), to D, ( $K=2, a=2$ ), on the Nichols chart as shown in Figure A-5. The process is continued until

the complete template is formed. For example, for  $a=0.5$ , vary  $K$  from 2 to 8 to obtain the line from A, ( $a=0.5$ ,  $K=2$ ), to B, ( $a=0.5$ ,  $K=8$ ). Templates are needed for a number of frequencies taken at regular intervals, such as every octave. A set of templates is shown in the figure to demonstrate the change in size and location of the range of uncertainty in  $P$  for different frequencies.

#### Nominal Plant

To facilitate the shaping of the loop transmission, the designer needs a reference or nominal plant transfer function. This nominal plant,  $P_0$ , chosen by the designer, is nothing more than a reference plant to be used in the definition and shaping of the nominal loop transmission,  $L_0 = GP_0$ . There are no rules or constraints on the selection of  $P_0$ . It doesn't even have to be from the set of possible  $P$ 's, but it is usually convenient to choose  $P_0$  such that it lies at a recognizable point on the templates. It is convenient, as is the case with the example, to select  $P_0$  such that it lies at the lower, left hand corner of the templates. This choice for  $P_0$  keeps the bounds on  $L_0$ , to be described next, as near the center of the Nichols chart as possible. Once selected, the  $P_0$  point should be marked on each template, as in Figure A-5. For the example, the plant described by  $P_0 = 2/(s + 0.5)$  is chosen as the nominal plant.

### Derivation of Bounds on L

The system step response  $y(t)$  is uniquely determined by the transfer function  $T(s)$ . Likewise,  $T(s)$ , for a stable, minimum phase system (no right-half-plane poles or zeros), is completely specified by the magnitude of the frequency response  $\underline{T}(j\omega)$  as described in References 13 and 14. From the design specifications, the frequency response of the output  $\underline{Y}(j\omega)$  can vary from the value of the bound  $(T_U)$  to the value on the bound  $(T_L)$  at a given frequency (see Figure A-4). For the given example, at the frequency,  $\omega = 1$ , assume that  $\underline{Y}(j1)$  can vary from 0.7db to -0.8db. The relative variation in  $\underline{Y}(j1)$  is  $(0.7)\text{db} - (-0.8)\text{db}$  or 1.5db. In general, the allowable relative change in  $\underline{Y}(j\omega)$  at a given frequency is expressed as:

$$\Delta \text{Lm} [\underline{Y}(j\omega)] = \Delta \text{Lm} [T_U(j\omega)] - \Delta \text{Lm} [T_L(j\omega)] \quad (\text{A-6})$$

where  $T_U(j\omega)$  and  $T_L(j\omega)$  are the frequency domain bounds on  $\underline{Y}(j\omega)$ .

The relative change in the output is related to the control ratio as follows. From Figure A-1 and Equation (A-1),  $\text{Lm} Y = \text{Lm} T = \text{Lm} [FL/(1+L)]$  where  $L = GP$  and it is assumed that no uncertainty exists in  $G$  and  $F$ . Then,

$$\Delta \text{Lm} [Y(j\omega)] = \Delta \text{Lm} [T(j\omega)] = \Delta \text{Lm} \frac{L(j\omega)}{[1 + L(j\omega)]} \quad (\text{A-7})$$

Likewise, the relative change in  $\underline{L}(j\omega)$  is equal to the relative change in the plant.

$$\Delta \text{Lm} [L(j, \omega)] = \Delta \text{Lm} [P(j, \omega)] \quad (\text{A-8})$$

The variation in  $P$  arises due to parameter uncertainty, thus the problem is to find an  $L$  such that the relative change requirements on the closed-loop response are satisfied for the entire uncertainty range of  $P$ . The design specifications state the requirements on the closed-loop response  $\underline{Y}(j, \omega)$  and thus  $\underline{T}(j, \omega)$  as given by Equation (A-7). Constraints on the loop transmission  $\underline{L}(j, \omega)$  are desired (14:291; 13:18).

#### L(j, ω) Bounds on the Nichols Chart

The relative uncertainty in  $L$  is shown to be equal to the range of uncertainty in  $P$  by Equation (A-8). As described earlier, the plant template is a plot on the Nichols chart of the range of uncertainty in  $P$  at a given frequency. Because  $\text{Lm} (L) = \text{Lm} (P) + \text{Lm} (G)$  and also  $\text{Ang} (L) = \text{Ang} (G)$ , a template may be translated (but not rotated) horizontally or vertically on the Nichols chart, where horizontal and vertical translations correspond to the angle and magnitude requirements on  $\underline{G}(j, \omega)$  respectively at a given frequency (14:290). Drawing a line on each of the templates parallel to the horizontal or vertical grid lines (see Figure A-5) of the Nichols chart is suggested to maintain correct template orientation.

With the template corresponding to  $\omega = 1$  of Figure A-5, translate it to position 1 shown in Figure A-6.

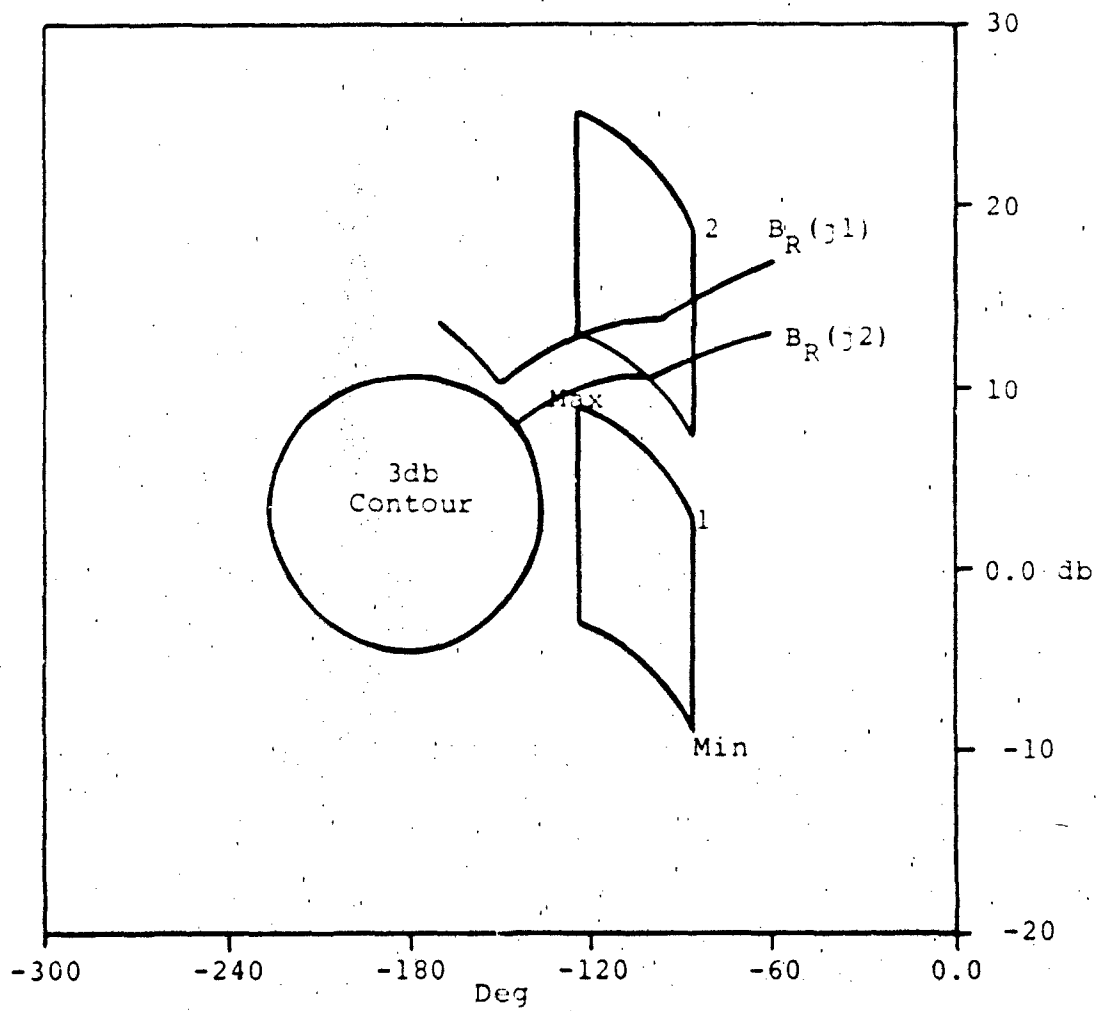


Fig. A-6.  $L_O(j\omega_1)$  Bounds on the Nichols Chart

Since the template is the range of uncertainty in  $P$  and  $L = GP$ , where  $G$  is to be precisely determined, it follows that the area now covered by the template corresponds to the variation in  $L$  and in  $T$  due to the uncertainty of  $P$ . Recall the correspondence between  $L$  and  $T$  on the Nichols chart. Using the curved magnitude contours, i.e., contours of constant  $Lm[T(j\omega)]$ , read the maximum and minimum values of  $T$  covered by the template. If the difference between the maximum and minimum values is greater than the allowable variation in  $T$  at the frequency  $\omega = 1$ , that is  $(\Delta Lm [T(j1)])$  as given by Equation (A-7) and determined from Figure A-4, shift the template vertically, as shown in Figure A-6, until the difference is equal to  $Lm[T(j1)]$  (to position 2). Conversely, if the difference is less than that allowed, move the template vertically downward until the equality is obtained. When the position of the template achieves the equality (position 2 of the example), mark the nominal point  $P_0$  of the template on the Nichols chart. The point marked corresponds to a bound on the magnitude and phase angle values of  $L_0(j1)$  read from the horizontal and vertical scales of the Nichols chart, where the nominal loop transmission,  $L_0(j\omega_i)$  is given by:

$$L_0(j\omega_i) = G(j\omega_i)P_0(j\omega_i) \quad (A-9)$$

Repeat the process horizontally across the chart at different values of  $Ang(L_0)$ . The points marked on the chart



form a curve,  $\underline{B}_R(j\omega_i)$ , representing the boundary of  $\underline{L}_O(j\omega_i)$  at the given frequency of the template. As long as  $\underline{L}_O(j\omega_i)$  lies outside or above the boundary,  $\underline{B}_R(j\omega_i)$ , corresponding to  $\omega = \omega_i$  at the frequency  $\omega = \omega_i$ , the variation in T due to the uncertainty in P is less than or equal to the relative change in T allowed by the design specifications at that frequency. Repeat this boundary,  $\underline{B}_R(j\omega_i)$ , derivation for various frequencies,  $\omega_i$  using the corresponding plant templates to obtain a series of bounds on  $\underline{L}_O(j\omega_i)$  (14: 291-292).

Likewise, the step disturbance response specification (line  $T_D$  on Figure A-4), is converted to bounds on  $\underline{L}_O(j\omega)$ . In order to effectively reject the disturbance the following inequality must be satisfied:

$$1/|1 + L(j\omega)| \geq |C(j\omega)| \quad (A-10)$$

where  $\underline{C}(j\omega)$  is the magnitude of the boundary, ( $T_D$ ), on Figure A-4. Converting the magnitudes to decibels and rearranging terms, the inequality can be expressed as:

$$\text{Lm } [1 + L(j\omega)] \geq -\text{Lm } [C(j\omega)] \quad (A-11)$$

Now a template is placed on the inverted Nichols chart such that its lowest point rests directly on the contour of constant  $\text{Lm } [1 + L(j\omega)]$  equal to  $-\text{Lm } [C(j\omega)]$  at the frequency,  $\omega_i$ , for which the template is drawn. The point,  $P_O$ , is marked and the template slid along the same contour

forming a bound,  $\underline{B}_D(j\omega_i)$  for  $L_o$ . Bounds are formed for each frequency, in this manner using each template. Using the rectangular ( $L_m L$ ) grid, transcribe the bounds,  $\underline{B}_D(j\omega_i)$ , on  $L_o$  onto the upright Nichols chart which already contains the command response bounds,  $\underline{B}_R(j\omega)$ , on  $L_o$  as shown in Figure A-7. For each frequency of interest, erase the lower of the two  $L$  bounds, where the remaining bound is labeled,  $\underline{B}_O(j\omega)$ . The point here is that the worst bound must be used in the shaping of  $L_o$ .

#### Universal Frequency Bound

The universal frequency (UF) bound ensures the loop transmission,  $L$ , has positive phase and gain margins, whose values depend on the oval of constant magnitude chosen (see Figure A-7). As the frequency,  $\omega$ , increases, the plant templates become narrower and can be considered vertical lines as  $\omega$  approaches infinity. The allowable variation in  $T$  increases with frequency also. The result is the bounds of  $\underline{L}_o(j\omega_i)$  tend to become a very narrow region around the 0db, -180 degree point (origin) of the Nichols chart at high frequency. To avoid placing closed-loop poles near the  $j\omega$  axis resulting in oscillatory disturbance response, a UF bound is needed on the Nichols chart. With increasing  $\omega$ , the bounds on  $L_o$  approximately follow the ovals encircling the origin. Choose one of the ovals near the origin. In Figure A-7, the contour of constant magnitude equal to 5db is used in this example.

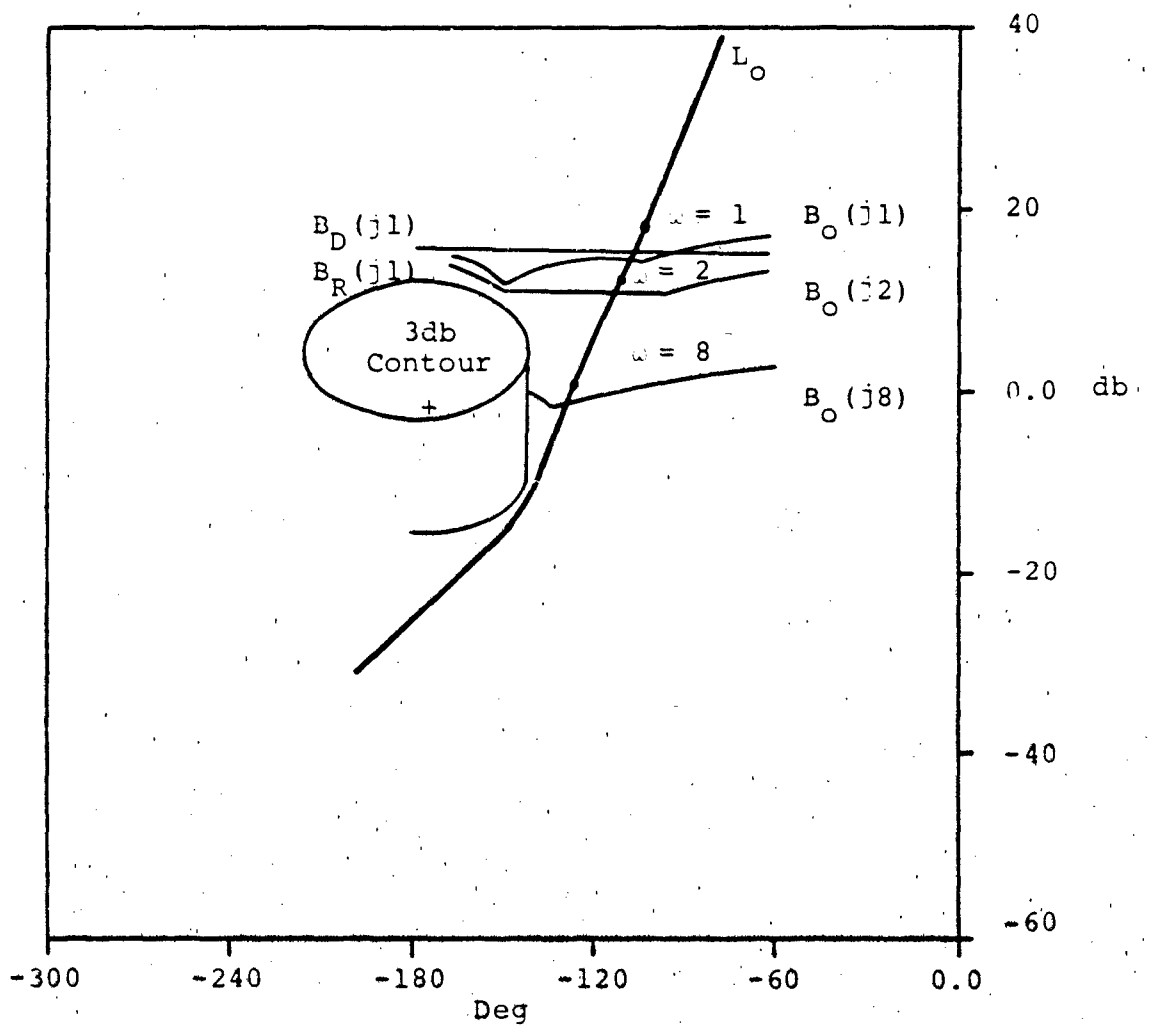


Fig. A-7. Nominal  $L_O(j\omega_i)$ .

From the templates corresponding to high frequency, find the template with the greatest vertical displacement,  $\Delta v$ , in db.  $\Delta v$  may be accurately determined by finding the maximum change in  $Lm[P(j\omega)]$  in the limit as  $\omega$  goes to infinity. Translate the lower half of the 5db oval down the length of the template, i.e.,  $\Delta v$  db, as shown, thus obtaining the UF bound (see Figure A-7). (Note: Professor Horowitz refers to this bound as the Universal High Frequency (UHF) Bound) (13:20-22.)

#### Shaping of the Nominal Loop Transmission

The shaping of a nominal loop transmission conforming to the boundaries of  $L_o$  is a most crucial step in the design process. A minimum bandwidth design has the value of  $L_o$  on its corresponding bound at each frequency. In practical designs, the goal is to have the value of  $L_o$  occurring above the corresponding bound, but as close as possible to keep the bandwidth to a minimum. Figure A-7 shows a practical design for  $L_o$ . Note, any right-half-plane (rhp) poles and/or zeros of  $P_o$  must be included in  $L_o$  to avoid any attempt to cancel them with zeros of  $P_o$  as a starting point in the design of  $L_o$  is suggested, to avoid any implicit cancellation of roots in determining  $G$ .

#### Solving for $G$

The compensator,  $G$ , is obtained from the relation:  
 $G = L_o/P_o$ . If the  $L_o$  found above does not contain the

roots of  $P_0$ , then the compensator  $G$  must cancel them. Note, cancellation occurs only for purposes of design using the nominal plant transfer function. In actual implementation, exact cancellation does not result (nor is it necessary) since  $P$  can vary over the entire uncertainty range.

Provided the nominal loop transmission,  $L_0$ , is shaped properly, i.e., meets the requirement of being on or above the bound,  $\underline{B}_0(j\omega_i)$ , at each corresponding frequency, the variation in  $T$  resulting from the uncertainty in  $P$  is guaranteed to be less than or equal to the allowable relative change in  $T$  allowed by the design specifications (14:291). The design of the pre-filter,  $F$ , is the final step in the design process.

#### Design of $F$

Design of a proper  $L_0$  only guarantees the variation in  $\underline{T}(j\omega)$  is less than or equal to that allowed. The purpose of the pre-filter is to position  $\text{Lm}[\underline{T}(j\omega)]$  within the frequency domain specifications. For the example given above, the magnitude of the frequency response must lie within the bounds shown in Figure A-4 which are redrawn in Figure A-8. One method for determining the bounds on the pre-filter,  $F$ , is as follows. Place the nominal point of the  $\omega = 1$  template on the Nichols chart where the  $\underline{L}_0(j1)$  point occurs. Record the maximum and minimum values of

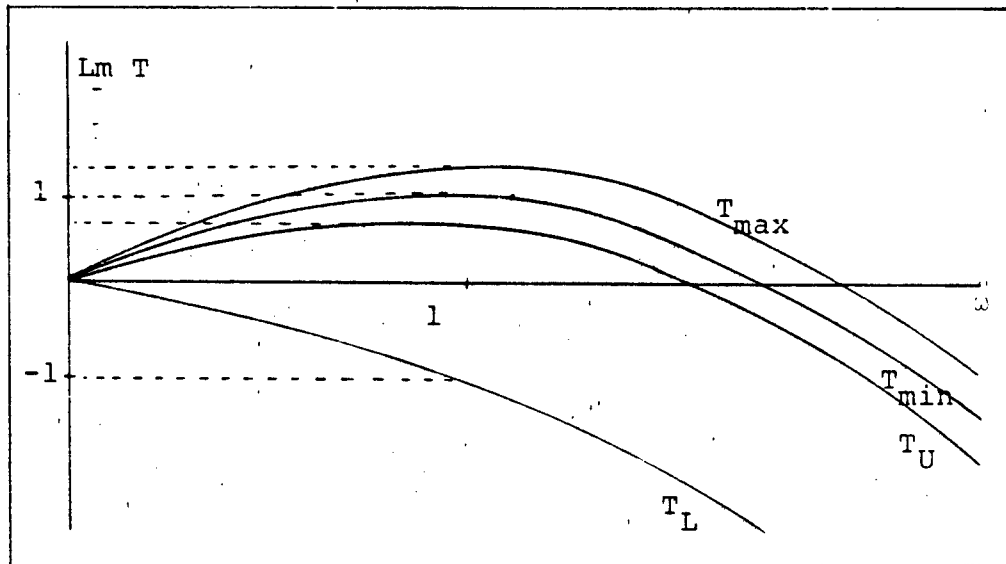


Fig. A-8. Requirements of F

$L_m(T)$ , 1.2 and 1.0 in the example, obtained from the curved magnitude contours. Compare the values found above to the maximum and minimum values allowed by the frequency domain specifications of Figure A-4 at  $\omega = 1$  (0.7db and -0.8db). Determine the range, in db,  $L_m(T)$  must be raised or lowered to fit within the bounds of the specifications. For example, at  $\omega = 1$ , the actual  $L_m(T)$  must be within  $[L_m(T_U) = 0.7 \text{ db}] > L_m[T(j1)] > [L_m(T_L) = -0.8\text{db}]$ . But, from the plot of  $L_o$ , the actual range of  $L_m(T)$  is:  $1.2\text{db} > L_m[T(j1)] > 1.0\text{db}$ . To lower  $L_m[T(j1)]$  from the actual range to the desired range, the pre-filter,  $L_m(F)$  is required:  $(0.7 - 1.2\text{db}) > L_m[F(j1)] > (-0.8 - 1.0\text{db})$ , or  $-0.5\text{db} > L_m[F(j1)] > -1.8\text{db}$  (see Figure A-8). The process is repeated for each frequency corresponding to the templates used in the design of  $L_o$ . Therefore,

in Figure A-9 the difference between the  $T_U$  and  $T_{\max}$  curves and the difference between the  $T_U$  and  $T_{\min}$  curves indicate the requirements for  $F$  as a function of frequency.

Bounds of  $F$ ,  $[\text{Lm}(T_U) - \text{Lm}(T_{\max})] > \text{Lm}(F) > [\text{Lm}(T_U) - \text{Lm}(T_{\min})]$ , are plotted as a function of frequency as shown in Figure A-9. By use of the straight line approximation, determine a transfer function,  $F$ , such that its magnitude lies within these bounds. The transfer function obtained in this manner is the pre-filter,  $F$  (14:301).

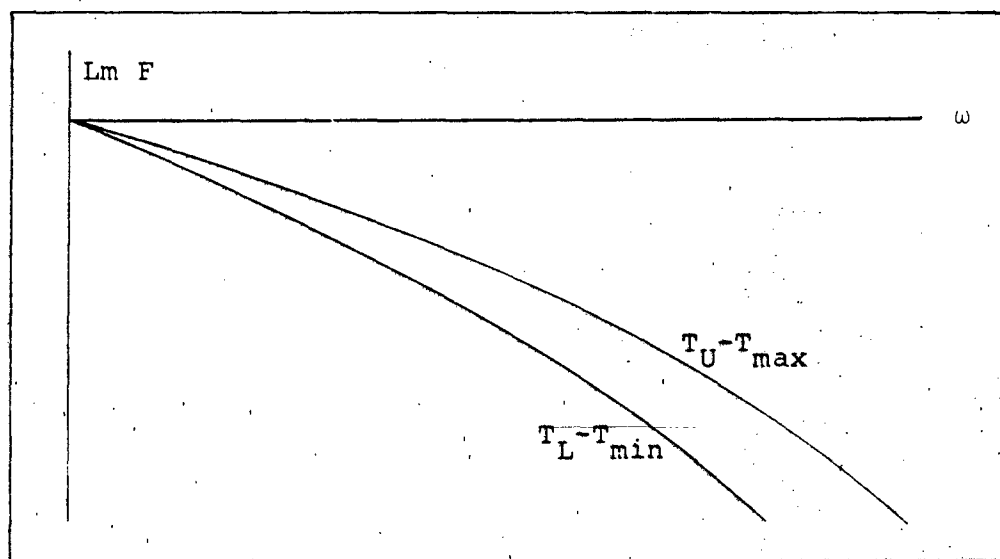


Fig. A-9. Frequency Bounds on the Pre-filter,  $F$

The single loop design is complete with the design of  $F$ . The system response is guaranteed to remain within the bounds of the design specifications, provided the uncertainty in  $P$  stays within the range assumed at the beginning of the design process (14:238).

### Summary

This appendix presents an overview of the SISO design technique of Professor Horowitz for the single loop systems with uncertain plants. The technique is entirely based in the frequency domain, and makes considerable use of the Nichols and Bode plots. Much of the designing can be done by graphical methods.

Design specifications are translated into the frequency domain and constitute limits or boundaries on the frequency response of the system control ratio and the loop transmission. Two compensator elements,  $G$  and  $F$ , are synthesized to control the system response to inputs and disturbances.



## Appendix B: Multiple Input-Multiple Output Theory

(This appendix was taken from Reference 3 with minor changes.)

### Introduction

The design approach for each loop of the MIMO system is identical to that for the SISO system described in Appendix A. But first the MIMO system must be separated into SISO loops which are equivalent to the actual MIMO model.

In general, an  $n \times n$  MIMO system can be represented in matrix notation as  $\underline{y} = \underline{P}\underline{u}$ , where  $\underline{y}$  is the vector of plant outputs,  $\underline{u}$  is the vector of plant inputs, and  $\underline{P}$  is the plant matrix of transfer functions relating  $\underline{u}$  to  $\underline{y}$ . This  $\underline{P}$  matrix is formed from either the linear differential equations describing the system or directly from the system state space representation.

Professor Horowitz has shown, by the use of fixed point theory, that the inverse of the  $\underline{P}$  matrix, referred to as  $\underline{Q}$ , contains elements which are the inverses of  $n^2$  single loop transfer functions equivalent to the original MIMO plant. The MIMO problem is then broken up into  $n$  loop designs and  $n$  pre-filter/disturbance problems, which are each handled as described in Chapter II (10:677).

### The MIMO Plant

Consider the multiple input-multiple output plant of Figure B-1. The  $n \times 1$  input vector,  $\underline{u}$  produces an  $n \times 1$  output vector,  $\underline{y}$ . The relationship between  $\underline{y}$  and  $\underline{u}$  is described by the  $n \times n$  plant matrix,  $\underline{P}$ , which is known only to be an element of a set of possible  $\underline{P}$ 's. It is assumed that the range of uncertainty in  $\underline{P}$  can be determined, probably in the form of empirical data relating  $\underline{u}$  to  $\underline{y}$ .

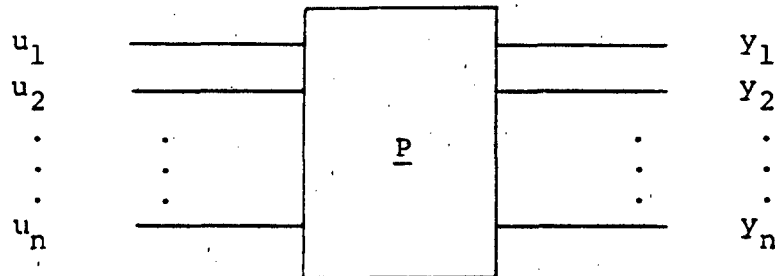


Fig. B-1. MIMO Plant

Note that the input and output vectors are assumed to be of the same dimension. Although this may appear to be a restrictive assumption, it can be shown that with  $n$  inputs, at most  $n$  outputs can be independently controlled (15: 530-536). Thus, if the existing model defines an unequal number of inputs and outputs, the first step is to modify the model such that the dimensions of the input and output vectors are equal. An example of such a modification is presented in Chapter IV.

The plant matrix  $\underline{P}$ , can be derived directly from the set of coupled, linear, time-invariant differential

equations describing the behavior of the plant in response to its inputs. Consider a general plant model of the form:

$$\begin{aligned} (a)y_1 + (bs + c)y_2 &= (f)u_1 + (g)u_2 \\ (ds)y_1 + (e)y_2 &= (h)u_1 + (i)u_2 \end{aligned} \quad (B-1)$$

where a through i are the constant coefficients, and Y's are the outputs, and the u's are the inputs to the plant. The system of Equation (B-1) can be represented in matrix notation as:

$$\begin{bmatrix} a & bs + c \\ ds & e \end{bmatrix} \underline{Y} = \begin{bmatrix} f & g \\ h & i \end{bmatrix} \underline{u} \quad (B-2)$$

Define the matrix multiplying the output vector as M and the matrix multiplying the input vector as N. The system is now described by:

$$\underline{My} = \underline{Nu} \quad (B-3)$$

The plant matrix needed is defined by:

$$\underline{Y} = \underline{Pu} \quad (B-4)$$

Thus the plant matrix, P is simply:

$$\underline{P} = \underline{M}^{-1}\underline{N} \quad (B-5)$$

The standard state space representation for a system is described by the equations (11:93):

$$\begin{aligned} \dot{\underline{x}} &= \underline{A}\underline{x} + \underline{B}\underline{u} \\ \underline{y} &= \underline{C}\underline{x} \end{aligned} \quad (\text{B-6})$$

The block diagram for this system is shown in Figure B-2.

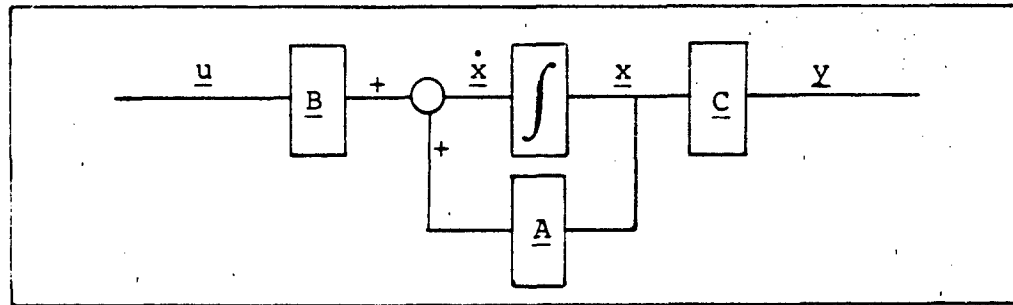


Fig. B-2. Standard State Space Diagram

Although any number of states may be represented, it is again assumed that the input and output vectors,  $\underline{u}$  and  $\underline{y}$  respectively, are of the same dimension. Assuming the system is linearized and the  $\underline{A}$ ,  $\underline{B}$ , and  $\underline{C}$  matrices are time invariant, the plant matrix is:

$$\underline{P} = \underline{C}[\underline{sI} - \underline{A}]^{-1} \underline{B} \quad (\text{B-7})$$

This plant matrix is actually a representative member of a set of possible plant matrices due to the uncertainty in the plant parameters. In practice, a finite set of  $\underline{P}$  matrices are formed representing the plant under varying conditions.

#### MIMO Compensation

The compensation scheme for the MIMO system is similar to that of the SISO system of Chapter II. The

basic MIMO control structure is shown in Figure B-3 where  $\underline{P}$  is the uncertain plant matrix,  $\underline{G}$  is a diagonal compensator matrix, and  $\underline{F}$  is a pre-filter matrix. Designs involving a non-diagonal  $\underline{G}$  matrix are not considered in this thesis (11:14).

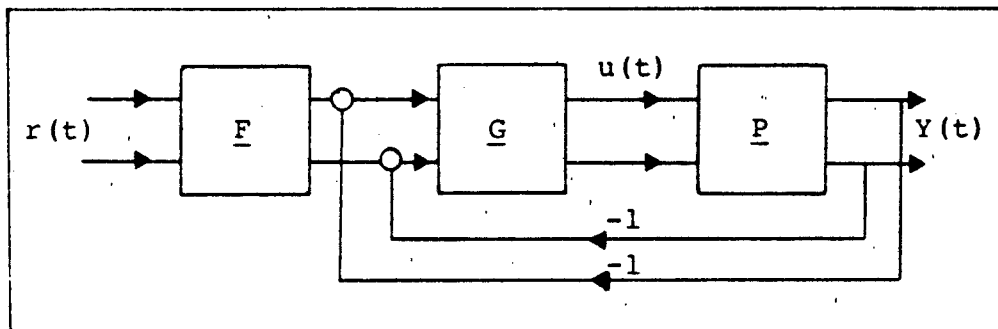


Fig. B-3. MIMO Control Structure

The functions of  $\underline{G}$  and  $\underline{F}$  are identical to those of  $G$  and  $F$  of the SISO system of Appendix A. Figure B-4 shows a more detailed breakdown of a 2x2 MIMO system where:

$$\underline{G} = \begin{bmatrix} g_1 & 0 \\ 0 & g_2 \end{bmatrix} \quad \underline{F} = \begin{bmatrix} f_{11} & f_{12} \\ f_{21} & f_{22} \end{bmatrix} \quad \underline{P} = \begin{bmatrix} P_{11} & P_{12} \\ P_{21} & P_{22} \end{bmatrix}$$

#### Constraints on the Plant Matrix

The set of  $\underline{P}$  matrices must be tested to ensure that two critical conditions are met (12:86-90):

1.  $\underline{P}$  must not be singular for any possible combination of plant parameters; i.e.,  $\underline{P}^{-1}$  must exist.
2. As  $s \rightarrow \infty$ ,  $|P_{11}P_{22}| > |P_{12}P_{21}|$  for all possible plants. This is the requirement for a 2x2 plant.

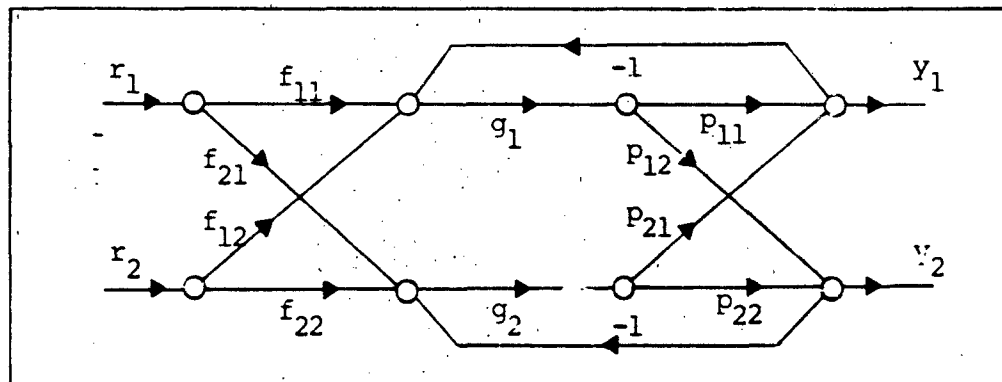


Fig. B-4. Two-by-Two MIMO System

For explanation of the constraint inequality for the 3x3 or higher cases, see Reference 12 and Chapter II.

The first condition is absolutely necessary to ensure controllability of the plant. The inverse of  $\underline{P}$  produces the effective transfer functions used in the design. If condition 2 is not satisfied, it may be possible to change the ordering of the input or output vector which changes the ordering of the  $\underline{P}$  matrix elements.

#### Effective SISO Loops

Now define a matrix  $\underline{Q}' = \underline{P}^{-1}$  which has elements,  $q'_{ij}$ . The  $n^2$  effective transfer functions needed are:  $q_{ij} = 1/q'_{ij}$ . Reference 12 contains the derivation and proof of this equivalence. The  $n \times n$  MIMO system is now treated as  $n^2$  SISO problems. Figure B-5 shows the four effective SISO loops resulting from the 2x2 MIMO system (10:682).

Each loop in Figure B-5 is handled as an individual SISO design problem in accordance with the procedures presented in Appendix A. The f's and g's are the

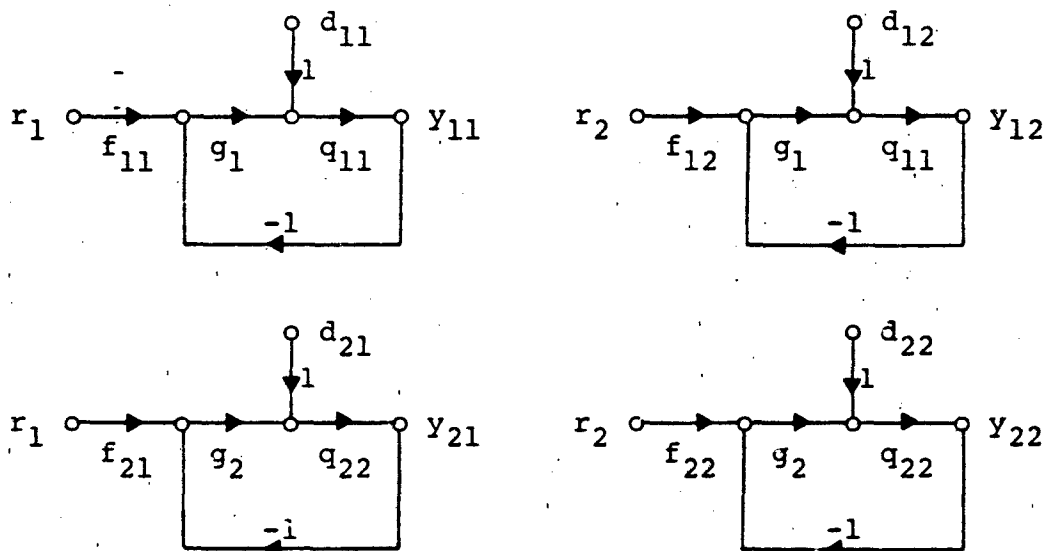


Fig. B-5. Effective SISO Loops

compensator elements  $F$  and  $G$  described previously. The disturbances,  $d_{ij}$  represent the interaction between the loops.

$$-d_{ij} = \sum_k \frac{b_{kj}}{q_{ik}}, \quad k \neq i \quad (\text{B-8})$$

The  $b_{kj}$  in the above equation is the upper response bound, ( $T_U$  or  $T_D$  in Figure B-4), for the respective input/output relationship. These are obtained from the design specifications (10:681-684). Note that the first digit of the subscript of  $b_{kj}$  refers to the output and the second digit to the input. Thus,  $b_{kj}$  is a function of the response requirements on the output,  $y_k$ , due to the input,  $r_j$ .

A recent improvement in the design technique involves modification of the  $a$ 's on the second and subsequent loops based on the  $g$ 's already designed. This reduces the overdesign inherent in the early part of the design process. During the design of the final loop the exact equation, representing the loop and the interactions of the other loops, is used (9:977). The use of this improvement is demonstrated in the actual design, Chapter IV.

#### Basically Non-interacting (BNIC) Loops

When the response of an output,  $y_k$ , due to an input,  $r_j$ , is ideally zero, the  $y_{kj}$  loop is called a basically non-interacting (BNIC) loop (10:679). Due to loop interaction and plant uncertainty, this ideal response is not achievable. Therefore, the performance specifications describe maximum responses and the loop is handled exclusively as a disturbance rejection problem.

#### Summary

This appendix describes the multiple input-multiple output plant and the plant matrix which describes it. Guidelines are presented for finding the  $P$  matrix, which relates the input vector to the output vector.

The division of the MIMO system into separate SISO loops is presented via inverse of the  $P$  matrix. After the



equivalent SISO loops are determined, each is designed in accordance with the SISO design theory presented in Appendix A.

## Appendix C: Aircraft Equations

(This appendix was taken from Reference 17 with minor changes.)

### Introduction

This appendix gives a description of the KC-135 aircraft and discusses the sign convention used in this thesis. The conversion of the nondimensional stability axis derivatives to the dimensional body axis system is outlined. The addition of the first and second body bending modes is also included.

### Aircraft Description (5)

The KC-135 is a four-engine jet-powered tanker/cargo aircraft. The swept wing is mounted low on the fuselage at an incidence of 2 degrees and is tailored for high subsonic cruise speeds. The aircraft has a basic weight of approximately 106,000 pounds, depending on equipment installed, and a maximum gross weight of 287,000 pounds. All control surfaces, except the spoilers, are aerodynamically balanced and operated by means of control tabs. A hydraulically boosted rudder is installed on all aircraft. The lateral control system is composed of integrated aileron and spoiler control surfaces. The spoilers may also be used as speed brakes when operated symmetrically. Movement of the inboard ailerons causes

a corresponding movement of the outboard ailerons if the wing flaps are extended beyond the 23 degree point. Such is the case for the flight condition representing the landing phase in this thesis. If the wing flaps are up, a lockout mechanism prevents the outboard ailerons from moving. Lateral trim of both the rudder and ailerons is accomplished manually by rotating a trim wheel which position trim tabs on respective control surfaces.

Longitudinal control is provided by an all moveable stabilizer and elevator system. The stabilizer position is set by a trim wheel which can be operated electrically or manually. All three F.C.'s used in this thesis assume a horizontal stabilizer setting, which results in no elevator deflection required to maintain that flight condition. It should be noted that no flight control surface, either lateral or longitudinal, is modified for the purpose of this thesis and all functions as described by the current Technical Order Specification at the time of this thesis (20).

The four Pratt and Whitney J57-P-59W or -43WB engines are mounted individually below the wing on forward swept struts. The engines are each rated at 12,845 pounds thrust for a standard day at sea level (15 deg. C, 29.29 inches of mercury). Other related geometric data as found in Reference 5 is as follows:

<u>Characteristic</u>	<u>Symbol</u>	<u>Dimension</u>
Fuselage	F	128.83 ft.
Wing Area	S	2433 sq.ft.
Wing Span	b	130.83 ft.
Wing M.A.C.	c	20.16 ft.
Distance from 25% Wing M.A.C. to 25% Horizontal Tail M.A.C.	$l_t$	61.39 ft.

The abbreviation, M.A.C., stands for mean aerodynamic chord. Further data for the KC-135 aircraft can be found in References 5 and 20.

#### Control Inputs

Control inputs available include two lateral controls, the rudder ( $\delta_r$ ) and the ailerons and spoilers ( $\delta_w$ ).  $\delta_w$  is modeled as the control wheel movement and its limits are set at  $\pm 90$  degrees. A control wheel movement corresponds to a combined aileron and spoiler displacement. Movement of the control wheel within its limits results in both aileron and spoiler movements within their limits.  $\delta_r$  is rudder displacement and its limits are set at  $\pm 17$  degrees. Longitudinal control includes the elevator ( $\delta_e$ ), the speed brakes ( $\delta_{sb}$ ), and the thrust ( $\delta_T$ ).  $\delta_e$  is elevator displacement and its limits are set at  $\pm 25$  degrees. It should be noted that constant elevator displacement represents an out of trim condition and is normally trimmed off by an appropriate horizontal stabilizer position. However,

this is not possible with the model representation used in this thesis.  $\delta_{sb}$  is speed brake deflection which is symmetrical spoiler deployment and has a limit of 0 to 60 degrees.  $\delta_T$  is modeled in terms of 100 percent of available thrust and limits vary depending upon altitude and gross weight.

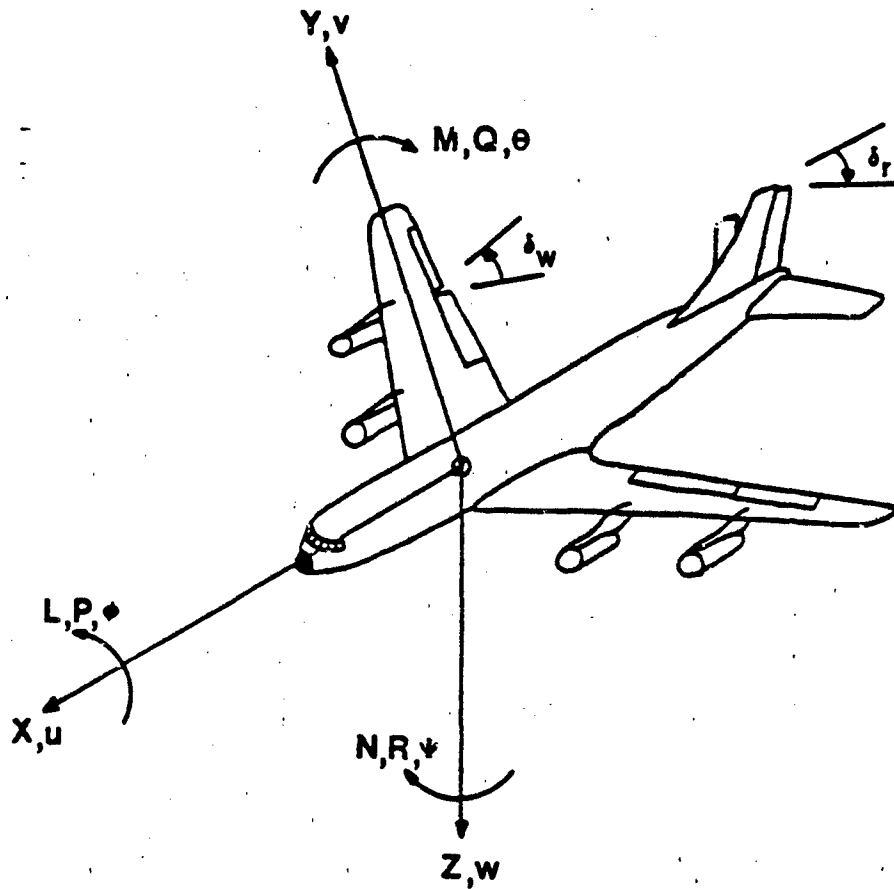
Since the equations are decoupled and the theory requires the same number of inputs and outputs, two lateral and three longitudinal outputs are chosen. The lateral outputs are the roll angle  $\phi$  and the sideslip  $\beta$ . The longitudinal outputs are the pitch angle  $\theta$ , the velocity in the x-direction  $v$ , and  $h$  is the velocity in the z-direction.

#### Sign Convention and Axes System

The sign convention for the forces and moments, as used throughout this thesis, are shown in Figures C-1, C-2, and C-3. Figure C-2 shows lateral sign conventions while Figure C-3 shows longitudinal sign convention.

Rudder ( $\delta_r$ ): Rudder deflection to the left is defined as positive. This produces a positive  $\beta$ , positive  $v$ , negative  $N$ , and negative  $R$ .

Control Wheel ( $\delta_w$ ): Control wheel deflection to the right, which cause right aileron up and right spoiler up along with left aileron down is defined as positive. This produces a positive  $L$ , positive  $\phi$ , and positive  $P$ . Note,



- |  |                        |
|--|------------------------|
| P - Roll Angular Velocity              | L - Rolling Moment     |
| Q - Pitch Angular Velocity             | M - Pitching Moment    |
| R - Yaw Angular Velocity               | N - Yawing Moment      |
| X, Y, Z - Aerodynamic Force Components | $\phi$ - Roll Angle    |
| u, v, w - Velocity Components          | $\theta$ - Pitch Angle |
|  | $\psi$ - Yaw Angle     |

Fig. C-1. Sign Convention

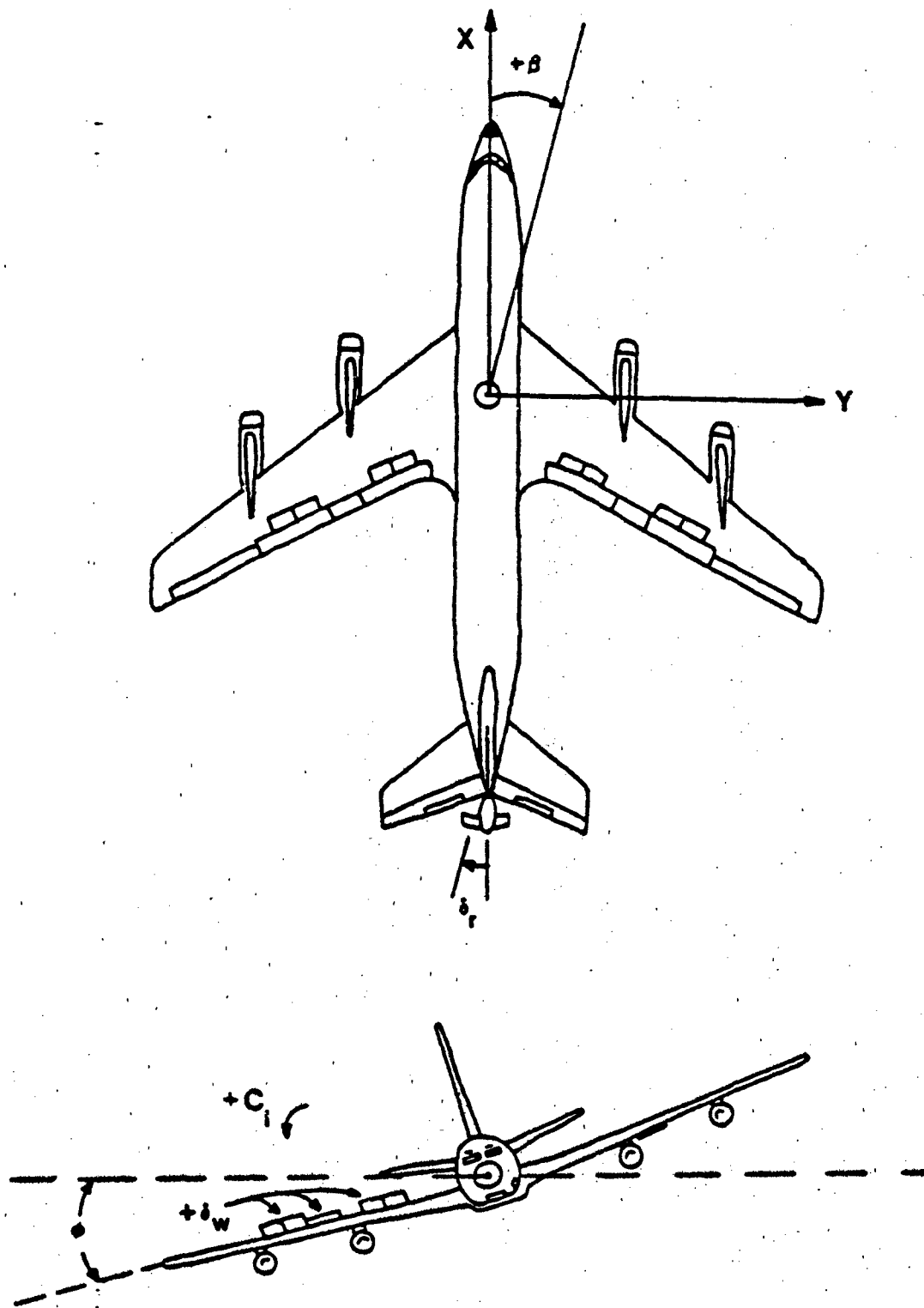


Fig. C-2. Lateral Sign Convention

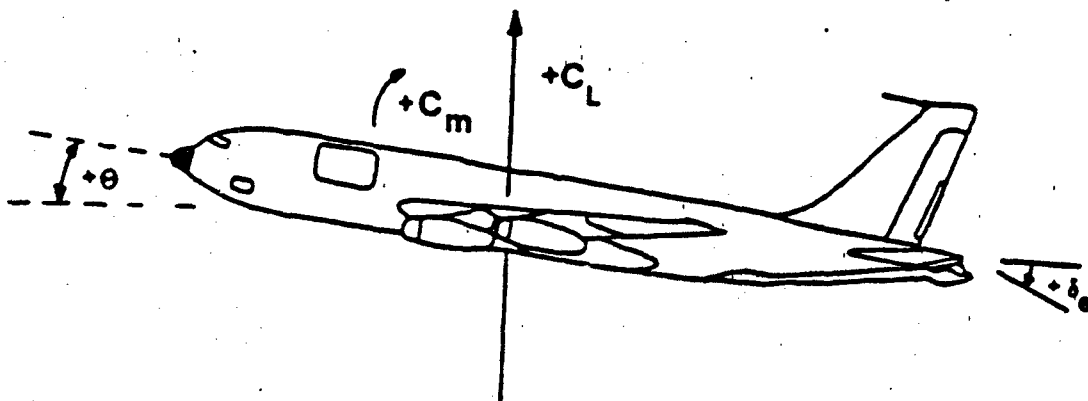


Fig. C-3. Longitudinal Sign Convention



that this definition of positive aileron is not standard, but does conform with Reference 4.

Elevator ( $\delta_e$ ): Control column movement forward which causes down elevator deflection is defined as positive. This positive elevator produces a negative  $\theta$ , negative M, and negative Q.

Speed Brakes ( $\delta_{sb}$ ): Spoilers when used symmetrically are defined as speed brakes, which when deflected positive are up.

Thrust ( $\delta_T$ ): Thrust is modeled as percent of available thrust and a positive  $\delta_T$  calls for an increase in thrust.

#### Conversion of Stability Axes to Body Axes

Control derivatives are given in Reference 6 as nondimensional stability axis coefficients (see Table C-2). These derivatives are converted to body axes and then dimensionalized in a manner found in Reference 18. The equations used to convert longitudinal stability axis derivatives to body axis are:

$$(C_{z_\alpha})_b = (-C_{L_\alpha} - C_D) \cos^2 \alpha_0 + (-C_D - 2C_D) \sin^2 \alpha_0 \\ + (-C_{L_u} - C_L - C_{D_\alpha}) \cos \alpha_0 \sin \alpha_0 \quad (C-1)$$

$$(C_{z_u})_b = -C_{L_q} \cos \alpha_0 \quad (C-2)$$

$$\begin{aligned} (C_{z_u})_b &= (-C_{L_u} - 2C_L)\cos^2\alpha_o + (C_{D_\alpha} - C_L)\sin^2\alpha_o \\ &\quad + (C_{L_\alpha} - C_{D_u} - C_D)\cos\alpha_o\sin\alpha_o \end{aligned} \quad (C-3)$$

$$(C_{z_\delta})_b = -C_{L_\delta}\cos\alpha_o - C_{D_\delta}\sin\alpha_o \quad (C-4)$$

$$\begin{aligned} (C_{x_\alpha})_b &= (-C_{D_\alpha} + C_{L_\alpha})\cos^2\alpha_o + (C_{L_u} + 2C_L)\sin^2\alpha_o \\ &\quad + (-C_{D_u} - C_D + C_{L_\alpha})\cos\alpha_o\sin\alpha_o \end{aligned} \quad (C-5)$$

$$(C_{x_q})_b = C_{L_q}\sin\alpha_o \quad (C-6)$$

$$\begin{aligned} (C_{x_u})_b &= (-C_{D_u} - 2C_D)\cos^2\alpha_o + (-C_{L_\alpha} - C_D)\sin^2\alpha_o \\ &\quad + (C_{D_\alpha} + C_{L_u} + C_L)\cos\alpha_o\sin\alpha_o \end{aligned} \quad (C-7)$$

$$(C_{x_\delta})_b = -C_{D_\delta}\cos\alpha_o + C_{L_\delta}\sin\alpha_o \quad (C-8)$$

$$(C_{M_\alpha})_b = C_{M_\alpha}\cos\alpha_o + (C_M + 2C_M)\sin\alpha_o \quad (C-9)$$

$$(C_{M_\alpha})_b = C_{M_\alpha}\cos\alpha_o \quad (C-10)$$

$$(C_{M_u})_b = (C_{M_u} + 2C_M)\cos\alpha_o - C_{M_\alpha}\sin\alpha_o \quad (C-11)$$

$$(C_{M_q})_b = C_{M_q} \quad (C-12)$$

$$(C_{M_\delta})_b = C_{M_\delta} \quad (C-13)$$

Where  $( )_b$  is used to distinguish body axes from stability axes. The equations used to convert lateral derivatives to body axes are:

$$(C_{l_\beta})_b = C_{L_\beta} \cos \alpha_o - C_{N_\beta} \sin \alpha_o \quad (C-14)$$

$$(C_{l_p})_b = C_{l_p} \cos^2 \alpha_o + C_{n_r} \sin^2 \alpha_o - (C_{l_r} + C_{n_p}) \sin \alpha_o \cos \alpha_o \quad (C-15)$$

$$(C_{l_r})_b = C_{l_r} \cos^2 \alpha_o - (C_{n_r} - C_{l_p}) \sin \alpha_o \cos \alpha_o + C_{n_p} \sin^2 \alpha_o \quad (C-16)$$

$$(C_{l_\delta})_b = C_{L_\delta} \cos \alpha_o - C_{N_\delta} \sin \alpha_o \quad (C-17)$$

$$(C_{n_\beta})_b = C_{n_\beta} \cos \alpha_o + C_{l_\beta} \sin \alpha_o \quad (C-18)$$

$$(C_{n_p})_b = C_{n_p} \cos^2 \alpha_o - (C_{n_r} - C_{l_p}) \sin \alpha_o \cos \alpha_o - C_{l_r} \sin^2 \alpha_o \quad (C-19)$$

$$(C_{n_r})_b = C_{n_r} \cos^2 \alpha_o + (C_{l_r} + C_{n_p}) \sin \alpha_o \cos \alpha_o + C_{l_p} \sin^2 \alpha_o \quad (C-20)$$

$$(C_{n_\delta})_b = C_{n_\delta} \cos \alpha_o + C_{l_\delta} \sin \alpha_o \quad (C-21)$$

$$(C_{y_\beta})_b = C_{y_\beta} \quad (C-22)$$

$$(C_{y_p})_b = C_{y_p} \cos \alpha_o - C_{y_p} \sin \alpha_o \quad (C-23)$$

$$(C_{y_r})_b = - C_{y_p} \cos \alpha_o + C_{y_p} \sin \alpha_o \quad (C-24)$$

$$(C_{y_\delta})_b = C_{y_\delta} \quad (C-25)$$

### Dimensional Body Axes Equations

Once the conversion to body axes is made it is desirable to dimensionalize the derivatives. The equations for dimensionalization of the longitudinal control derivatives as given in Reference 16 are as follows:

$$z_\alpha = z C_{z_\alpha} \quad (C-26)$$

$$z_q = [(z C) / (2U_o)] C_{z_q} \quad (C-27)$$

$$z_u = (z / U_o) C_{z_u} \quad (C-28)$$

$$z_\delta = z C_{z_\delta} \quad (C-29)$$

$$x_\alpha = x C_{x_\alpha} \quad (C-30)$$

$$x_q = [(x C) / (2U_o)] C_{x_q} \quad (C-31)$$

$$x_u = (x / U_o) C_{x_u} \quad (C-32)$$

$$x_\delta = x C_{x_\delta} \quad (C-33)$$

$$M_\alpha = M (C_{M_\alpha})_b \quad (C-34)$$

$$M_q = [(M C) / (2U_o)] (C_{M_q})_b \quad (C-35)$$

$$M_q = [(M C) / (2U_o)] (C_{M_q})_b \quad (C-36)$$

$$M_u = (M/U_o) (C_{M_u})_b \quad (C-37)$$

$$M_\delta = M (C_{M_\delta})_b \quad (C-38)$$

Where  $Z = (qs)/m$ ,  $X = (qs)/m$ ,  $M = (qsc)/I_{yy}$ , and  $q =$  dynamic pressure,  $s =$  surface area of the wing,  $m =$  mass of the aircraft, and  $I_{yy} =$  body axes moment of inertia about the y-axis. The equations for dimensionalization of the lateral control derivatives as given in Reference 16 are as follows:

$$N_C = N (C_{n_\beta})_b \quad (C-39)$$

$$N_p = [(N b) / (2U_o)] (C_{n_p})_b \quad (C-40)$$

$$N_r = [(N b) / (2U_o)] (C_{n_r})_b \quad (C-41)$$

$$N_\delta = N (C_{n_\delta})_b \quad (C-42)$$

$$L_\beta = L (C_{l_\beta})_b \quad (C-43)$$

$$L_p = -[(L b) / (2U_o)] (C_{l_p})_b \quad (C-44)$$

$$L_r = [(L b) / (2U_o)] (C_{l_r})_b \quad (C-45)$$

$$L_\delta = L (C_{l_\delta})_b \quad (C-46)$$

$$Y_\beta = Y (C_{y_\beta})_b \quad (C-47)$$

$$Y_p = [(Y b) / (2U_o)] (C_{y_p})_b \quad (C-48)$$

$$Y_r = [(Yb)/(2U_o)] (C_{y_r})_b \quad (C-49)$$

$$Y_{\delta} = Y(C_{y_{\delta}})_b \quad (C-50)$$

Where  $N = (qsb)/(I_{zz})$ ,  $L = (qsb)/(I_{xx})$ , and  $Y = (qsb)/m$  and  $q =$  dynamic pressure,  $s =$  surface area of wing,  $m =$  mass of the aircraft,  $b =$  wing span,  $I_{zz} =$  body axes moment of inertia about z-axis, and  $I_{xx} =$  body axes moment about x-axis.

Appropriate dimensional body axes derivatives are changed to the prime notation using:

$$X_{u'} = -g \cos \theta_o \quad (C-51)$$

$$X_{q'} = X_q - U_o \dot{\theta}_o \quad (C-52)$$

$$Z_{\theta'} = (-g/U_o) \sin \theta_o \quad (C-53)$$

$$Z_{u'} = Z_q/U_o \quad (C-54)$$

$$Z_{q'} = (Z_q/U_o) + 1 \quad (C-55)$$

$$Z_{\alpha'} = Z_{\alpha}/U_o \quad (C-56)$$

$$Z_{\delta'} = Z_{\delta}/U_o \quad (C-57)$$

$$M_{\theta'} = M Z_{\theta'} \quad (C-58)$$

$$M_{u'} = M_u + M_{\alpha} (Z_u/U_o) \quad (C-59)$$

$$M_{\alpha'} = M_{\alpha} + M_{\alpha} (Z/U_o) \quad (C-60)$$

$$M_{q'} = M_q + M_{\dot{\alpha}} [(Z_q/U_0) + 1] \quad (C-61)$$

$$M_{\delta_r'} = M_{\delta_r} + M_{\dot{\alpha}} (Z/U_0) \quad (C-62)$$

$$Y_{\phi'} = g/U_0 \quad (C-63)$$

$$Y_{\beta'} = Y_{\beta}/U_0 \quad (C-64)$$

$$Y_{p'} = (Y_p/U_0) + \alpha_0 \quad (C-65)$$

$$Y_{r'} = Y_r/U_0 \quad (C-66)$$

$$Y_{\delta'} = Y_{\delta}/U_0 \quad (C-67)$$

$$L_i = \frac{L_i + (I_{xz}/I_{zz})N_i}{1 - (I_{xz})/(I_{xx}I_{zz})} \quad (C-68)$$

$$N_i = \frac{N_i + (I_{xz}/I_{zz})L_i}{1 - (I_{xz})/(I_{xx}I_{zz})} \quad (C-69)$$

$$U_0 = (U_0)/57.3 \quad (C-70)$$

Note that  $i$  in Equations (C-68) and (C-69) represents  $b$ ,  $p$ ,  $r$ ,  $\delta_r$ , and  $\delta_w$  and that in Equations (C-57), (C-62), and (C-67) implies  $\delta_e$ ,  $\delta_{sb}$ ,  $\delta_r$ , or  $\delta_w$  as appropriate. Also body axes inertias are used.

Now actual transformation from nondimensional stability axes derivatives to dimensional body axes is accomplished using a computer program created by A. Finley Barfield (2) which utilizes the equations summarized in this appendix. A sample run of this program for F.C.

number 2 is shown in Appendix D. Data received from this program has the units of radians, radians per second, and feet per second. This data was converted by Capt. J. Locken (17) into units of degrees, degrees per second, and feet per second. Body axes derivatives for the three F.C.'s are listed in Tables C-5, C-6, and C-7.

Percent thrust is modeled in terms of thrust available and is given by

$$X = \frac{\text{Thrust available ft/sec}^2}{(\text{Mass}) \times 100\% \text{ R.M}}$$

where  $M = g/w$  is the mass of the aircraft and thrust is measured in pounds.

#### KC-135 Aircraft Models

The three F.C.'s as discussed in Chapter III are:

- F.C. #1: High altitude, high speed cruise at Mach 0.77 and 45,000 feet.
- F.C. #2: Medium altitude, heavy weight cruise at Mach 0.77 and 28,500 feet.
- F.C. #3: Landing configuration at Mach 0.21 and sea level.

Pertinent aircraft data for each of the three F.C.'s as found in References 5 and 19 is listed in Table C-1. The nondimensional stability axes derivatives as found in Reference 6 are listed in Tables C-2, C-3, and C-4 for F.C.'s #1, #2, and #3 respectively. The dimensional body axes derivatives for the input and output matrices are listed in Tables C-5, C-6, and C-7 for F.C.'s #1, #2, and #3 respectively. All derivatives not listed in these tables are assumed to be zero.



TABLE C-1  
KC-135 AIRCRAFT DATA

Condition	#1	#2	#3	Units
Altitude	45,600	28,500	sea level	ft
Mach	0.77	0.77	0.21	--
Weight	130,000	284,000	130,000	lbs
Centre of Gravity	32.1	24.2	32.1	%MAC
$\bar{y}$	124.8	279.7	65.9	lbs/ft <sup>2</sup>
s (wing area)	2433	2433	2433	ft <sup>2</sup>
b (wing span)	130.83	130.83	130.83	ft
c (wing MAC)	20.16	20.16	20.16	ft
$U_o$ (true)	745	771	235	ft/sec
$\theta_o$ (body)	2.4	2.4	-0.1	deg
$\alpha_o$ (wing)	4.4	4.4	4.4	deg
$\alpha_o$ (body)	2.4	2.4	2.4	deg
$I_{xx}$	2,050,000	2,930,000	2,050,000	slug ft <sup>2</sup>
$I_{yy}$	2,460,000	4,660,000	2,460,000	slug ft <sup>2</sup>
$I_{zz}$	4,360,000	7,480,000	4,360,000	slug ft <sup>2</sup>
$I_{xz}$	--	--	--	--

Note: All inertias are in body axis reference system.

TABLE C-2  
 NONDIMENSIONAL STABILITY AXES DERIVATIVES  
 FOR F.C. #1

$C_L$	0.426	$C_M$	0.0	$C_D$	0.024
$C_{L_u}$	0.0	$C_{M_\alpha}$	-6.79	$C_{D_u}$	0.0
$C_{L_\alpha}$	5.329	$C_{M_\alpha}$	-1.1747	$C_{D_\alpha}$	0.2417
$C_{L_q}$	5.1545	$C_{m_q}$	-15.65	--	--
$C_{L_{\delta_e}}$	0.2114	$C_{M_{\delta_e}}$	-0.6647	$C_{D_{\delta_e}}$	0.0
$C_{L_{\delta_{sb}}}$	-0.3189	$C_{M_{\delta_{sb}}}$	0.07259	$C_{D_{\delta_{sb}}}$	0.0497
$C_{l_\beta}$	-0.223	$C_{n_\beta}$	0.166	$C_{y_\beta}$	-0.762
$C_{l_p}$	-0.435	$C_{n_p}$	-0.005	$C_{y_p}$	-0.233
$C_{l_r}$	0.155	$C_{n_r}$	-0.194	$C_{y_r}$	0.428
$C_{l_{\delta_r}}$	0.0315	$C_{n_{\delta_r}}$	-0.113	$C_{y_{\delta_r}}$	0.264
$C_{l_{\delta_w}}$	0.0189	$C_{n_{\delta_w}}$	0.00149	$C_{y_{\delta_w}}$	-0.0074

Note: Units are radians<sup>-1</sup>.

TABLE C-3

NONDIMENSIONAL STABILITY AXES DERIVATIVES  
FOR F.C. #2

$C_L$	0.426	$C_M$	0.0	$C_D$	0.024
$C_{L_u}$	0.0	$C_{M_\alpha}$	-6.57	$C_{D_U}$	0.0
$C_{L_\alpha}$	4.727	$C_{M_\alpha}$	-0.8595	$C_{D_\alpha}$	0.2143
$C_{L_q}$	4.825	$C_{M_q}$	-14.65	--	--
$C_{L_{\delta_e}}$	0.1862	$C_{M_{\delta_e}}$	-0.5988	$C_{D_{\delta_e}}$	0.0
$C_{L_{\delta_{sb}}}$	-0.2751	$C_{M_{\delta_{sb}}}$	0.07639	$C_{D_{\delta_{sb}}}$	0.04779
$C_{l_\beta}$	-0.198	$C_{n_\beta}$	0.166	$C_{y_\beta}$	-0.762
$C_{l_p}$	-0.345	$C_{n_p}$	-0.005	$C_{y_p}$	-0.211
$C_{l_r}$	0.155	$C_{n_r}$	-0.194	$C_{y_r}$	0.428
$C_{l_{\delta_r}}$	0.0315	$C_{n_{\delta_r}}$	-0.113	$C_{y_{\delta_r}}$	0.264
$C_{l_{\delta_w}}$	0.0153	$C_{n_{\delta_w}}$	0.00149	$C_{y_{\delta_w}}$	-0.0074

Note: Units are radians<sup>-1</sup>.

TABLE C-4  
 NONDIMENSIONAL STABILITY AXES DERIVATIVES  
 FOR F.C. #3

$C_L$	0.8108	$C_M$	0.0	$C_D$	0.0905
$C_{L_u}$	0.0	$C_{M_\alpha}$	-5.52	$C_{D_u}$	0.0
$C_{L_\alpha}$	4.475	$C_{M_\alpha}$	-1.0027	$C_{D_\alpha}$	0.3863
$C_{L_q}$	4.6275	$C_{M_q}$	-14.05	--	--
$C_{L_{\delta_e}}$	0.2222	$C_{M_{\delta_e}}$	-0.7105	$C_{D_{\delta_e}}$	0.0
$C_{L_{\delta_{sb}}}$	-0.3857	$C_{M_{\delta_{sb}}}$	0.0879	$C_{D_{\delta_{sb}}}$	0.075
$C_{l_\beta}$	-0.229	$C_{n_\beta}$	0.132	$C_{Y_\beta}$	-0.768
$C_{l_p}$	-0.385	$C_{n_p}$	-0.055	$C_{Y_p}$	-0.202
$C_{l_r}$	0.248	$C_{n_r}$	-0.186	$C_{Y_r}$	0.380
$C_{l_{\delta_r}}$	0.0287	$C_{n_{\delta_r}}$	-0.098	$C_{Y_{\delta_r}}$	0.226
$C_{l_{\delta_w}}$	0.0372	$C_{n_{\delta_w}}$	0.0024	$C_{Y_{\delta_w}}$	-0.0143

Note: Units are radians<sup>-1</sup>.

TABLE C-5  
 DIMENSIONAL INPUT AND OUTPUT MATRIX COEFFICIENTS  
 FOR F.C. #1

$X_u$	-0.0029646	1/sec	$L_{\beta'}$	-4.4499	1/sec <sup>2</sup>
$X_\alpha$	0.53477	$\frac{ft/sec^2}{deg}$	$L_{p'}$	-0.75011	1/sec
$X_{q'}$	-0.53477	$\frac{ft/sec}{deg}$	$L_{r'}$	0.24613	1/sec
$X_{\theta'}$	-0.56146	$\frac{ft/sec^2}{deg}$	$L_{\delta' r}$	.701583	1/sec <sup>2</sup>
$X_{\delta' e}$	0.011617	$\frac{ft/sec^2}{deg}$	$L_{\delta' w}$	0.36464	1/sec <sup>2</sup>
$X_{\delta' sb}$	-0.82712	$\frac{ft/sec^2}{deg}$	$N_{\beta'}$	1.42597	1/sec <sup>2</sup>
$X_{\delta' T}$	0.0495	$\frac{ft/sec}{\%RPM}$	$N_{p'}$	-0.012277	1/sec
$M_u$	0.010529	$\frac{deg}{ft(sec)}$	$N_{r'}$	-0.15052	1/sec
$M_\alpha$	-2.7963	1/sec <sup>2</sup>	$N_{\delta' r}$	-1.01653	1/sec <sup>2</sup>
$M_{q'}$	-0.7537	1/sec	$N_{\delta' w}$	.020775	1/sec <sup>2</sup>
$M_{\theta'}$	.00041339	1/sec <sup>2</sup>	$Y_{\beta'}$	-0.076917	1/sec
$M_{\delta' e}$	-1.64897	1/sec <sup>2</sup>	$Y_{p'}$	0.039665	--
$M_{\delta' sb}$	0.173339	1/sec <sup>2</sup>	$Y_{r'}$	-0.99629	--

TABLE C-5--Continued

$Z_{u'}$	-0.004883	deg/ft	$Y_{\delta' r}$	0.026647	1/sec
$Z_{\alpha'}$	-0.54223	1/sec	$Y_{\delta' w}$	-0.000746	1/sec
$Z_{q'}$	0.992966	--	$Y_{\phi'}$	0.04322	1/sec
$Z_{\theta'}$	-0.0018099	1/sec	$Z_{\delta' sb}$	0.031962	1/sec
$Z_{\delta' e}$	-0.021319	1/sec	$U_o$	13.001715	$\frac{\text{ft/sec}}{\text{deg}}$

TABLE C-6  
 DIMENSIONAL INPUT AND OUTPUT MATRIX COEFFICIENTS  
 FOR F.C. #2

$X_u$	-0.0029479	1/sec	$L_{\beta'}$	-6.22193	1/sec <sup>2</sup>
$X_{\alpha}$	.551527	$\frac{\text{ft/sec}^2}{\text{deg}}$	$L_{p'}$	-0.936318	1/sec
$X_{q'}$	-0.56006	$\frac{\text{ft/sec}}{\text{deg}}$	$L_{r'}$	0.395991	1/sec
$X_{\theta'}$	-0.56146	$\frac{\text{ft/sec}^2}{\text{deg}}$	$L_{\delta' r}$	1.10013	1/sec <sup>2</sup>
$X_{\delta' e}$	0.010498	$\frac{\text{ft/sec}^2}{\text{deg}}$	$L_{\delta' w}$	0.46253	1/sec <sup>2</sup>
$X_{\delta' sb}$	-0.079813	$\frac{\text{ft/sec}^2}{\text{deg}}$	$N_{\beta'}$	1.87524	1/sec <sup>2</sup>
$X_{\delta' T}$	0.034	$\frac{\text{ft/sec}}{\% \text{RFM}}$	$N_{p'}$	-0.012103	1/sec
$M_u'$	0.0091035	$\frac{\text{deg}}{\text{ft}(\text{sec})}$	$N_{r'}$	-0.196469	1/sec
$M_{\alpha'}$	-2.40739	1/sec <sup>2</sup>	$N_{\delta' r}$	-1.32796	1/sec <sup>2</sup>
$M_{q'}$	-0.814938	1/sec	$N_{\delta' w}$	0.02541	1/sec <sup>2</sup>
$M_{\theta'}$	0.0004419	1/sec <sup>2</sup>	$Y_{\beta'}$	-0.078921	1/sec
$M_{\delta' e}$	-0.018616	1/sec <sup>2</sup>	$Y_{p'}$	0.0399458	--
$M_{\delta' sb}$	0.0273034	1/sec <sup>2</sup>	$Y_{r'}$	-0.996444	--

TABLE C-6--Continued

$Z_{u'}$	-0.004865	deg/ft	$Y_{\delta'}$ <sub>r</sub>	0.0273552	1/sec
$Z_{\alpha'}$	-0.477268	1/sec	$Y_{\delta'}$ <sub>w</sub>	-0.000766	1/sec
$Z_{q'}$	0.993693	--	$Y_{\phi'}$	0.041764	1/sec
$Z_{\theta'}$	-0.001749	1/sec	$Z_{\delta'}$ <sub>sb</sub>	0.218002	1/sec
$Z_{\delta'}$ <sub>e</sub>	-1.758	1/sec	$U_o$	13.4555	$\frac{\text{ft/sec}}{\text{deg}}$



TABLE C-7  
 DIMENSIONAL INPUT AND OUTPUT MATRIX COEFFICIENTS  
 FOR F.C. #3

$X_u$	-0.0234233	1/sec	$L_{\beta'}$	-2.39756	1/sec <sup>2</sup>
$X_{\alpha}$	0.4228202	$\frac{\text{ft/sec}^2}{\text{deg}}$	$L_{p'}$	-1.11861	1/sec
$X_{q'}$	-0.1660307	$\frac{\text{ft/sec}}{\text{deg}}$	$L_{r'}$	0.681707	1/sec
$X_{\theta'}$	-0.5619546	$\frac{\text{ft/sec}^2}{\text{deg}}$	$L_{\delta' r}$	0.335391	1/sec <sup>2</sup>
$X_{\delta' e}$	0.0064484	$\frac{\text{ft/sec}^2}{\text{deg}}$	$L_{\delta' w}$	0.379249	1/sec <sup>2</sup>
$X_{\hat{c}'_{sb}}$	-0.063125	$\frac{\text{ft/sec}^2}{\text{deg}}$	$L_{\beta'}$	0.588344	1/sec <sup>2</sup>
$X_{\hat{c}'_T}$	0.1268	ft/sec <sup>2</sup>	$N_{p'}$	-0.085262	1/sec <sup>2</sup>
$M_u'$	0.0318452	$\frac{\text{deg}}{\text{ft}(\text{sec})}$	$N_{r'}$	-0.238751	1/sec
$M_{\alpha'}$	-1.07422	1/sec <sup>2</sup>	$N_{\delta' r}$	-0.465479	1/sec <sup>2</sup>
$M_{q'}$	-1.09229	1/sec	$N_{\delta' w}$	0.0190316	1/sec <sup>2</sup>
$M_{\theta'}$	-0.000074	1/sec <sup>2</sup>	$Y_{\beta'}$	-0.129778	1/sec
$M_{\delta' e}$	-0.92184	1/sec <sup>2</sup>	$Y_{p'}$	0.0316453	--
$M_{\delta' sb}$	0.095412	1/sec <sup>2</sup>	$Y_{r'}$	-0.982538	--

TABLE C-7--Continued

$Z_u'$	-0.0591737	deg/ft	$Y_{\delta'}_r$	0.03819	1/sec
$Z_\alpha'$	-0.778653	1/sec	$Y_{\delta'}_r$	-0.002421	1/sec
$Z_q'$	0.966486	--	$Y_{\phi'}$	0.1370213	1/sec
$Z_\theta'$	0.000239	1/sec	$Z_{\delta'}_{sb}$	0.064588	1/sec
$Z_{\delta'}_e$	-0.037515	1/sec	$U_o$	4.101222	$\frac{\text{ft/sec}}{\text{deg}}$

### Body Bending Modes

To eliminate the rigid body assumption stated in Chapter I, the elastic mode information is taken from Reference 7. The first and second body bending modes are included in the design for a longitudinal controller. The following equations and matrices (7) are used in the development of the elastic model for the longitudinal plane:

$$\begin{aligned} & [I_s] \{\ddot{\epsilon}_s\} + ([2\xi\omega_n I_s] + \rho_o V_o [C_{\dot{\epsilon}_s}]) \{\dot{\epsilon}_s\} \\ & + ([\omega_n^2 I_s] + \rho_o V_o^2 [C_{\epsilon_s}]) \{\epsilon_s\} \\ = & -\rho_o V_o^2 [(C_{\hat{q}}) \hat{q} + (C_{\alpha}) \alpha + (C_{\delta_e}) \delta_e + (C_{\delta_{sp}}) \delta_{sp}] \\ & + (C_{\alpha_g}) \alpha_g \end{aligned} \quad (C-71)$$

$$\{\ddot{z}\} = [C_{nz}] \{\ddot{\epsilon}_s\} \quad (C-72)$$

$$\{\ddot{\theta}\} = [C_{\ddot{\theta}}] \{\ddot{\epsilon}_s\} \quad (C-73)$$

where:

$I$  = Mass moment of inertia, slug--in.<sup>2</sup>

$\{\epsilon\}$  = Elastic mode displacement, in.

$\xi$  = Viscous damping factor.

$\omega_n$  = Frequency, rad/sec.

$\rho_o$  = Air density, lb-sec<sup>2</sup>/in.<sup>4</sup>

$V_o$  = True airspeed, in/sec.

C = Derivative for structural modes.

$\ddot{z}$  = Vertical acceleration, up pos., g.

$\ddot{\theta}$  = Pitch acceleration nose up pos., rad/sec.

$\hat{q}$  = Pitch rate, rad/sec  $\times \frac{MAC}{2V}$ , nose up pos.

$\alpha$  = Angle of attack, wind from below pos., radians.

$\delta_e$  = Elevator displacement, T.E. down pos., radians.

$\delta_{sp}$  = Spoiler displacement, (L + R)/2, R. spoiler up pos., radians.

$\alpha_g$  = Vertical gust angle, from below pos., radians.

For aircraft gross weight of 120,000 pounds (used for F.C.'s #1 and #2) the given data in matrix form is:

$$I = \begin{bmatrix} 15.12 & 0 & 0 \\ 0 & 101.5 & 0 \\ 0 & 0 & 15.87 \end{bmatrix}; \quad \omega_n = \begin{bmatrix} 11.44 \\ 23.41 \\ 17.94 \end{bmatrix} \quad (C-74)$$

$$\xi = \begin{bmatrix} .02 \\ .02 \\ .02 \end{bmatrix}; \quad C_\alpha = \begin{bmatrix} 7.425(10)^4 \\ 3.617(10)^4 \\ 6.363(10)^4 \end{bmatrix}; \quad (C-75)$$

$$C_{\hat{q}} = \begin{bmatrix} 5.970(10)^4 \\ -7.664(10)^4 \\ 4.174(10)^4 \end{bmatrix} \quad (C-76)$$

$$C_{\epsilon} = \begin{bmatrix} 6.709(10)^4 & 5.561(10)^4 & 2.118(10)^3 \\ 3.899(10)^4 & 9.183(10)^4 & -6.194(10)^3 \\ 5.753(10)^3 & 6.461(10)^3 & 6.793(10)^4 \end{bmatrix} \quad (C-77)$$

$$C_{\epsilon} = \begin{bmatrix} 27.92 & 270.5 & -61.68 \\ 36.65 & -175.8 & -131.8 \\ -16.02 & 19.10 & 256.6 \end{bmatrix} \quad (C-78)$$

$$C_{\delta_e} = \begin{bmatrix} -1.430(10)^4 \\ -1.583(10)^4 \\ 4.027(10)^4 \end{bmatrix} ; C_{\delta_{sp}} = \begin{bmatrix} 0.0 \\ 0.0 \\ 0.0 \end{bmatrix} \quad (C-79)$$

$$C_{nz} = \begin{bmatrix} 2.618(10)^4 & 1.764(10)^3 & -1.334(10)^3 \\ 2.469(10)^4 & 5.952(10)^4 & -3.496(10)^5 \\ 2.578(10)^4 & 2.165(10)^4 & 4.522(10)^4 \\ 3.992(10)^4 & 2.086(10)^4 & 1.697(10)^4 \\ 5.024(10)^4 & 4.141(10)^4 & -4.741(10)^4 \end{bmatrix} \begin{matrix} BS^* = 194.5 \\ BS = 584.2 \\ BS = 855.6 \\ BS = 1321.0 \\ BS = 1504.5 \end{matrix} \quad (C-80)$$

$$C_{\alpha_g} = \begin{bmatrix} 7.348(10)^4 \\ 3.574(10)^4 \\ 6.236(10)^4 \end{bmatrix} \quad (C-81)$$

\*Note: BS = Body Station.

$$C_{\theta}'' = \begin{bmatrix} 1.924(10)^{-5} & 1.275(10)^{-3} & -1.406(10)^{-3} \\ -3.975(10)^{-7} & 8.091(10)^{-4} & -9.473(10)^{-4} \\ -4.636(10)^{-5} & 3.024(10)^{-4} & -4.068(10)^{-4} \\ -1.877(10)^{-4} & -2.925(10)^{-4} & 9.671(10)^{-4} \\ -2.445(10)^{-4} & -5.753(10)^{-4} & 1.772(10)^{-3} \end{bmatrix} \begin{array}{l} \text{BS} = 194.5 \\ \text{BS} = 584.2 \\ \text{BS} = 855.6 \\ \text{BS} = 1321.0 \\ \text{BS} = 1504.5 \end{array} \quad (\text{C-82})$$

For aircraft gross weight of 260,000 pounds (use for F.C.

#2) the given data matrices are:

$$I = \begin{bmatrix} 19.03 & 0 & 0 \\ 0 & 113.1 & 0 \\ 0 & 0 & 22.47 \end{bmatrix}; \quad \omega_n = \begin{bmatrix} 8.76 \\ 22.76 \\ 23.62 \end{bmatrix} \quad (\text{C-83})$$

$$\xi = \begin{bmatrix} .02 \\ .02 \\ .02 \end{bmatrix}; \quad C = \begin{bmatrix} 8.403(10)^4 \\ 2.114(10)^4 \\ 8.659(10)^4 \end{bmatrix}; \quad C_{\dot{q}} = \begin{bmatrix} 7.538(10)^4 \\ 2.461(10)^5 \\ 5.080(10)^5 \end{bmatrix} \quad (\text{C-84})$$

$$C_{\ddot{e}} = \begin{bmatrix} 6.778(10)^4 & 2.795(10)^4 & -1.366(10)^4 \\ 1.777(10)^3 & 7.691(10)^4 & -3.34(10)^4 \\ -4.213(10)^3 & -2.239(10)^4 & 7.839(10)^4 \end{bmatrix} \quad (\text{C-85})$$

$$C_{\dot{e}} = \begin{bmatrix} 80.35 & 181.7 & -108.4 \\ 31.22 & -281.2 & -216.7 \\ -9.809 & -109.3 & 254.9 \end{bmatrix} \quad (\text{C-86})$$

$$c_{\varepsilon_e} = \begin{bmatrix} -1.358(10)^4 \\ -2.629(10)^4 \\ 4.781(10)^4 \end{bmatrix} ; \quad c_{\varepsilon_{sp}} = \begin{bmatrix} 0.0 \\ 0.0 \\ 0.0 \end{bmatrix} \quad (C-87)$$

$$c_{\alpha_g} = \begin{bmatrix} 8.309(10)^4 \\ 1.809(10)^3 \\ 8.594(10)^4 \end{bmatrix} \quad (C-88)$$

$$c_{nz} = \begin{bmatrix} 2.300(10)^5 & 1.592(10)^3 & -1.246(10)^3 \\ 1.107(10)^4 & 4.018(10)^4 & -1.444(10)^4 \\ 1.772(10)^4 & 3.072(10)^5 & 2.583(10)^4 \\ 3.784(10)^4 & 2.087(10)^4 & -2.049(10)^4 \\ 4.863(10)^4 & 5.600(10)^4 & -9.129(10)^4 \end{bmatrix} \begin{matrix} \text{BS} = 194.5 \\ \text{BS} = 584.2 \\ \text{BS} = 855.6 \\ \text{BS} = 1321.0 \\ \text{BS} = 1504.6 \end{matrix} \quad (C-89)$$

$$c_{\theta} = \begin{bmatrix} -8.642(10)^5 & 1.288(10)^3 & -1.180(10)^3 \\ -8.873(10)^5 & 8.307(10)^4 & -8.143(10)^4 \\ -1.159(10)^4 & 2.467(10)^4 & -2.827(10)^4 \\ -2.099(10)^4 & -5.501(10)^4 & 1.125(10)^4 \\ -2.420(10)^4 & -9.325(10)^4 & 1.866(10)^4 \end{bmatrix} \begin{matrix} \text{BS} = 194.5 \\ \text{BS} = 584.2 \\ \text{BS} = 855.6 \\ \text{BS} = 1321.0 \\ \text{BS} = 1504.0 \end{matrix} \quad (C-90)$$

It is to be noted that the above matrices are for the first, second, and third bending modes and there is coupling between modes as can be seen from the nondiagonal matrices. However, for this thesis it is assumed that there is no cross coupling between the first and second

body bending modes. Also, the units are converted by the author to correspond to the units of the rigid aircraft equations. The elastic equations of motion for the longitudinal mode are:

F.C. #1:

First Body Bending Mode:

$$\ddot{e} + 1.318\dot{e} + 134.074e = -119.45q - 148.56\alpha + 28.612\delta_e \quad (C-91)$$

Second Body Bending Mode:

$$\ddot{e} + 1.112\dot{e} + 545.026e = 22.843q - 10.781\alpha + 5.523\delta_e \quad (C-92)$$

F.C. #2:

First Body Bending Mode:

$$\ddot{e} + 1.848\dot{e} + 93.164e = -268.953q - 299.816\alpha + 48.456\delta_e \quad (C-93)$$

Second Body Bending Mode:

$$\ddot{e} + 1.196\dot{e} + 517.212e = 147.744q - 1.269\alpha + 15.783\delta_e \quad (C-94)$$

F.C. #3:

First Body Bending Mode:

$$\ddot{e} + 1.893\dot{e} + 131.014e = -62.847q - 78.164\alpha + 15.054\delta_e \quad (C-95)$$

Second Body Bending Mode:

$$\ddot{e} + 1.229\dot{e} + 547.77e = 12.019q - 5.672\alpha + 2.906\delta_e \quad (C-96)$$

Using Equations (C-72) and (C-73) the body bending modes are converted to the desired matrix form, which is in an equivalent form as the equation for the rigid aircraft. The final form is:



$$\begin{bmatrix} a & b & 0 \\ c & d & 0 \\ 0 & 0 & 1 \end{bmatrix} \begin{bmatrix} h \\ e \\ u \end{bmatrix} = \begin{bmatrix} e & 0 & 0 \\ f & 0 & 0 \\ 0 & 0 & 0 \end{bmatrix} \begin{bmatrix} \delta_e \\ \delta_{sb} \\ \delta_T \end{bmatrix} \quad (C-97)$$

Where for F.C. #1:

$$a = -0.0769S^2 - (0.00023/A + 0.000113/A)S$$

$$b = (1 + 0.00241/A - 0.0031/B)S + 0.00299/A + 0.0031/B$$

$$c = -(0.00022/A + 0.00106/B)S$$

$$d = S^2 + (0.0023/A - 0.02912/B)S + 0.00286/A + 0.0137/A$$

$$e = 0.000576/A + 0.000749/B$$

$$f = 0.00055/A + 0.00704/B$$

$$A = S^2 + 1.318S + 134.074$$

$$B = S^2 + 1.112S + 545.026$$

For F.C. #2:

$$a = -0.0743S^2 - (0.000038/A + 0.000011/B)S$$

$$b = (1 + 0.00046/A - 0.01748/B)S + 0.00051/A + 0.0015/B$$

$$c = (0.00189/A - 0.000121/B)S$$

$$d = S^2 + (0.02276/A + 0.1903/B)S - 0.02537/A + 0.00163/B$$

$$e = 0.000083/A + 0.00187/B$$

$$f = -0.0041/A + 0.0203/B$$

$$A = S^2 + 1.848S + 93.164$$

$$B = S^2 + 1.196S + 517.212$$

For F.C. #3:

$$a = -0.2438S^2 - (0.00122/A + 0.00059/A)S$$

$$b = (1 + 0.00401/A - 0.00517/B)S + 0.00499/A + 0.00244/B$$

$$c = - (0.000366/A + 0.00178/B)S$$

$$d = S^2 + (0.00121/A - 0.01548/B)S + 0.0015/A + 0.00731/B$$

$$e = 0.000961/A + 0.00125/B$$

$$f = 0.00029/A + 0.00374/B$$

$$A = (S^2 + 1.893S + 131.014)$$

$$B = (S^2 + 1.229S + 547.77)$$

The above bending mode equations are developed for body station 194.5 which is located at the pilot/copilot area.

#### Summary

This appendix summarizes the KC-135 aircraft. Sign convention is highlighted and the nondimensional stability axis derivatives are converted to the dimensional body

axis derivatives using a computer program described in Reference 2. Tabular listings of all deviations are given for each of the three flight conditions studied. The development of the body bending modes is highlighted with conversion to a form comparable with the rigid longitudinal equations. These equations are to be used in the longitudinal design (Chapter V).

Appendix D: Sample Run of CAT Program

COMMAND- ATTACH,CAT1,ID=T820366  
PFN IS  
CAT1  
AT CY= 001 SM-AFIT  
COMMAND- CAT1

\*\*\*\*\*  
\*\*\*\*\* AXIS TRANSFORMATION PROGRAM \*\*\*\*\*  
\*\*\*\*\*

ENTER STABILITY AXIS COEFFICIENTS FOR TRANSFORMATION  
TO BODY AXIS. TRIM ALPHA IS NEEDED FOR CONVERSION.  
MOMENT COEFFICIENTS AND SIDEFORCE COEFFICIENTS NOT  
REQUESTED REMAIN UNCHANGED.

NOTE: ALL COEFFICIENTS ARE REQUESTED WHEN COMPUTING  
DIMENSIONAL DERIVATIVES.

\*\*\*\*\*  
TO TRANSFORM ONLY LONGITUDINAL DATA - TYPE LONG  
TO TRANSFORM ONLY LATERAL-DIRECTIONAL DATA - TYPE LAT  
TO TRANSFORM BOTH LONG AND LAT-DIR DATA - TYPE BOTH  
KEYWORD =BOTH

ARE DIMENSIONAL BODY AXIS DERIVATIVES REQUIRED ? (YES/NO)YES

\*\*\*\*\*  
Q (DYNAMIC PRESSURE - LBS/FT2) =124.8

S (WING REFERENCE AREA - FT2) =2433

C (WING MEAN AERODYNAMIC CORD - FT) =29.16

B (WING SPAN - FT) =139.83

VT (TRIM VELOCITY - FT/SEC) =745

THETA (PITCH ANGLE - DEGS) =2.4

W (WEIGHT - LBS) =130000

INERTIAS MUST BE INPUT IN BODY AXIS.

IXX (SLUG-FT2) =2050000

IYY (SLUG-FT2) =2460000

IZZ (SLUG-FT2) =4360000

Ixz (SLUG-FT2) =0

\*\*\*\*\*

AIRCRAFT PARAMETERS

Q (DYNAMIC PRESSURE - LBS/FT2) = 124.800  
S (WING REFERENCE AREA - FT2) = 2433.00  
C (WING MEAN AERODYNAMIC CORD - FT) = 20.1600  
B (WING SPAN - FT) = 130.830  
VT (TRIN VELOCITY - FT/SEC) = 745.000  
THETA = 2.40000  
W (WEIGHT - LBS) = 130000.  
IXX (SLUG-FT2) = .205000E+07  
IYY (SLUG-FT2) = .246000E+07  
IZZ (SLUG-FT2) = .436000E+07  
IXZ (SLUG-FT2) = 0.

\*\*\*\*\*  
IS THE ENTERED DATA CORRECT? (YES/NO)YES

\*\*\*\*\*  
ALPHA (DEG) =2.4

CL =.4260

CLA (1/DEG) =.093

CLDE (1/DEG) =.003689

CLDF (1/DEG) =-.005367

CLB (1/RAD) =5.1545

CLAD (1/RAD) =0

CLU (1/(FT/SEC)) =0

CD =.0240

CDA (1/DEG) =.004218

CODE (1/DEG) =0

CDDF (1/DEG) =.0000674

CDU (1/(FT/SEC)) =0

CN =0

CNA (1/DEG) =-.0205

CNDE (1/DEG) =-.0116

CNDF (1/DEG) =.001267

CNB (1/RAD) =-15.65

CNAD (1/RAD) =-6.79

CNU (1/(FT/SEC)) = 0

\*\*\*\*\*

LONGITUDINAL STABILITY AXIS COEFFICIENTS

ALPHA = 2.40000

CL = .426000	CH = 0.	CD = .240000E-01
CLA = .930000E-01	CHA = -.205000E-01	CDA = .421000E-02
CLDE = .360000E-02	CHDE = -.116000E-01	CDE = 0.
CLDF = -.556700E-02	CHDF = .126700E-02	CDF = .867400E-03
CLG = 5.15450	CHG = -15.6500	
CLAD = 0.	CHAD = -6.79000	
CLU = 0.	CHU = 0.	CDU = 0.

\*\*\*\*\*

IS THE ENTERED DATA CORRECT ? (YES/NO)YES

\*\*\*\*\*

LONGITUDINAL BODY AXIS COEFFICIENTS (1/RAD)

CZ = -.426631	CNA = -1.17333	CX = -.613992E-02
CZA = -5.37114		CXA = .467432
CZDE = -.211179		CXDE = .805101E-02
CZDF = .316605		CXDF = -.630117E-01
CZG = -5.14990		CXG = .215040
CZAD = 0.	CMAD = -6.70404	CIAD = 0.
CZU = -.620094	CNU = .491056E-01	CIU = -.293671E-01

\*\*\*\*\*

LONG BODY AXIS DIMENSIONAL DERIVATIVES

Z = -129542.	H = 0.	Y = -1064.32
ZA = -403.950	HA = -2.92017	YA = 30.6425
ZDE = -15.0025	HDE = -1.65304	YDE = .665675
ZDF = 23.0115	HDF = .100639	YDF = -4.73904
ZG = -5.24057	HG = -.526903	YG = .219645
ZAD = 0.	HAD = -.220405	YAD = 0.
ZU = -.634070E-01	HU = .164203E-03	YU = -.296465E-02

\*\*\*\*\*

LONG BODY AXIS PRIMED DIMENSIONAL DERIVATIVES

ZA' = -.542225	HA' = -2.79632	YA' = 30.6425
ZDE' = -.213100E-01	HDE' = -1.64097	YDE' = .665675
ZDF' = .319617E-01	HDF' = .173339	YDF' = -4.73904
ZG' = .992966	HG' = -.733701	YG' = -30.9060
ZU' = -.052106E-04	HU' = .103740E-03	YU' = -.296465E-02
ZTHETA' = -.100993E-02	HTHETA' = .413396E-03	YTHETA' = -32.1710

\*\*\*\*\*

CNB (1/DEG) = .002097 ←

CNP (1/RAD) = -.005

CNR (1/RAD) = -.194

CNDR (1/DEG) = -.001972

CNDA (1/DEG) = .000026

CNDDT (1/DEG) =0  
 CNDC (1/DEG) =0  
 CLD (1/DEG) =-.00309  
 CLP (1/RAD) =-.4330  
 CLR (1/RAD) =.155  
 CLDR (1/DEG) =.0005497  
 CLDA (1/DEG) =.0003298  
 CLDDT (1/DEG) =0  
 CLDC (1/DEG) =0  
 CYB (1/DEG) =-.013298  
 CYP (1/RAD) =-.233  
 CYR (1/RAD) =.428  
 CYDR (1/DEG) =.004607  
 CYDA (1/DEG) =-.000129  
 CYDDT (1/DEG) =0  
 CYDC (1/DEG) =0

\*\*\*\*\*

LAT-DIR STABILITY AXIS COEFFICIENTS

CND = .209700E-02	CLD = -.389000E-02	CYB = -.132900E-01
CNP = -.500000E-02	CLP = -.433000	CYP = -.233000
CNR = -.194000	CLR = .155000	CYR = .428000
CNDR = -.197200E-02	CLDR = .549700E-03	CYDR = .460700E-02
CNDA = .260000E-04	CLDA = .329800E-03	CYDA = -.129000E-03
CNDDT = 0.	CLDDT = 0.	CYDDT = 0.
CNDC = 0.	CLDC = 0.	CYDC = 0.

\*\*\*\*\*

IS THE ENTERED DATA CORRECT ? (YES/NO)YES

\*\*\*\*\*

LAT-DIR BODY AXIS COEFFICIENTS

CND = .156507	CLD = -.229636	CYB = -.761919
CNP = -.153462E-01	CLP = -.440853	CYP = -.250710
CNR = -.180147	CLR = .144654	CYR = .417868
CNDR = -.996992E-01	CLDR = .319410E-01	CYDR = .263962
CNDA = .227967E-02	CLDA = .180172E-01	CYDA = -.739116E-02
CNDDT = 0.	CLDDT = 0.	CYDDT = 0.

CNDC = 0.                      CLDC = 0.                      CYDC = 0.  
\*\*\*\*\*

LAT-DIR BODY AXIS DIMENSIONAL DERIVATIVES

NB = 1.42597	LB = -4.44990	YB = -57.3031
NP = -.122772E-01	LP = -.750111	YP = -1.63568
NR = -.150520	LR = .246128	YR = 2.75949
NDR = -.908384	LDR = .618955	YDR = 19.8523
NDA = .207706E-01	LDA = .364641	YDA = -.535881
NDDT = 0.	LDDT = 0.	YDDT = 0.
NDC = 0.	LDC = 0.	YDC = 0.

\*\*\*\*\*

LAT-DIR BODY AXIS PRIMED DIMENSIONAL DERIVATIVES

NB' = 1.42597	LB' = -4.44990	YB' = -.769169E-01
NP' = -.122772E-01	LP' = -.750111	YP' = .396635E-01
NR' = -.150520	LR' = .246128	YR' = -.996296
NDR' = -.908384	LDR' = .618955	YDR' = .266473E-01
NDA' = .207706E-01	LDA' = .364641	YDA' = -.746149E-03
NDDT' = 0.	LDDT' = 0.	YDDT' = 0.
NDC' = 0.	LDC' = 0.	YDC' = 0.

\*\*\*\*\*  
IS ANOTHER PROGRAM RUN DESIRED ? (YES/NO)NO

\*\*\*\*\*  
END CAT  
024300 MAXIMUM EXECUTION FL.  
0.312 CP SECONDS EXECUTION TIME.



## Appendix E: Time Response Models

### Introduction

This appendix outlines the response models developed for each of the maneuvers in the lateral design of a robust controller. These models are developed using Reference 2 as a guide. Also the required 2x2 equation for F.C.'s #2 and #3 are included and, finally, the required templates for the design of loops one and two are shown.

### Response Models--Bank Angle Command

The upper bound or optimal response selected for the bank angle response is a settling time of approximately 5 seconds for a 30 degree command input. The derived equation for this bound is:

$$b_{11} = \frac{50}{(s + 1)(s + 5)(s + 10)} \quad (E-1)$$

The time domain specification for this model is given in Table E-1. The log magnitude of  $b_{11}$  over the frequency of interest is shown in Table E-2.

The worst acceptable response for a 30 degree bank angle command is selected as having a settling time of

TABLE E-1

 $b_{11}$ --TIME DOMAIN SPECIFICATION

---



---

Rise time = 2.29 seconds
Settling time = 4.24 seconds
Peak value = 30.0
Final value = 30.0

---

TABLE E-2

LOG MAGNITUDE-- $b_{11}$ 


---



---

Frequency (Rad/Sec)	Magnitude (db)	Frequency (Rad/Sec)	Magnitude (db)
0.1	-0.045	10	-30.0
0.2	-0.179	20	-45.3
0.5	-1.02	50	-68.2
1.0	-3.22	100	-86.1
2.0	-7.80	200	-104
5.0	-18.1	500	-128

---

approximately 10 seconds. The derived equation for this bound is:

$$a_{11} = \frac{25.0}{(s + .5)(s + 1)(s + 5)(s + 10)} \quad (E-2)$$

The time domain specification for this model is given in Table E-3. The log magnitude of  $a_{11}$  over the frequency of interest is shown in Table E-4.

TABLE E-3

 $a_{11}$ --TIME DOMAIN SPECIFICATIONS

Rise time = 5.21 seconds
Settling time = 9.51 seconds
Peak value = 30.0
Final value = 30.0

TABLE E-4

LOG MAGNITUDE-- $a_{11}$ 

Frequency (Rad/Sec)	Magnitude (db)	Frequency (Rad/Sec)	Magnitude (db)
0.1	-0.216	10	-56.1
0.2	-0.824	20	-77.4
0.5	-4.03	50	-108
1.0	-10.2	100	-132
2.0	-20.1	200	-156
5.0	-38.2	500	-188

The upper bound or maximum acceptable response for the sideslip response due to a bank angle command is a peak value of 1 degree which settles to zero. The derived equation for this bound is:

$$b_{12} = \frac{1.859 s(s + 5)}{(s + .5)(s + 1.3)(s + 20)} \quad (E-3)$$

The time domain specification model is given in Table E-5  
 The log magnitude of  $b_{12}$  over the frequency of interest  
 is shown in Table E-6.

A plot of log magnitude vs frequency for each of  
 the response models is shown in Figure E-1.

TABLE E-5

$b_{12}$ --TIME DOMAIN SPECIFICATIONS

Settling time = 15 seconds
Time to peak = 1 second
Peak value = 1.0
Final value = 0.0

TABLE E-6

LOG MAGNITUDE-- $b_{12}$

Frequency (Rad/Sec)	Magnitude (db)	Frequency (Rad/Sec)	Magnitude (db)
0.1	-23.1	10	-20.7
0.2	-17.6	20	-23.4
0.5	-12.5	50	-29.2
1.0	-11.8	100	-34.8
2.0	-13.9	200	-40.8
5.0	-18.2	500	-48.6

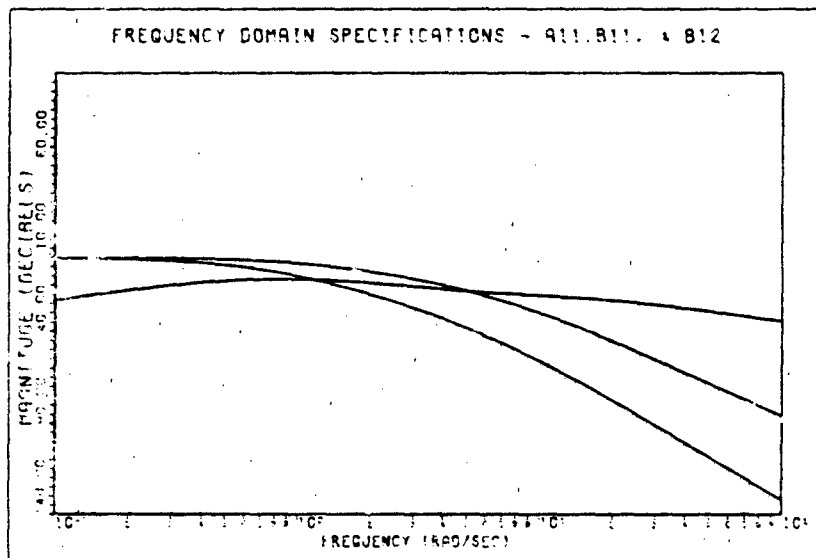


Fig. E-1. Frequency Response-- $a_{11}$ ,  $b_{11}$  and  $b_{12}$

Response Model--Sideslip Command

The upper bound or optimal response selected on the sideslip response is a settling time of approximately 9 seconds for a 5 degree command input. The derived equation for this bound is

$$b_{22} = \frac{2.25}{(s + .45)(s + 5)} \quad (E-4)$$

The time domain specifications for this model are given in Table E-7. The log magnitude of  $b_{22}$  over the frequency of interest is shown in Table E-8.

TABLE E-7

 $b_{22}$ --TIME DOMAIN SPECIFICATIONS

Rise time = 4.91 seconds
Settling time = 8.90 seconds
Peak value = 5.0
Final value = 5.0

TABLE E-8

LOG MAGNITUDE-- $b_{22}$ 

Frequency (Rad/Sec)	Magnitude (db)	Frequency (Rad/Sec)	Magnitude (db)
0.1	-0.211	10	-33.9
0.2	-0.790	20	-45.3
0.5	-3.54	50	-61.0
1.0	-7.91	100	-73.0
2.0	-13.8	200	-85.0
5.0	-24.0	500	-100.0

The worst acceptable response for a 5 degree side-slip command is selected as having a settling time of approximately 15 seconds. The derived equation for this bound is:

$$a_{22} = \frac{1.5}{(s + .3)(s + 1)(s + 5)} \quad (E-5)$$

The time domain specifications for this model are given in Table E-9. The log magnitude of  $a_{22}$  over the frequency of interest is shown in Table E-10.

TABLE E-9  
 $a_{22}$ --TIME DOMAIN SPECIFICATIONS

Rise time = 7.87 seconds
Settling time = 14.4 seconds
Peak value = 5.0
Final value = 5.0

TABLE E-10  
 LOG MAGNITUDE-- $a_{22}$

Frequency (Rad/Sec)	Magnitude (db)	Frequency (Rad/Sec)	Magnitude (db)
0.1	-0.503	10	-57.5
0.2	-0.77	20	-74.8
0.5	-6.78	50	-98.5
1.0	-14.0	100	-116.0
2.0	-24.2	200	-134.0
5.0	-41.6	500	-152.0

The upper and lower bounds or maximum acceptable response for bank angle response due to a sideslip command is a peak value of 2 degrees which settles to zero. The derived equation for this bound is:

$$b_{21} = \frac{.7643 (s) (s + 6)}{(s + .5) (s + 2.3) (s + 20)} \quad (E-6)$$

The time domain specifications for this model are given in Table E-11. The log magnitude of  $b_{21}$  over the frequency of interest is shown in Table E-12.

A plot of log magnitude vs frequency for each of the response models is shown in Figure E-2.

TABLE E-11

$b_{21}$ --TIME DOMAIN SPECIFICATIONS

---

---

Time to peak = .681 seconds

Settling time = 20 seconds

Peak value = 2.0

Final value = 0.0

---



TABLE E-12

LOG MAGNITUDE-- $b_{21}$

Frequency (Rad/Sec)	Magnitude (db)	Frequency (Rad/Sec)	Magnitude (db)
0.1	-34.2	10	-28.2
0.2	-28.7	20	-31.1
0.5	-22.3	50	-36.9
1.0	-21.6	100	-42.5
2.0	-22.3	200	-48.4
5.0	-25.6	500	-56.3

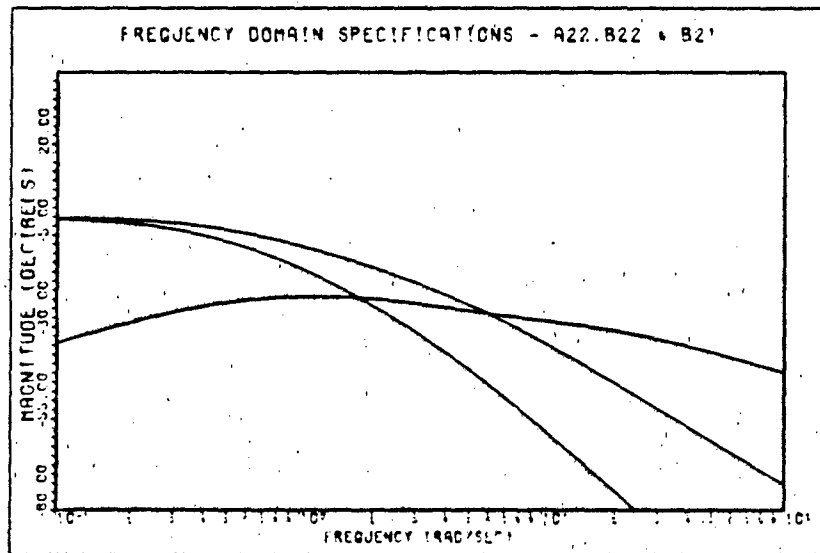


Fig. E-2. Frequency Response-- $a_{22}$ ,  $b_{22}$ , and  $b_{21}$

Equations for F.C.'s #2 and #3

The required equations for F.C. #2 and F.C. #3 are:

$$\psi = \frac{1}{.99644s} [ (.0399458s + .04176)\phi - (s + .07625)\beta - .007655\delta_w + .0273552\delta_r ] \quad (E-7)$$

$$(s^2 + .920643s - .016597)\phi + (.3974s + 6.25223)\beta = .46223\delta_w + 1.111\delta_r \quad (E-8)$$

$$(.0399466s^2 + .06167s + .00821)\phi - (s^2 + .272719s + 1.88358)\beta = (.0007655s + .02547)\delta_w - (.0273552s + 1.3286)\delta_r \quad (E-9)$$

and in matrix form

$$\begin{bmatrix} (s^2 + .920643s - .016597) & (.3974s + 6.25223) \\ (.0399458s^2 + .06167s + .00821) & -(s^2 + .272719s + 1.88358) \end{bmatrix} \begin{bmatrix} \phi \\ \beta \end{bmatrix} = \begin{bmatrix} .46223 & 1.111 \\ .0007655s + .02547 & -.0273552s - 1.3286 \end{bmatrix} \begin{bmatrix} \delta_w \\ \delta_r \end{bmatrix} \quad (E-10)$$

F.C. #3:

$$\psi = \frac{1}{.982538s} [ (.0316453s + .1370213)\phi - (s + .129778)\beta - .0024207\delta_w + .03819\delta_r ] \quad (E-11)$$

$$(s^2 + 1.11801s - .09548)\phi + (.69382s + 2.4876)\beta$$

$$= .37757\delta_w = .36189\delta_r \quad (E-12)$$

$$(.0316453s^2 + .22835s + .03271)\phi - (s^2 + .36853s + .60905)\beta$$

$$= (.0024207s + .01926)\delta_w - (.03819s + .46618)\delta_r \quad (E-13)$$

and in matrix form

$$\begin{bmatrix} (s^2 + 1.11801s - .09548) & (.69382s + 2.4876) \\ (.0316453s^2 + .22835s + .03271) & -(s^2 + .36853s + .60905) \end{bmatrix} \begin{bmatrix} \phi \\ \beta \end{bmatrix}$$

$$= \begin{bmatrix} .37757 & .36189 \\ .0024207s + .01926 & -.03819s - .46618 \end{bmatrix} \begin{bmatrix} \delta_w \\ \delta_r \end{bmatrix} \quad (E-14)$$

### Templates

The templates for  $q_{22}$  are shown in Figure E-3 and the templates for  $q_{11e}$  are shown in Figure E-4.

### Summary

This appendix outlines the response model developed for the lateral design. One set of models is for the commanded bank angle maneuver while the second set of models is for the commanded sideslip maneuver. Also included are the required lateral equations for FC #2 and #3 and, finally, the templates used in the design are shown.

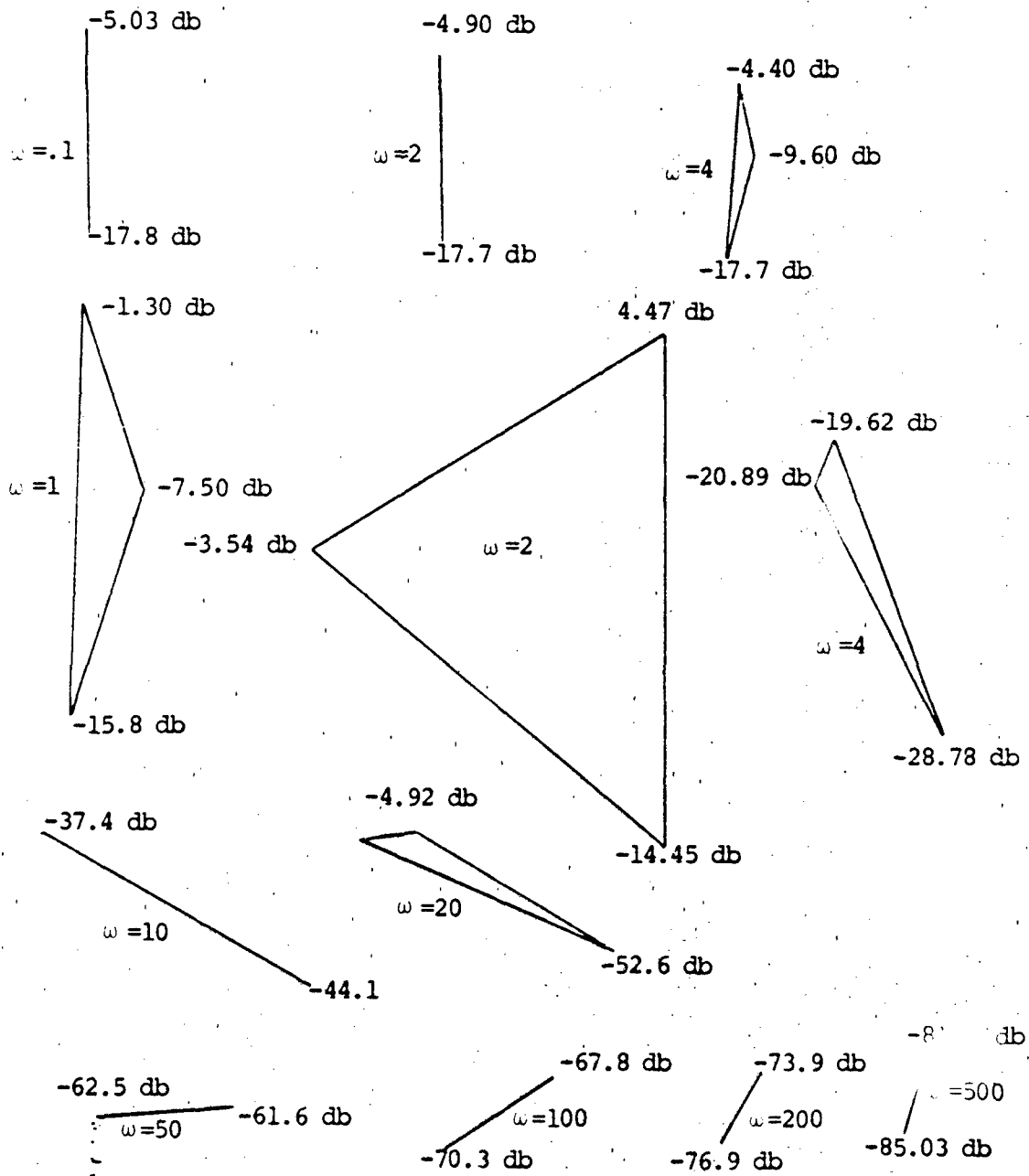


Fig. E-3. Templates for  $q_{22}$

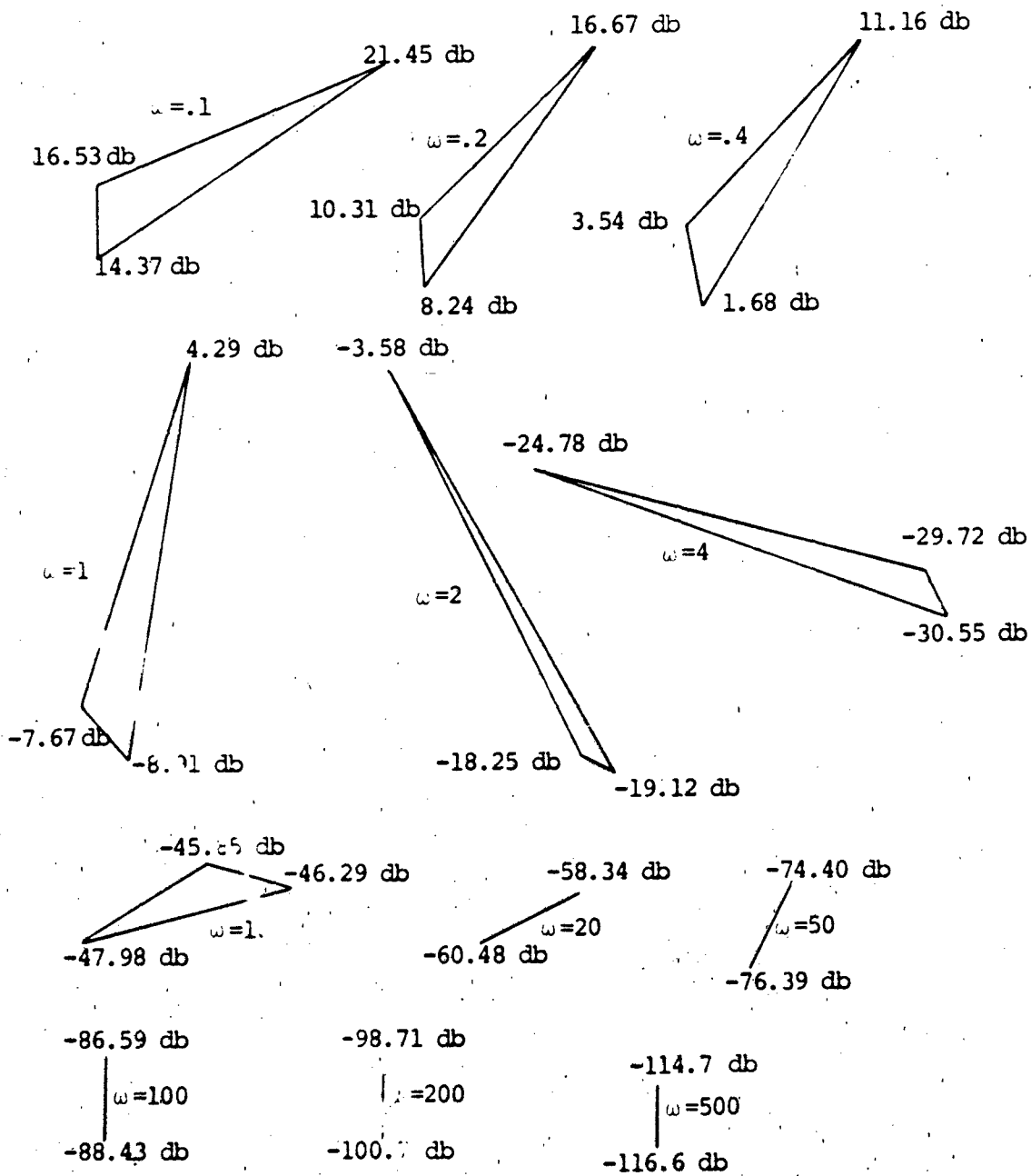


Fig. E-4. Templates for  $q_{11e}$

Appendix F: The 3x3 Design Data  
and Response Models

Introduction

This appendix contains the required data for the design of the Longitudinal 3x3 MIMO System. This data is obtained using the computer programs listed in Reference 19. The first set of data is for the rigid aircraft while the second set of data is for the rigid aircraft plus the first and second body bending modes. Also included are the 3x3 equations of the rigid aircraft for F.C.'s #2 and #3. The next section contains the derived time domain specifications for the pitch pointing maneuver and, finally, the templates of  $q_{11}$ ,  $q_{22}$  and  $q_{33}$  for both the rigid and non-rigid aircraft are included.

Rigid Aircraft Data

The data listed in Tables F-1 through F-10 is only given over the desired frequency of interest. Each table gives the magnitude of the desired  $q_{ij}$  for each of the three F.C.'s. For each  $q_{11}$ ,  $q_{22}$  and  $q_{33}$  the magnitude and phase are given. Phase angle is given in degrees.

TABLE F-1

MAGNITUDE (db) AND PHASE (Deg) --  $q_{11}$ 

Frequency (Rad/Sec)	F.C. #1		F.C. #2		F.C. #3	
	Mag	Phase	Mag	Phase	Mag	Phase
0.01	82.49	-291.7	63.73	-273.2	73.23	-281.0
0.1	51.04	-345.5	42.53	-299.6	46.61	-332.8
0.2	39.21	-352.7	34.13	-318.6	35.31	-345.6
0.5	23.35	-357.0	20.20	-340.6	19.62	-345.1
1.0	11.32	-358.5	8.535	-350.0	7.616	-357.1
2.0	0.7195	-359.3	-3.407	-355.5	-4.416	-358.5
5.0	-16.64	-359.7	-19.30	-358.0	-20.23	-359.4
10.0	-28.68	-359.9	-31.33	-359.0	-32.37	-359.7
20.0	-40.72	-359.8	-43.37	-359.5	-44.41	-359.9
50.0	-56.64	-360.0	-59.29	-359.8	-60.33	-359.9
100.0	-68.68	-360.0	-71.33	-359.9	-72.37	-360.0
200.0	-80.72	-360.0	-83.37	-359.9	-84.41	-360.0
500.0	-96.64	-360.0	-99.29	-360.0	-100.3	360.0

TABLE F-2  
MAGNITUDE (db)-- $q_{12}$

Frequency (Rad/Sec)	F.C. #1	F.C. #2	F.C. #3
0.01	20.20	1.106	21.10
0.1	18.86	1.033	16.16
0.2	16.20	.817	11.21
0.5	9.123	-.5276	2.983
1.0	1.018	-3.946	-4.755
2.0	-9.135	-10.87	-14.46
5.0	-24.38	-24.39	-29.41
10.0	-36.32	-36.01	-41.30
20.0	-48.34	-47.94	-53.30
50.0	-64.25	-63.83	-69.21
100.0	-76.29	-75.87	-81.25
200.0	-88.33	-87.91	-93.29
500.0	-104.2	-103.8	-109.2



TABLE F-3  
MAGNITUDE (db)-- $q_{13}$

Frequency (Rad/Sec)	F.C. #1	F.C. #2	F.C. #3
0.01	32.34	30.47	17.23
0.1	32.34	30.47	17.23
0.2	32.34	30.47	17.23
0.5	32.34	30.47	17.23
1.0	32.34	30.47	17.23
2.0	32.34	30.47	17.23
5.0	32.34	30.47	17.23
10.0	32.34	30.47	17.23
20.0	32.34	30.47	17.23
50.0	32.34	30.47	17.23
100.0	32.34	30.47	17.23
200.0	32.34	30.47	17.23
500.0	32.34	30.47	17.23

TABLE F-4  
MAGNITUDE (db) --  $q_{21}$

Frequency (Rad/Sec)	F.C. #1	F.C. #2	F.C. #3
0.01	37.67	37.43	30.60
0.1	17.50	17.22	10.52
0.2	11.02	10.63	4.267
0.5	0.7319	-1.884	-5.033
1.0	-9.236	-10.27	-13.95
2.0	-20.56	-21.72	-24.67
5.0	-36.25	-37.46	-40.13
10.0	-48.26	-49.47	-52.10
20.0	-60.29	-61.51	-64.12
50.0	-76.21	-77.42	-80.03
100.0	-88.25	-89.46	-92.07
200.0	-100.3	-101.5	-104.1
500.0	-116.2	-117.4	-120.0

TABLE F-5

MAGNITUDE (db) AND PHASE (Deg)-- $q_{22}$ 

Freq. (Rad /Sec)	F.C. #1		F.C. #2		F.C. #3	
	Mag	Phase	Mag	Phase	Mag	Phase
0.01	-24.64	-.1848	-25.18	-.1763	-21.66	-.2665
0.1	-24.64	-1.848	-25.18	-1.763	-21.66	-2.664
0.2	-24.65	-3.695	-25.19	-3.525	-21.68	-5.326
0.5	-24.70	-9.221	-25.23	-8.797	-21.78	-13.27
1.0	-24.86	-18.32	-25.38	-17.49	-22.12	-26.18
2.0	-25.50	-35.76	-25.97	-34.21	-23.36	-49.89
5.0	-28.99	-77.77	-29.22	-75.14	-29.09	-98.61
10.0	-35.77	-116.4	-35.72	-114.0	-37.80	-133.5
20.0	-45.78	-145.6	-45.58	-144.0	-48.76	-155.7
50.0	-61.04	-165.9	-60.77	-165.2	-64.34	-170.2
100.0	-72.98	-172.9	-72.70	-172.6	-76.34	-175.1
200.0	-84.99	-176.9	-84.71	-176.3	-88.37	-177.5
500.0	-100.91	-178.6	-100.6	-178.1	-104.3	-179.0

TABLE F-6  
MAGNITUDE (db) AND PHASE (Deg) --  $q_{22e}$

Frequency (Rad, Sec)	F.C. #1		F.C. #2		F.C. #3	
	Mag	Phase	Mag	Phase	Mag	Phase
0.01	-24.64	-359.9	-25.17	-359.9	-21.65	-359.9
0.1	-24.62	-359.9	-25.62	-359.8	-21.62	-359.8
0.2	-24.62	-359.8	-25.15	-359.6	-21.61	-359.6
0.5	-24.65	-359.4	-25.20	-358.8	-21.58	-357.9
1.0	-24.80	-357.2	-25.39	-356.3	-21.91	-347.1
2.0	-27.58	-343.5	-29.47	-340.1	-29.79	-302.3
5.0	-47.92	-224.1	-45.36	-204.3	-57.53	-111.3
10.0	-57.29	-186.1	-54.77	-181.3	-59.99	-132.7
20.0	-68.48	-172.5	-66.13	-171.3	-68.85	-125.8
50.0	-82.71	-154.5	-80.68	-155.3	-78.89	-107.8
100.0	-92.98	-139.9	-91.04	-140.4	-85.34	-99.41
200.0	-101.6	-121.3	-99.72	-121.6	-91.49	-94.77
500.0	-110.7	-103.7	-108.9	-103.9	-99.48	-91.92
1000.0	-117.0	-96.97	-115.1	-97.06	-105.5	-90.96
2000.0	-123.0	-93.50	-121.1	-93.55	-111.5	-90.48
5000.0	-131.0	-91.41	-129.1	-91.42	-119.5	-90.20
10000.0	-137.0	-90.71	-135.1	-90.72	-125.5	-90.10

TABLE F-7  
MAGNITUDE (db)--q<sub>23</sub>

Frequency (Rad/Sec)	F.C. #1	F.C. #2	F.C. #3
0.01	15.43	13.98	.0323
0.1	15.43	13.98	.0323
0.2	15.43	13.98	.0323
0.5	15.43	13.98	.0323
1.0	15.43	13.98	.0323
2.0	15.43	13.98	.0323
5.0	15.43	13.98	.0323
10.0	15.43	13.98	.0323
20.0	15.43	13.98	.0323
50.0	15.43	13.98	.0323
100.0	15.43	13.98	.0323
200.0	15.43	13.98	.0323
500.0	15.43	13.98	.0323

TABLE F-8  
MAGNITUDE (db)-- $q_{31}$

Frequency (Rad/Sec)	F.C. #1	F.C. #2	F.C. #3
0.01	37.37	34.28	43.67
0.0	16.96	13.77	23.30
0.2	9.907	6.490	16.31
0.5	-2.010	-5.883	4.541
1.0	-12.99	-17.06	-6.371
2.0	-24.72	-28.86	-18.08
5.0	-40.55	-44.70	-33.90
10.0	-52.58	-56.73	-45.92
20.0	-64.62	-68.77	-57.96
50.0	-80.53	-84.69	-73.88
100.0	-92.57	-96.73	-85.92
200.0	-104.6	-108.8	-97.96
500.0	-120.5	-124.7	-113.9

TABLE F-9  
 MAGNITUDE (db)--q<sub>32</sub>

Frequency (Rad/Sec)	F.C. #1	F.C. #2	F.C. #3
0.01	-28.3	-32.47	-13.84
0.1	-28.94	-32.48	-13.85
0.2	-28.96	-32.50	-13.87
0.5	-29.13	-32.67	-14.03
1.0	-29.68	-33.23	-14.57
2.0	-31.39	-34.94	-16.31
5.0	-36.70	-40.24	-22.55
10.0	-42.75	-46.22	-30.83
20.0	-50.51	-53.79	-41.40
50.0	-63.84	-66.87	-56.82
100.0	-75.35	-78.30	-68.79
200.0	-87.25	-90.18	-80.81
500.0	-103.1	-106.0	-96.72

TABLE F-10

MAGNITUDE (db) AND PHASE (Deg)-- $q_{33}$ 

Frequency (Rad/Sec)	F.C. #1		F.C. #2		F.C. #3	
	Mag	Phase	Mag	Phase	Mag	Phase
0.01	8.102	-30.90	4.159	-28.35	3.377	-6.681
0.1	-6.228	-80.52	-9.517	-79.50	-3.151	-49.52
0.2	-12.16	-85.23	-15.43	-84.71	-4.685	-66.89
0.5	-20.09	-88.09	-23.36	-87.88	-12.04	-80.32
1.0	-26.11	-89.05	-29.37	-88.94	-17.97	-85.13
2.0	-32.13	-89.53	-35.39	-89.48	-23.97	-87.56
5.0	-40.09	-89.82	-43.35	-89.79	-31.92	-89.03
10.0	-46.11	-89.91	-49.37	-89.90	-37.94	-89.52
20.0	-52.13	-89.96	-55.39	-89.95	-43.96	-89.76
50.0	-60.09	-89.99	-63.35	-89.99	-51.92	-89.91
100.0	-66.11	-90.00	-69.37	-90.00	-57.94	-89.96
200.0	-72.13	-90.00	-75.39	-90.00	-63.96	-89.98
500.0	-80.09	-90.00	-83.35	-90.00	-71.92	-90.00



Aircraft Data--Rigid, First and  
Second Bending Mode

The data listed in the following tables is obtained using the programs listed in Reference 19. The natural frequency for the first bending mode occurs at approximately 11.6 rad/sec and the natural frequency of the second bending mode occurs at approximately 23.4 rad/s. For the design of the longitudinal controller, the frequencies at and around the bending modes natural frequencies are of interest because of changes in both magnitude and phase. Thus the data in Tables F-11 through F-20 is expanded around the natural frequencies of the first and second body bending modes. Note: the change in magnitude and phase of the non-rigid model is very small from that of the rigid model.

TABLE F-11  
MAGNITUDE AND PHASE  $q_{11}$

Frequency (Rad/Sec)	F.C. #1		F.C. #2		F.C. #3	
	Mag	Phase	Mag	Phase	Mag	Phase
0.01	82.48	-290.8	63.73	-273.2	73.23	-280.9
0.1	51.04	-345.5	42.53	-299.6	46.61	-332.7
0.2	39.21	-352.6	34.13	-318.6	35.31	-345.6
0.5	23.35	-357.0	20.20	-340.6	19.62	-354.1
1.0	11.32	-358.5	8.54	-350.0	7.62	-357.1
2.0	-7.19	-359.3	-3.41	-355.0	-4.42	-358.5
5.0	-16.64	-359.7	-19.30	-358.0	-20.33	-359.4
*10.0	-28.68	-359.9	-31.33	-359.0	-32.37	-359.7
11.0	-30.33	-359.9	-32.99	-359.1	-34.03	-359.7
11.5	-31.11	-359.9	-33.76	-359.1	-34.80	-359.7
12.0	-31.85	-359.9	-34.50	-359.2	-35.54	-359.8
12.5	-32.55	-359.9	-35.21	-359.2	-36.25	-359.8
13.0	-33.24	-359.9	-35.89	-359.2	-36.93	-359.8
**20.0	-40.72	-359.9	-43.37	-359.2	-44.41	-359.9
22.0	-42.37	-359.9	-45.03	-359.5	-46.07	-359.9
22.5	-42.77	-359.9	-45.42	-359.5	-46.46	-359.9
23.0	-43.15	-359.9	-45.80	-359.5	-46.84	-359.9
23.5	-43.52	-359.9	-46.17	-359.6	-47.21	-359.9
24.0	-43.89	-359.9	-46.54	-359.6	-47.58	-359.9
50.0	-56.64	-360.0	-59.29	-359.8	-60.33	-359.9
100.0	-68.68	-360.0	-71.33	-359.9	-72.37	-360.0
200.0	-80.72	-360.0	-83.37	-359.9	-84.41	-360.0
500.0	-96.64	-360.0	-99.29	-360.0	-100.30	-360.0

\* First bending mode.

\*\* Second bending mode.

TABLE F-12  
MAGNITUDE (db) --  $q_{12}$

Frequency (Rad/Sec)	F.C. #1	F.C. #2	F.C. #3
0.01	20.19	1.10	21.10
0.1	18.86	1.03	16.16
0.2	16.20	0.82	11.21
0.5	9.12	-0.53	2.98
1.0	1.08	-3.95	-4.76
2.0	-9.14	-10.87	-14.46
5.0	-24.38	-24.39	-29.41
10.0	-36.32	-36.01	-41.30
11.0	-37.97	-37.64	-42.95
11.5	-38.74	-38.41	-43.71
12.0	-39.48	-39.14	-44.45
12.5	-40.19	-39.84	-45.16
13.0	-40.86	-40.51	-45.84
20.0	-48.34	-47.94	-53.30
22.0	-49.99	-49.59	-54.95
22.5	-50.38	-49.98	-55.34
23.0	-50.76	-50.36	-55.72
23.5	-51.13	-50.73	-56.10
24.0	-51.50	-51.10	-56.46
50.0	-64.25	-63.83	-69.21
100.0	-76.29	-75.87	-81.25
200.0	-88.33	-87.91	-93.29
500.0	-104.20	-103.80	-109.20

TABLE F-13  
MAGNITUDE (db)-- $q_{13}$

Frequency (Rad/Sec)	F.C. #1	F.C. #2	F.C. #3
0.01	32.34	30.47	17.23
0.1	32.34	30.47	17.23
0.2	32.34	30.47	17.23
0.5	32.34	30.47	17.23
1.0	32.34	30.47	17.23
2.0	32.34	30.47	17.23
5.0	32.34	30.47	17.23
10.0	32.34	30.47	17.23
11.0	32.34	30.47	17.23
11.5	32.34	30.47	17.23
12.0	32.34	30.47	17.23
12.5	32.34	30.47	17.23
13.0	32.34	30.47	17.23
20.0	32.34	30.47	17.23
22.0	32.34	30.47	17.23
22.5	32.34	30.47	17.23
23.0	32.34	30.47	17.23
23.5	32.34	30.47	17.23
24.0	32.34	30.47	17.23
50.0	32.34	30.47	17.23
100.0	32.34	30.47	17.23
200.0	32.34	30.47	17.23
500.0	32.34	30.47	17.23

TABLE F-14  
MAGNITUDE (db)-- $q_{21}$

Frequency (Rad/Sec)	F.C. #1	F.C. #2	F.C. #3
0.01	37.67	37.42	30.60
0.1	17.50	17.22	10.52
0.2	11.02	10.63	4.27
0.5	7.32	-0.02	-5.03
1.0	-9.24	-10.27	-13.95
2.0	-20.56	-21.72	-24.67
5.0	-36.25	-37.46	-40.13
10.0	-48.26	-49.47	-52.10
11.0	-49.91	-51.13	-53.75
11.5	-50.68	-51.90	-54.52
12.0	-51.42	-52.64	-55.26
12.5	-52.13	-53.35	-55.97
13.0	-52.81	-54.03	-56.65
20.0	-60.29	-61.51	-64.12
22.0	-61.94	-63.16	-65.78
22.5	-62.34	-63.55	-66.17
23.0	-62.72	-63.93	-66.55
23.5	-63.09	-64.31	-66.92
24.0	-63.46	-64.67	-67.29
50.0	-76.21	-77.42	-80.03
100.0	-88.25	-89.46	-92.07
200.0	-100.30	-101.50	-104.10
500.0	-116.20	-117.40	-120.00

TABLE F-15  
MAGNITUDE (db) and PHASE--q<sub>22</sub>

Frequency (Rad/Sec)	F.C. #1		F.C. #2		F.C. #3	
	Mag	Phase	Mag	Phase	Mag	Phase
0.01	-24.64	-360.0	-25.18	-360.0	-21.66	-360.0
0.1	-24.65	-360.0	-25.18	-360.0	-21.66	-359.9
0.2	-24.65	-359.9	-25.18	-359.9	-21.68	-359.8
0.5	-24.70	-359.8	-25.23	-359.9	-21.78	-359.6
1.0	-24.86	-359.7	-25.38	-359.7	-22.12	-359.2
2.0	-25.49	-359.4	-25.95	-359.5	-23.40	-358.6
5.0	-28.92	-359.1	-29.17	-359.1	-29.21	-358.2
10.0	-35.63	-359.1	-35.64	-359.1	-37.96	-359.7
11.0	-36.85	-358.8	-36.83	-359.1	-39.38	-358.8
11.5	-37.44	-358.9	-37.40	-359.1	-40.06	-358.9
12.0	-38.03	-358.9	-37.96	-359.2	-40.72	-358.9
12.5	-38.59	-358.9	-38.52	-359.2	-41.35	-358.9
13.0	-39.14	-359.3	-39.05	-359.2	-41.97	-358.9
20.0	-45.61	-359.3	-45.45	-359.4	-48.95	-359.3
22.0	-47.13	-359.5	-46.95	-359.5	-50.53	-359.3
22.5	-47.49	-359.5	-47.30	-359.6	-50.91	-359.4
23.0	-47.84	-359.5	-47.68	-359.7	-51.28	-359.4
23.5	-48.20	-359.6	-48.03	-359.6	-51.65	-359.4
24.0	-48.54	-359.6	-48.37	-359.6	-52.00	-359.4
50.0	-60.85	-360.0	-60.46	-360.0	-64.54	-360.0
100.0	-72.79	-360.0	-72.57	-360.0	-76.54	-360.0
200.0	-84.81	-360.0	-84.58	-360.0	-88.57	-360.0
500.0	-100.70	-360.0	-100.50	-360.0	-104.50	-360.0

TABLE F-16

MAGNITUDE (db)-- $q_{23}$ 

Frequency (Rad/Sec)	F.C. #1	F.C. #2	F.C. #3
0.01	15.43	13.98	32.45
0.1	15.43	13.98	32.45
0.2	15.43	13.98	32.45
0.5	15.43	13.98	32.45
1.0	15.43	13.98	32.45
2.0	15.43	13.98	32.45
5.0	15.43	13.98	32.45
10.0	15.43	13.98	32.45
11.0	15.43	13.98	32.45
11.5	15.43	13.98	32.45
12.0	15.43	13.98	32.45
12.5	15.43	13.98	32.45
13.0	15.43	13.98	32.45
20.0	15.43	13.98	32.45
22.0	15.43	13.98	32.45
22.5	15.43	13.98	32.45
23.0	15.43	13.98	32.45
23.5	15.43	13.98	32.45
24.0	15.43	13.98	32.45
50.0	15.43	13.98	32.45
100.0	15.43	13.98	32.45
200.0	15.43	13.98	32.45
500.0	15.43	13.98	32.45

TABLE F-17  
MAGNITUDE (db) --  $q_{31}$

Frequency (Rad/Sec)	F.C. #1	F.C. #2	F.C. #3
0.01	37.46	34.45	43.74
0.1	16.97	13.77	23.30
0.2	9.91	6.49	16.31
0.5	-2.00	-5.88	4.54
1.0	-12.99	-17.06	-6.37
2.0	-24.72	-28.86	-18.08
5.0	-40.55	-44.70	-33.90
10.0	-52.58	-56.73	-45.92
11.0	-54.23	-58.39	-47.58
11.5	-55.01	-59.16	-48.35
12.0	-55.75	-59.90	-49.09
12.5	-56.45	-60.61	-49.80
13.0	-57.14	-61.29	-50.48
20.0	-64.62	-68.77	-57.96
22.0	-66.27	-70.43	-59.62
22.5	-66.66	-70.82	-60.01
23.0	-67.04	-71.20	-60.39
23.5	-67.42	-71.58	-60.76
24.0	-67.78	-71.94	-61.13
50.0	-80.53	-84.69	-73.88
100.0	-92.57	-96.73	-85.92
200.0	-104.60	-108.80	-97.96
500.0	-120.50	-124.70	-113.90



TABLE F-18

MAGNITUDE (db) --  $q_{32}$ 

Frequency (Rad/Sec)	F.C. #1	F.C. #2	F.C. #3
0.01	-15.80	-19.17	-4.96
0.1	-16.18	-19.77	-4.87
0.2	-16.56	-20.14	-4.90
0.5	-18.52	-22.12	-5.10
1.0	-22.14	-25.76	-5.82
2.0	-27.31	-30.93	-8.45
5.0	-35.21	-38.81	-18.27
10.0	-41.94	-45.44	-29.15
11.0	-42.95	-46.42	-30.74
11.5	-43.44	-46.89	-31.49
12.0	-43.91	-47.35	-32.21
12.5	-44.36	-47.80	-32.90
13.0	-48.80	-48.23	-33.56
20.0	-50.07	-53.35	-40.90
22.0	-51.35	-54.59	-42.54
22.5	-51.65	-54.90	-42.92
23.0	-51.96	-55.21	-43.30
23.5	-52.26	-55.50	-43.68
24.0	-52.55	-55.78	-44.05
50.0	-63.73	-66.75	-56.74
100.0	-75.32	-78.27	-68.77
200.0	-87.24	-90.17	-80.81
500.0	-103.10	-106.00	-96.72

TABLE F-19

MAGNITUDE (db) AND PHASE (Deg) --  $q_{33}$ 

Frequency (Rad/Sec)	F.C. #1		F.C. #2		F.C. #3	
	Mag	Phase	Mag	Phase	Mag	Phase
0.01	9.02	-34.58	4.39	-28.97	3.79	-6.97
0.1	-6.23	-80.53	-9.52	-79.50	-3.12	-49.54
0.2	-12.16	-85.23	-15.43	-84.71	-4.69	-66.89
0.5	-20.09	-88.09	-23.36	-87.88	-12.04	-80.32
1.0	-26.11	-89.05	-29.37	-88.94	-17.97	-85.13
2.0	-32.13	-89.53	-35.39	-89.48	-23.97	-87.56
5.0	-40.09	-89.82	-43.35	-89.79	-31.92	-89.03
10.0	-46.11	-90.00	-49.37	-90.00	-37.94	-90.00
11.0	-46.94	-90.00	-50.20	-90.00	-38.77	-90.00
11.5	-47.32	-90.00	-50.58	-90.00	-39.15	-90.00
12.0	-47.69	-90.00	-50.95	-90.00	-39.52	-90.00
12.5	-48.05	-90.00	-51.31	-90.00	-39.88	-90.00
13.0	-48.39	-90.00	-51.65	-90.00	-40.22	-90.00
20.0	-52.13	-90.00	-55.39	-90.00	-43.96	-90.00
22.0	-52.96	-90.00	-56.22	-90.00	-44.79	-90.00
22.5	-53.15	-90.00	-56.41	-90.00	-44.98	-90.00
23.0	-53.34	-90.00	-56.60	-90.00	-45.17	-90.00
23.5	-53.53	-90.00	-56.79	-90.00	-45.36	-90.00
24.0	-53.71	-90.00	-56.97	-90.00	-45.54	-90.00
50.0	-60.09	-90.00	-63.35	-90.00	-51.92	-90.00
100.0	-66.11	-90.00	-69.37	-90.00	-57.94	-90.00
200.0	-72.13	-90.00	-75.39	-90.00	-63.96	-90.00
500.0	-80.09	-90.00	-83.35	-90.00	-71.92	-90.00

TABLE F-20

MAGNITUDE (db) AND PHASE (Deg) --  $q_{22e}$ 

Frequency (Rad/Sec)	F.C. #1		F.C. #2		F.C. #3	
	Mag	Phase	Mag	Phase	Mag	Phase
0.01	-24.64	-360.0	-25.17	-360.0	-21.66	-360.0
0.1	-24.64	-359.9	-25.17	-359.9	-21.67	-359.9
0.2	-24.64	-359.9	-25.18	-359.7	-31.66	-359.7
0.5	-24.67	-359.5	-25.25	-359.0	-21.64	-358.2
1.0	-24.85	-357.4	-25.49	-356.4	-22.00	-347.7
2.0	-27.63	-343.3	-29.52	-339.8	-29.85	-302.9
5.0	-47.92	-224.1	-45.36	-204.3	-57.54	-111.3
10.0	-57.29	-186.1	-54.77	-181.3	-59.99	-132.7
11.0	-58.77	-183.9	-56.28	-179.9	-61.17	-132.6
11.5	-59.47	-183.0	-57.00	-179.2	-61.73	-132.5
12.0	-60.15	-182.1	-57.69	-178.6	-62.27	-132.3
12.5	-60.80	-181.3	-58.35	-178.0	-62.79	-132.0
13.0	-61.43	-180.5	-58.99	-177.5	-63.30	-131.7
20.0	-68.48	-172.5	-66.13	-171.3	-68.85	-125.8
22.0	-70.05	-170.6	-67.72	-169.9	-70.04	-124.0
22.5	-70.41	-170.2	-68.10	-169.5	-70.32	-123.5
23.0	-70.77	-169.7	-68.46	-169.1	-70.59	-123.1
23.5	-71.13	-169.3	-68.81	-168.7	-70.84	-122.6
24.0	-71.47	-168.8	-69.16	-168.4	-71.09	-122.2
50.0	-82.71	-154.5	-80.68	-155.3	-78.89	-107.8
100.0	-92.98	-139.9	-91.04	-140.4	-85.34	-99.41
200.0	-101.60	-121.3	-99.72	-121.6	-91.49	-94.77
500.0	-110.70	-103.7	-108.90	-103.9	-99.48	-91.92

Rigid Aircraft Equations

Listed below are the derived equations of the longitudinal mode for F.C.'s #2 and #3. Note that these equations are derived in the same manner as the equation derived in Chapter V for F.C. #1.

F.C. #2:

$$\begin{bmatrix} .0411S & .560066S - .02669 & S + .0029646 \\ -.074319S^2 - .03547S & .006307S + .47902 & .004865 \\ -.17891 & S^2 + .814938S + 2.46095 & -.009104 \end{bmatrix} \begin{bmatrix} h \\ \theta \\ u \end{bmatrix}$$

$$= \begin{bmatrix} .010498 & -.079813 & .034 \\ -.01862 & .027303 & 0 \\ -1.75799 & .217951 & 0 \end{bmatrix} \begin{bmatrix} \delta_e \\ \delta_{sb} \\ \delta_T \end{bmatrix}$$

F.C. #3:

$$\begin{bmatrix} .10310S & .1660307S - .13914 & S + .1234233 \\ -.24383S^2 & .18986S & .033514S + .77841 & .1591737 \\ -.261927S & S^2 + 1.09229S + 1.0743 & -.0318452 \end{bmatrix} \begin{bmatrix} h \\ \theta \\ u \end{bmatrix}$$

$$= \begin{bmatrix} .0064484 & -.063125 & .1268 \\ -.0375145 & .064588 & 0 \\ -.921844 & .194512 & 0 \end{bmatrix} \begin{bmatrix} \delta_e \\ \delta_{sb} \\ \delta_T \end{bmatrix}$$

Response Models--Pitch  
Angle Command

The upper bound or optimal response selected for the pitch angle response is a settling time of approximately 6 seconds for a 4 degree command input. The derived equation for this bound is:

$$b_{22} = \frac{0.9550}{(s + 1.018)(s + 0.6665 \pm j0.7028)}$$

The time domain specifications for this model are given in Table F-21.

TABLE F-21

$b_{22}$ --TIME DOMAIN SPECIFICATIONS

---

Rise Time = 2.93 seconds

Settling Time = 6.26 seconds

Peak Value = 4.08 seconds

Final Value = 4.00 seconds

---

The log magnitude of  $b_{22}$  over the frequency of interest is shown in Table F-22.

TABLE F-22

LOG MAGNITUDE-- $b_{22}$ 

Frequency (Rad/Sec)	Magnitude (db)	Frequency (Rad/Sec)	Magnitude (db)
0.1	-0.038	10	-60.4
0.2	-0.153	20	-78.5
0.5	-1.12	50	-102
1.0	-5.99	100	-120
2.0	-19.59	200	-138
5.0	-42.5	500	-162

The worst acceptable case for a 4 degree pitch angle command is selected as having a settling time of approximately 10 seconds. The derived equation for this bound is:

$$a_{22} = \frac{0.4875}{(S + 0.51)(S + 1.018)(S + 0.6665 \pm j0.7028)}$$

The time domain specifications for this model are given in Table F-23.

TABLE F-23

 $a_{22}$ --TIME DOMAIN SPECIFICATIONS

Rise Time = 5.08 seconds

Settling Time = 10.1 seconds

Peak Value = 4.00 seconds

Final Value = 4.00 seconds

The log magnitude of  $a_{22}$  over the frequency of interest is shown in Table F-24.

TABLE F-24  
LOG MAGNITUDE-- $a_{22}$

Frequency (Rad/Sec)	Magnitude (db)	Frequency (Rad/Sec)	Magnitude (db)
0.1	-0.193	10	-86.3
0.2	-0.766	20	-110
0.5	-4.04	50	-142
1.0	-12.8	100	-166
2.0	-31.7	200	-190
5.0	-62.4	500	-222

The upper bound or maximum acceptable response for the altitude response,  $h$ , due to a pitch angle command is a peak value of 0.5 ft. which approaches zero as time increases. The derived equation for this bound is:

$$b_{12} = \frac{11.86S(S + 5)}{(S + 0.4 \pm j0.3165)(S + 10)(S + 10)}$$

The time domain specifications for this model are given in Table F-25. The log magnitude of  $b_{12}$  over the frequency of interest is shown in Table F-26.

TABLE F-25

b<sub>12</sub>--TIME DOMAIN SPECIFICATIONS

Time to Peak = 2.11 seconds
Settling Time = 9.92 seconds
Peak Value = 0.500 seconds
Final Value = 0 seconds

TABLE F-26

LOG MAGNITUDE--b<sub>12</sub>

Frequency (Rad/Sec)	Magnitude (db)	Frequency (Rad/Sec)	Magnitude (db)
0.1	-12.9	10	-23.6
0.2	-7.22	20	-32.2
0.5	-2.59	50	-46.8
1.0	-10.4	200	-70.6
5.0	-17.5	500	-86.5

The upper bound or maximum acceptable response for the perturbation velocity,  $u$ , due to a pitch angle command is a peak value of 1.0 ft/sec which approaches zero as time increases. The derived equation for this bound is:

$$b_{32} = \frac{4.75S(S + 5)}{(S + 0.4 \pm j0.3165)(S + 20)}$$



The time domain specifications for this model are given in Table F-27. The log magnitude of  $b_{32}$  over the frequency of interest is shown in Table F-28.

TABLE F-27

$b_{32}$ --TIME DOMAIN SPECIFICATIONS

Time to Peak = 1.94 seconds
Settling Time = 9.76 seconds
Peak Value = 1.00 seconds
Final Value = 0 seconds

Table F-28

LOG MAGNITUDE-- $b_{32}$

Frequency (Rad/Sec)	Magnitude (db)	Frequency (Rad/Sec)	Magnitude (db)
0.1	-6.89	10	-12.5
0.2	-1.18	20	-15.2
0.5	3.47	50	-21.1
1.0	0.906	100	-26.6
2.0	-4.07	200	-32.5
5.0	-9.76	500	-40.5

A plot of Log Magnitude vs Frequency for each of the response models is shown in Figure F-1.

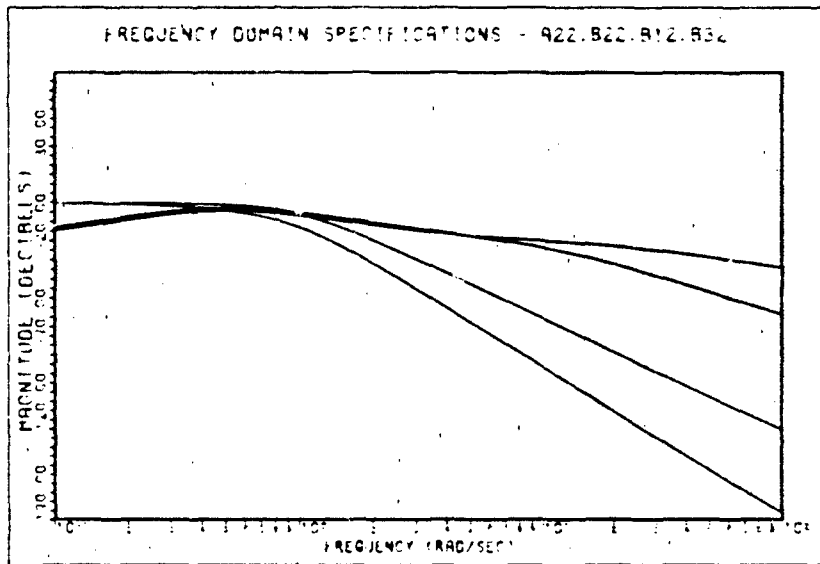
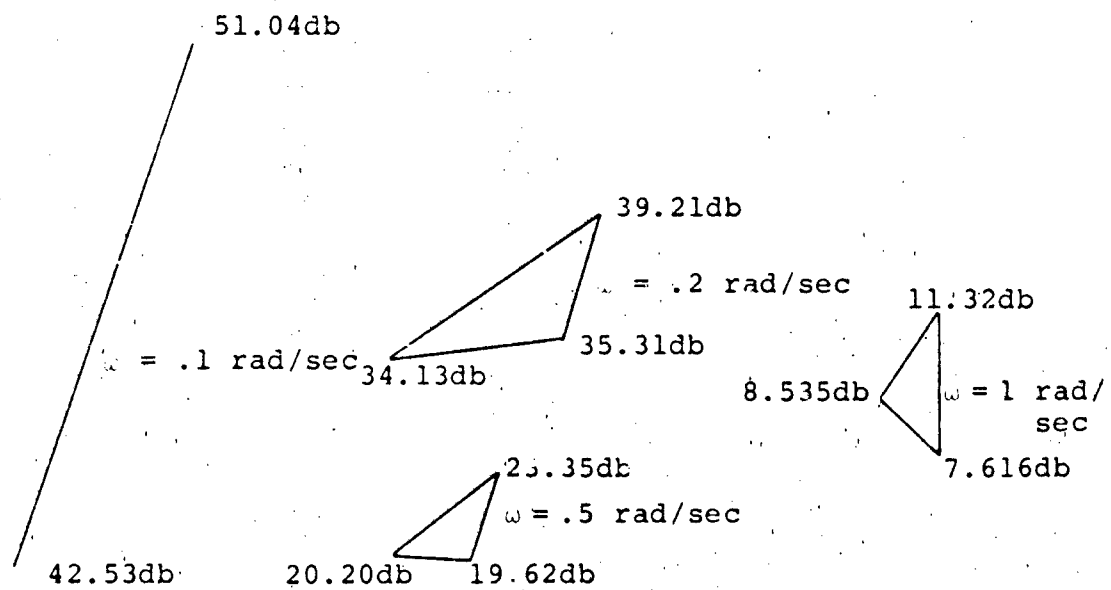


Fig. F-1. Frequency Response-- $a_{22}$ ,  $b_{22}$ ,  $b_{12}$  and  $b_{32}$

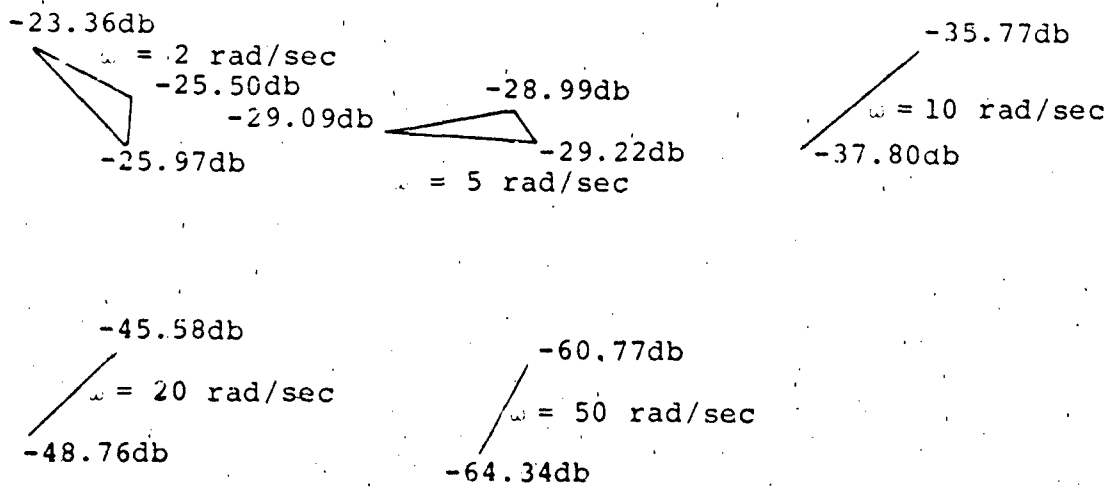
Templates of  $g_{11}$ ,  $g_{22}$ ,  $g_{22e}$  and  $g_{33}$   
for the Rigid and Non-Rigid Design

The templates for the design of the rigid and non-rigid aircraft models are shown in Figures F-2 through F-8.



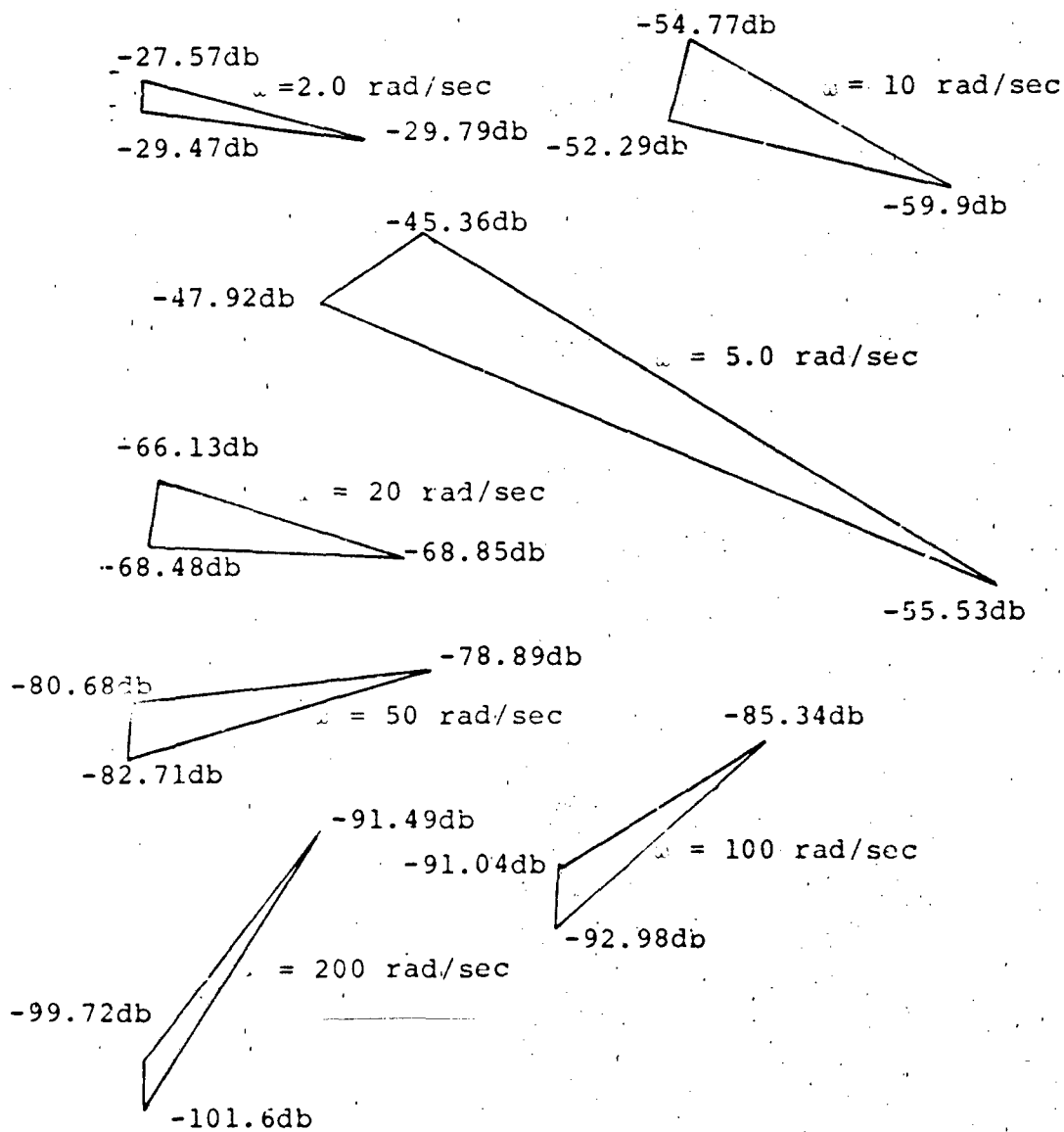
Note that the templates for  $\omega > 2 \text{ rad/sec}$  are straight lines with magnitude of 3.69db.

Fig. F-2. Templates-- $q_{11}$ --Rigid Aircraft



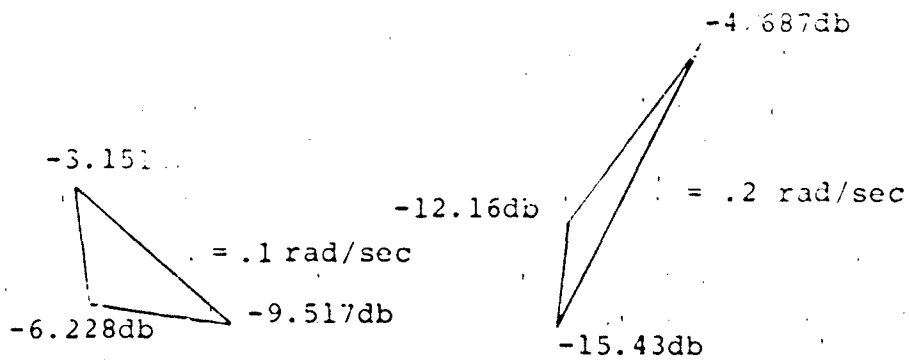
Note that the templates for  $0.1 < \omega < 1.0$  rad/sec and  $\omega > 100$  rad/sec are straight lines with magnitude of 3.50db and 3.64db respectively.

Fig. F-3. Templates-- $J_{22}$ --Rigid Aircraft



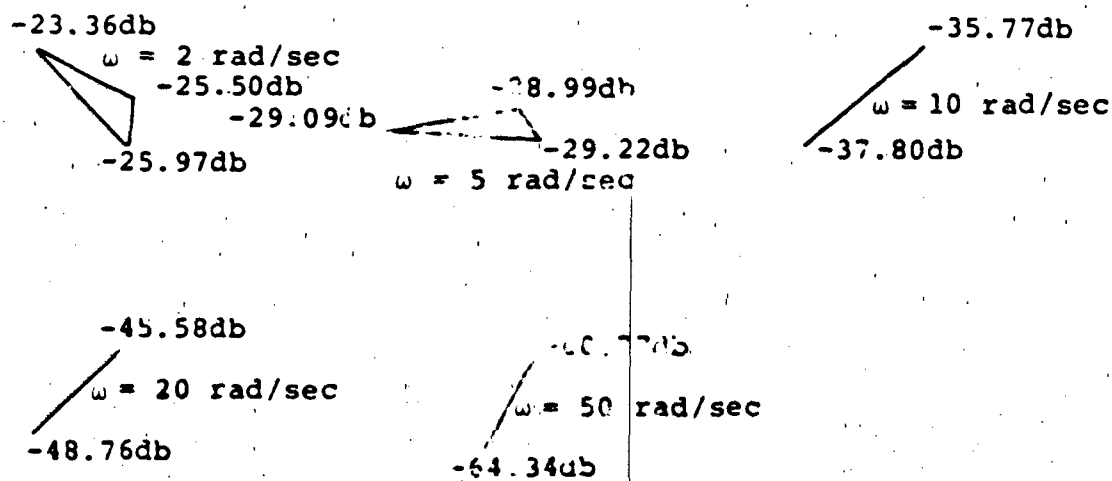
Note that the templates for  $\omega \leq 1.0$  rad/sec are straight lines with magnitude of 3.48db and  $\omega \geq 500$  rad/sec straight lines with magnitude 11.5db.

Fig. F-4. Templates-- $q_{22e}$ --Rigid Aircraft



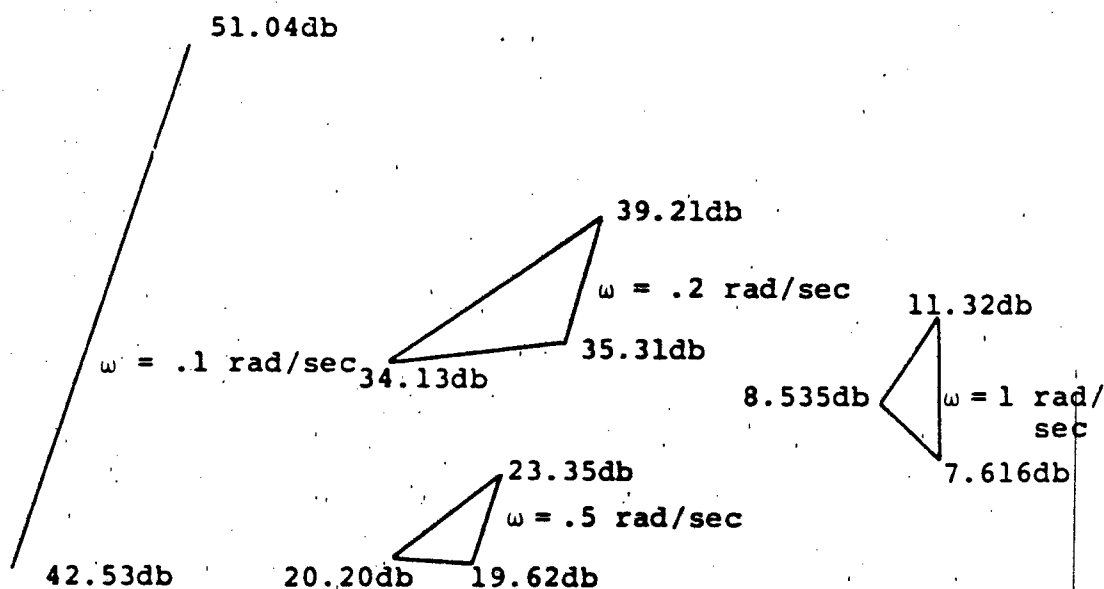
Note that the templates for  $\omega = 2.0 \text{ rad/sec}$  are straight lines with magnitude of  $11.40\text{db}$ .

Fig. F-5. Templates-- $q_{33}$ --Rigid and Non-Rigid Aircraft



Note that the templates for  $0.1 < \omega < 1.0$  rad/sec and  $\omega > 100$  rad/sec are straight lines with magnitude of 3.50db and 3.64db respectively.

Fig. F-6. Templates-- $q_{22}$ --Non-Rigid Aircraft



Note that the templates for  $\omega > 2$  rad/sec are straight lines with magnitude of 3.69db.

Fig. F-7. Templates-- $q_{11}$ --Non-Rigid Aircraft



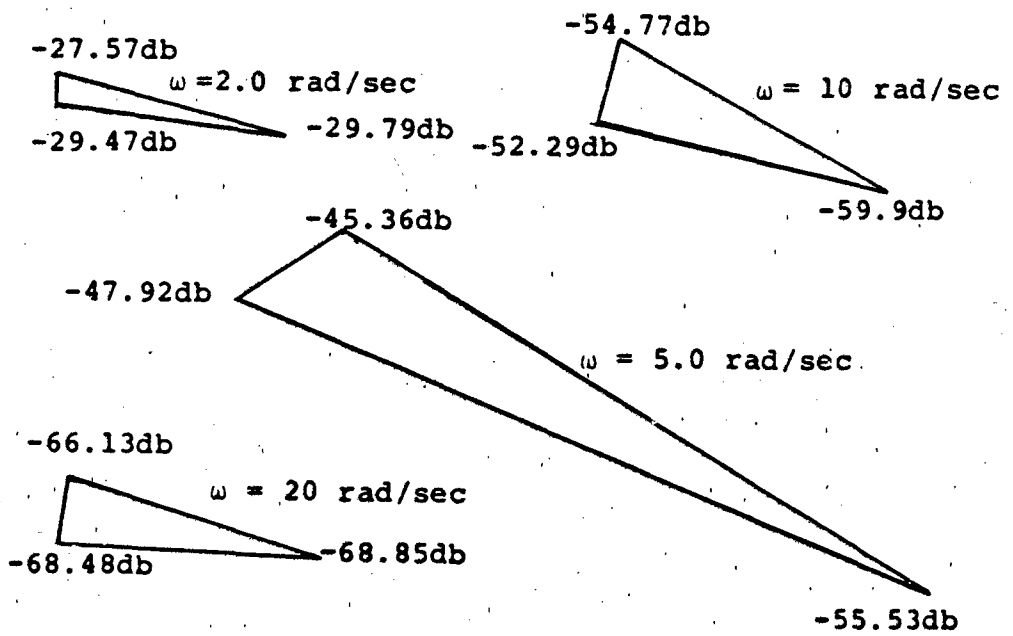
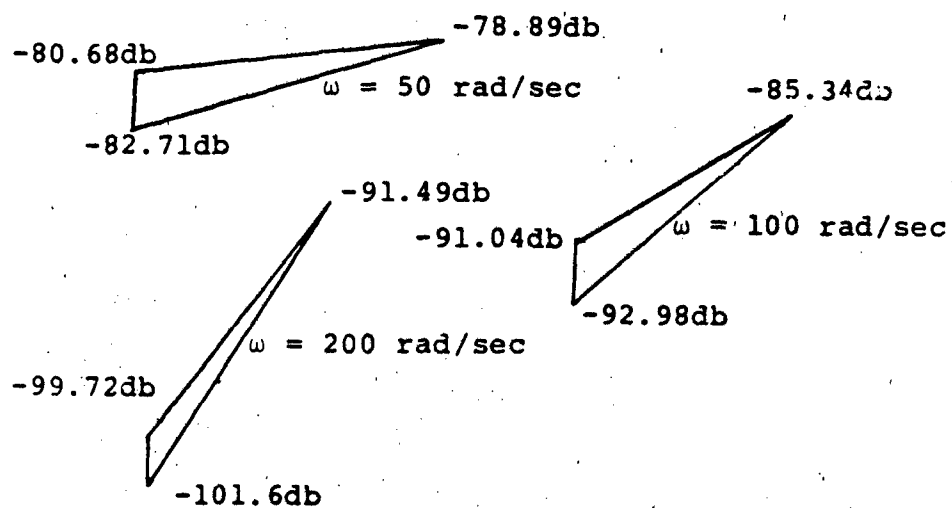


Fig. F-8(a). Templates-- $q_{22e}$ --Non-Rigid Aircraft



Note that the templates for  $\omega < 1.0$  rad/sec are straight lines with magnitude of 3.48db and  $\omega \geq 500$  rad/sec straight lines with magnitude 11.5db.

Fig. F-8(b). Templates-- $q_{22e}$ --Non-Rigid Aircraft

### Summary

This appendix contains the required magnitudes for each of the  $q_{ij}$ 's for the design of the 3x3 longitudinal controllers for both the rigid and nonrigid models. The aircraft equations for F.C.'s #2 and #3 are highlighted and the time domain specification models are presented. These models are used in the development of a pitch angle controller for the longitudinal mode. Finally, the templates required in the design of each controller are included.

## Appendix G: 2x2 Simulation Programs

### Introduction

This appendix contains the computer programs used in the simulation of the 2x2 design. The programs used during the 3x3 design phase for the numerical analysis and simulations are contained in Reference 19.

### 2x2 Simulation

The following programs are used in the simulation of the 2x2 design. Shown in Figure G-1 is the feedback structure used in this simulation.

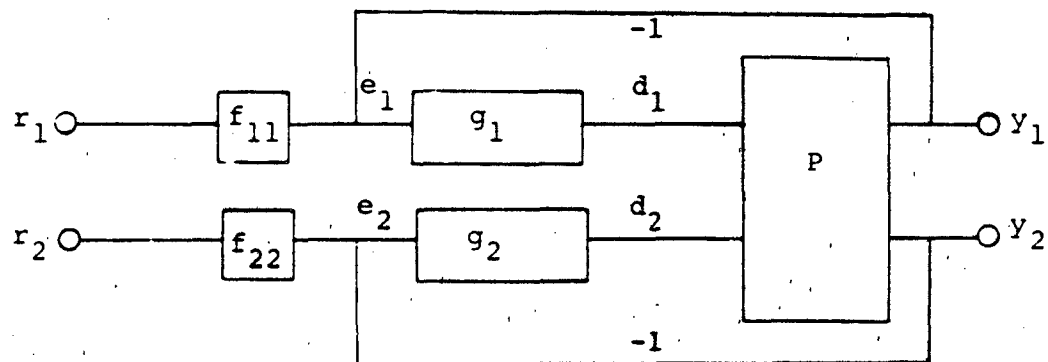


Fig. G-1. Simulation Block Diagram

Where  $P$  is the plant matrix,  $G_1$  and  $G_2$  are the two designed compensators, and  $f_{11}$  and  $f_{22}$  are the two desired pre-filters. The first program is the procedure file used to compile, load and run the desired simulation programs.

```

.PROC, YR1.
* YR1
*
**
** THIS PROGRAM COMPILES, LOADS AND RUNS THE REQUIRED **
** ROUTINES FOR THE 2X2 SIMULATION **
**
CLEAR.
RFL, 130000.
GET, DERV.
FTNS, I=DERV, L=DERLIST, ANSI=0, LO=R/A/S/M.
*LIBGEN(P=SUBY.
GET, YDATA.
FTNS, I=YDATA, L=DATLIST, ANSI=0, LO=R/A/S/M.
*LIBGEN(P=SUBYD.
GET, YSIMU.
FTNS, I=YSIMU, L=SIMLIST, ANSI=0, LO=R/A/S/M.
*SETPLOT(PEN1=BLACK/LIQ3, PEN2=RED/LIQ2).
GET, DEGOL.
FTNS, I=DEGOL, L=DEGLIST, ANSI=0, LO=R/A/S/M.
*GET, PLOT.
*FTNS, I=PLOT, L=PLOLIST, ANSI=0, LO=R/A/S/M.
*ATTACH, HCRSLIB/PLIB, POOL.
GET, SUBLP.
FTNS, I=SUBLP, L=SUBLIST, ANSI=0, LO=R/A/S/M.
LOAD(DERV, YDATA, YSIMU, DEGOL, SUBLP).
*GET, SUBD.
*GET, SUB.
*LOADER, LIB=HCRSLIB/SUB/SUBD/SUBYD/SUBY.
SETTL=7000.
*SETLIM, CP=5500.
LGO.
REPLACE, DATALP.
REPLACE, DATAOUT.
DAYFILE, YLIST.
REPLACE, YLIST.
EXIT.
DAYFILE, YLIST.
REPLACE, YLIST.
REVERT, NQLIST.
END OF FILE

```

This subroutine contains the required data for the input/output equations over the three flight conditions of interest.

SUBROUTINE DATA

```
C
C 2X2 SYSTEM
C
C
C ** THIS SUBROUTINE CONTAINS THE DATA OF THE 2X2 **
C ** INPUT/OUTPUT MATRICIES. THE EQUATIONS ARE IN **
C ** THE FORM: MY = N DELTA WHERE M IS THE OUTPUT **
C ** MATRIX AND N IS THE INPUT MATRIX. Y IS THE **
C ** OUTPUT VECTOR AND DELTA IS THE INPUT VECTOR **
C
C
C----- DIMENSION -----
C
C      DIMENSION VM11A(3),VM11B(3),VM11C(3)
C      DIMENSION VM12A(3),VM12B(3)
C      DIMENSION VM21A(3),VM21B(3),VM21C(3)
C      DIMENSION VM22A(3),VM22B(3),VM22C(3)
C
C      DIMENSION VN11A(3)
C      DIMENSION VN12A(3)
C      DIMENSION VN21A(3),VN21B(3)
C      DIMENSION VN22A(3),VN22B(3)
C
C----- COMMON -----
C
C      COMMON /VM11/ VM11A,VM11B,VM11C
C      COMMON /VM12/ VM12A,VM12B
C      COMMON /VM21/ VM21A,VM21B,VM21C
C      COMMON /VM22/ VM22A,VM22B,VM22C
C
C      COMMON /VN11/ VN11A
C      COMMON /VN12/ VN12A
C      COMMON /VN21/ VN21A,VN21B
C      COMMON /VN22/ VN22A,VN22B
C
```

C----- OUTPUT MATRIX DATA -----

C  
C

DATA VM11A/1.,1.,1./  
DATA VM11B/.74028,.920643,1.09665/  
DATA VM11C/-.010714,-.016597,-.09548/  
DATA VM12A/.24789,.3974,.69382/  
DATA VM12B/4.46897,6.25223,2.4876/  
DATA VM21A/.039665,.0399458,.031645/  
DATA VM21B/.06142,.06167,.22835/  
DATA VM21C/.0065,.00821,.03271/  
DATA VM22A/-1.,-1.,-1./  
DATA VM22B/-.227437,-.272719,-.368629/  
DATA VM22C/-1.43226,-1.88298,-.609055/

C  
C-----

INPUT MATRIX DATA

C

DATA VN11A/.364455,.46223,.37757/  
DATA VN12A/.708183,1.111,.36189/  
DATA VN21A/.00074615,.0007655,.0024207/  
DATA VN21B/.020812,.02546,.01926/  
DATA VN22A/-.026647,-.0273552,-.038190/  
DATA VN22B/-1.01677,-1.3286,-.46618/  
RETURN  
END

END OF FILE

This subroutine contains the state space equations of the plant, compensators and pre-filters. The remainder of the equations in this program are derived from Figure G-1.

```

SUBROUTINE DERV(T,Y,YF)
C
C   UPDATE% 08/21/84
C
C **
C ** THIS SUBROUTINE CONTAINS THE AIRCRAFT EQUATIONS, **
C ** PRE-FILTER EQUATIONS, AND COMPENSATOR EQUATIONS. **
C ** IN STATE SPACE FORM. THE TERM YF IS THE **
C ** DERIVATIVE OF Y WHERE Y IS THE STATE. **
C **
C
C
C   DIMENSION Y(18),YF(18)
C
C***** COMMON *****
C
C   COMMON /C11/ C11A,C11B,C11C
C   COMMON /C12/ C12A,C12B
C   COMMON /C21/ C21A,C21B,C21C
C   COMMON /C22/ C22A,C22B,C22C
C
C   COMMON /D11/ D11A,D12A,D21A,D21B,D22A,D22B
C
C   COMMON /F/ F1K,F1P1,F1P2,F2K,F2P1,F2P2
C
C   COMMON /G1/ G1K,G1Z1,G1Z2,G1Z3,G1Z4
C   COMMON /G1P/ G1P1,G1P2,G1P3,G1P4,G1P5,G1P6
C
C   COMMON /G2/ G2K,G2Z1,G2P1,G2P2,G2P3
C
C   COMMON /R/ R1,R2
C   COMMON /C/ C1,C2
C   COMMON /D/ D1,D2,DD1,DD2
C
C----- P(S) -----
C **
C ** INPUT/OUTPUT MATRICIES IN EQUATION FORM **
C **
C
C   YF(1) = Y(2)
C   YF(2) = -C11B*Y(2) - C11C*Y(1) - C12A*Y(4) - C12B*Y(3)
C   YF(2) = YF(2) + D11A*D1 + D12A*D2
C   YF(2) = YF(2)/C11A

```



```

C1 = Y(1)
C
YP(3) = Y(4)
YP(4) = -C21A*YP(2) - C21B*Y(2) - C21C*Y(1)
YP(4) = YP(4) - C22B*Y(4) - C22C*Y(3)
YP(4) = YP(4) + D21A*DD1 + D21B*DD1
YP(4) = YP(4) + D22A*DD2 + D22B*DD2
YP(4) = YP(4)/C22A
C
C2 = Y(3)
C
C----- F1(S) -----
C
C **
C ** PRE-FILTER/LOOP TWO **
C **
C      YP(18) = R1 - .58*Y(18)
C      F1A = .58*Y(18)
C
C
C      YP(5) = Y(6)
C      YP(6) = F1A - F1P1*Y(6) - F1P2*Y(5)
C
C      F1 = F1K*Y(5)
C
C      YP(5) = R1 - F1P1*Y(5)
C      YP(6) = F1K*Y(5) - F1P2*Y(6)
C
C      F1 = Y(6)
C
C----- F2(S) -----
C
C **
C ** PRE-FILTER/LOOP TWO **
C **
C      YP(7) = Y(8)
C      YP(8) = R2 - F2P1*Y(8) - F2P2*Y(7)
C
C      F2 = F2K*Y(7)
C
C      YP(7) = R2 - F2P1*Y(7)
C      YP(8) = F2K*Y(7) - F2P2*Y(8)
C
C      F2 = Y(8)

```

```

C----- G1(S) -----
C
C **
C ** COMPENSATOR DESIGNED FOR LOOP ONE **
C **
      E1 = F1 - C1
C
      YP(9) = Y(10)
      YP(10) = E1 - G1P1*Y(10) - G1P2*Y(9)
      G1A = G1K*(Y(10) + G1Z1*Y(9))
C
      YP(11) = G1A - G1P3*Y(11)
      G1B = YP(11) + G1Z2*Y(11)
C
      YP(12) = G1B - G1P4*Y(12)
      G1C = YP(12) + G1Z3*Y(12)
C
      YP(13) = G1C - G1P5*Y(13)
      G1D = YP(13) + G1Z4*Y(13)
C
      YP(14) = G1D - G1P6*Y(14)
C
      D1 = Y(14)
      DD1 = YP(14)
C
C----- G2(S) -----
C
C **
C ** COMPENSATOR DESIGNED FOR LOOP TWO **
C **
      E2 = F2 - C2
C
      YP(15) = Y(16)
      YP(16) = E2 - G2P1*Y(16) - G2P2*Y(15)
      G2A = G2K*(Y(16) + G2Z1*Y(15))
C
      YP(17) = G2A - G2P3*Y(17)
C
      D2 = Y(17)
      DD2 = YP(17)
C
C **
C ** CONTROL SURFACE SATURATION.   **
C ** CONTROL WHEEL AND RUDDER.    **
C **
C
      IF (D1 .GT. 90.) D1 = 90.
      IF (D1 .LT. -90.) D1 = -90.
      IF (D2 .GT. 17.) D2 = 17.
      IF (D2 .LT. -17.) D2 = -17.
C
      RETURN
      END
END OF FILE

```

This subroutine contains the required program that calculates the desired time response from the system of equations developed in the other subroutines.

```

SUBROUTINE DEGOL(F,NEQN,Y,T,TOUT,RELERR,
+ ABSERR,IFLAG,ITMAX)
C ** THIS SUBROUTINE IS USED IN DETERMINING **
C ** THE DESIRED RESPONSE FROM A GIVEN **
C ** SYSTEM OF EQUATIONS. **
INTEGER K
REAL HOLD
LOGICAL START,CRASH,STIFF
DIMENSION Y(NEQN),PSI(12)
DIMENSION YY(30),WT(30),PHI(30,16),F(30),YF(30)
DIMENSION YPOUT(30)
EXTERNAL F
DATA FOURU/.44E-15/
MAXNUM=MAX0(500,ITMAX)
IF(NEQN .LT. 1 .OR. NEQN .GT. 30) GO TO 10
IF(T .EQ. TOUT) GO TO 10
IF(RELERR .LT. 0.0 .OR. ABSERR .LT. 0.0) GO TO 10
EPS = AMAX1(RELERR,ABSERR)
IF(EPS .LE. 0.0) GO TO 10
IF(IFLAG .EQ. 0) GO TO 10
ISN = ISIGN(1,IFLAG)
IFLAG = IABS(IFLAG)
IF(IFLAG .EQ. 1) GO TO 20
IF(IFLAG .GE. 2 .AND. IFLAG .LE. 5) GO TO 20
10 IFLAG = 6
RETURN
20 DEL = TOUT - T
ABSDEL = ABS(DEL)
TEND = T + 10.0*DEL
IF(ISN .LT. 0) TEND = TOUT
NOSTEP = 0
KLE4 = 0
STIFF = .FALSE.
RELEPS = RELERR/EPS
ABSEPS = ABSERR/EPS
IF(IFLAG .EQ. 1) GO TO 30
IF(ISNOLD .LT. 0) GO TO 30
IF(DELSGN*DEL .GT. 0.0) GO TO 50
C
C ON START AND RESTART ALSO SET WORK VARIABLES X
C AND YY(*), STORE THE DIRECTION OF INTEGRATION
C AND INITIALIZE THE STEP SIZE
30 START = .TRUE.
X = T
DO 40 L = 1,NEQN
40 YY(L) = Y(L)
DELSGN = SIGN(1.0,DEL)
H = SIGN(AMAX1(ABS(TOUT-X),FOURU*ABS(X)),TOUT-X)

```

```

50 IF(ABS(X-T) .LT. ABSDEL) GO TO 60
   CALL INTRF(X,YY,TOUT,Y,YFOUT,NEQN,KOLD,FHI,PSI)
   IFLAG = 2
   T = TOUT
   TOLD = T
   ISNOLD = ISN
   RETURN

```

```

C
C IF CANNOT GO PAST OUTPUT POINT AND SUFFICIENTLY CLOSE,
C EXTRAPOLATE AND RETURN
C

```

```

60 IF(ISN .GT. 0 .OR. ABS(TOUT-X) .GE. FOURU*ABS(X)) GO TO 80
   H = TOUT - X
   CALL F(X,YY,YF)
   DO 70 L = 1,NEQN
70   Y(L) = YY(L) + H*YF(L)
   IFLAG = 2
   T = TOUT
   TOLD = T
   ISNOLD = ISN
   RETURN

```

```

C
C TEST FOR TOO MUCH WORK
C

```

```

80 IF(NOSTEP .LT. MAXNUM) GO TO 100
   IFLAG = ISN*4
   IF(STIFF) IFLAG = ISN*5
   DO 90 L = 1,NEQN
90   Y(L) = YY(L)
   T = X
   TOLD = T
   ISNOLD = 1
   RETURN

```

```

C
C LIMIT STEP SIZE, SETWEIGHT VECTOR AND A STEP
C

```

```

100 H = SIGN(AMINI(ABS(H),ABS(TEND-X)),H)
   DO 110 L = 1,NEQN
110   WT(L) = RELEPR*ABS(YY(L)) + ABSEPS
   CALL STEP(X,YY,F,NEQN,H,EPS,WT,START,
+   HOLD,N,KOLD,CRASH,FHI,F,YF,PSI)

```

```

C
C TEST FOR TOLERANCE S TOO SMALL

```

```

   IF(.NOT. CRASH) GO TO 130
   IFLAG = ISN*3
   RELEPR = EPS*RELEPR
   ABSERR = EPS*ABSEPS
120 DO 120 L = 1,NEQN
   Y(L) = YY(L)
   T = X
   TOLD = T
   ISNOLD = 1
   RETURN

```

```

C
C AUGMENT COUNTER, ON WORK AND TEST FOR STIFFNESS

```

```

130 NOSTEP = NOSTEP + 1
    KLE4 = KLE4 + 1
    IF(KOLD .GT. 4) KLE4 = 0
    IF(KLE4, GE. 50) STIFF = .TRUE.
    GO TO 50
END
C*****
C SUBROUTINE STEP
C*****
SUBROUTINE STEP(X,Y,F,NEQN,H,EPS,WT,START,
+ HOLD,K,NOLD,CRASH,FHI,F,YF,FSI)
LOGICAL START,CRASH,PHASE1,NORD
DIMENSION Y(NEQN),WT(NEQN),FHI(NEQN,16),F(NEQN)
DIMENSION YF(NEQN),FSI(12)
DIMENSION ALPHA(12),BETA(12),SIG(13),W(12),V(12),G(13),
+ GSTR(13),TWO(13)
EXTERNAL F
DATA TWO/.22E-15/
DATA FOUR/.44E-15/
DATA TWO/2.0,4.0,8.0,16.0,32.0,64.0,128.0,256.0,512.0,
+ 1024.0,2048.0,4096.0,8192.0/
DATA GSTR/0.500,0.0833,0.0417,0.0264,0.0188,0.0143,
+ 0.0114,0.00936,0.00789,0.00679,0.00592,0.00524,0.00468/
DATA G(1),G(2)/1.0,0.5/,SIG(1)/1.0/
CRASH = .TRUE.
IF(ABS(H) .GE. FOUR*ABS(Y)) GO TO 5
H = SIGN(FOUR*ABS(Y),H)
RETURN
5 PSEPS = 0.5*LPS
C
C IF ERROR TOLERANCE IS TOO SMALL, INCREASE IT TO AN
C ACCEPTABLE VALUE
C
ROUND = 0.0
DO 10 L = 1,NEQN
10 ROUND = ROUND + (Y(L)/WT(L))**2
ROUND = TWO*SQR(ROUND)
IF(PSEPS .GE. ROUND) GO TO 15
EPS = 2.0*ROUND*(1.0 + FOUR)
RETURN
15 CRASH = .FALSE.
IF(.NOT.START) GO TO 99
C
C INITIALIZE. COMPUTE APPROPRIATE STEP SIZE FOR FIRST STEP
C
CALL F(X,Y,YF)
SUM = 0.0
DO 20 L = 1,NEQN
PHI(L,1) = YF(L)
PHI(L,2) = 0.0
20 SUM = SUM + (YF(L)/WT(L))**2
SUM = SQR(SUM)
ABSH = ABS(H)
IF(LPS.LT. 16.0*SUM**H) ABSH = 0.25*SQR(EPS/SUM)
H = SIGN(AMAX1(ABSH,FOUR*ABS(Y)),H)
HOLD = 0.0

```

```

      K = 1
      KOLD = 0
      START = .FALSE.
      PHASE1 = .TRUE.
      NORND = .TRUE.
      IF(PSEPS .GT. 100.0*FQUND) GO TO 99
      NORND = .FALSE.
      DO 25 L = 1,NEQN
25      PHI(L,15) = 0.0
99      IFAIL = 0
C      ***      END BLOCK 0      ***
C
C      ***      BEGIN BLOCK 1      ***
C      COMPUTE COEFFICIENTS OF FORMULAS FOR THIS STEP. AVOID
C      COMPUTING THOSE QUANTITIES NOT CHANGED WHEN STEP SIZE IS
C      NOT CHANGED.
C      ***
C
100     KP1 = K+1
        KP2 = K+2
        KM1 = K-1
        KM2 = K-2
C
C      NS IS THE NUMBER OF STEPS TAKEN WITH SIZE H, INCLUDING
C      THE CURRENT ONE. WHEN K.LT.NS, NO COEFFICIENTS CHANGE
C
        IF(H .NE. HOLD) NS = 0
        NS = MINO(NS+1,KOLD+1)
        NSP1 = NS+1
        IF(K .LT. NS) GO TO 199
C
C      COMPUTE THOSE COMPONENTS OF ALPHA(*),BETA(*),PSI(*),SIG(*)
C      WHICH ARE CHANGED
C
        BETA(NS) = 1.0
        REALNS = NS
        ALPHA(NS) = 1.0/REALNS
        TEMP1 = H*REALNS
        SIG(NSP1) = 1.0
        IF(K .LT. NSP1) GO TO 110
        DO 105 I = NSP1,K
            IM1 = I-1
            TEMP2 = PSI(IM1)
            PSI(IM1) = TEMP1
            BETA(I) = BETA(IM1)*PSI(IM1)/TEMP2
            TEMP1 = TEMP2 + H
            ALPHA(I) = H/TEMP1
            REALI = I
105     SIG(I+1) = REALI*ALPHA(I)*SIG(I)
110     PSI(K) = TEMP1
C
C      COMPUTE COEFFICIENTS G(*)
C
C      INITIALIZE V(*) AND W(*), G(2) IS SET DATA STATEMENT
C
        IF(NS .GT. 1) GO TO 120

```

```

DO 115 IQ = 1,K
  TEMP3 = IQ*(IQ+1)
  V(IQ) = 1.0/TEMP3
115  W(IQ) = V(IQ)
  GO TO 140
C
C IF ORDER WAS RAISED, UPDATE DIAGONAL PART OF V(*)
C
120 IF(K .LE. KOLD) GO TO 130
  TEMP4 = K*KF1
  V(K) = 1.0/TEMP4
  NSM2 = NS-2
  IF(NSM2 .LT. 1) GO TO 130
  DO 125 J = 1,NSM2
    I = K-J
125  V(I) = V(I) - ALPHA(J+1)*V(I+1)
C
C UPDATE V(*) AND SET W(*)
C
130 LIMIT1 = KF1 - NS
  TEMP5 = ALPHA(NS)
  DO 135 IQ = 1,LIMIT1
    V(IQ) = V(IQ) - TEMP5*V(IQ+1)
135  W(IQ) = V(IQ)
  G(NSF1) = W(1)
C
C COMPUTE THE G(*) IN THE WORK VECTOR W(*)
C
140 NSF2 = NS + 2
  IF(KF1 .LT. NSF2) GO TO 199
  DO 150 I = NSF2,KF1
    LIMIT2 = KF2 - I
    TEMP6 = ALPHA(I-1)
    DO 145 IQ = 1,LIMIT2
145  W(IQ) = W(IQ) - TEMP6*W(IQ+1)
150  G(I) = W(1)
199 CONTINUE
C
C *** END BLOCK 1 ***
C
C *** BEGIN BLOCK 2 ***
C PREDICT A SOLUTION P(*), EVALUATE DERIVATIVES USING
C PREDICTED SOLUTION, ESTIMATE LOCAL ERROR AT ORDER K AND
C ERRORS AT ORDERS K, K-1, K-I AS IF CONSTANT STEP SIZE WERE USED.
C
C CHANGL PHI TO PHI STAR
C
  IF(K .LT. NSF1) GO TO 215
  DO 210 I = NSF1,K
    TEMP1 = BETA(1)
    DO 205 L = 1,NEQN
205  PHI(L,I) = TEMP1*PHI(L,I)
210 CONTINUE
C
C PREDICT SOLUTION AND DIFFERENCES

```

```

215 DO 220 L = 1,NEQN
      PHI(L,NP2) = PHI(L,NP1)
      PHI(L,NP1) = 0.0
220   P(L) = 0.0
      DO 230 J = 1,K
          I = NP1 - J
          IP1 = I+1
          TEMP2 = G(I)
          DO 225 L = 1,NEQN
              P(L) = P(L) + TEMP2*PHI(L,I)
225     PHI(L,I) = PHI(L,I) + PHI(L,IP1)
230   CONTINUE
      IF(NORND) GO TO 240
      DO 235 L = 1,NEQN
          TAU = H*P(L) - PHI(L,15)
          P(L) = Y(L) + TAU
235     PHI(L,16) = (P(L) - Y(L)) - TAU
          GO TO 250
240   DO 245 L = 1,NEQN
245     P(L) = Y(L) + H*P(L)
250   XOLD = X
      X = X + H
      ABSH = ABS(H)
      CALL F(X,P,YP)

```

```

C
C ESTIMATE ERRORS AT ORDERS K, K-1, K-2
C

```

```

      ERKM2 = 0.0
      ERKM1 = 0.0
      ERK = 0.0
      DO 265 L = 1,NEQN
          TEMP3 = 1.0/WT(L)
          TEMP4 = YP(L) - PHI(L,1)
          IF(KM2)265,260,255
255     ERKM2 = ERKM2 + ((PHI(L,KM1)+TEMP4)*TEMP3)**2
260     ERKM1 = ERKM1 + ((PHI(L,K)+TEMP4)*TEMP3)**2
265     ERK = ERK + (TEMP4*TEMP3)**2
          IF(KM2)280,275,270
270     ERKM2 = ABSH*SIG(KM1)*GSTR(KM2)*SQRT(ERKM2)
275     ERKM1 = ABSH*SIG(K)*GSTR(KM1)*SQRT(ERKM1)
280     TEMPS = ABSH*SQRT(ERK)
          ERR = TEMPS*(G(K) - G(NP1))
          ERK = TEMPS*SIG(NP1)*GSTR(K)
          NNEW = K

```

```

C
C TEST IF ORDER SHOULD BE LOWERED
C

```

```

      IF(KM2)299,290,285
295   IF(AMAX1(ERKM1,ERKM2) .LE. ERK) NNEW = KM1
      GO TO 299
290   IF(ERKM1 .LE. 0.5*ERK) NNEW = NM1

```

```

C
C TEST IF STEP SUCCESSFUL
C

```

```

299   IF(ERR .LE. EPS) GO TO 400

```



```

C      ***      END BLOCK 2      ***
C
C      ***      BEGIN BLOCK 3      ***
C      THE STEP IS UNSUCCESSFUL. RESTORE X, PHI(*,*),
C      PSI(*). IF THIRD CONSECUTIVE FAILURE, SET ORDER TO ONE.
C      IF STEP FAILS MORE THAN THREE TIMES, CONSIDER AN OPTIMAL
C      STEP SIZE. DOUBLE ERROR TOLERANCE AND RETURN IF ESTIMATED
C      STEP SIZE IS TOO SMALL FOR MACHINE PRECISION.
C      ***
C      RESTORE X, PHI(*,*) AND PSI(*)
C
C      PHASE1 = .FALSE.
C      X = XOLD
C      DO 310 I = 1,K
C          TEMP1 = 1.0/BETA(I)
C          IP1 = I+1
C          DO 305 L = 1,NEQN
305             PHI(L,I) = TEMP1*(PHI(L,I) - PHI(L,IP1))
310         CONTINUE
C          IF(K .LT. 2) GO TO 320
C          DO 315 I = 2,K
315             PSI(I-1) = PSI(I) - H
C
C      ON THIRD FAILURE, SET ORDER TO ONE. THEREAFTER, USE
C      OPTIMAL STEP SIZE
C
C      320 IFAIL = IFAIL + 1
C          TEMP2 = 0.5
C          IF(IFAIL - 3) 335,330,325
325         IF(PSEPS .LT. 0.25*ERK) TEMP2 = SQRT(PSEPS/ERK)
330         KNEW = 1
335         H = TEMP2*H
C          K = KNEW
C          IF(ABS(H) .GE. FOURU*ABS(X)) GO TO 340
C          CRASH = .TRUE.
C          H = SIGN(FOURU*ABS(X),H)
C          EPS = EPS + EPS
C          RETURN
340         GO TO 100
C      ***      END BLOCK 3      ***
C
C      ***      BEGIN BLOCK 4      ***
C      THE STEP IS SUCCESSFUL. CORRECT THE PREDICTED SOLUTION,
C      EVALUATE THE DERIVATIVES USING THE CORRECTED SOLUTION
C      AND UPDATE THE DIFFERENCES. DETERMINE BEST AND SIZE
C      FOR NEXT STEP.
C
C      400 KOLD = K
C          HOLD = H
C
C      CORRECT AND EVALUATE
C
C          TEMP1 = H*G(NP1)
C          IF(NOPND) GO TO 410

```

```

DO 405 L = 1,NEQN
  RHO = TEMP1*(YF(L) - PHI(L,1)) - PHI(L,16)
  Y(L) = F(L) + RHO
405 PHI(L,15) = (Y(L) - F(L)) - RHO
  GO TO 420
410 DO 415 L = 1,NEQN
415   Y(L) = F(L) + TEMP1*(YF(L) - PHI(L,1))
420 CALL F(X,Y,YF)

```

```

C
C  UPDATE DIFFERENCES FOR NEXT STEP
C

```

```

DO 425 L = 1,NEQN
  PHI(L,KP1) = YF(L) - PHI(L,1)
425  PHI(L,KP2) = PHI(L,KP1) - PHI(L,KP2)
  DO 435 I = 1,K
  DO 430 L = 1,NEQN
430    PHI(L,I) = PHI(L,I) + PHI(L,KP1)
435 ASE1 = .FALSE.
  IF(PHASE1) GO TO 450
  IF(KNEW .EQ. KM1) GO TO 455
  IF(KP1 .GT. NS) GO

```

```

TO 460
  DO 440 L = 1,NEQN
440    ERKP1 = ERKP1 + (PHI(L,KP2)/WT(L))**2
  ERKP1 = ABSH*GSTK(KP1)*SQRT(ERKP1)

```

```

C
C  USING ESTIMATED ERROR AT ORDER K+1, DETERMINE
C  APPROPRIATE ORDER FOR NEXT STEP
C

```

```

  IF(N .GT. 1) GO TO 445
  IF(ERKP1 .GE. 0.5*ERK) GO TO 460
  GO TO 450
445  IF(ERKM1 .LE. AMIN1(ERK,ERKP1)) GO TO 455
  IF(ERKP1 .GE. ERK .OR. K .EQ. 12) GO TO 460

```

```

C
C  HERE ERKP1 .LT. ERK .LT. AMAX1(ERKM1,ERKM2) ELSE
C  ORDER WOULD HAVE BEEN LOWERED IN BLOCK 2. THUS ORDER
C  IS TO BE RAISED
C

```

```

C  RAISE ORDER
C

```

```

450  K = KP1
  ERK = ERKP1
  GO TO 460

```

```

C
C  LOWER ORDER
C

```

```

455  K = KM1
  ERK = ERKM1

```

```

C
C  WITH NEW ORDER DETERMINE APPROPRIATE STEP SIZE FOR NEXT STEP
C

```

```

460  HNEW = H + H
  IF(PHASE1) GO TO 465
  IF(PSEPS .GE. ERK*TWO(K+1)) GO TO 465
  HNEW = H
  IF(PSEPS .GE. ERK) GO TO 465

```

```

TEMP2 = K+1
R = (F5EPS/ERK)**(1.0/TEMP2)
HNEW = ABSH*AMAX1(0.5,AMAX1(0.9,R))
HNEW = SIGN(AMAX1(HNEW,FOURU*ABS(X)),H)
465 H = HNEW
RETURN
C      ***      END BLOCK 4      ***
      END
C*****
C      SUBROUTINE INTRP
C*****
      SUBROUTINE INTRP(X,Y,XOUT,YOUT,YFOUT,NEQN,KOLD,FHI,PSI)
      DIMENSION Y(NEQN),YOUT(NEQN),YFOUT(NEQN),FHI(NEQN,16)
      DIMENSION PSI(12)
      DIMENSION G(13),W(13),RHO(13)
      DATA G(1)/1.0/,RHO(1)/1.0/
      HI = XOUT - X
      KI = KOLD + 1
      KIP1 = KI + 1
C
C      INITIALIZE W(*) FOR COMPUTING G(*)
C
      DO 5 I = 1,KI
          TEMP1 = I
          W(I) = 1.0/TEMP1
          TERM = 0.0
C
C      COMPUTE G(*)
C
      DO 15 J = 2,KI
          JM1 = J - 1
          PSIJM1 = PSI(JM1)
          GAMMA = (HI + TERM)/PSIJM1
          ETA = HI/PSIJM1
          LIMIT1 = KIP1 - J
          DO 10 I = 1,LIMIT1
              W(I) = GAMMA*W(I) - ETA*W(I+1)
              G(J) = W(1)
              RHO(J) = GAMMA*RHO(JM1)
              TERM = PSIJM1
          10
          15
C
C      INTERPOLATE
C
      DO 20 L = 1,NEQN
          YFOUT(L) = 0.0
          YOUT(L) = 0.0
          20
          DO 30 J = 1,KI
              I = KIP1 - J
              TEMP2 = G(I)
              TEMP3 = RHO(I)
              DO 25 L = 1,NEQN
                  YOUT(L) = YOUT(L) + TEMP2*FHI(L,I)
                  YFOUT(L) = YFOUT(L) + TEMP3*FHI(L,I)
              25
              30
          CONTINUE
          DO 35 L = 1,NEQN

```

35 YOUT(L) = Y(L) + HI\*YOUT(L)  
RETURN  
END  
END OF FILE

This subroutine generates a plot of the desired response which can be printed on a line printer.

```

SUBROUTINE LPLOTS(NXPMAX,NYPMAX,IPLOT)
C *****
C LIBRARY OF PLOT SUBROUTINES
C PRINT OUT ON LINE PRINTER ONLY.
C *****
C *****
C SUB LPLOTS
C *****
C
C DIMENSION IXY(101,71),IBUF(100)
C COMMON /HOPY/ IPO,XOLD,YOLD,ANXD
C COMMON /LIXY/ IXY,NX,NY
C DATA IBLANK/' '/
C NX = NXPMAX
C NY = NYPMAX
C DO 1 I = 1,NX
C   DO 1 J = 1,NY
C     IXY(I,J) = IBLANK
1 CONTINUE
C IPO = IPLOT
C IF(IPO .GE. 1) CALL PLOTS(IBUF,100,8.5,11.,'PRIN300*')
C IF(IPO .GE. 1) CALL PLOTS(0,0,4HPLOT)
C RETURN
C END

C *****
C SUB LTITLE
C *****
C
C SUBROUTINE LTITLE(NITT,ITT)
C DIMENSION IT(4),ITT(4)
C COMMON /LIT/ NIT,IT
C
C NIT = NITT
C DO 1 I = 1,4
C   IT(I) = ITT(I)
1 CONTINUE
C
C RETURN
C END

C *****
C SUB LXAXIS
C *****

```

C JAN. 27, 1984

C  
SUBROUTINE LXAXIS(XXMIN,XXMAX,NXXD,ITX,NITX)  
DIMENSION ITX(4),ITTX(60)  
DIMENSION IXY(101,71),XLABL(11)  
COMMON /LIXY/ IXY,NX,NY  
COMMON /LITX/ NITTX,ITTX  
COMMON /LXX/ XMIN,XMAX,NXD,XD,NXPT  
COMMON /LXL/ NXLABL,XLABL  
COMMON /HOPY/ IPO,XOLD,YOLD,ANXD  
DATA IBLANK/' ',IDASH/'----'/,IFLUS/'++++'/

C  
NXD = NXXD  
ANXD = NXD  
XMIN = XXMIN  
XMAX = XXMAX

C  
C--- X-LINE ---  
NXD1 = NXD + 1  
NXPT = NXD\*10 + 1  
DO 1 I = 1,NXPT  
IXY(I,1) = IDASH  
1 CONTINUE

C  
C--- X-MARK ---  
IX = 1 - 10  
DO 2 I = 1,NXD1  
IX = IX + 10  
IXY(IX,1) = IPLUS  
2 CONTINUE

C  
C--- X-LABEL ---  
XD = (XMAX - XMIN)/NXD  
NXLABL = NXD1  
X = XMIN - XD  
DO 3 I = 1,NXLABL  
X = X + XD  
XLABL(I) = X  
3 CONTINUE

C  
C--- X-TITLE ---  
DO 4 I = 1,60  
ITTX(I) = IBLANK  
4 CONTINUE

C  
NBLANK = (NXD\*10 - NITX)/2  
IF(NBLANK.LT. 1) NBLANK = 1  
NITTX = NBLANK + NITX  
REWIND 9  
WRITE(9,101)(ITX(I),I=1,4)  
REWIND 9  
N1 = NBLANK + 1  
READ(9,102)(ITTX(I),I=N1,NITTX)

C  
101 FORMAT(1X,4A10)  
102 FORMAT(1X,40A1)

```

C
C--- FRAME ---
      IF(IPO .GE. 1) THEN
C          CALL NEWPEN(2)
C          CALL PLOT(1.,1.,-3)
C          CALL SYMBOL(0.,0.,0.28,3,0,-1)
C          CALL SYMBOL(0.,11.,0.28,3,0.,-1)
C          CALL SYMBOL(8.5,0.,0.28,3,0.,-1)
C          CALL SYMBOL(8.5,11.,0.28,3,0.,-1)
C
C          IF(IPO .GE. 3) THEN
C              CALL SYMBOL(0.,12.,0.28,3,0.,-1)
C              CALL SYMBOL(0.,23.,0.28,3,0.,-1)
C              CALL SYMBOL(8.5,12.,0.28,3,0.,-1)
C              CALL SYMBOL(8.5,23.,0.28,3,0.,-1)
C          ENDIF
C          CALL PLOT(1.5,2.5,-3)
C          CALL NEWPEN(1)
C      ENDIF
C
C--- AXIS ---
C
C      IF(IPO .GE. 1) CALL AXIS(0.,0.,ITX,-NITX,ANXD,0.,XXMIN,XD)
C
C      IF(IPO .GE. 3) CALL AXIS(0.,12.,ITX,-NITX,ANXD,0.,XXMIN,XD)
C
C      XOLD = 1.E+9
C      RETURN
C      END
C
C*****
C      SUB LYAXIS
C*****
C      JAN. 27, 1984
C
C      SUBROUTINE LYAXIS(YYMIN,YYMAX,NYYD,ITY,NITY)
C      DIMENSION IT(4)
C      DIMENSION ITY(4),ITTY(71)
C      DIMENSION IXY(101,71),YLABL(8)
C      COMMON /LIXY/ IXY,NX,NY
C      COMMON /LIT/ NIT,IT
C      COMMON /LITY/ NITY,ITTY
C      COMMON /LXX/ XMIN,XMAX,NXD,XD,NXPT
C      COMMON /LYY/ YMIN,YMAX,NYD,YD,NYPT
C      COMMON /LYL/ NYLABL,YLABL
C      COMMON /HOPY/ IPO,XOLD,YOLD,ANXD
C      DATA IBLANK/' ',ISLOT/'.....',IFLUS/'++++'
C
C      NYD = NYYD
C      ANYD = NYD
C      YMIN = YYMIN
C      YMAX = YYMAX
C
C--- Y-LINE ---
C      NYD1 = NYD + 1

```

```

NYPT = NYD*10 + 1
DO 1 I = 1,NYPT
  IXY(1,I) = ISLOT
1 CONTINUE
C
C--- Y-MARK ---
  IY = 1 - 10
  DO 2 I = 1,NYD1
    IY = IY + 10
    IXY(1,IY) = IPLUS
2 CONTINUE
C
C--- Y-LABEL ---
  YD = (YMAX - YMIN)/NYD
  NYLABL = NYD1
  Y = YMIN - YD
  DO 3 I = 1,NYLABL
    Y = Y + YD
    YLABL(I) = Y
3 CONTINUE
C
C--- Y-TITLE ---
  DO 4 I = 1,71
    ITTY(I) = IBLANK
4 CONTINUE
C
  NBLANK = (NYD*10 - NITY)/2
  IF(NBLANK .LT. 1) NBLANK = 1
  NITTY = NBLANK + NITY
  REWIND 9
  WRITE(9,101)(ITTY(I),I=1,4)
  REWIND 9
  N1 = NBLANK + 1
  READ(9,102)(ITTY(I),I=N1,NITTY)
C
101 FORMAT(1X,4A10)
102 FORMAT(1X,40A1)
C
C--- PLOT TITLE ---
C IF(IPO .GE. 1) CALL SYMBOL(1.,ANYD+1.,0.14,IT,0.,NIT)
C IF(IPO .GE. 1) CALL SYMBOC(1.,ANYD+12.+1.,0.14,IT,C.,NIT)
C
C IF(IPO .GE. 1) CALL PLOT(ANXD,0.,3)
C IF(IPO .GE. 1) CALL PLOT(ANXD,ANYD,2)
C IF(IPO .GE. 1) CALL PLOT(0.,ANYD,2)
C IF(IPO .GE. 1) CALL PLOT(0.,0.,3)
C
C IF(IPO .GE. 1) CALL AXIS(0.,0.,ITY,NITY,ANYD,90.,YYMIN,YD)
C IF(IPO .GE. 2) CALL AXIS(0.,ANYD," ",1,ANXD,0.,XMIN,XD)
C IF(IPO .GE. 2) CALL AXIS(ANXD,0.," ",-1,ANYD,90.,YYMIN,-D)
C
C IF(IPO .GE. 3) CALL AXIS(0.,12.,ITY,NITY,ANYD,90.,YYMIN,YD)
C IF(IPO .GE. 3) CALL AXIS(0.,ANYD+12.," ",1,ANXD,0.,XMIN,XD)
C IF(IPO .GE. 3) CALL AXIS(ANXD,12.," ",-1,ANYD,90.,YYMIN,YD)
YOLD = 1.E+9
RETURN

```



```

      END
C
C*****
C   SUB LGRID
C*****
C
C   JAN. 27, 1984
C
      SUBROUTINE LGRID(XGRID,YGRID)
      DIMENSION IXY(101,71)
      COMMON /LIXY/ IXY,NX,NY
      COMMON /LXX/ XMIN,XMAX,NXD,XD,NXPT
      COMMON /LYY/ YMIN,YMAX,NYD,YD,NYPT
      DATA IDOT/'.....'/
C
C--- X-GRID ---
      GD = XGRID/XD*10.
      GX = 0
      DO 1 I = 1,101
          GX = GX + GD
          IX = GX + 1.5
          IF(IX .GT. NXPT) GO TO 2
          DO 3 J = 2,NYPT
              IXY(IX,J) = IDOT
          3      CONTINUE
      1      CONTINUE
      2      CONTINUE
C
C--- Y-GRID ---
      GD = YGRID/YD*10.
      GY = 0
      DO 4 I = 1,71
          GY = GY + GD
          IY = GY + 1.5
          IF(IY .GT. NYPT) GO TO 5
          DO 6 J = 2,NXPT
              IXY(J,IY) = IDOT
          6      CONTINUE
      4      CONTINUE
      5      CONTINUE
C
      RETURN
      END
C
C*****
C   SUB LPLOT
C*****
C
C   UPDATE%  MAY. 31, 1984
C   ORIGINAL% JAN. 27, 1984
C
      SUBROUTINE LPLOT(X,Y,IMARK,HMARK,ILINE)
      DIMENSION IXY(101,71),ICH(40)
      COMMON /LIXY/ IXY,NX,NY
      COMMON /LXX/ XMIN,XMAX,NXD,XD,NXPT
      COMMON /LYY/ YMIN,YMAX,NYD,YD,NYPT

```

```

COMMON /HCOFY/ IFO,XOLD,YOLD,ANXD
DATA ICH/1H1,1H2,1H3,1H4,1H5,1H6,1H7,1H8,1H9,1H0,
+      1HA,1HE,1HC,1HD,1HE,1HF,1HG,1HH,1HI,1HJ,
+      1HK,1HL,1HM,1HN,1HO,1HP,1HQ,1HR,1HS,1HT,
+      1HU,1HV,1HW,1HX,1HY,1HZ,1H?,1H*,1H-,1H+/
C
IX = (X - XMIN)/XD*10. + 1.5
IY = (Y - YMIN)/YD*10. + 1.5
IF(IX .LT. 1) IX = 1
IF(IX .GT. NXPT) IX = NXPT
IF(IY .LT. 1) IY = 1
IF(IY .GT. NYPT) IY = NYPT
IXY(IX,IY) = ICH(IMARK)
C
IF(IFO .LT. 1) GO TO 21
IF(X .GT. XMAX .OR. X .LT. XMIN) GO TO 21
IF(Y .GT. YMAX .OR. Y .LT. YMIN) GO TO 21
X = (X - XMIN)/XD
Y = (Y - YMIN)/YD
DIST = SQRT((XOLD - X)*(XOLD - X) + (YOLD - Y)*(YOLD - Y))
IF(DIST .LT. 0.1 .AND. DIST .LT. 0.1) GO TO 11
HIGH = 0.07*HMARK
IF(HIGH .LT. 0.07) HIGH = 0.07
IF(HIGH .GT. 1.) HIGH = 0.07
C IF(ILINE .LT. 1) CALL SYMBOL(X,Y,HIGH,ICH(IMARK),0.,1)
C IF(IFO .GE. 3) CALL SYMBOL(X,Y+12.,HIGH,ICH(IMARK),0.,1)
XOLD = X
YOLD = Y
11 X = XMIN + X*XD
Y = YMIN + Y*YD
21 CONTINUE
RETURN
END
C
C*****
C SUB LLINE
C*****
C
C MAY. 30, 1984
C
SUBROUTINE LLINE(X,Y,N)
DIMENSION X(N),Y(N),X1(1000),Y1(1000)
COMMON /LXX/ XMIN,XMAX,NXD,YD,NYPT
COMMON /LYY/ YMIN,YMAX,NYD,YD,NYPT
COMMON /HCOFY/ IFO,XOLD,YOLD,ANXD
C
IF(IFO .LT. 1) GO TO 3
C
C--- LINE ---
DO 1 I = 1,N
XX = X(I)
YY = Y(I)
IF(XX .LT. XMIN) XX = XMIN
IF(YY .LT. YMIN) YY = YMIN
IF(XX .GT. XMAX) XX = XMAX
IF(YY .GT. YMAX) YY = YMAX

```

```

          X1(I) = XX
          Y1(I) = YY
1      CONTINUE
      NF = N + 2
      X1(NF-1) = XMIN
      X1(NF) = XD
      Y1(NF-1) = YMIN
      Y1(NF) = YD
C      CALL LINE(X1,Y1,N,1,0,0)
3      CONTINUE
      RETURN
      END

C
C*****
C      SUB LSYMB0
C*****

C      UPDATE% MAY. 31, 1984
C      ORIGINAL% MAY. 31, 1984
C
      SUBROUTINE LSYMB0(XS,YS,ITTS,NITTS)
      DIMENSION ITTS(4)
C      COMMON /LXX/ XMIN,XMAX,NXD,XD,NXPT
C      COMMON /LYY/ YMIN,YMAX,NYD,YD,NYPT
C      COMMON /HCOFY/ IFO,XOLD,YOLD,ANXD
C
C---  SYMBOL ---
      X = (XS - XMIN)/XD
      Y = (YS - YMIN)/YD
C      IF(IFO .GE. 1) CALL SYM1QL(X,Y,0.14,ITTS,0.,NITTS)
C      IF(IFO .GE. 3) CALL SYM1QL(X,Y+12.,0.14,ITTS,0.,NITTS)
C
      RETURN
      END

C
C*****
C      SUB LPRINT
C*****

C      UPDATE% APR. 13, 1984
C      ORIGINAL% JAN. 27, 1984
C
      SUBROUTINE LPRINT(IPAGE)
      DIMENSION IXY(101,71)
      DIMENSION IT(4)
      DIMENSION ITTX(60),XLABL(11)
      DIMENSION ITTY(71),YLABL(8)
      COMMON /LIXY/ IXY,NX,NY
      COMMON /LIT/ NIT,IT
      COMMON /LITX/ NITTX,ITTX
      COMMON /LXX/ XMIN,XMAX,NXD,XD,NXPT
      COMMON /LXL/ NXLABL,YLABL
      COMMON /LITY/ NITTY,ITTY
      COMMON /LYY/ YMIN,YMAX,NYD,YD,NYPT
      COMMON /LYL/ NYLABL,YLABL
      COMMON /HOPY/ IFO,XOLD,YOLD,ANXD

```

```

DATA IBLANK/' */
C
C--- PRINT PAGE ---
-IF(IPAGE .GE. 1) WRITE(7,100)
C IF(IPAGE .GE. 1 .AND. IFO .GE. 1) CALL FLOT(8.,-3.5,-3)
C IF(IPAGE .LT. 1 .AND. IFO .GE. 1) CALL FLOT(8.,-3.5,-3)
C IF(IPAGE .GE. 2 .AND. IFO .GE. 1) CALL FLOT(0.,0.,999)
C
C--- PRINT TITLE ---
WRITE(7,106)IT
WRITE(7,105)
C
C--- PRINT IXY ---
ICOUNT = 0.
ILABL = 0
DO 1 I = 1,NYPT
  K = NYPT - I + 1
  ICOUNT = ICOUNT + 1
  IF(ICOUNT .EQ. 10) ICOUNT = 0
  IF(ICOUNT .EQ. 1) ILABL = ILABL + 1
  IF(ICOUNT .NE. 1) GO TO 2
  IL = NYLABL - ILABL + 1
  WRITE(7,101)ITTY(I),YLABL(IL),(IXY(J,K),J=1,NXPT)
2
  CONTINUE
C
C--- CLEAN IXY ---
C
DO 4 I = 1,NX
  DO 4 J = 1,NY
    IXY(I,J) = IBLANK
4
CONTINUE
C
C--- FORMAT ---
100 FORMAT(1H1)
101 FORMAT(1X,A1,1X,F7.2,1X,101A1)
102 FORMAT(1X,A1,1X,7X,1X,101A1)
103 FORMAT(1X,4X,11(F9.2,1X))
104 FORMAT(/,1X,11X,101A1)
105 FORMAT(//)
106 FORMAT(12X,10X,4A10)
C
RETURN
END
END OF FILE

```

This routine is the main program for the simulation. It calls all subroutines listed above and the final output is the tabulated data of the desired time response for a given input and desired output(s). This data is used in the generation of the CALCOMP plots of each response and control surface deflection.

```

PROGRAM YSIMU(INPUT,OUTPUT,DATAP,DATAOUT,PLOT,TAPE9,
+           TAPE6=OUTPUT,TAPE7=DATAP,TAPE8=DATAOUT)
C
C 2X2 SYSTEM
C
C ** THIS IS THE MAIN SIMULATION PROGRAM. THIS **
C ** PROGRAM CALLS ALL SUBROUTINES REQUIRED IN **
C ** THE SIMULATION PROCESS. **
C **
C***** DIMENSION *****
C
C----- CASE -----
      DIMENSION IRV(10),ICV(10)
C----- DEGOL -----
      REAL Y(30)
      EXTERNAL DERV
      DIMENSION XX(500),YY(500),YY1(500),YY2(500),YY3(500),YY4(500)
      DIMENSION YY5(500),YY6(500)
C
C----- PLANT -----
C
      DIMENSION UM1A(3),UM1B(3),UM1C(3)
      DIMENSION UM12A(3),UM12B(3)
      DIMENSION UM2A(3),UM2B(3),UM2C(3)
      DIMENSION UM22A(3),UM22B(3),UM22C(3)
      DIMENSION UN1A(3)
      DIMENSION UN12A(3)
      DIMENSION UN2A(3),UN2B(3)
      DIMENSION UN22A(3),UN22B(3)
C
C***** COMMON *****
C
      COMMON /C11/ C11A,C11B,C11C
      COMMON /C12/ C12A,C12B
      COMMON /C13/ C13A,C13B,C13C
      COMMON /C22/ C22A,C22B,C22C
      COMMON /D11/ D11A,D11B,D11C,D21B,D22A,D22B
      COMMON /F/ F1A,F1B,F1C,F2A,F2B,F2C
      COMMON /G1/ G1A,G1B,G1C,G1D,G1E,G1F
      COMMON /G1F/ G1F1,G1F2,G1F3,G1F4,G1F5,G1F6

```

```

C
C      COMMON /G2/ G2K,G2Z1,G2F1,G2F2,G2F3
C
C      COMMON /R/ R1,R2
C      COMMON /C/ C1,C2
C      COMMON /D/ D1,D2,DD1,DD2
C
C----- DATA -----
C
C      COMMON /VM11/ VM11A,VM11B,VM11C
C      COMMON /VM12/ VM12A,VM12B
C      COMMON /VM21/ VM21A,VM21B,VM21C
C      COMMON /VM22/ VM22A,VM22B,VM22C
C
C      COMMON /VN11/ VN11A
C      COMMON /VN12/ VN12A
C      COMMON /VN21/ VN21A,VN21B
C      COMMON /VN22/ VN22A,VN22B
C
C----- CASE -----
C
C      DATA NC/1/
C      DATA IRV/2,1,1,1,1,1,4*0/
C      DATA ICV/3,1,1,1,1,1,4*0/
C
C***** MAIN PROGRAM *****
C
C----- F(S) -----
C
C      CALL DATA
C
C----- F1(S) -----
C
C      **
C      ** PRE-FILTER VALUES FOR LOOP ONE **
C      **
C
C      F1K = .63*.63
C      F1K = .9
C
C      F1P1 = 2.*.7*.63
C      F1P1 = .9
C      F1P2 = .63*.63
C      F1P2 = 1.
C
C----- F2(S) -----
C
C      **
C      ** PRE-FILTER VALUES FOR LOOP TWO **
C      **
C
C      F2K = 1.2*1.2
C      F2K = .512
C
C      F2P1 = 2.*.7*1.2
C      F2P1 = .5

```

```

C      F2F2 = 1.2*1.2
      F2F2 = 1.
C
C----- G1(S) -----
C
C **
C **- COMPENSATOR VALUES FOR LOOP ONE **
C **
C
      G1K = 1.946E+10
C
      G1Z1 = 4.
      G1Z2 = 4.
      G1Z3 = 17.
      G1Z4 = 50.
C
      G1P1 = 1800.
      G1P2 = 2.25E06
      G1P3 = 10.
      G1P4 = 10.
      G1P5 = 83.
      G1P6 = 100.
C
C----- G2(S) -----
C
C **
C **- COMPENSATOR VALUES FOR LOOP TWO **
C **
C
      G2K = 2.36E07
C
      G2Z1 = 7.
C
      G2P1 = 192.
      G2P2 = 25600.
      G2P3 = 50.
C
C----- INPUT R(I) -----
      R1 = 30.
      R2 = 5.
C
C***** DATA CHECK *****
C      IF(NC .NE. NC) THEN
C          DO 9 I = 1,3
C              WRITE(7,*)//,/,,'CASE = ',I
C
C              WRITE(7,*)//,/,,'M11',UM11A(I),UM11B(I),UM11C(I)
C              WRITE(7,*)//,/,,'M12',UM12A(I),UM12B(I)
C              WRITE(7,*)//,/,,'M21',UM21A(I),UM21B(I),UM21C(I)
C              WRITE(7,*)//,/,,'M22',UM22A(I),UM22B(I),UM22C(I)
C
C              WRITE(7,*)//,/,,'N11',UN11A(I)
C              WRITE(7,*)//,/,,'N12',UN12A(I)
C              WRITE(7,*)//,/,,'N21',UN21A(I),UN21B(I)
C              WRITE(7,*)//,/,,'N22',UN22A(I),UN22B(I)

```

```

C
C 9 CONTINUE
C
C WRITE(7,*)//,/'F1(S)',/, 'GAIN = ',F1K
C WRITE(7,*)//,/'POLE %',/,F1P1,/,F1P2
C
C WRITE(7,*)//,/'F2(S)',/, 'GAIN = ',F2K
C WRITE(7,*)//,/'POLE %',/,F2P1,/,F2P2
C
C WRITE(7,*)//,/'G1(S)',/, 'GAIN = ',G1K
C WRITE(7,*)//,/'ZERO %',/,G1Z1,/,G1Z2,/,G1Z3,/,G1Z4
C WRITE(7,*)//,/'POLE %',/,G1P1,/,G1P2,/,G1P3,/,G1P4,
C + /,G1P5,/,G1P6
C WRITE(7,*)//,/'G2(S)',/, 'GAIN = ',/,G2K
C WRITE(7,*)//,/'ZERO %',/,G2Z1
C WRITE(7,*)//,/'POLE %',/,G2P1,/,G2P2,/,G2P3
C
C STOP
C ENDIF
C
C ***** DO CASES *****
C
C DO 10 III = 1,NC
C
C IR = IRV(III)
C IC = ICV(III)
C
C R1 = 0.
C R2 = 0.
C IF(IR .EQ. 1) R1 = 0.
C IF(IR .EQ. 2) R2 = 0.
C
C
C----- M11 -----
C
C C11A = VM11A(IC)
C C11B = VM11B(IC)
C C11C = VM11C(IC)
C
C----- M12 -----
C
C C12A = VM12A(IC)
C C12B = VM12B(IC)
C
C----- M21 -----
C
C C21A = VM21A(IC)
C C21B = VM21B(IC)
C C21C = VM21C(IC)
C
C----- M22 -----
C
C C22A = VM22A(IC)
C C22B = VM22B(IC)
C C22C = VM22C(IC)

```



```

C
C----- N11 -----
C
          D11A = VN11A(IC)
C
C----- N12 -----
C
          D12A = VN12A(IC)
C
C----- N21 -----
C
          D21A = VN21A(IC)
          D21B = VN21B(IC)
C
C----- N22 -----
C
          D22A = VN22A(IC)
          D22B = VN22B(IC)
C
C***** INTEGRATION *****
C
C **
C ** SET-UP REQUIRED VALUES FOR SUBROUTINE DEGOL **
C **
C
          NE = 17
          AE = 1.E-5
          RE = 1.E-6
          MAX = 1000
          H = 2.E-4
          N = 100000
          NP = 100
          TO = 0.
          T1 = H
C
C----- INITIAL CONDITION -----
          C1 = 0.
          C2 = 0.
          D1 = 0.
          D2 = 0.
          DD1 = 0.
          DD2 = 0.
C
          DO 30 I = 1,NE
30          Y(I) = 0.
C
C----- ITERATION -----
          II = 0
          IIXY = 1
          KKXY = N/NP
          IF(KKXY .LT. 1) KKXY = 1
C
          DO 40 I = 1,N
C
C----- YY(II) -----
          IF(I .EQ. IIXY) THEN

```

```

        II = II + 1
        PRINT 122,II,T0,C1,C2,D1,DD1,D2,DD2
        XX(II) = T0
        YY1(II) = C1
        YY2(II) = C2
        YY3(II) = D1
        YY4(II) = DD1
        YY5(II) = D2
        YY6(II) = D2
        IIXY = IIXY + KKXY
    ENDIF
C
C----- CALL DEGOL -----
C        PRINT 122,I,T0,C1,C2,D1,DD1,D2,DD2
        IK = 1
        CALL DEGOL(DERV,NE,Y,T0,T1,RE,AE,IK,MAX)
        IF( IK .NE. 2 ) THEN
            PRINT *,IK,T0,T1
            STOP
        ENDIF
        T1 = T1 + H
C
C **
C ** RAMP INPUT **
C **
C
        IF( IR .EQ. 1 .AND. T1 .LE. 1 ) R1 = 30.*T1
        IF( IR .EQ. 1 .AND. T1 .GT. 1 ) R1 = 30.
        IF( IR .EQ. 2 .AND. T1 .LE. 1 ) R2 = 5.*T1
        IF( IR .EQ. 2 .AND. T1 .GT. 1 ) R2 = 5.
40    CONTINUE
C
C***** PLOT *****
        NXY = II
        PRINT *,NXY
C
        WRITE(8,121)NXY
C        WRITE(7,121)NXY
        DO 50 I = 1,NXY
            WRITE(8,122)I,XX(I),YY1(I),YY2(I),YY3(I),YY4(I),
            CALL LPL(NXY,XX,YY1,1)
            CALL LPRINT(2
        )
C
C
C***** FORMAT *****
121  FORMAT(1X,I5)
122  FORMAT(1X,I5,7(1X,E9.3))
C
        STOP
        END
C
C*****
C        SUB LPL
C*****
C

```

```

C UPDATE% AUG. 12, 1984
C ORIGINAL% AUG. 12, 1984
C
SUBROUTINE LPL(N,X,Y,IC)
DIMENSION X(N),Y(N)
DIMENSION IIM(10),ITT(4),ITY(4),ITX(4)
C
DATA NITT/ 23/,ITT(4)/"FLT COND" /
DATA NITX/10/,ITX(4)/"TIME (SEC)" /
DATA NITY/5/,ITY(4)/"Y1" /
DATA IPLOT/0/,ILINE/1/,HMARK/1./
DATA IIM/11,12,13,14,15,16,17,18,19,20/
DATA NX/5/,XMIN/0./,XMAX/10./,XG/2./
DATA NY/4/,YMIN/0./,YMAX/40./,YG/10./
C
IF(IC .EQ. 1) THEN
C CALL LPLOTS(101,71,IPLOT)
IF(IPLOT .GE. 1) CALL FACTOR(.5)
CALL LTITLE(NITT,ITT)
CALL LXAXIS(XMIN,XMAX,NX,ITX,NITX)
CALL LYAXIS(YMIN,YMAX,NY,ITY,NITY)
CALL LGRID(XG,YG)
ENDIF
C
C----- LPLOT -----
IMARK = IIM(IC)
DO 2 I = 1,N
CALL LPLOT(X(I),Y(I),IMARK,HMARK,ILINE)
2 CONTINUE
C
C----- LINE -----
IF(IILINE .GE. 1 .AND. IPLOT .GE. 1) THEN
CALL LLINE(X,Y,N)
ENDIF
C
C
RETURN
END
C
C*****
C SUB LPL1
C*****
C
C UPDATE% AUG. 12, 1984
C ORIGINAL% AUG. 12, 1984
C
SUBROUTINE LPL1(N,X,Y,IC)
DIMENSION X(N),Y(N)
DIMENSION IIM(10),ITT(4),ITY(4),ITX(4)
C
DATA NITT/23/,ITT(4)/"FLT COND" /
DATA NITX/10/,ITX(4)/"TIME (SEC)" /
DATA NITY/5/,ITY(4)/"Y2" /
DATA IPLOT/0/,ILINE/1/,HMARK/1./
DATA IIM/1,2,3,4,5,6,7,8,9,10/
DATA NX/5/,XMIN/0./,XMAX/10./,XG/2./

```

```

DATA NY/5/,YMIN/0./,YMAX/6.25/,YG/1.25/
C
IF(IC .EQ. 1) THEN
  CALL LPLOTS(101,71,IPLOT)
  CALL LTITLE(NITT,ITT)
  CALL LXAXIS(XMIN,XMAX,NX,ITX,NITX)
  CALL LYAXIS(YMIN,YMAX,NY,ITY,NITY)
  CALL LGRID(XG,YG)
ENDIF
C
C----- LPLOT -----
IMARK = IIM(IC)
DO 2 I = 1,N
  CALL LPLOT(X(I),Y(I),IMARK,HMARK,ILINE)
2 CONTINUE
C
C----- LINE -----
IF(ILINE .GE. 1 .AND. IPLOT .GE. 1) THEN
  CALL LLINE(X,Y,N)
ENDIF
C
C
RETURN
END
END OF FILE

```

### Conclusion

- This appendix gives a brief overview of the program and subroutine used in the simulations of the 2x2 lateral design. A more detailed explanation of programs and subroutines is contained in Reference 19.

Appendix H: Simulation Responses for  
F.C.'s #1 and #2

Introduction

This appendix contains the simulation responses for F.C.'s #1 and #2. The characteristics for each response are shown in the accompanying tables.

Simulation Responses for F.C. #1--  
Bank Angle Command

The responses for a 30 degree step input bank angle command are shown in Figures H-1 and H-2 (complex pre-filter roots). The control surface deflections are shown in Figures H-3 and H-4. The characteristics for this F.C. are outlined in Table H-1.

TABLE H-1  
BANK ANGLE COMMAND--F.C. #1

	Peak Value	Final Value	Rise Time	Settling Time
$\phi$ (deg)	30.6	30.6	5.45	7.35
$\beta$ (deg)	0.002	0.0016	--	--
$\delta_r$ (deg)	-0.264	--	--	--
$\delta_w$ (deg)	16.6	--	--	--

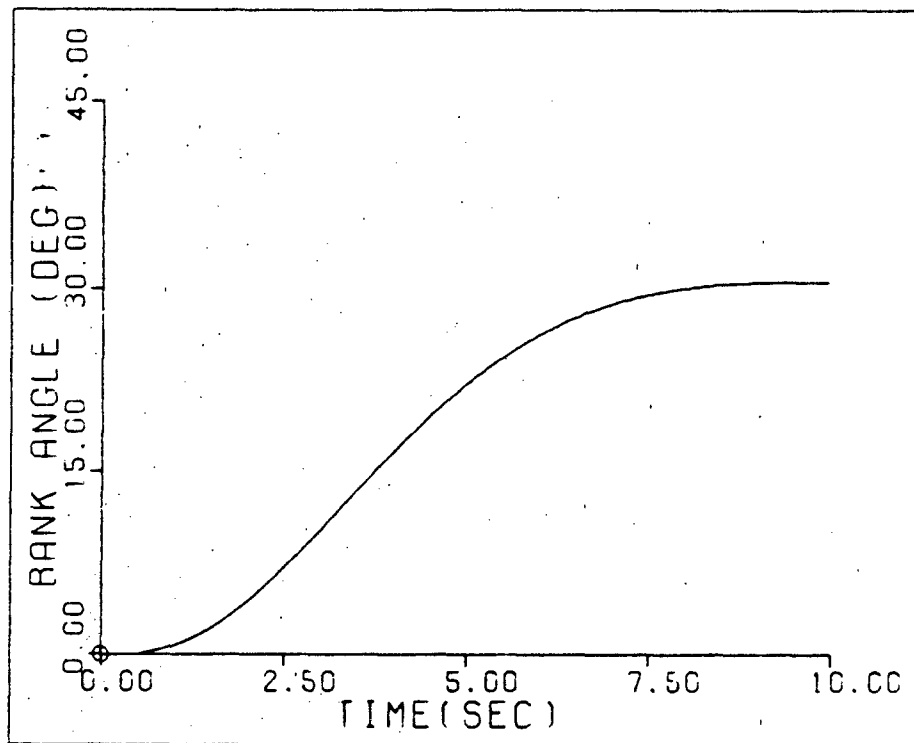


Fig. H-1. Bank Angle Response--F.C. #1

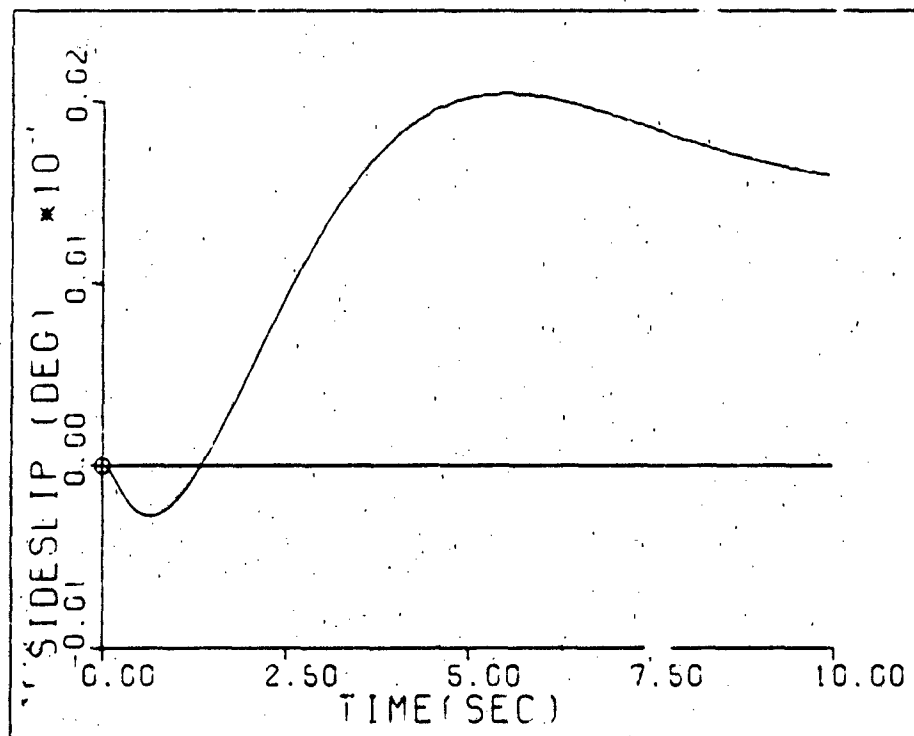


Fig. H-2. Sideslip Response--F.C. #1

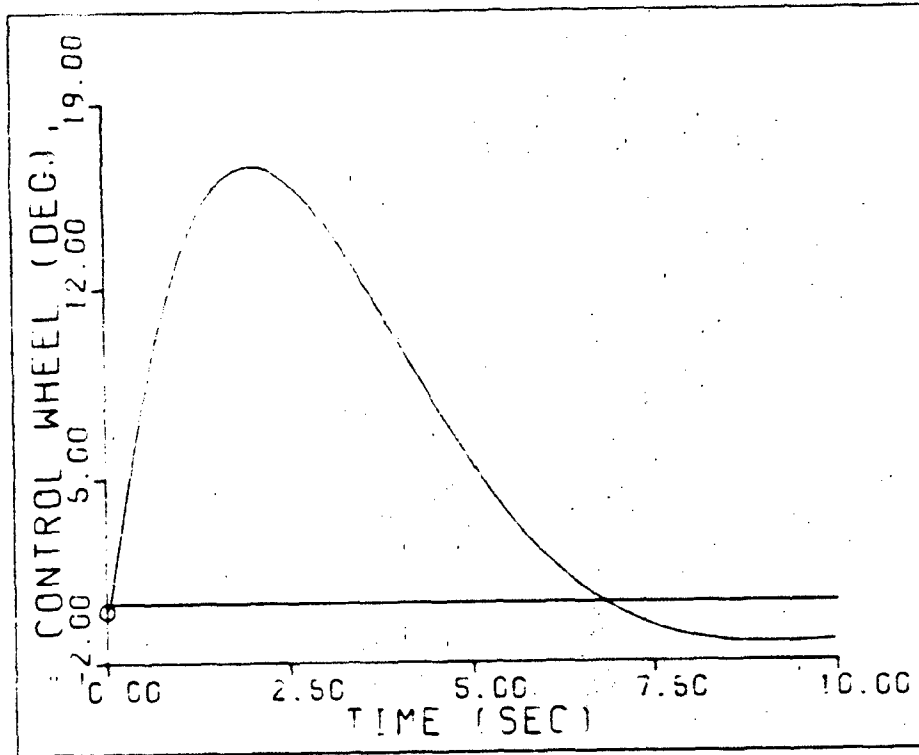


Fig. H-3. Control Wheel Deflection--F.C. #1

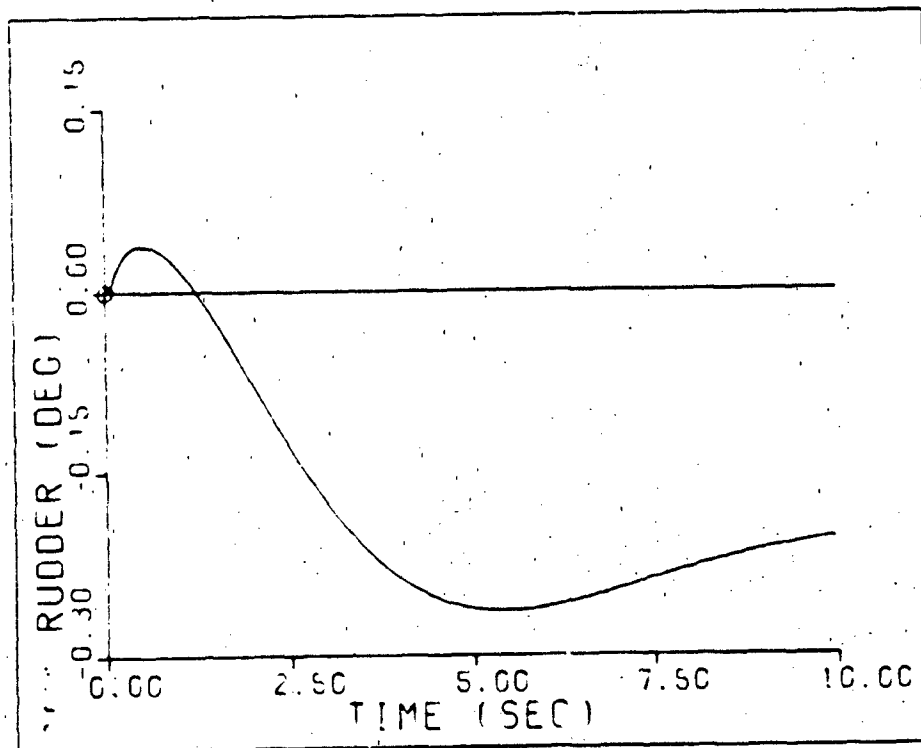


Fig. H-4. Rudder Deflection--F.C. #2



The responses for a 30 degree step input bank angle command are shown in Figures H-5 and H-6 (real pre-filter poles). The control surface deflections are shown in Figures H-7 and H-8 while the response characteristics are outlined in Table H-2.

TABLE H-2

BANK ANGLE COMMAND--F.C. #1

	Peak Value	Final Value	Rise Time	Settling Time
$\delta$ (deg)	30.0	30.0	3.60	6.10
$\delta$ (deg)	0.003	0.0016	--	--
$\delta_r$ (deg)	0.328	--	--	--
$\delta_w$ (deg)	66.0	--	--	--

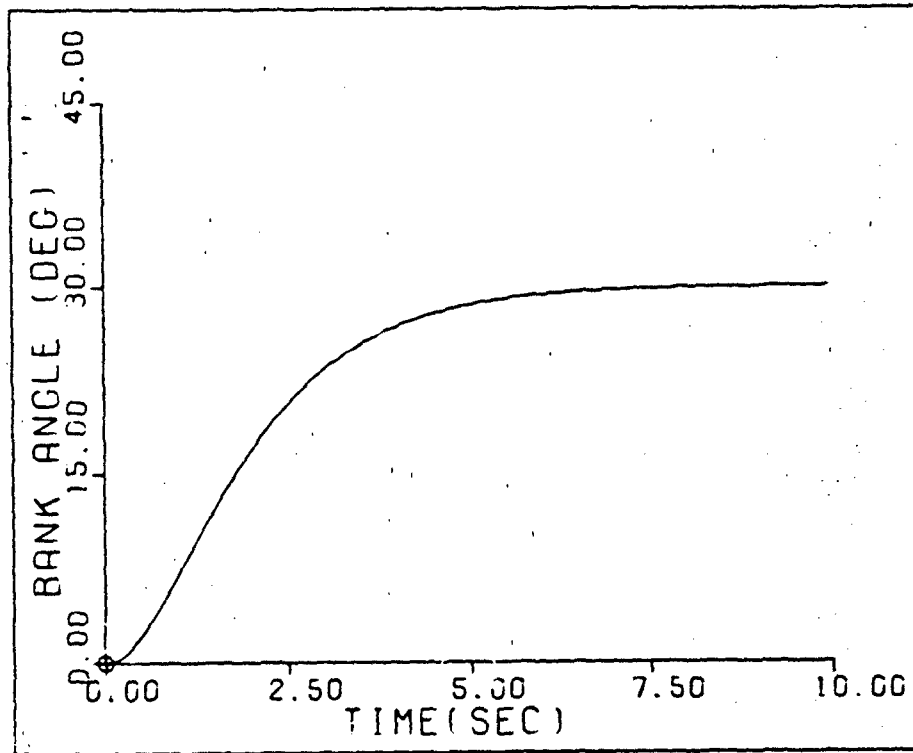


Fig. H-5. Bank Angle Response--F.C. #1

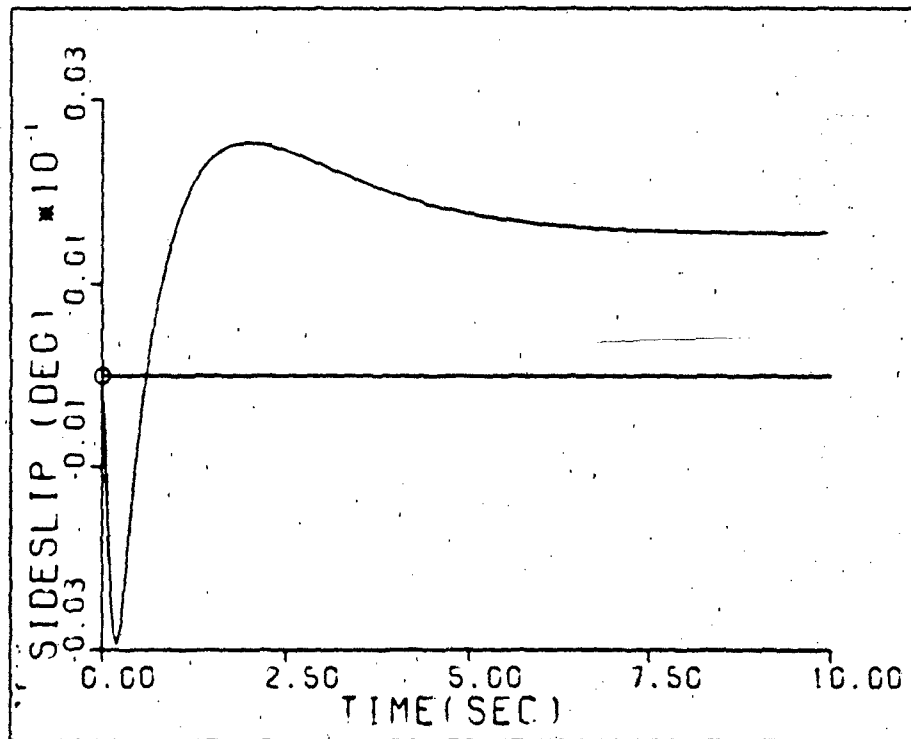


Fig. H-6. Sideslip Response--F.C. #1

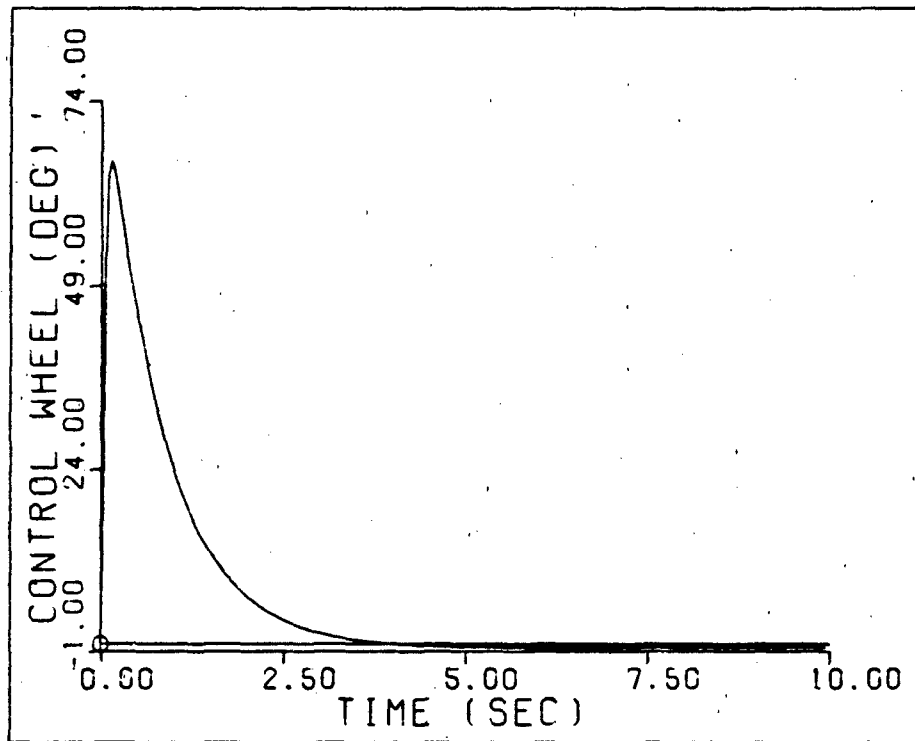


Fig. H-7. Control Wheel Deflection--F.C. #1

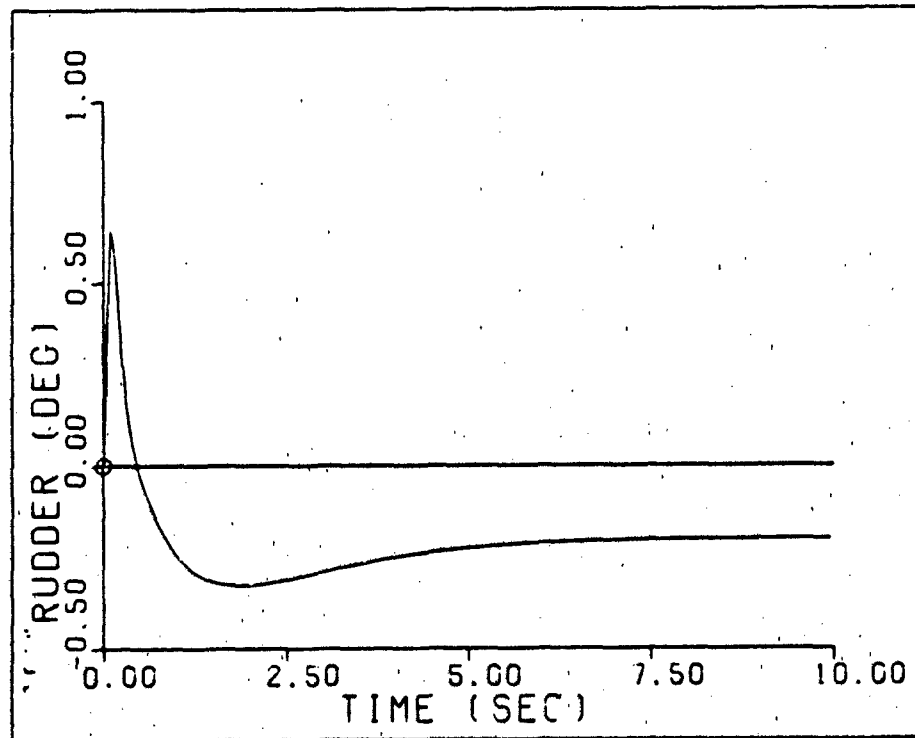


Fig. H-8. Rudder Deflection--F.C. #1

The responses shown in Figures H-9 through H-12 are for a 30 degree bank angle command with real pre-filter zeros. The command input is a ramp with a rise time of 1 second. Table H-3 outlines the characteristics of the responses.

TABLE H-3  
BANK ANGLE COMMAND--F.C. #1

	Peak Value	Final Value	Rise Time	Settling Time
$\phi$ (deg)	30.0	30.0	3.48	6.60
$\beta$ (deg)	0.0025	0.0016	--	--
$\delta_r$ (deg)	0.323	--	--	--
$\delta_w$ (deg)	43.5	--	--	--

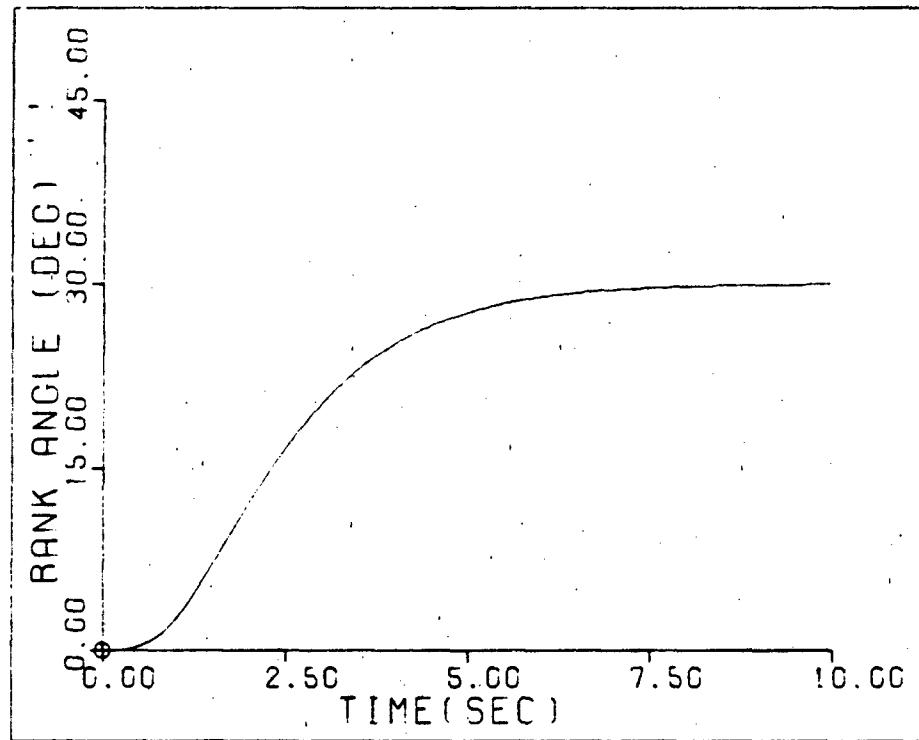


Fig. H-9. Bank Angle Response--F.C. #1

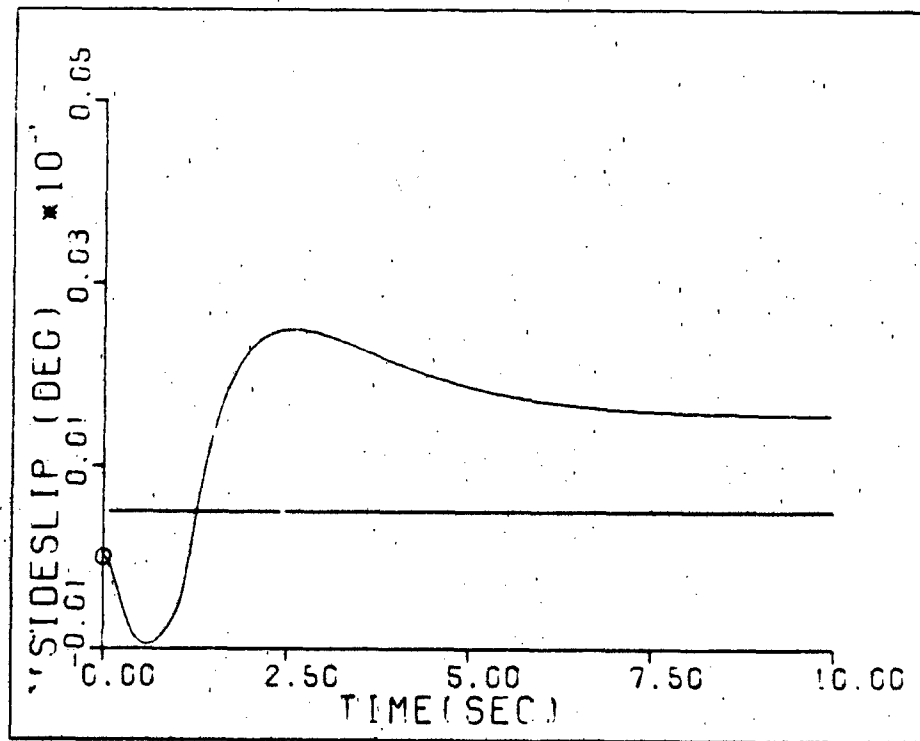


Fig. H-10. Sideslip Response--F.C. #1

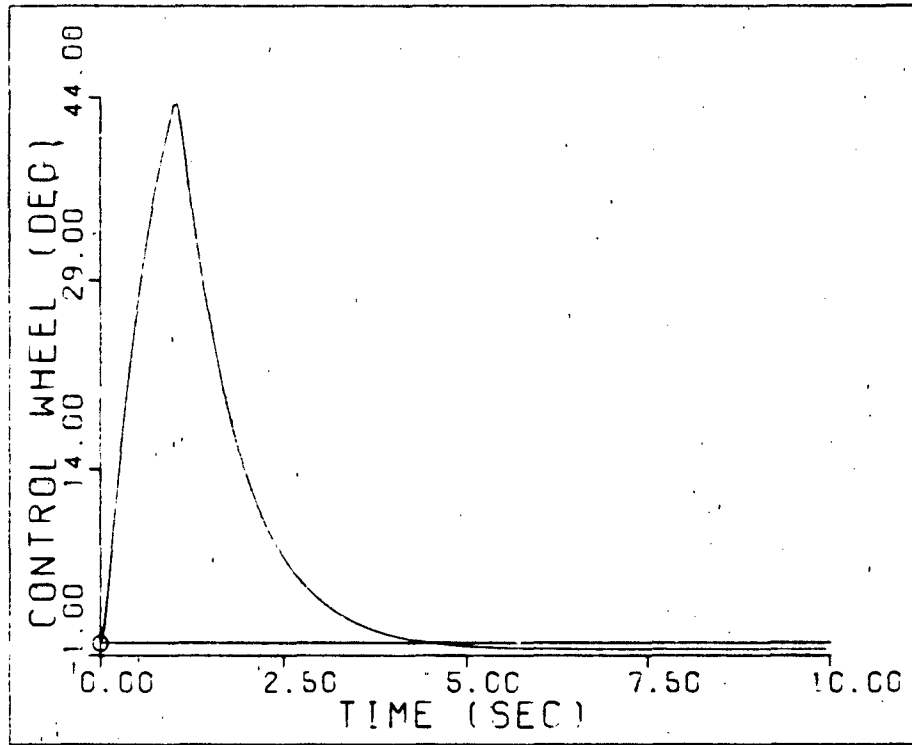


Fig. H-11. Control Wheel Deflection--F.C. #1

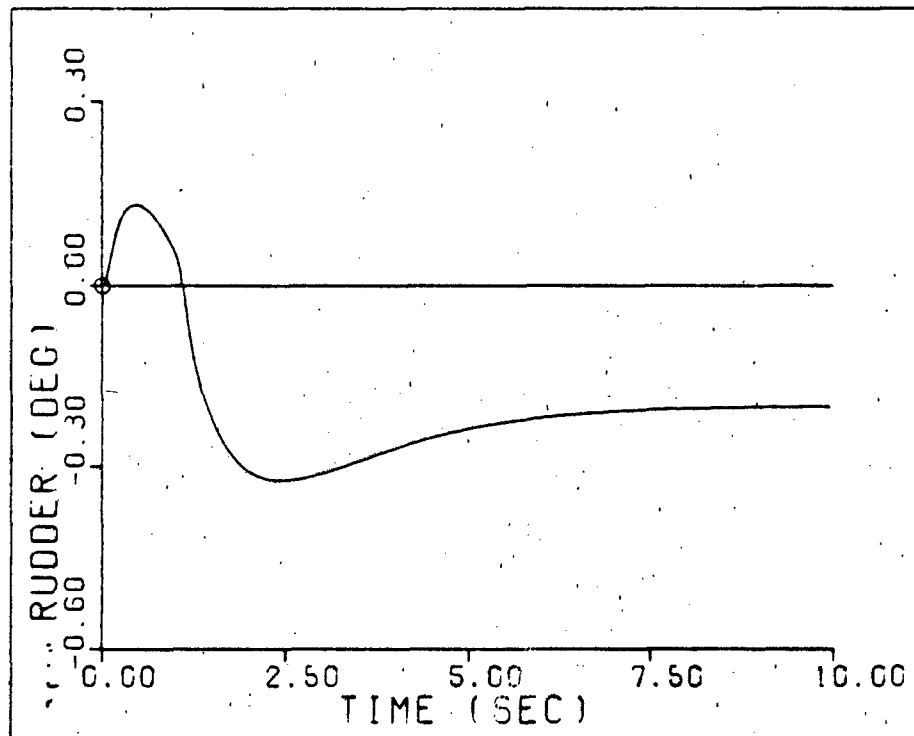


Fig. H-12. Rudder Deflection--F.C. #1

Simulation Response for F.C. #2--  
Bank Angle Command

The responses shown in Figures H-13 and H-14 are for a 30 degree step input bank angle command (complex pre-filter poles). The control surface deflections are shown in Figures H-15 and H-16. Table H-4 outlines the characteristics of each response.

TABLE H-4

BANK ANGLE COMMAND--F.C. #2

	Peak Value	Final Value	Rise Time	Settling Time
$\phi$ (deg)	30.6	30.6	4.32	7.35
$\beta$ (deg)	0.0017	0.0016	--	--
$\delta_r$ (deg)	-0.216	--	--	--
$\delta_w$ (deg)	15.0	--	--	--

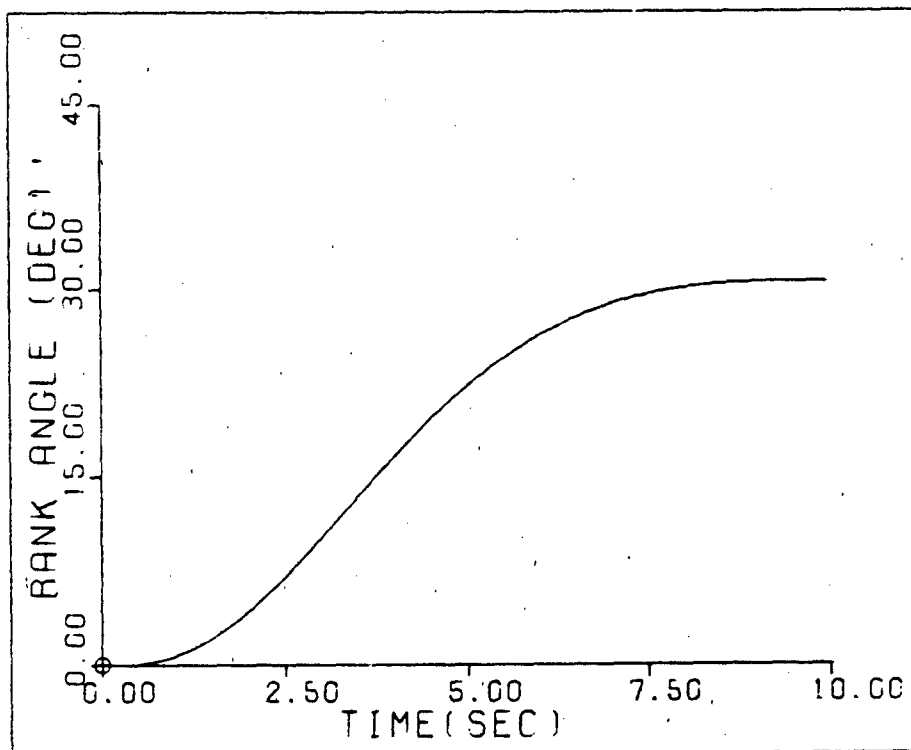


Fig. H-13. Bank Angle Response--F.C. #2

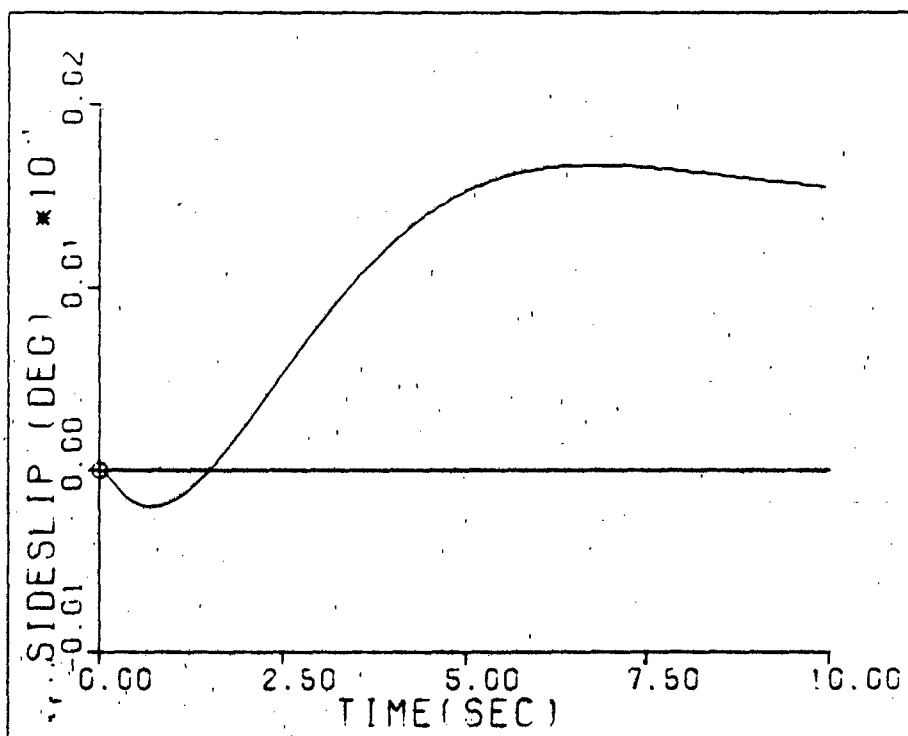


Fig. H-14. Sideslip Response--F.C. #2



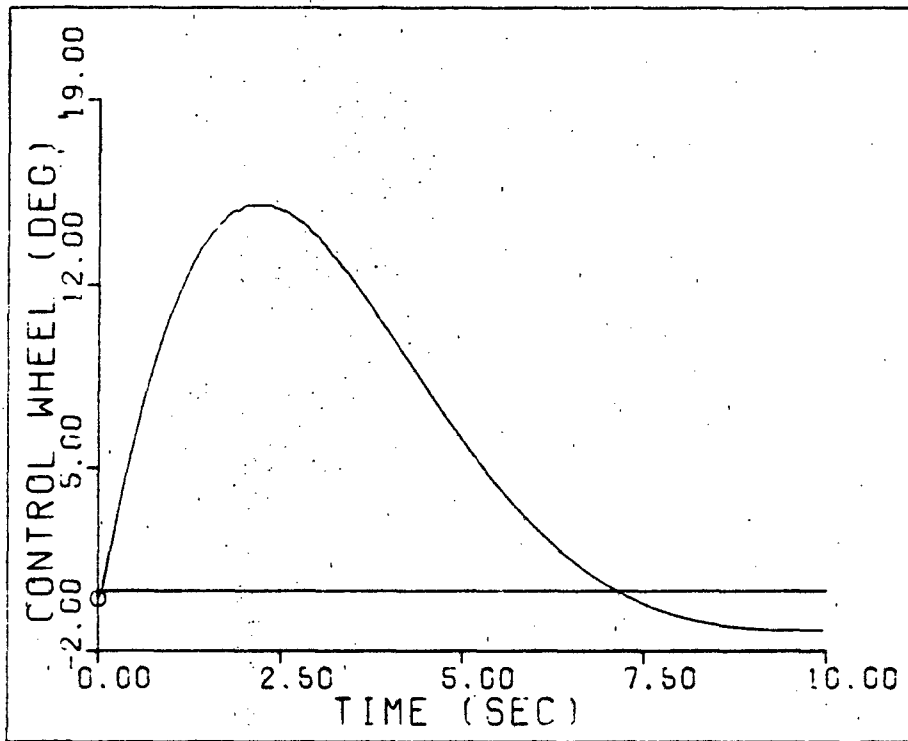


Fig. H-15. Control Wheel Deflection--F.C. #2

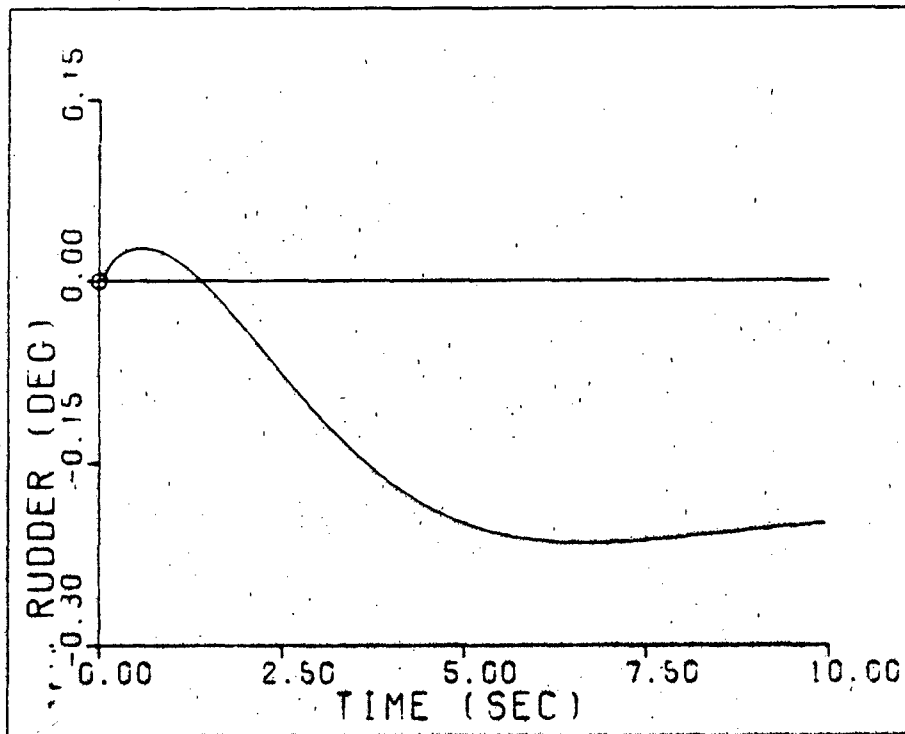


Fig. H-16. Rudder Deflection--F.C. #2

The responses shown in Figures H-17 and H-18 are for a 30 degree step input bank angle command (real pre-filter poles). The control surface deflections are shown in Figures H-19 and H-20. Table H-5 outlines the characteristics of each response.

TABLE H-5

BANK ANGLE COMMAND--F.C. #2

	Peak Value	Final Value	Rise Time	Settling Time
$\phi$ (deg)	30.0	30.0	3.40	6.10
$\beta$ (deg)	0.0017	0.0015	--	--
$\delta_r$ (deg)	-0.223	--	--	--
$\delta_w$ (deg)	53.0	--	--	--

PAGES 309,310,311,312,313,314  
ARE  
MISSING  
IN  
ORIGINAL  
DOCUMENT

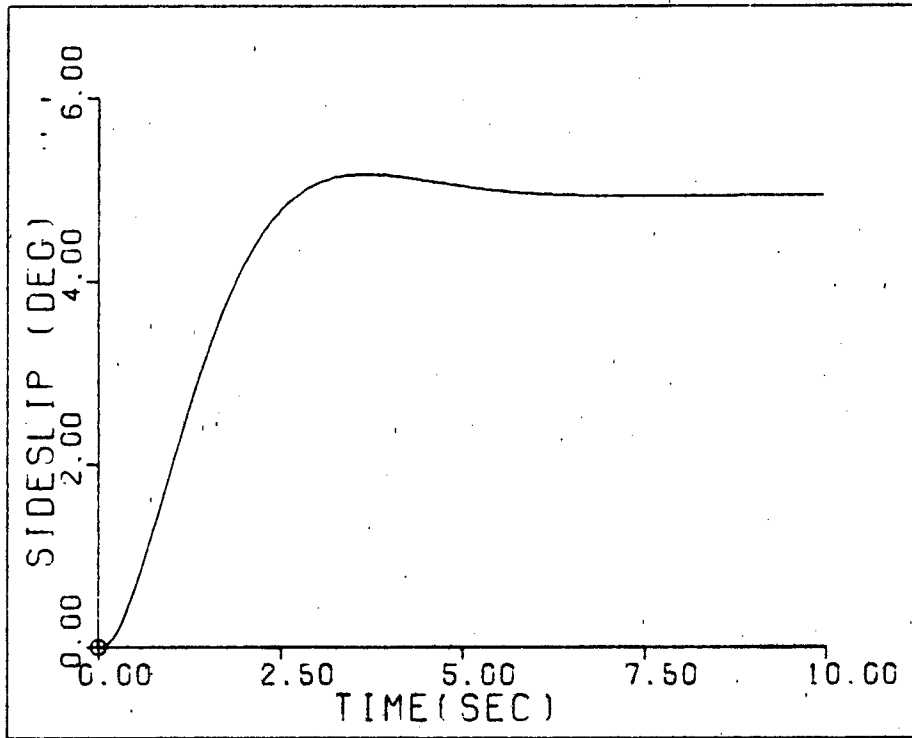


Fig. H-25. Sideslip Response--F.C.#1

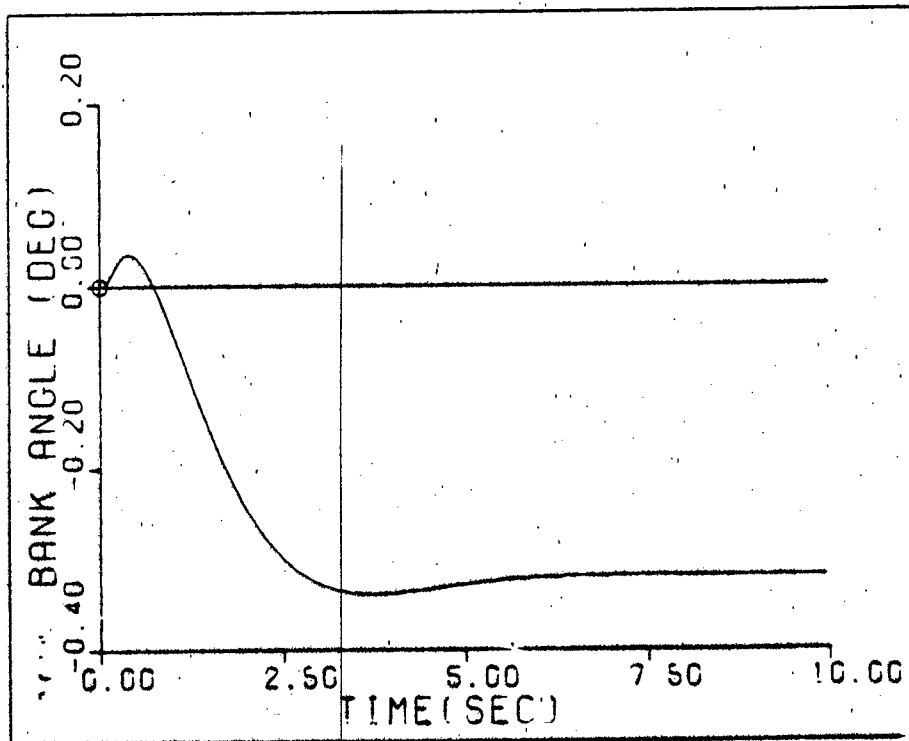


Fig. H-26. Bank Angle Response--F.C.#1

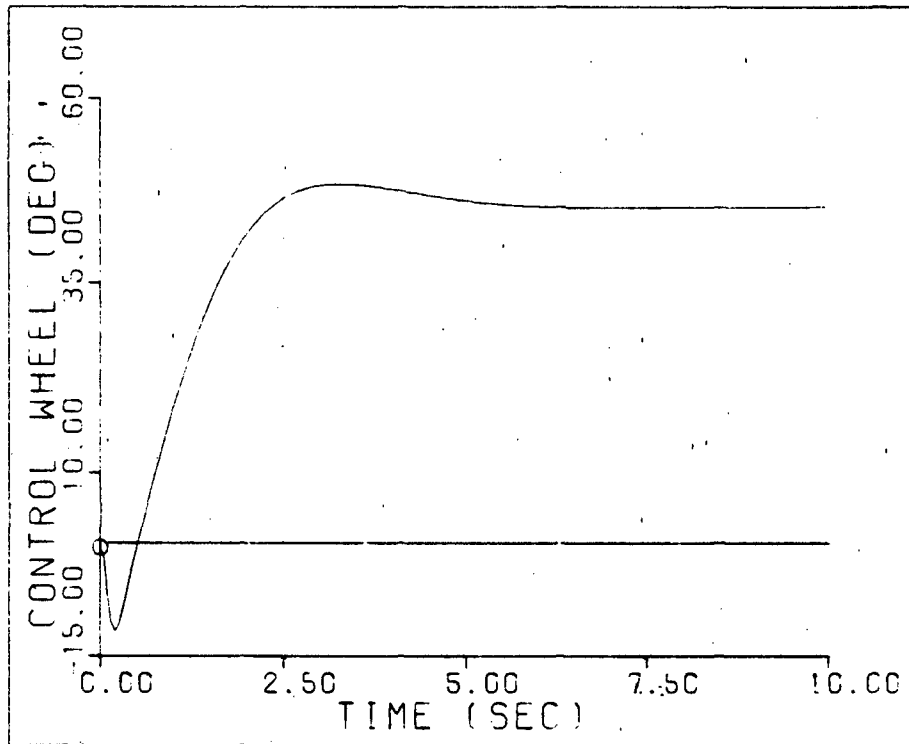


Fig. H-27. Control Wheel Deflection--F.C. #1

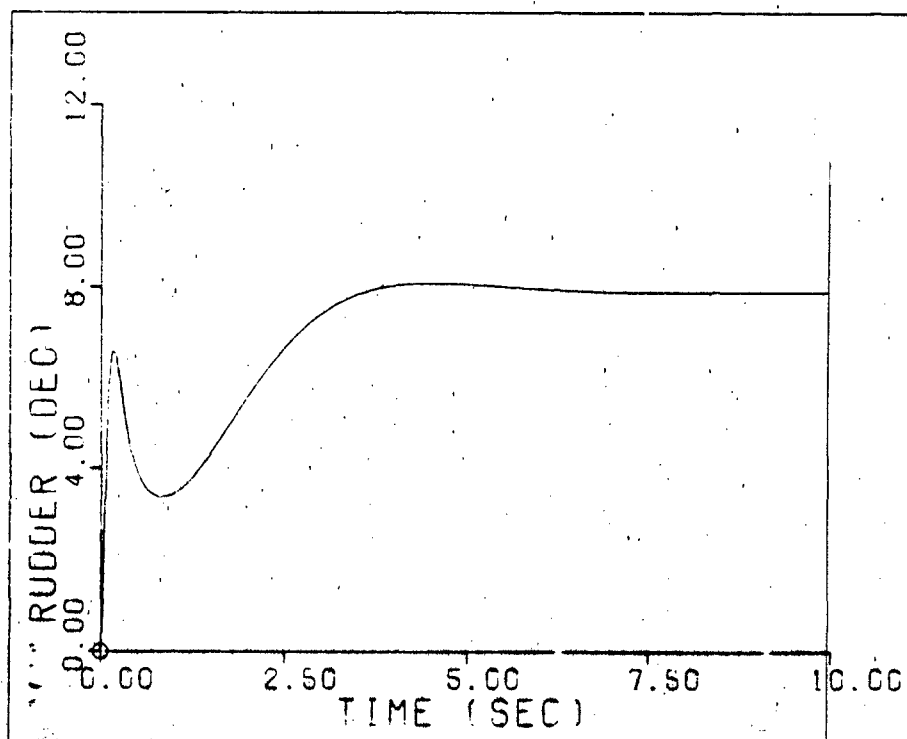


Fig. H-28. Rudder Deflection--F.C. #1

The responses shown in Figures H-29 and H-30 are for a 5 degree step input sideslip command (real pre-filter poles). The control surface deflections are shown in Figures H-31 and H-32. Table H-8 outlines the characteristics of each response.

TABLE H-8  
SIDESLIP COMMAND---F.C. #1

	Peak Value	Final Value	Rise Time	Settling Time
$\beta$ (deg)	5.0	5.0	4.99	8.85
$\phi$ (deg)	-0.322	-0.322	--	--
$\delta_r$ (deg)	7.95	--	--	--
$\delta_w$ (deg)	45.7	--	--	--

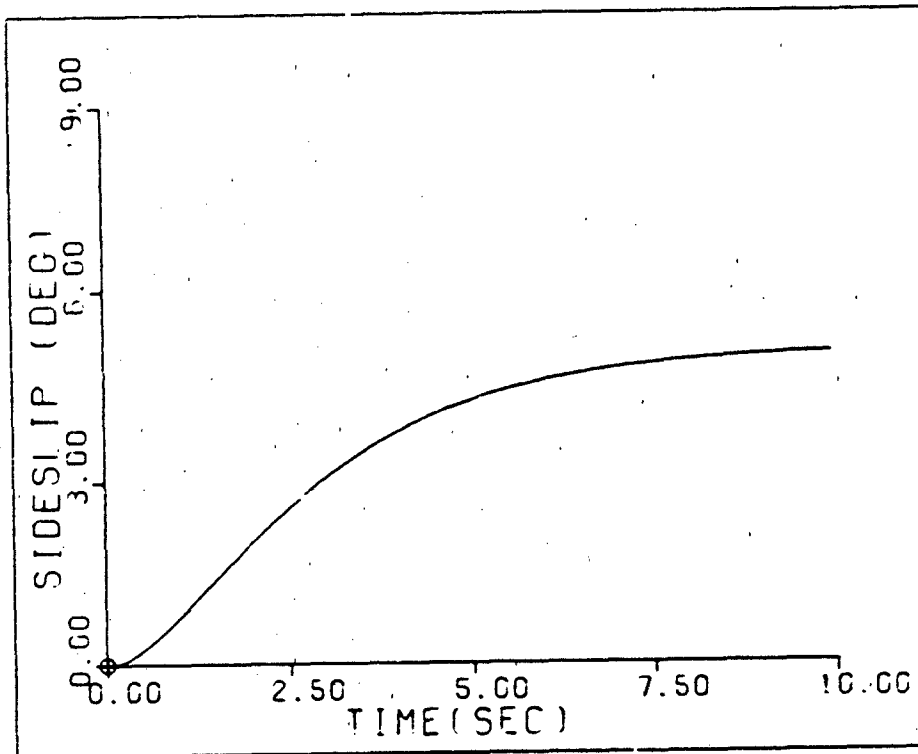


Fig. H-29. Sideslip Response--F.C. #1

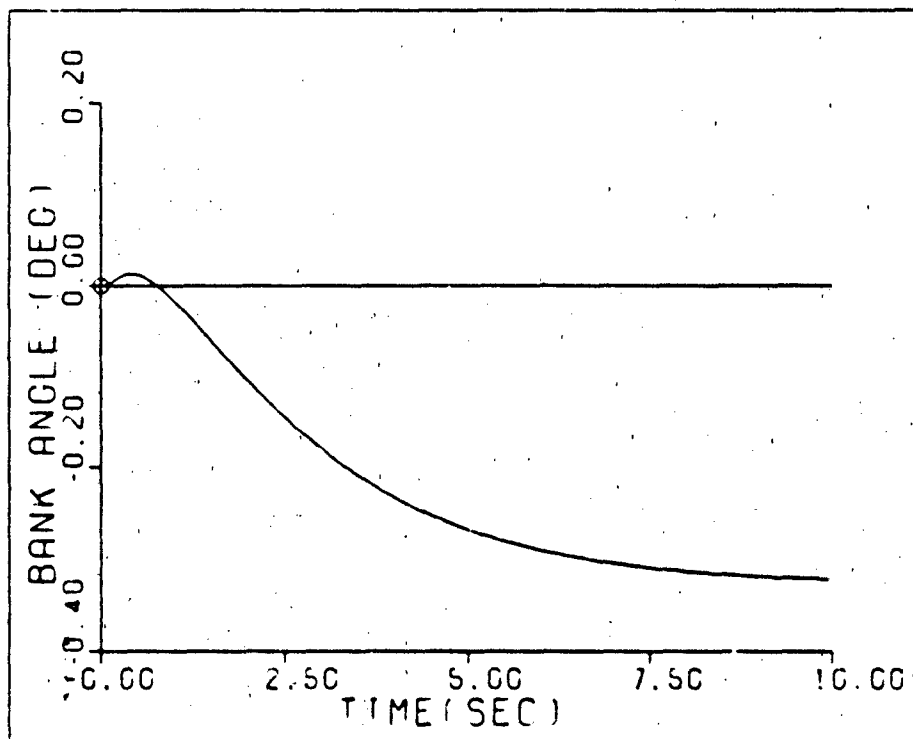


Fig. H-30. Bank Angle Response--F.C. #1

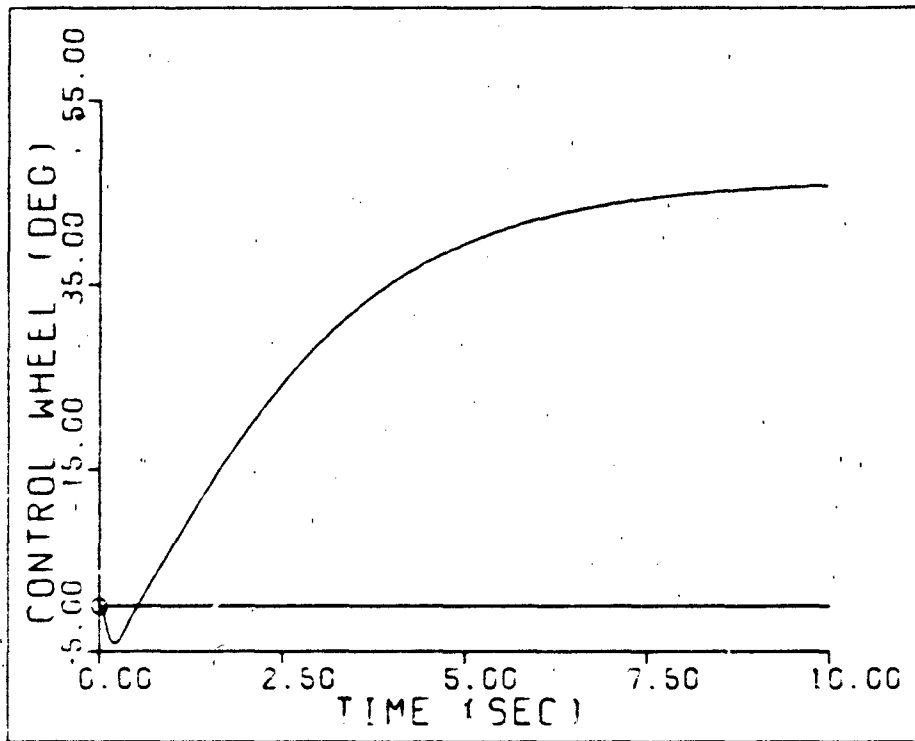


Fig. H-31. Control Wheel Deflection--F.C. #1

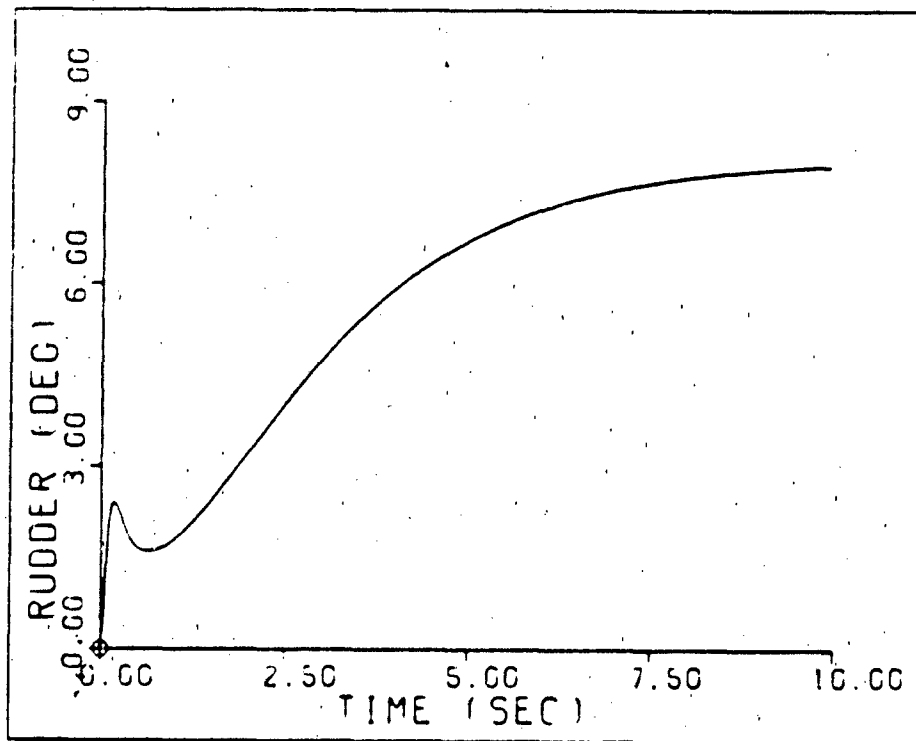


Fig. H-32. Rudder Deflection--F.C. #1



The responses shown in Figures H-33 and H-34 are for a 5 degree sideslip command (real pre-filter pole). The input is a ramp with a rise time of 1 second. The control surface deflections are shown in Figures H-35 and H-36. Table H-9 outlines the characteristics of each response.

TABLE H-9

SIDESLIP COMMAND--F.C. #1

	Peak Value	Final Value	Rise Time	Settling Time
$\delta$ (deg)	5.0	5.0	5.0	8.85
$\delta_r$ (deg)	-0.320	-0.320	--	--
$\delta_r$ (deg)	7.92	--	--	--
$\delta_w$ (deg)	45.6	--	--	--

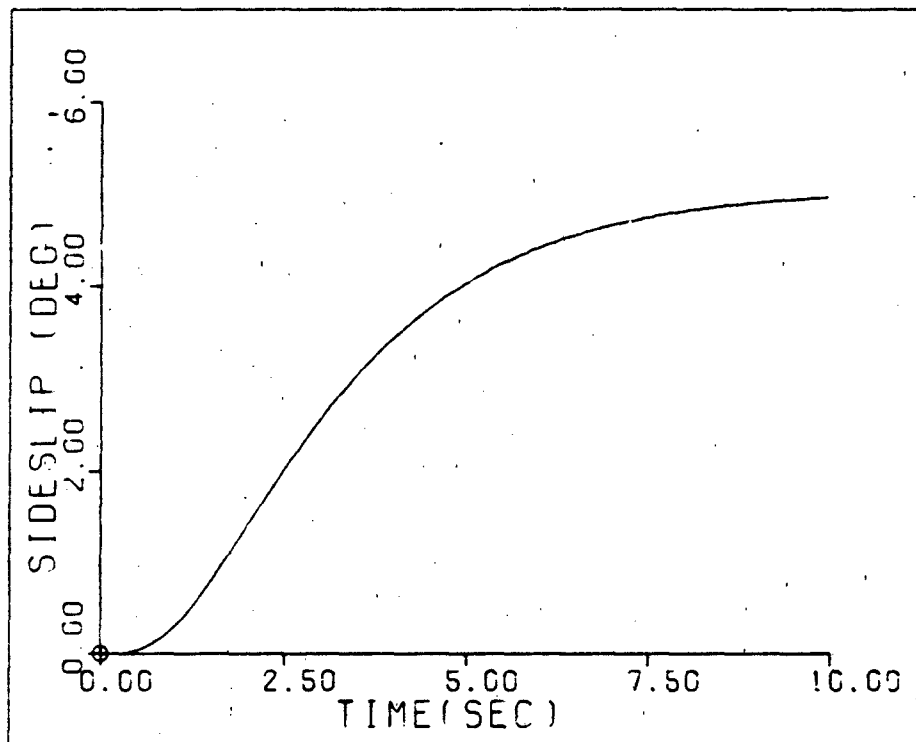


Fig. H-33. Sideslip Response--F.C. #1

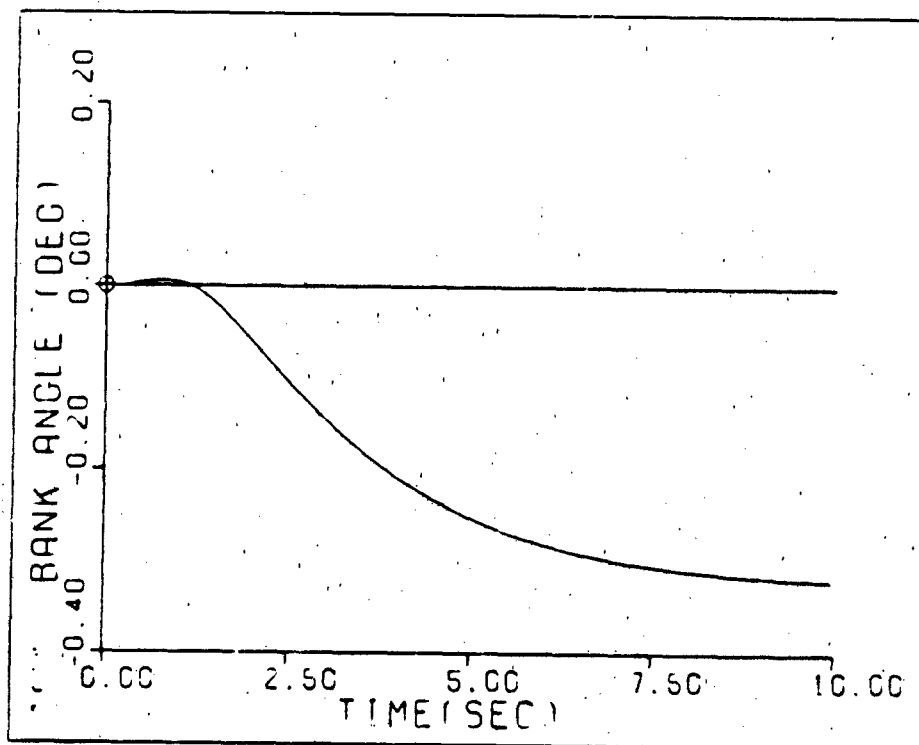


Fig. H-34. Bank Angle Response--F.C. #1

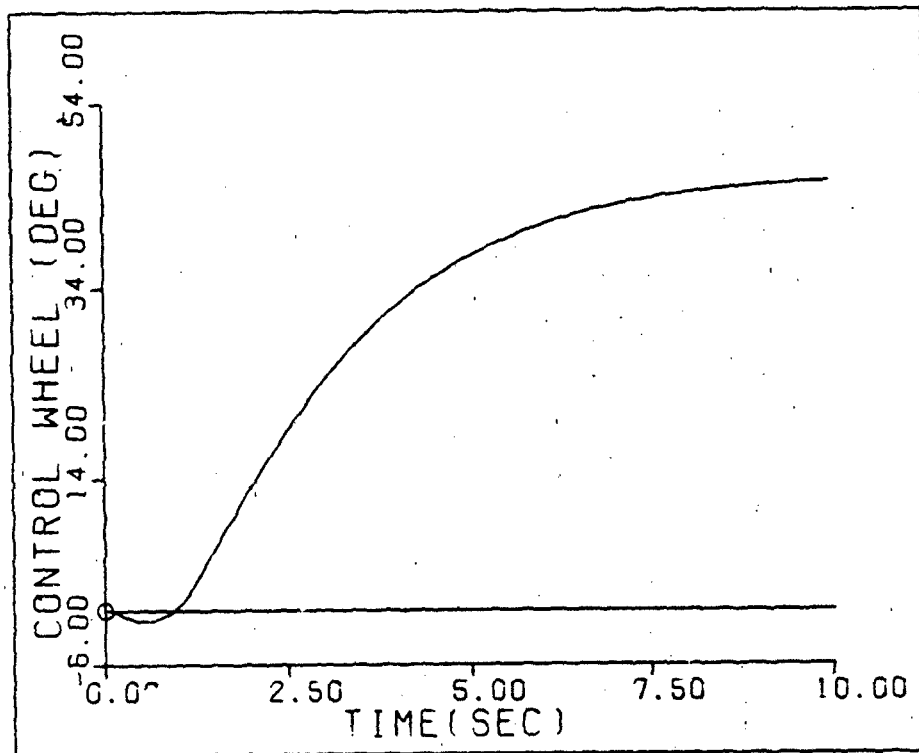


Fig. H-35. Control Wheel Deflection--F.C. #1

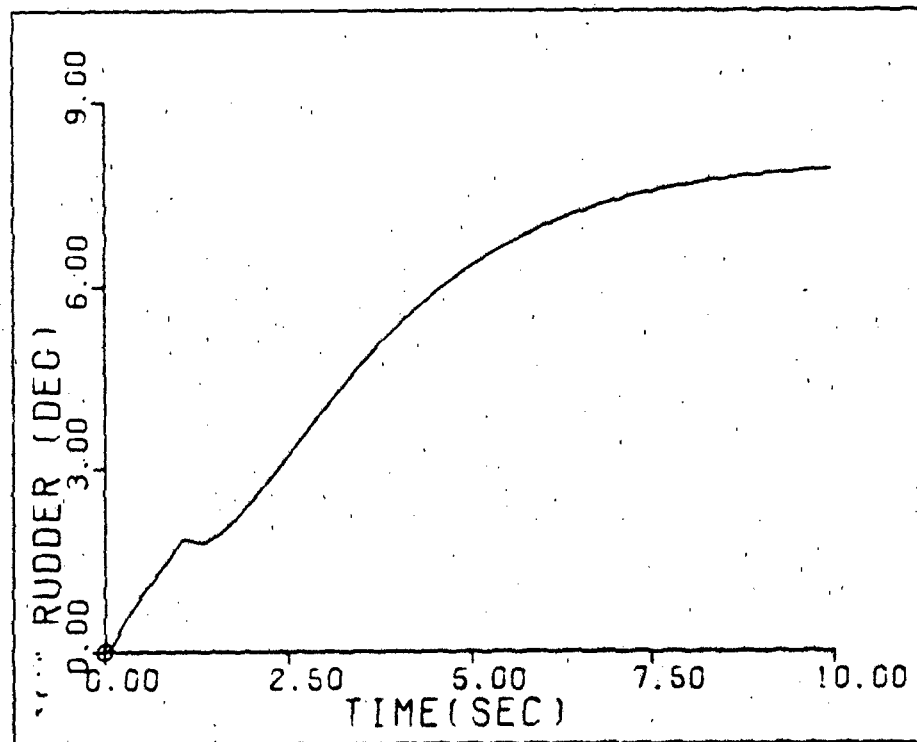


Fig. H-36. Rudder Deflection--F.C. #1

Simulation Responses for F.C. #2--  
Sideslip Command

The responses shown in Figures H-37 and H-38 are for a 5 degree step input sideslip command (complex pre-filter poles). The control surface deflections are shown in Figures H-39 and H-40. Table H-10 outlines the characteristics of each response.

TABLE H-10

SIDESLIP COMMAND--F.C. #2

	Peak Value	Final Value	Rise Time	Settling Time
$\beta$ (deg)	5.17	4.94	4.86	8.85
$\phi$ (deg)	-0.337	-0.337	--	--
$\delta_r$ (deg)	7.92	--	--	--
$\delta_w$ (deg)	50.9	--	--	--

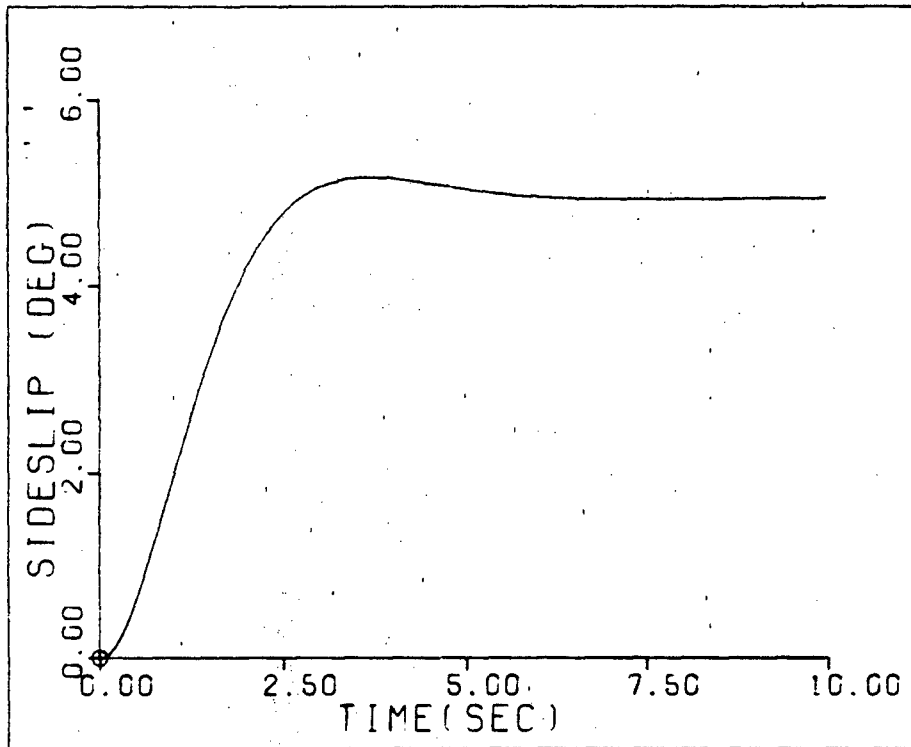


Fig. H-37. Sideslip Response--F.C. #2

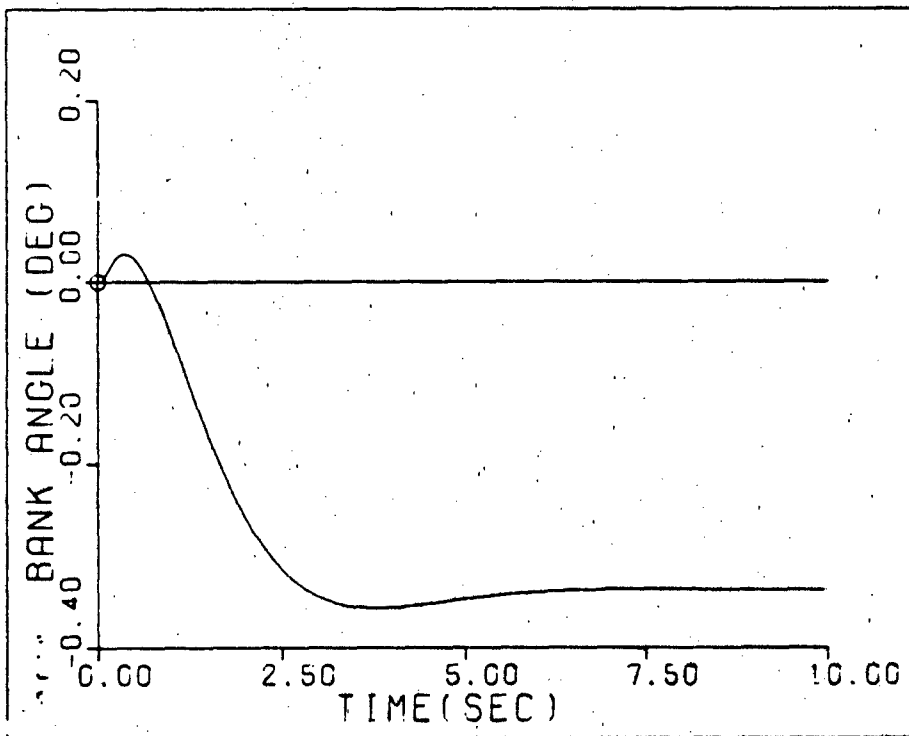


Fig. H-38. Bank Angle Response--F.C. #2

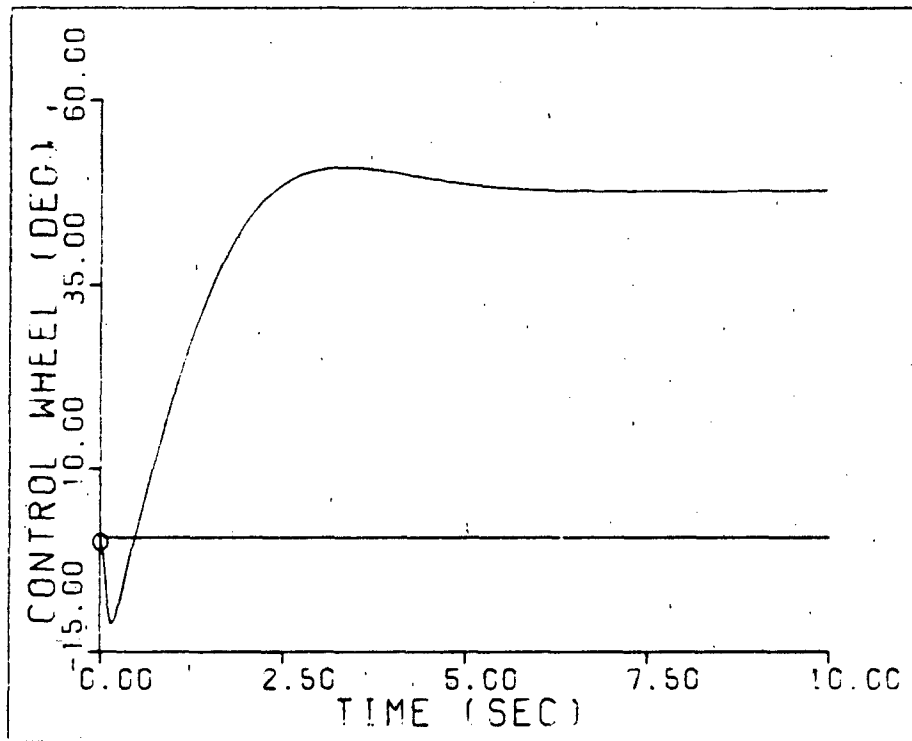


Fig. H-39. Control Wheel Deflection--F.C. #2

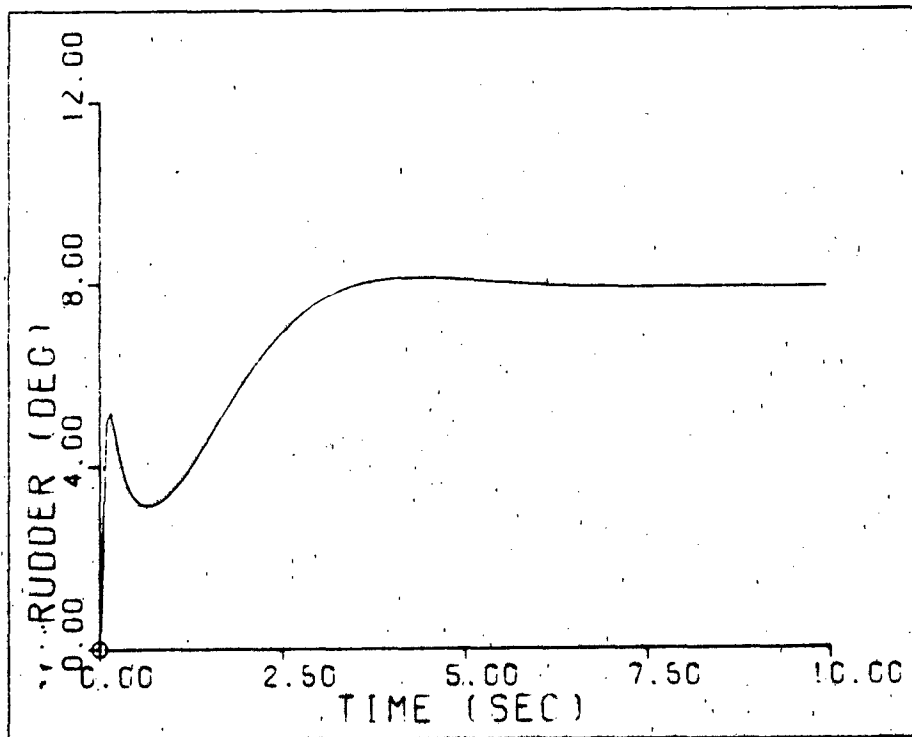


Fig. H-40. Rudder Deflection--F.C. #2

The responses shown in Figures H-41 and H-42 are for a 5 degree step input sideslip command (real pre-filter poles). The control surface deflections are shown in Figures H-43 and H-44. Table H-11 outlines the characteristics of each response.

TABLE H-11  
SIDESLIP COMMAND--F.C. #2

	Peak Value	Final Value	Rise Time	Settling Time
$\beta$ (deg)	5.0	5.0	4.95	8.25
$\phi$ (deg)	-0.340	-0.340	--	--
$\delta_r$ (deg)	7.99	--	--	--
$\delta_w$ (deg)	48.3	--	--	--

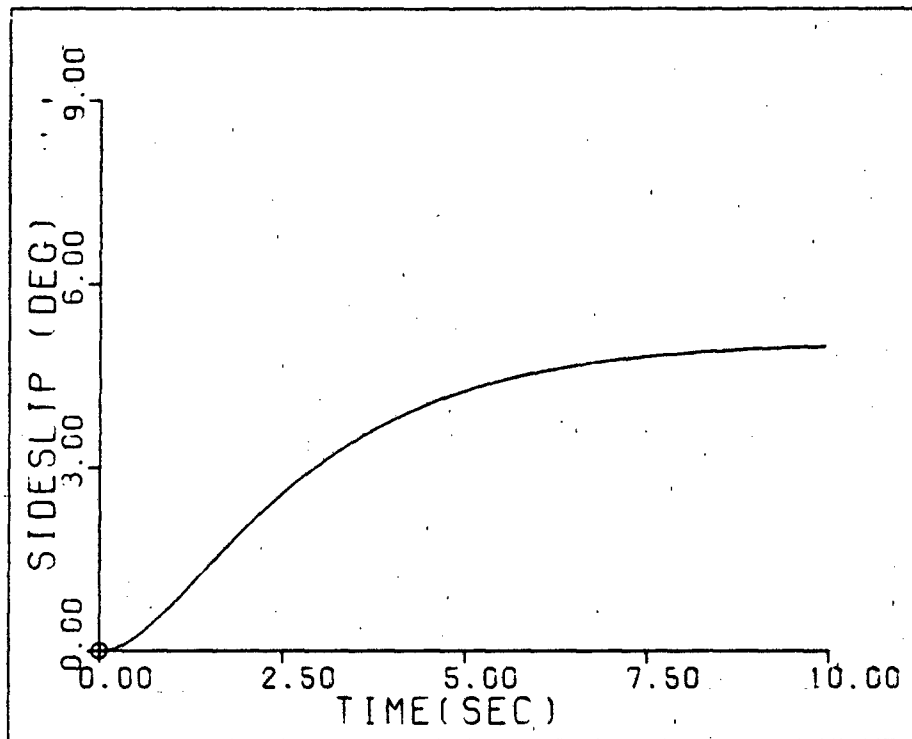


Fig. H-41. Sideslip Response--F.C. #2

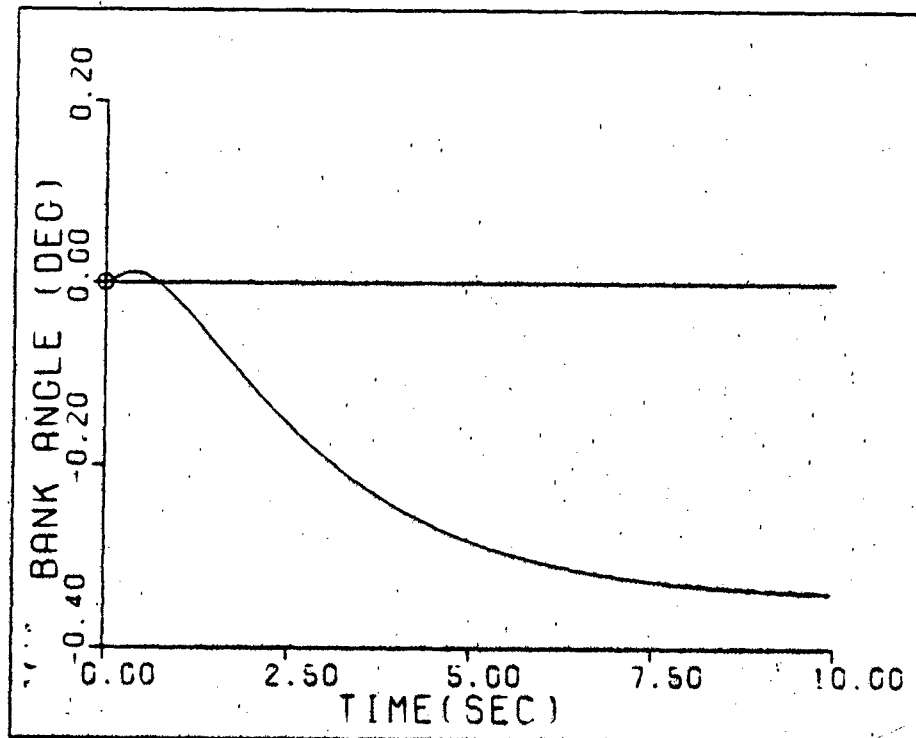


Fig. H-42. Bank Angle Response--F.C. #2



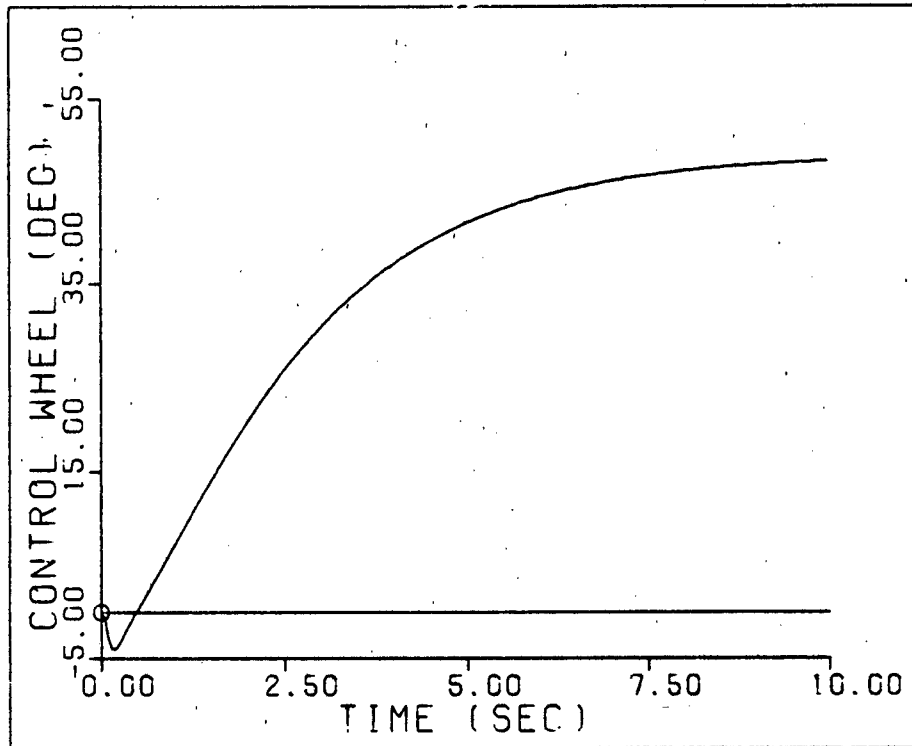


Fig. H-43. Control Wheel Deflection--F.C. #2

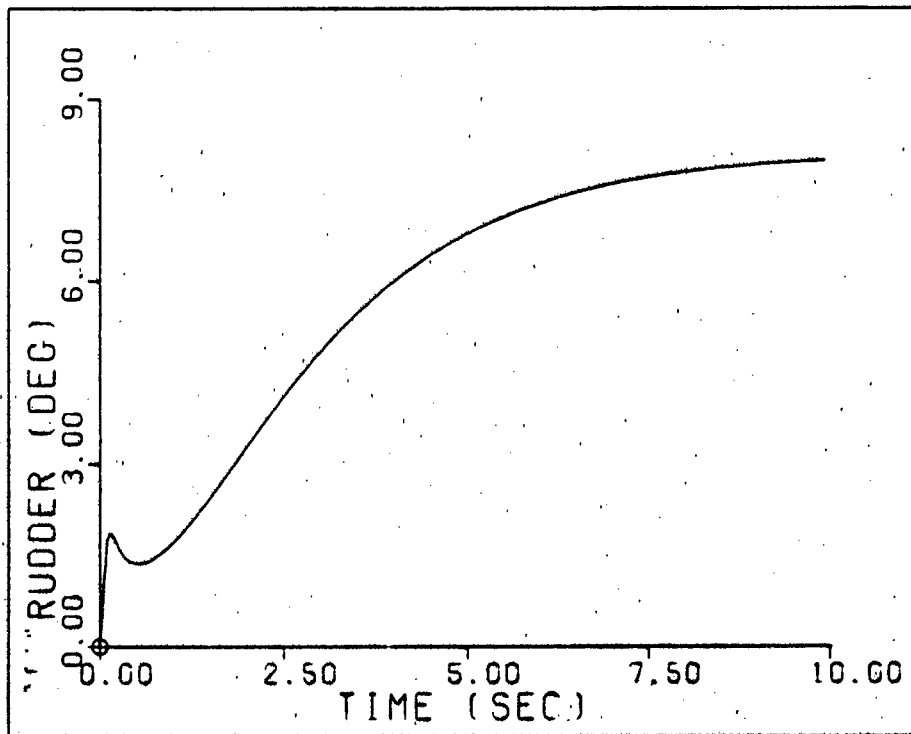


Fig. H-44. Rudder Deflection--F.C. #2

The responses shown in Figures H-45 and H-46 are for a 5 degree sideslip command. The input is a ramp with a rise time of 1 second. The control surface deflections are shown in Figures H-47 and H-48. Table H-12 outlines the characteristics of each response.

TABLE H-12

SIDESLIP COMMAND--F.C. #2

	Peak Value	Final Value	Rise Time	Settling Time
$\beta$ (deg)	5.0	5.0	4.0	9.35
$\phi$ (deg)	-0.338	-0.338	--	--
$\delta_r$ (deg)	7.96	--	--	--
$\delta_w$ (deg)	48.1	--	--	--

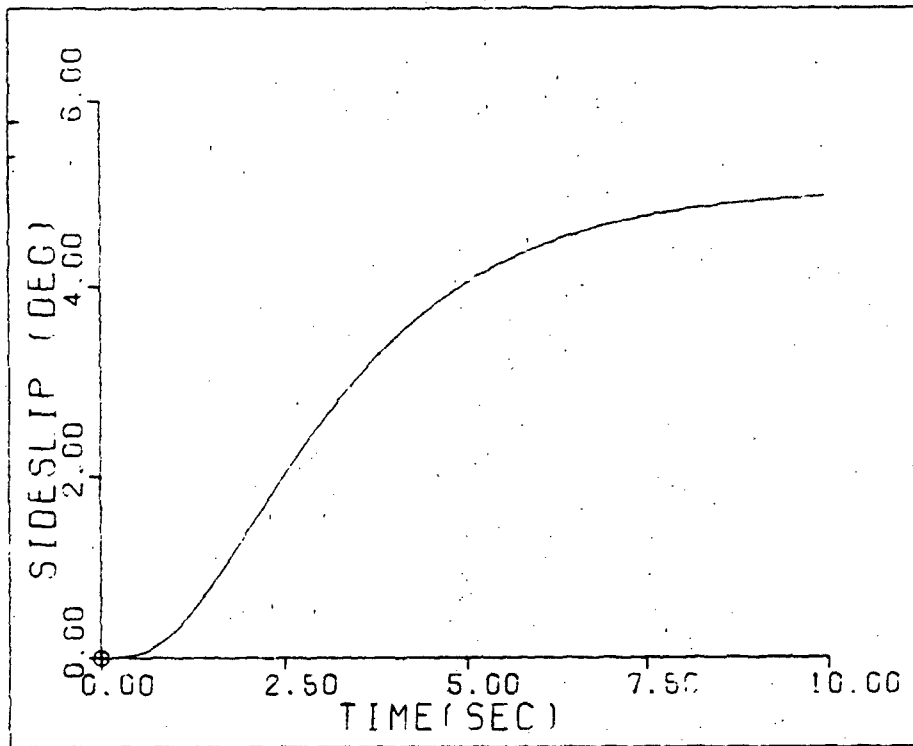


Fig. H-45. Sideslip Response--F.C. #2

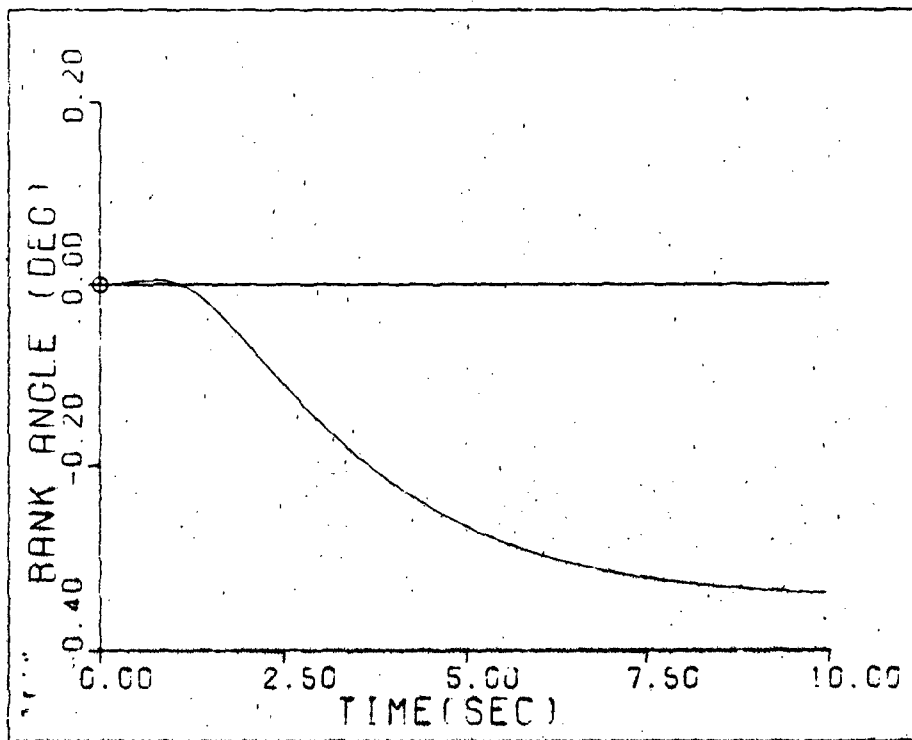


Fig. H-46. Bank Angle Response--F.C. #2

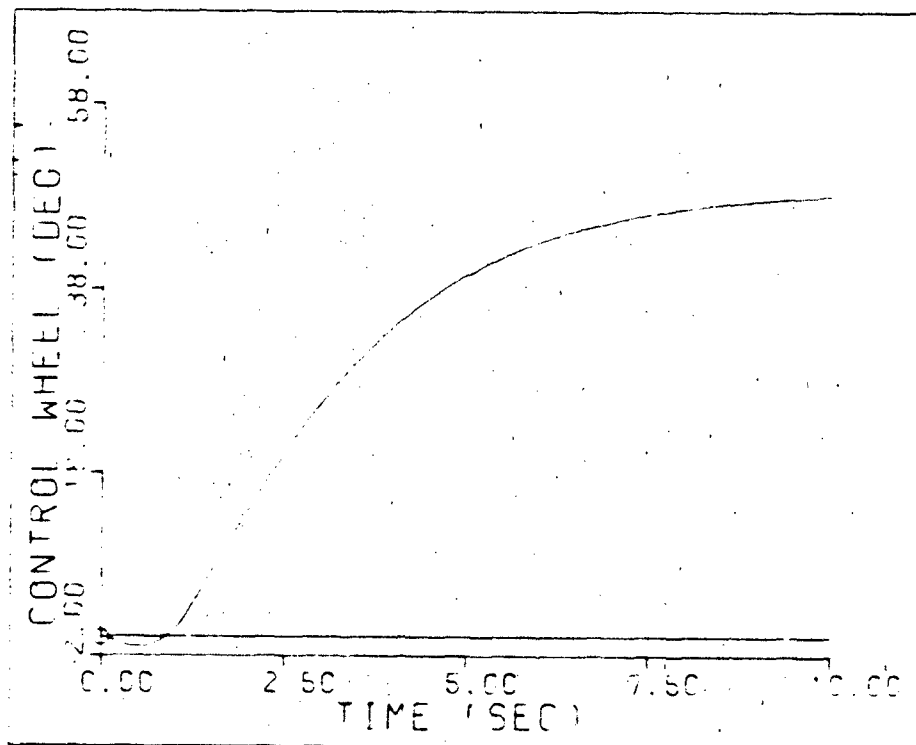


Fig. H-47. Control Wheel Deflection--F.C. #2

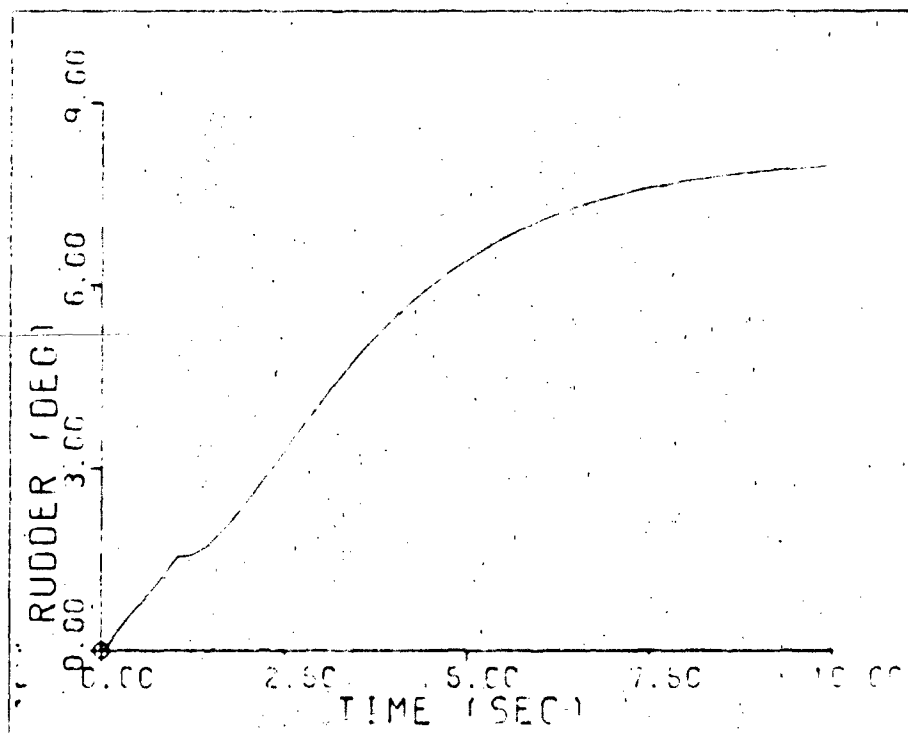


Fig. H-48. Rudder Deflection--F.C. #2

Simulation Response for F.C. #1--  
Pitch Angle Command (Rigid Aircraft)

The responses for a 1 degree pitch angle command are shown in Figures H-49 through H-51 and the control surface deflections are shown in Figures H-52 through H-54. Table H-13 outlines the characteristics of each response.

TABLE H-13  
 PITCH ANGLE COMMAND--F.C. #1

	Peak Value	Final Value	Rise Time	Settling Time
	1.0	1.0	4.76	8.45
h	-0.0503	-0.0242	--	--
u	-0.286	-0.243	--	--
e	-0.198	--	--	--
sb	16.0	--	--	--
T	26.4	--	--	--

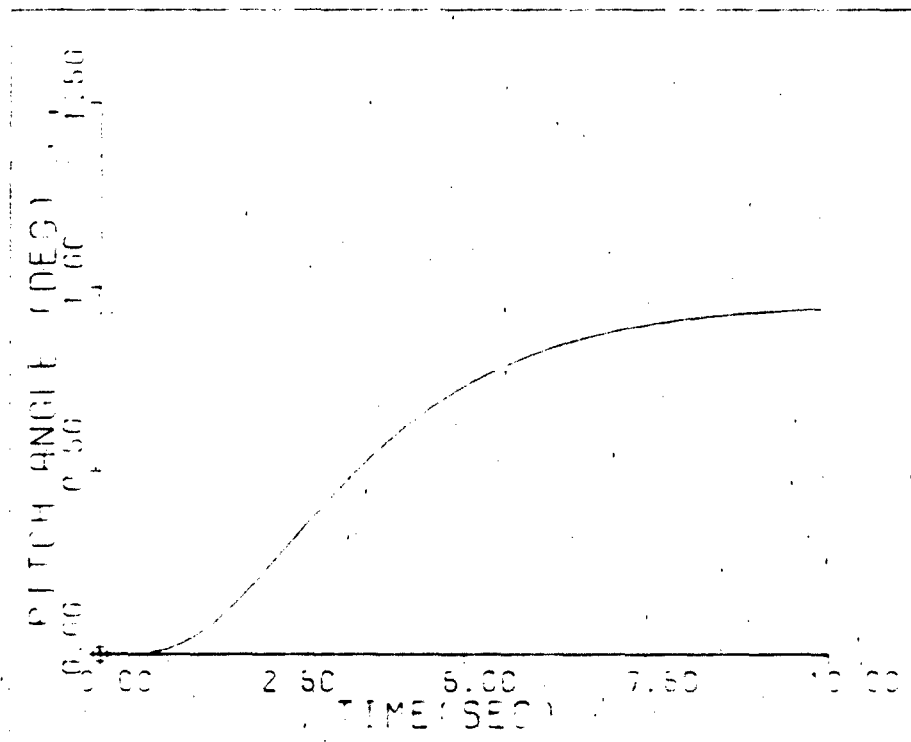


Fig. H-49. Pitch Angle Response--F.C. #1

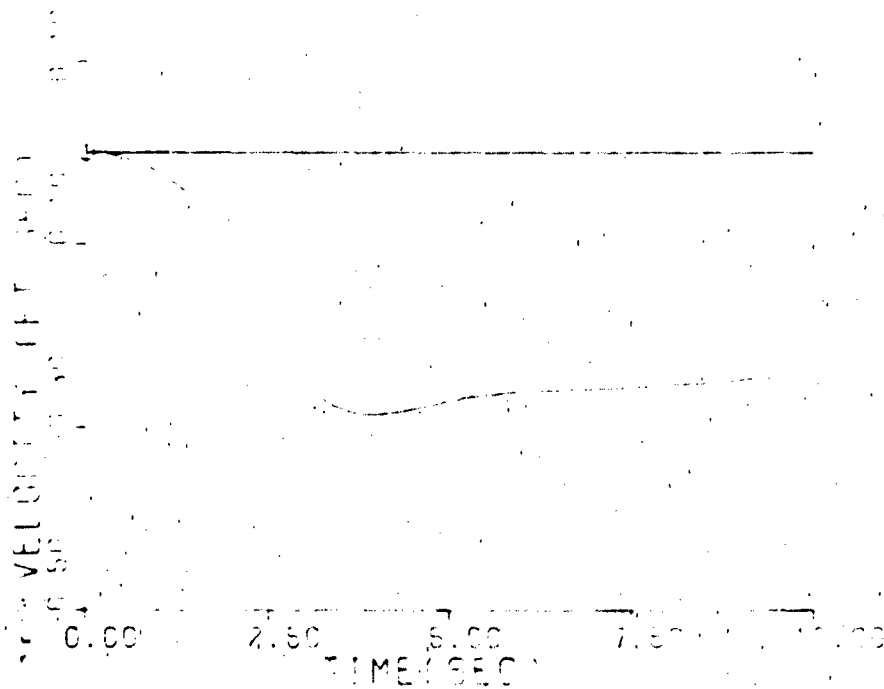


Fig. H-50. Perturbation Velocity Response--F.C. #1

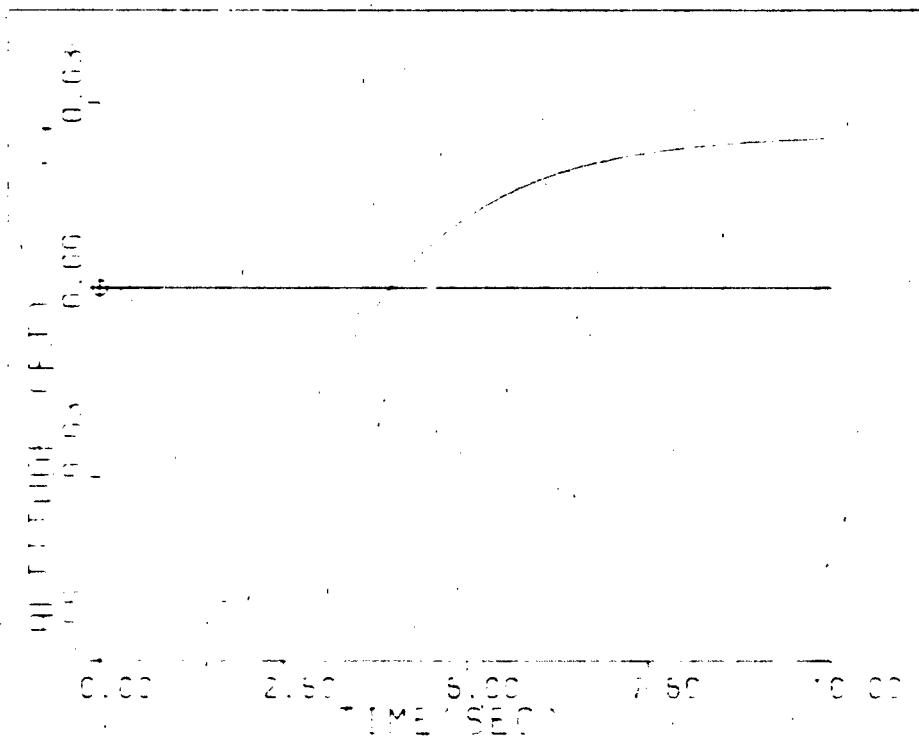


Fig. H-51. Altitude Response--F.C. #1

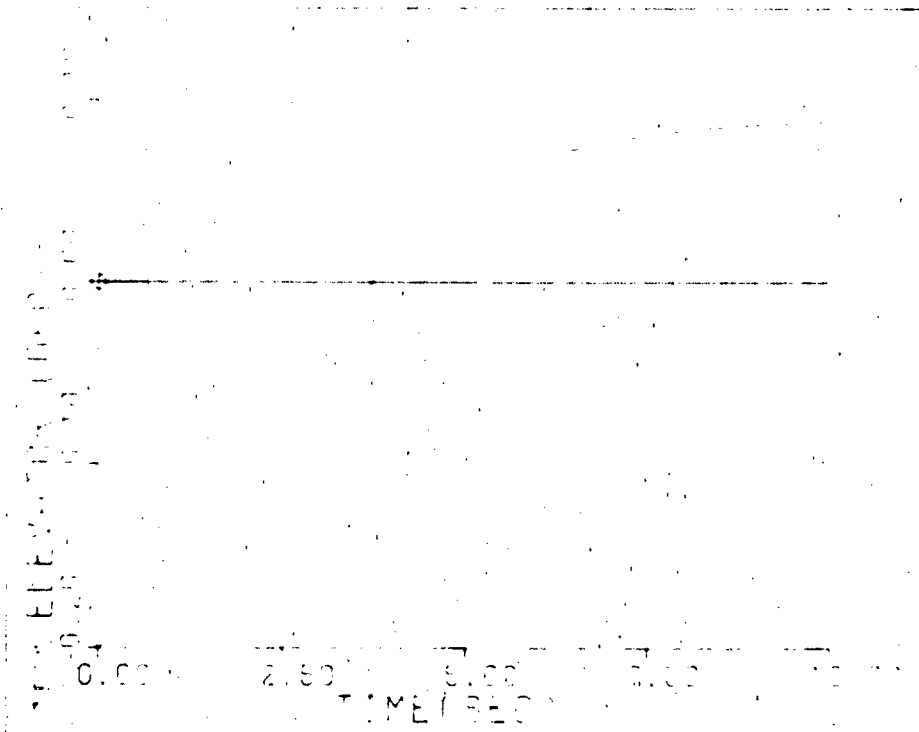


Fig. H-52. Elevator Deflection--F.C. #1

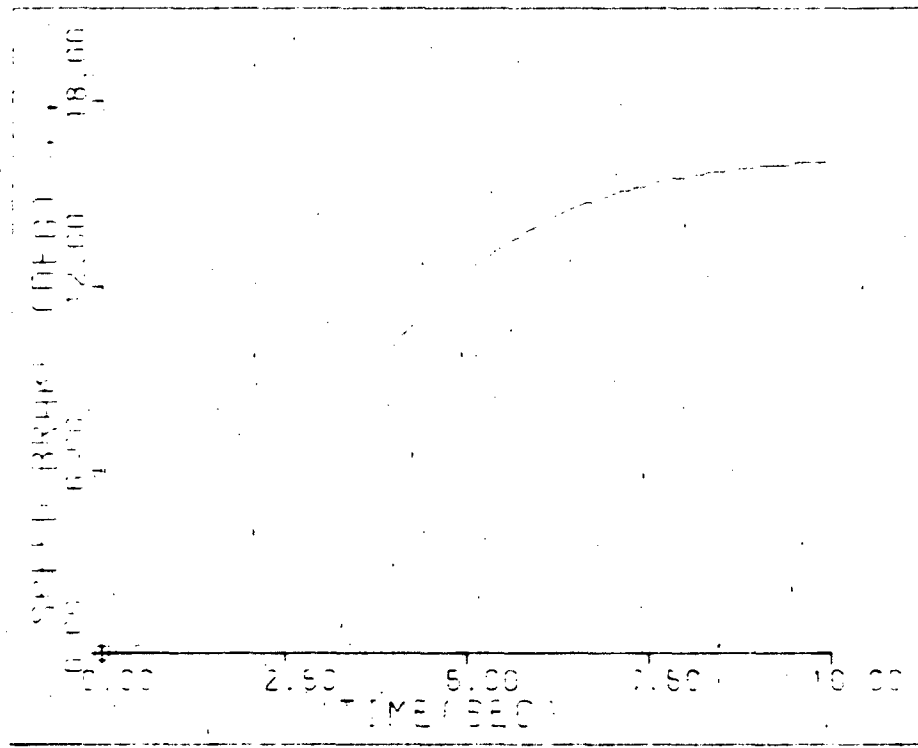


Fig. H-53. Speed Brake Deflection--F.C. #1

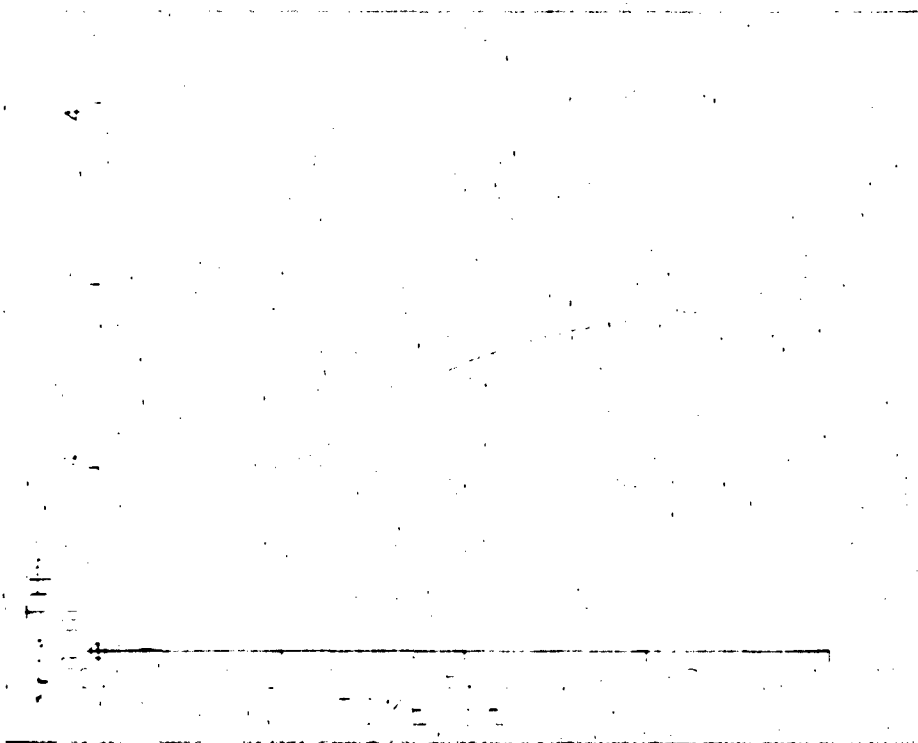


Fig. H-54. Thrust Increase--F.C. #1



Simulation Responses for F.C. #2--  
Pitch Angle Command (Rigid Aircraft)

The responses for a 4 degree pitch angle command are shown in Figures H-55 through H-57 and the control surface deflections are shown in Figures H-58 through H-60. Table H-14 outlines the characteristics of each response.

TABLE H-14

PITCH ANGLE COMMAND--F.C. #1

	Peak Value	Final Value	Rise Time	Settling Time
$\dot{\delta}$	1.0	1.0	6.1	7.70
h	0.219	0.219	--	--
u	-0.450	-0.374	--	--
$\delta_e$	0.802	--	--	--
$\delta_{sb}$	16.7	--	--	--
$\delta_T$	39.1	--	--	--

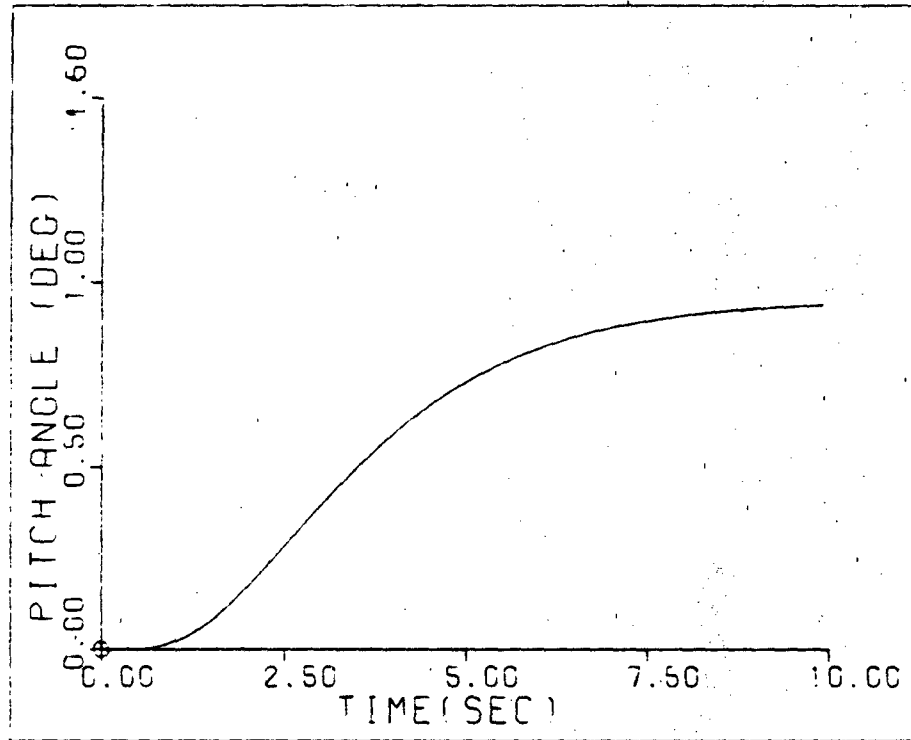


Fig. H-55. Pitch Angle Response--F.C. #2

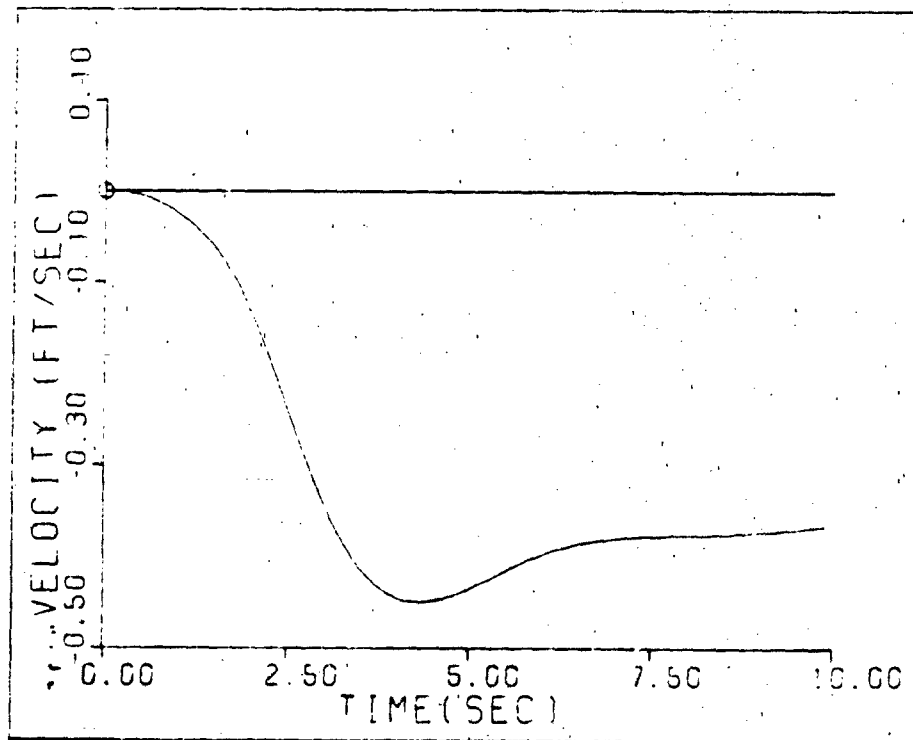


Fig. H-56. Perturbation Velocity Response--F.C. #3

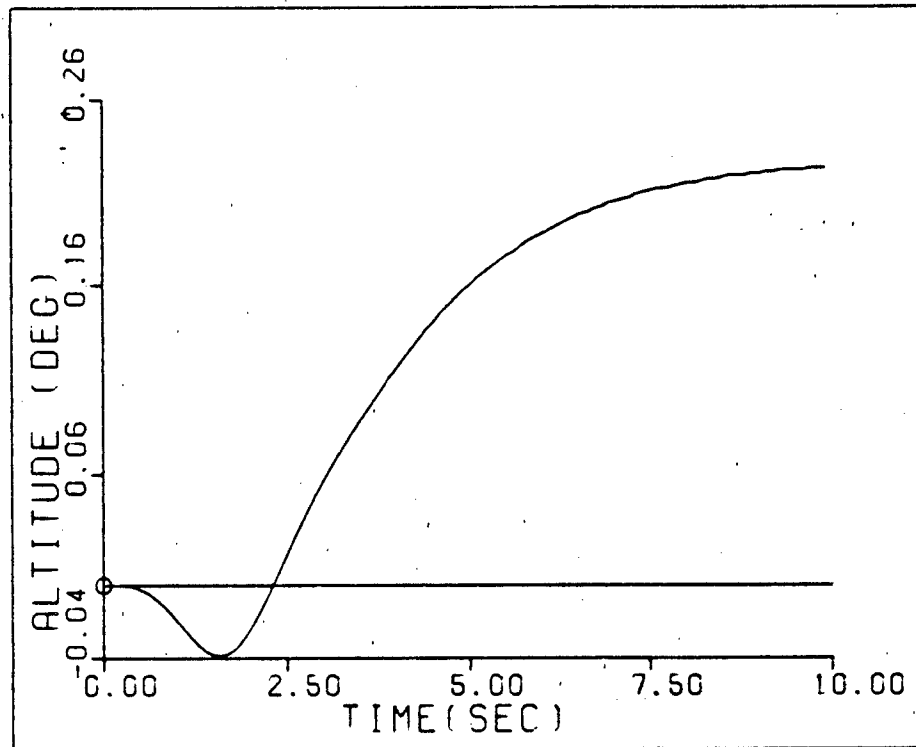


Fig. H-57. Altitude Response--F.C. #2

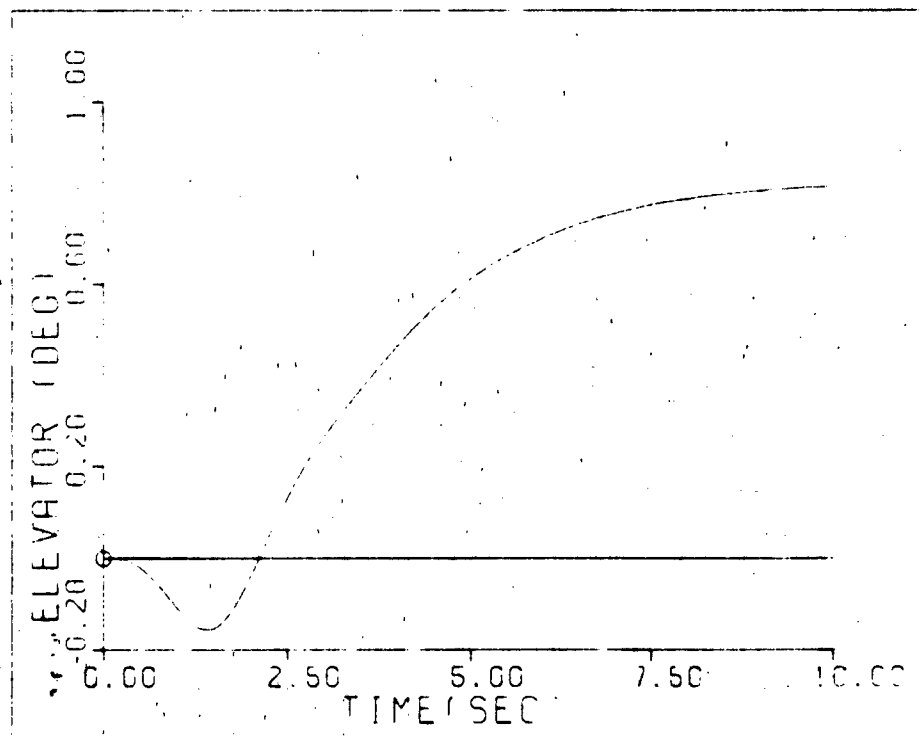


Fig. H-58. Elevator Deflection--F.C. #2

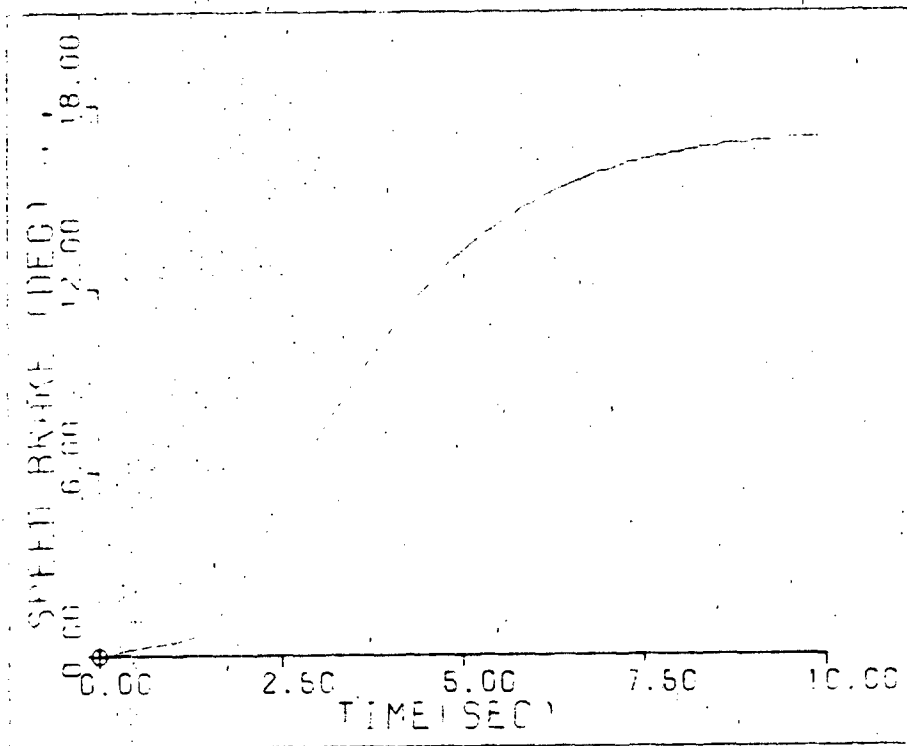


Fig. H-59. Speed Brake Deflection--F.C. #2

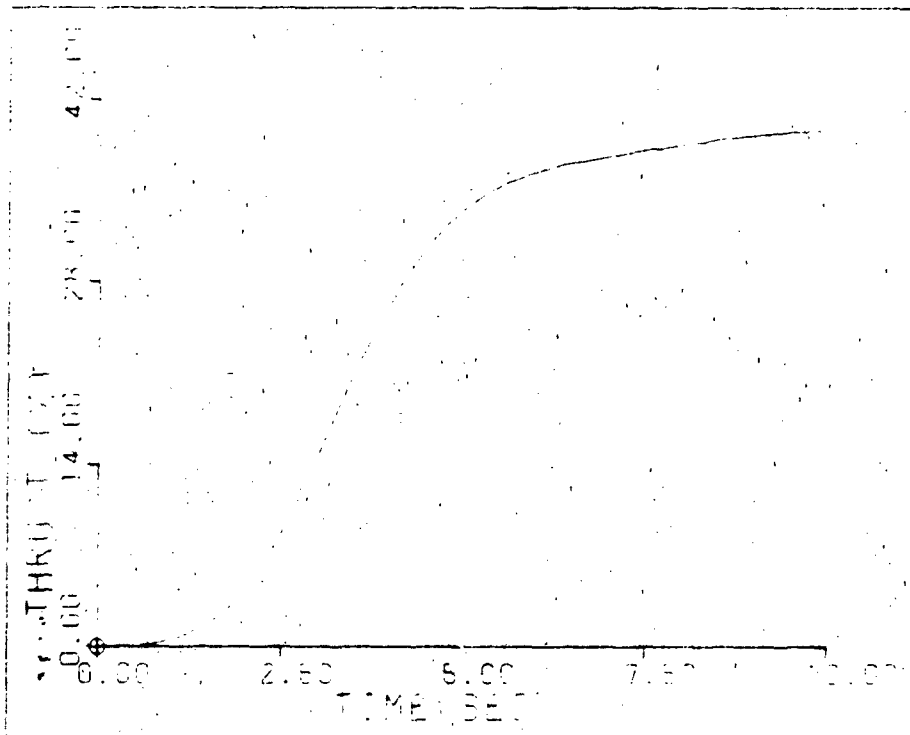


Fig. H-60. Thrust Increase--F.C. #2

Simulation Response for F.C. #1--  
Pitch Angle Command (Non-rigid Aircraft)

The responses for a 1 degree pitch angle command are shown in Figures H-61 through H-63 and the control surface deflections are shown in Figures H-64 through H-66. Table H-15 outlines the characteristics of each response.

TABLE H-15  
 PITCH ANGLE COMMAND--F.C. #1

	Peak Value	Final Value	Rise Time	Settling Time
$\theta$	1.0	1.0	5.1	8.4
$h$	0.50	0.50	--	--
$u$	-0.318	-0.267	--	--
$\delta_e$	1.82	--	--	--
$\delta_{sb}$	17.2	--	--	--
$\delta_T$	29.0	--	--	--

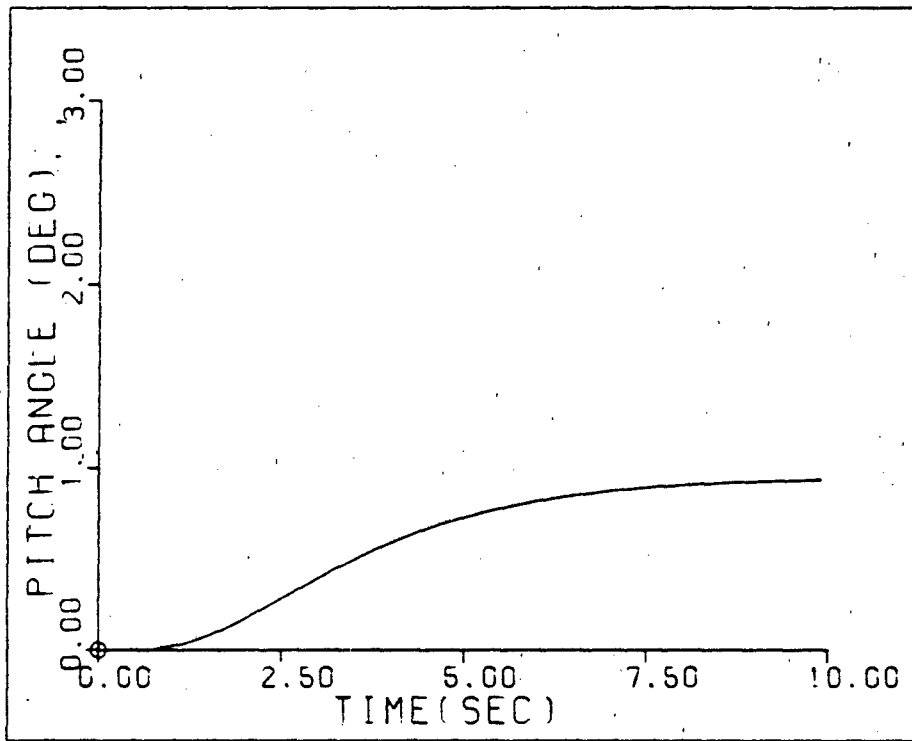


Fig. H-61. Pitch Angle Response--F.C. #1

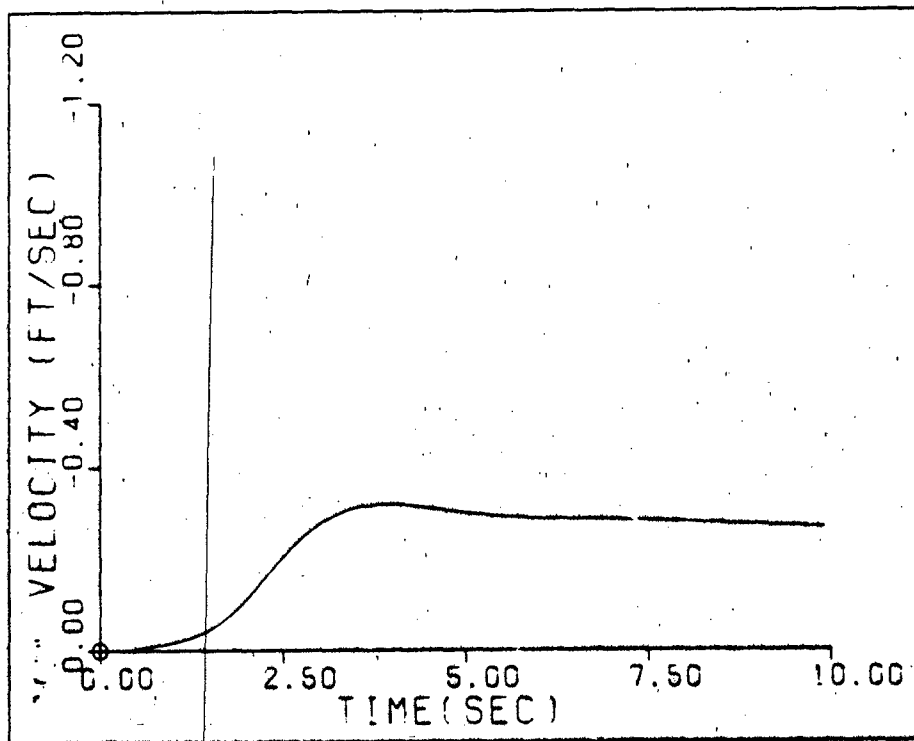


Fig. H-62. Perturbation Velocity--F.C. #1

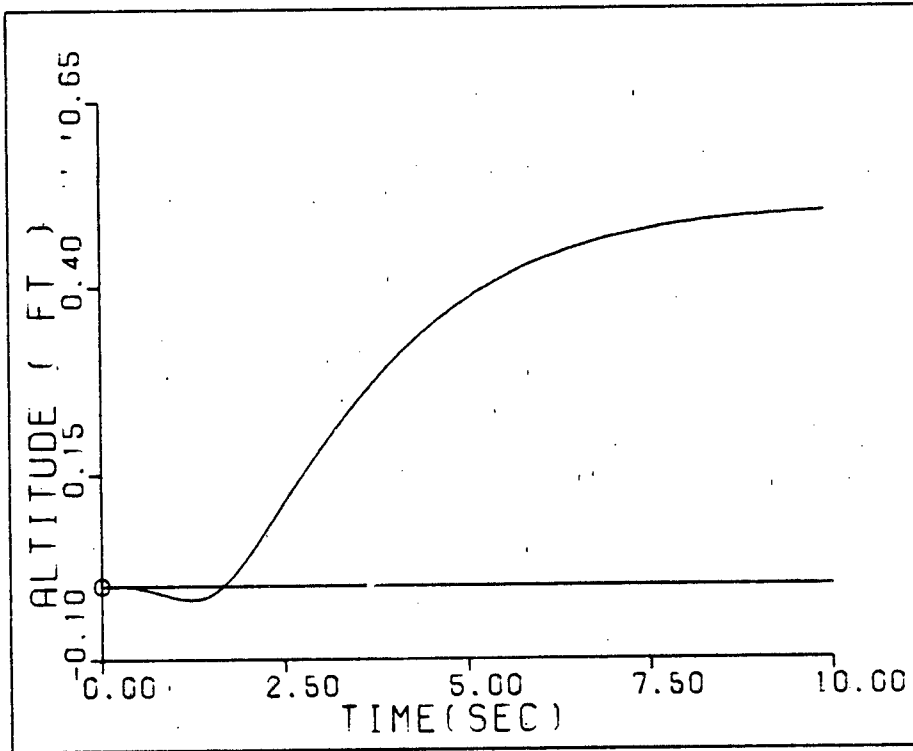


Fig. H-63. Altitude Response--F.C. #1

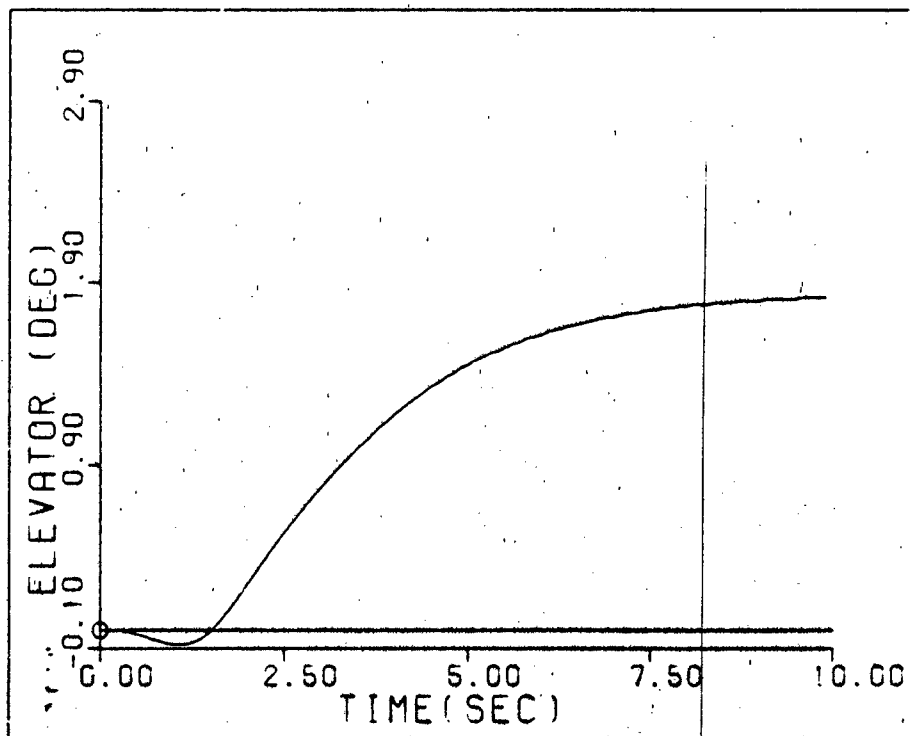


Fig. H-64. Elevator Deflection--F.C. #1

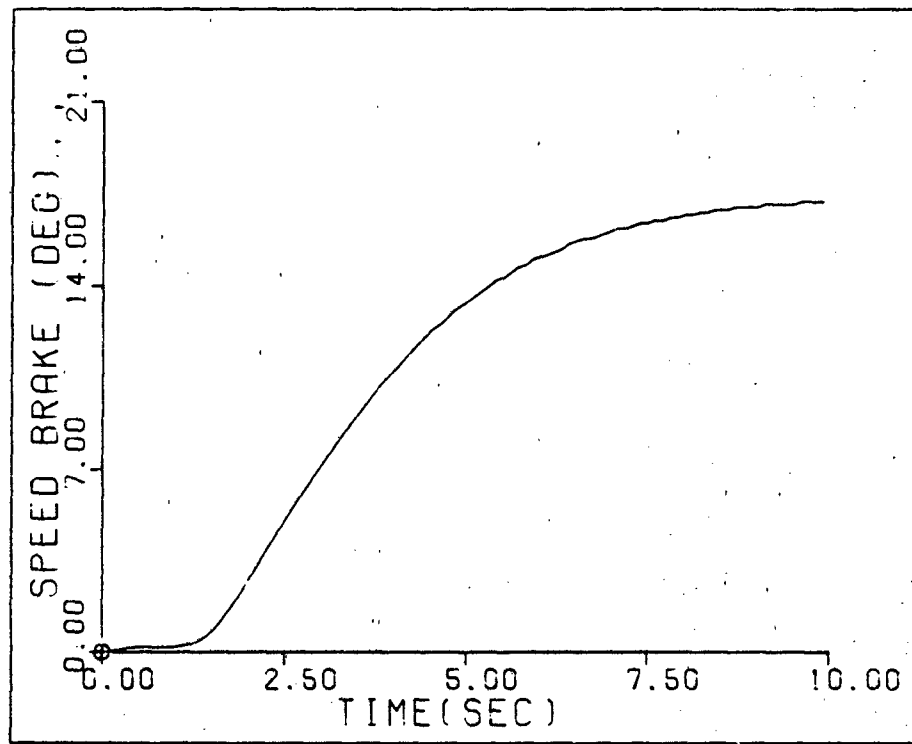


Fig. H-65. Speed Brake Deflection--F.C. #1

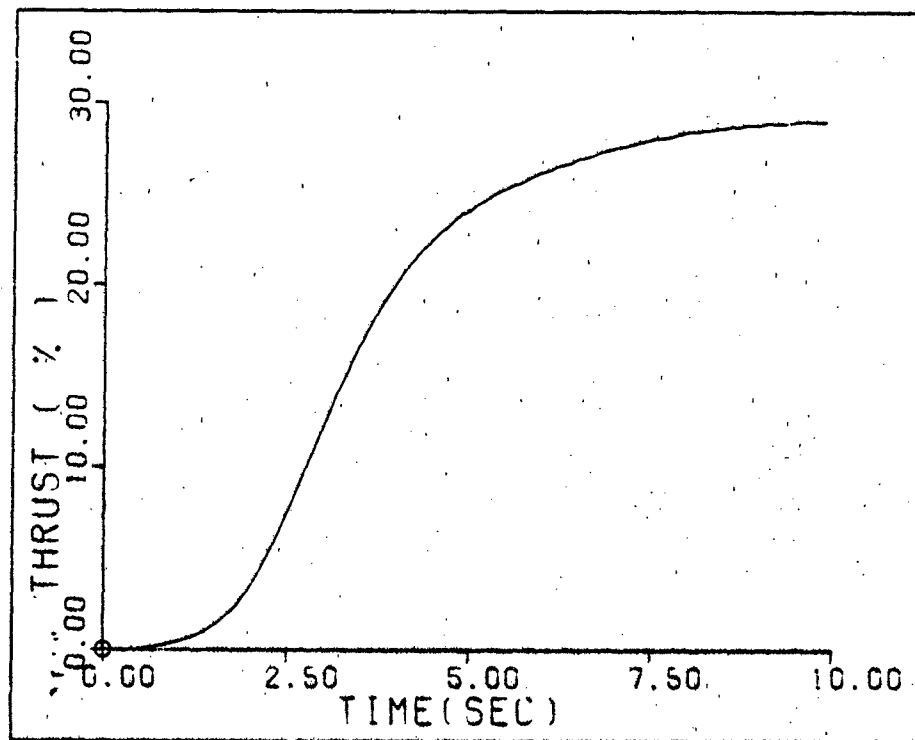


Fig. H-66. Thrust Increase--F.C. #1



Simulation Responses for F.C. #2--  
Pitch Angle Command (Non-rigid Aircraft)

The responses for a 1 degree pitch angle command are shown in Figures H-67 through H-69 and the control surface deflections are shown in Figures H-70 through H-72. Table H-16 outlines the characteristics of each response.

TABLE H-16  
 PITCH ANGLE COMMAND--F.C. #2

	Peak Value	Final Value	Rise Time	Settling Time
$\theta$	1.0	1.0	5.2	8.4
h	0.661	0.661	--	--
u	-0.498	-0.425	--	--
$\delta_e$	2.42	--	--	--
$\delta_{sb}$	19.3	--	--	--
$\delta_T$	45.1	--	--	--

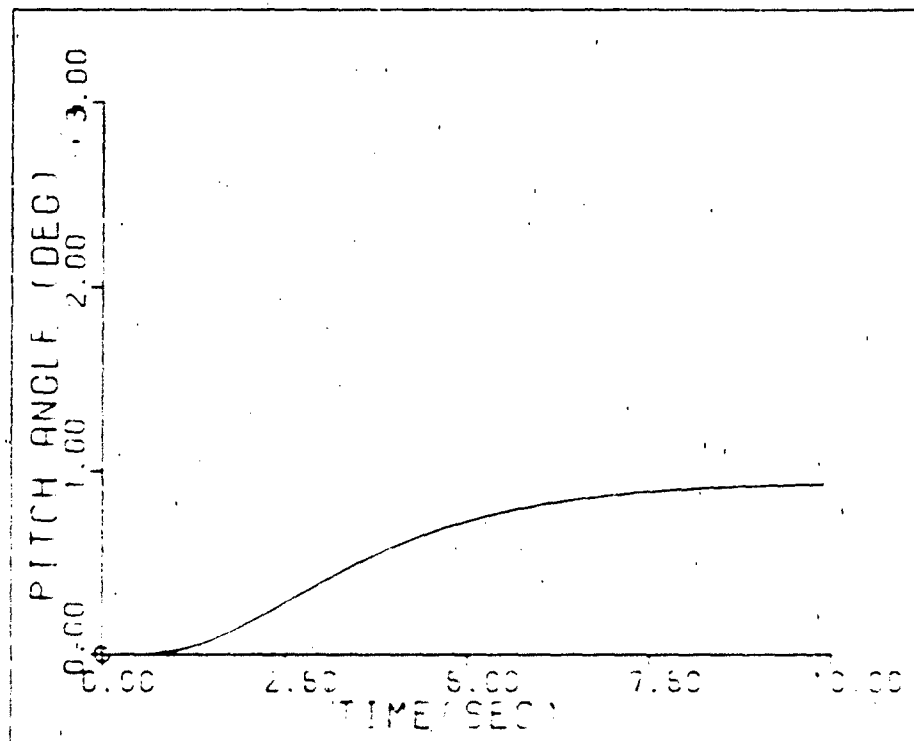


Fig. H-67. Pitch Angle Response--F.C. #2

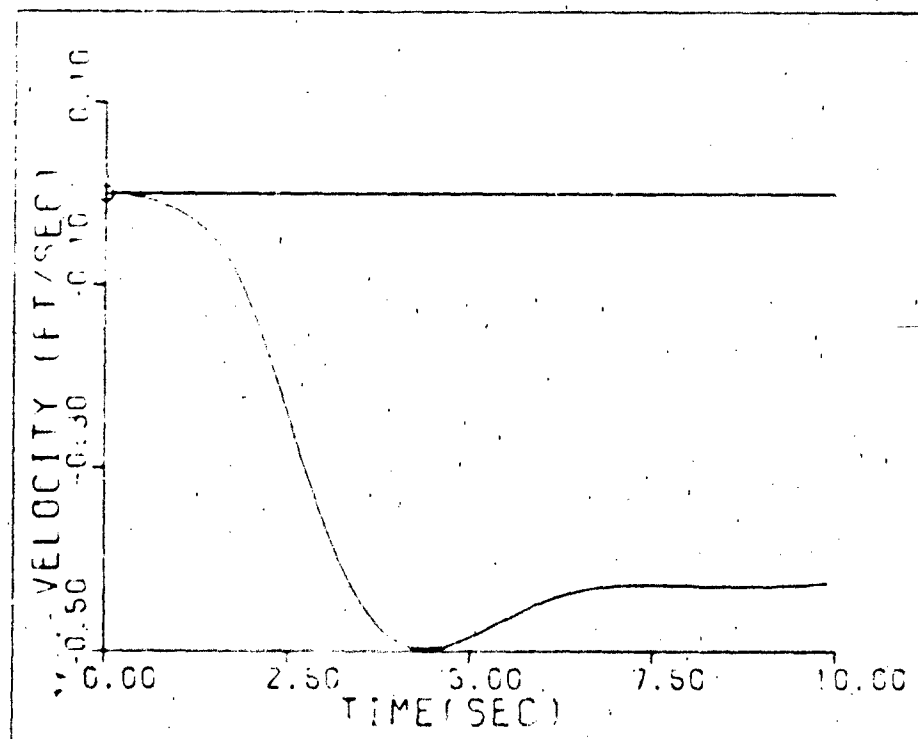


Fig. H-68. Perturbation Velocity Response--F.C. #2

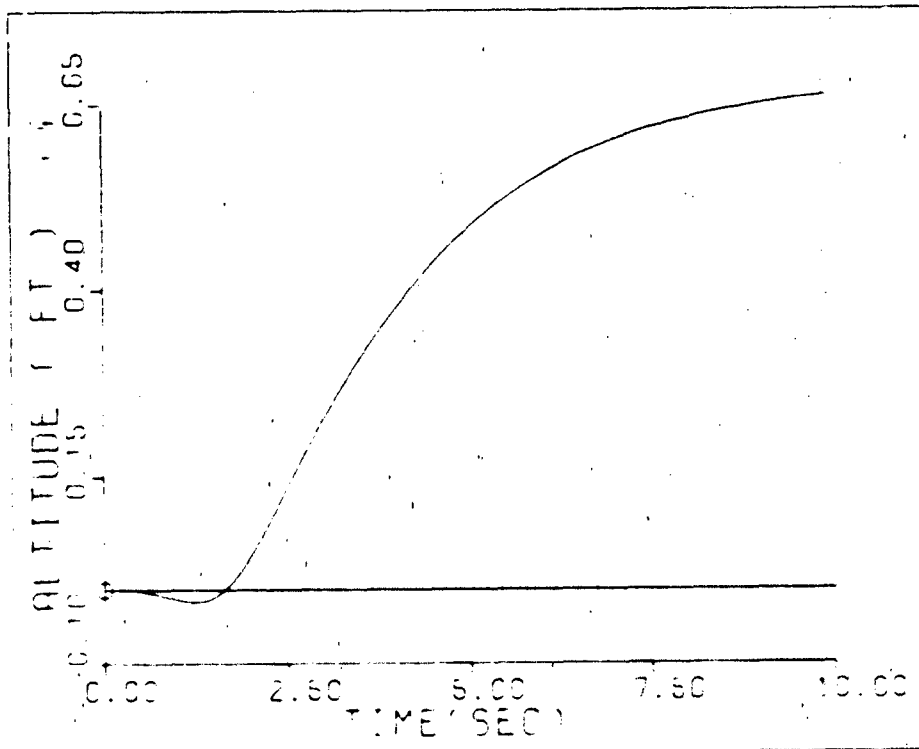


Fig. H-69. Altitude Response--F.C. #2

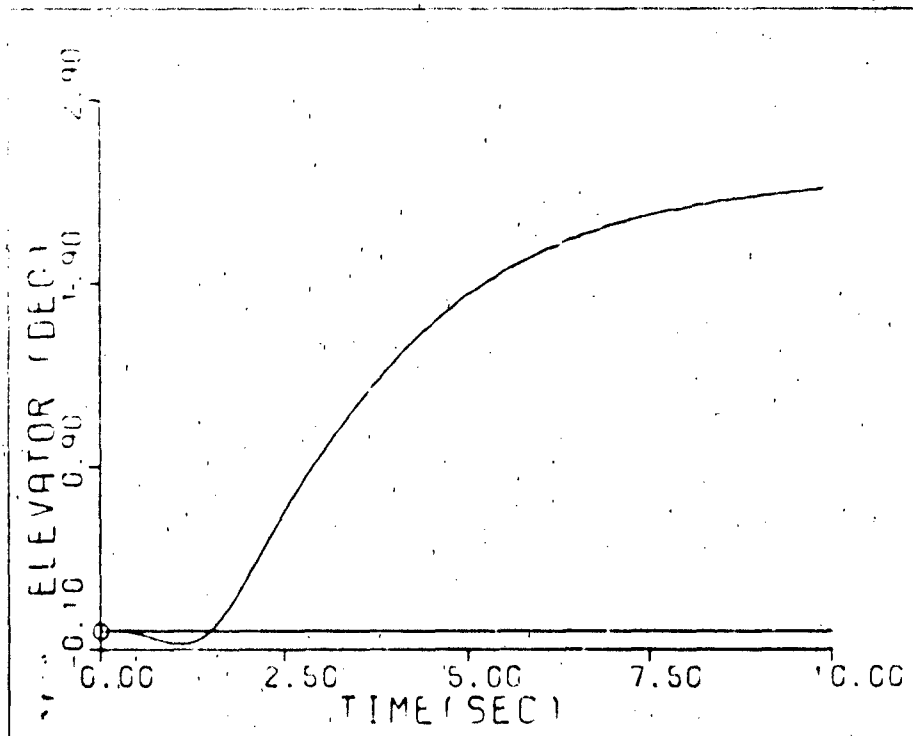


Fig. H-70. Elevator Deflection--F.C. #2

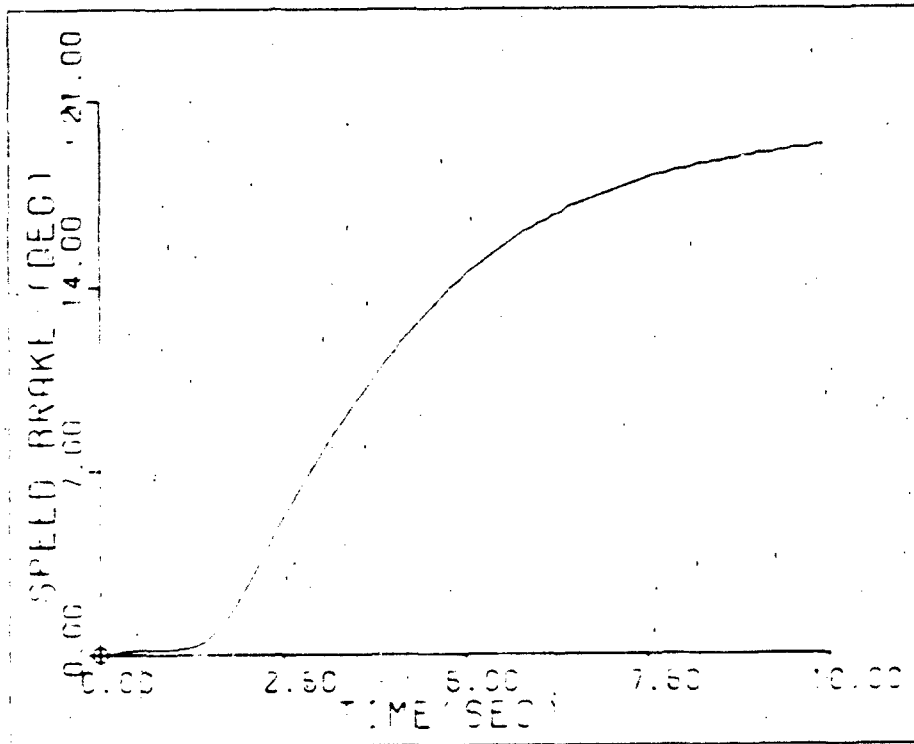


Fig. H-71. Speed Brake Deflection--F.C. #2

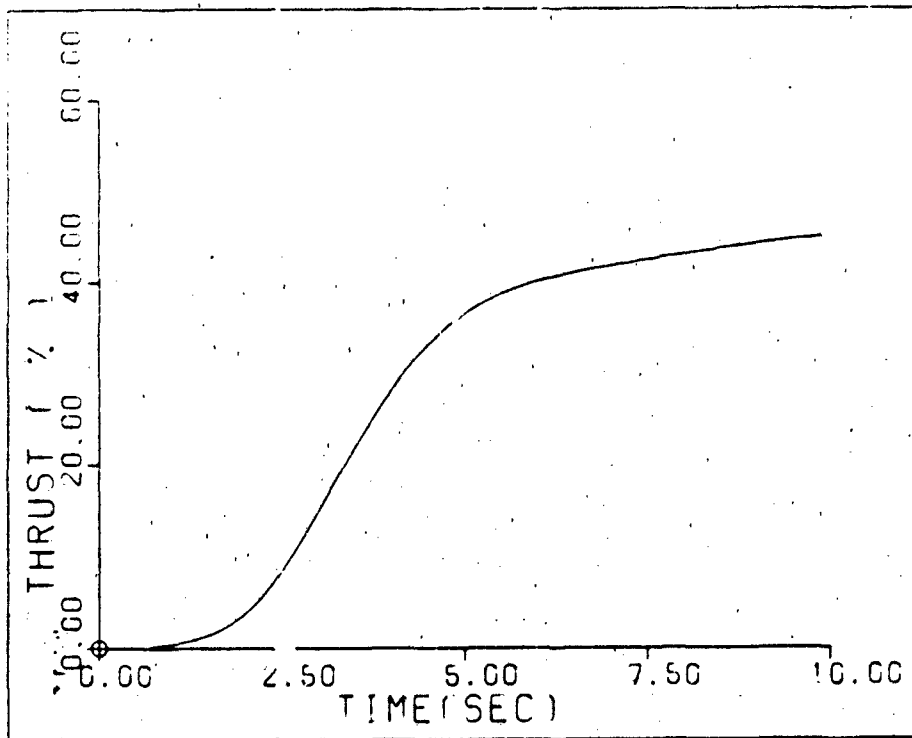


Fig. H-72. Thrust Increase--F.C. #3

Summary

This appendix contains the simulated responses for both the lateral and longitudinal designs for F.C.'s #1 and #2.

## Bibliography

1. Ashworth, M. J. Feedback Design of Systems with Significant Uncertainty. Chichester: Research Studies Press, 1982.
2. Barfield, Finley A. Multivariable Control Laws for the AFIT/F-16. MS Thesis. Air Force Institute of Technology, Wright-Patterson AFB OH, July 1983 (AFIT/GE/EE/835-4).
3. Betzold, Robert W. Multiple Input-Multiple Output Flight Control Design with Highly Uncertain Parameters; Application to the C-135 Aircraft. MS Thesis. Air Force Institute of Technology, Wright-Patterson AFB OH, December 1983 (AFIT/GE/EE/830-11).
4. Blakelock, John H. Automatic Control of Aircraft and Missiles. New York: John Wiley and Sons, Inc., 1965.
5. Boeing Company. KC/EC/RC-135 Aerodynamic Characteristics Mission Simulators. Document number D3-9782-2, Contract No. F34601-74-A-001, May 1976.
6. Boeing Company. KC/EC/RC-135 Aerodynamic Characteristics. Document number D3-9090, Contract No. F34601-74-A-001, April 1976.
7. Boeing Company. KC/EC/RC-135 System Characteristics-Mission Simulators. Document number D3-9782-5, Contract No. F34601-74-A-0001, April 1976.
8. D'Azzo, John J. and Constantine H. Houpis. Linear Control System Analysis and Design, Conventional and Modern (Second Edition). New York: McGraw-Hill Book Company, 1981.
9. Horowitz, Isaac. "Improved Design Technique for Uncertain Multiple Input-Multiple Output Feedback Systems," International Journal of Control, 36(6): 977-988 (1982).
10. Horowitz, Isaac and Clayton Loecher. "Design of 3x3 Multivariable Feedback System with Large Plant Uncertainty," International Journal of Control, 33(4): 677-699 (1981).

11. Horowitz, Isaac and T. Kopelman. Multivariable Flight Control Design with Uncertain Parameters. Department of Applied Mathematics, The Weizmann Institute of Science, Rehovot, Israel. Final Report, September 1982.
12. Horowitz, Isaac. "Quantitative Synthesis of Uncertain Multiple Input-Multiple Output Feedback Systems," International Journal of Control, 30(1): 81-106 (1979).
13. Horowitz, Isaac et al. Research in Advanced Flight Control Design. AFFDC-TR-79-3120. Department of Applied Mathematics, The Weizmann Institute of Science, Rehovot, Israel, January 1980.
14. Horowitz, Isaac and Marcel Sidi. "Synthesis of Feedback Systems with Large Plant Ignorance for Prescribed Time-Domain Tolerances," International Journal of Control, 16(2): 287-309 (1972).
15. Horowitz, Isaac M. Synthesis of Feedback Systems. New York: Academic Press, 1963.
16. Larimer, S. J. Total--An Interactive Computer-Aided Design Program for Digital and Continuous Control System Analysis and Synthesis. MS Thesis. Air Force Institute of Technology, Wright-Patterson AFB OH, March 1978.
17. Locken, William J. Digital Multivariable Tracker Control Laws for the KC-135A. MS Thesis. Air Force Institute of Technology, Wright-Patterson AFB OH, December 1983 (AFIT/GE/EE/83D-40).
18. Roskam, J. Airplane Flight Dynamics and Automatic Flight Control. Lawrence KS: Roskam Aviation and Engineering Corporation, 1976.
19. Russell, Harvey H. "Software for Quantitative Feedback Theory (QFT)," AFIT/EN, Wright-Patterson AFB OH, December 1984.
20. USAF Technical Orders, KC-135A Dash-1, T.O. IC-135 (K) A-1, Change 47, Tinker Air Force Base OK, December 1981.

Vita

Harvey H. Russell was born in Princeton, Bonavista Bay, Newfoundland on 30 September 1950. He joined the Canadian Armed Forces in 1968 and was employed by the Fire Department until 1976. He attended the Royal Roads Military College and the Royal Military College from 1976 to 1980 and received a Bachelor of Science Degree in Electrical Engineering in May, 1980.

After graduation, he was employed as an engineer at the Aerospace Maintenance Development Unit in Trenton, Ontario.

He entered the Graduate Electrical Engineering Program at the School of Engineering, Air Force Institute of Technology in June 1983.

Permanent Address: Princeton,  
Bonavista Bay,  
Newfoundland



**END**

**FILMED**

5-85

**DTIC**